TECHNISCHE UNIVERSITÄT MÜNCHEN
Ingenieurfakultät Bau Geo Umwelt
Professur für Hangbewegungen

Rock-Slope Failures Impacting Lakes – Frequency, Magnitude and Interactive Processes Deciphered from Lacustrine and Terrestrial Deposits

Sibylle Knapp

Vollständiger Abdruck der von der Ingenieurfakultät Bau Geo Umwelt der Technischen Universität München zur Erlangung des akademischen Grades eines

Doktors der Naturwissenschaften
(Dr. rer. nat.)

genehmigten Dissertation.

Vorsitzender:	Prof. Dr. Kurosch Thuro
Prüfende der Dissertation:	1. Prof. Dr. Michael Krautblatter
	2. Prof. Dr. Flavio Anselmetti, Universität Bern, Schweiz
	3. Prof. Dr. Jürgen Geist

Die Dissertation wurde am 09.07.2020 bei der Technischen Universität München eingereicht und durch die Ingenieurfakultät Bau Geo Umwelt am 01.10.2020 angenommen.

Declaration of authorship

I, Sibylle Knapp, declare that this thesis entitled *"Rock-Slope Failures Impacting Lakes – Frequency, Magnitude and Interactive Processes Deciphered from Lacustrine and Terrestrial Deposits"* and the work presented in the thesis are both my own, and have been generated by me based on my own original research. I confirm that:

- where I have quoted work from others, the source is always given
- this work was wholly or mainly done while in candidature for a doctoral degree at the Technical University of Munich
- where any parts of this thesis have been previously submitted for a degree at the Technical University of Munich or any other institution, this has been clearly stated
- I have acknowledged all main sources of help
- all published own work (authorship) or co-authored published work regarding paper and conference proceedings originating from this thesis are given in the following.

This thesis is written in accordance to the "Promotionsordnung der Technischen Universität München vom 12. März 2012 in der Fassung der 2. Änderungssatzung vom 1. September 2013" (implemented January 1, 2014), the "Leitfaden BGU Promotionen" (issued April 6, 2016) and the "Leitfaden Kumulative Promotionen" (issued July 2015).

The following articles and conference proceedings originate from this thesis:

ISI-listed publications (full research paper, peer-reviewed):

Accepted manuscripts:

Knapp, S., Gilli, A., Anselmetti, F.S., Krautblatter, M., Hajdas, I. (2018): Multistage Rock-Slope Failures Revealed in Lake Sediments in a Seismically Active Alpine Region (Lake Oeschinen, Switzerland). *Journal of Geophysical Research: Earth Surface 123(4): 658-677*. https://doi.org/10.1029/2017JF004455

Knapp, S. and Krautblatter, M. (2020): Conceptual Framework of Energy Dissipation During Disintegration in Rock Avalanches. *Frontiers in Earth Science, 8(263).* https://doi.org/10.3389/feart.2020.00263

Knapp, S., Mamot, P., Lempe, B., Krautblatter, M. (2020): Impact of an 0.2 km³ Rock Avalanche on Lake Eibsee (Bavarian Alps, Germany) – Part I: Reconstruction of the Paleolake and Effects of the Impact. *Earth Surface Processes and Landforms.* https://doi.org/10.1002/esp.5024

Knapp, S., Anselmetti, F. S., Lempe, B., Krautblatter, M. (2020): Impact of an 0.2 km³ Rock Avalanche on Lake Eibsee (Bavarian Alps, Germany) – Part II: Catchment Response to Consecutive Debris Avalanche and Debris Flow. *Earth Surface Processes and Landforms.* https://doi.org/10.1002/esp.5025

The mentioned articles above have been incorporated in the thesis according to Wiley's "Copyright Transfer Agreement" regarding the "Final Published Version" of a paper, and the "Frontiers Copyright Statement" including the Creative Commons attribution licence.

Published raw data

The data sets presented in the publication *Knapp et al. (2018)* are available at https://doi.org/10.14459/2018md1432577.

Conference proceedings (oral presentations):

Knapp, S., Gilli, A., Anselmetti, F.S., Hajdas, I. (2016): Reconstruction of multistage massive rock slope failure: Polymethodical approach in Lake Oeschinen (CH). EGU General Assembly 2016, Vol. 18, EGU2016-8468-4, Vienna, Austria.

Knapp, S., Anselmetti, F.S., Krautblatter, M. (2016): Large rock slope failures impact on lakes – Event reconstruction and interaction analysis using sedimentology and geophysics. Annual Meeting of the German Geomorphology Group „AK Geomorphologie" 2016, Jena.

Knapp, S., Gilli, A., Anselmetti, F.S., Krautblatter, M., Hajdas, I. (2018): Frequency, age and magnitude of rock-slope failures derived from lake sediments (Lake Oeschinen, CH). EGU General Assembly 2018, Vol. 20, EGU2018-9976, Vienna, Austria.

Knapp, S. (2018): Wiederkehrintervalle von Fels- und Bergstürzen abgeleitet aus sedimentologischen Untersuchungen (Öschinensee und Eibsee). 18. Fachtagung Rutschungen, Forschungsstelle JGU Mainz, 06.06.2018, Tagungsband: 10-12.

Knapp, S., Gilli, A., Anselmetti, F.S., Krautblatter, M., Hajdas, I. (2018): Towards refined recurrence rates and distribution patterns of rock-slope failures by studying lake sediments (Lake Oeschinen, CH, and Lake Eibsee, D). 20th International Sedimentological Congress 2018, Quebec City, Quebec, Canada.

Knapp, S., Anselmetti, F.S., Krautblatter, M., Gilli, A., Hajdas, I. (2018): Large rock-slope failures impacting on lakes – Insights from lacustrine and terrestrial deposits at Lake Oeschinen (CH), Lake Eibsee (D) and Flims (CH). Central European Conference on Geomorphology and Quaternary Sciences 2018, Giessen.

Knapp, S., Mamot, P., Lempe, B., Krautblatter, M. (2020): Lake pushed out by 200 m³ rock avalanche (Zugspitze / Lake Eibsee, D) - New geophysical and sedimentological insights into interactive processes. EGU General Assembly 2020, EGU2020-13810, Vienna, Austria. https://doi.org/10.5194/egusphere-egu2020-13810

Biannual PhD Conferences with oral presentations, German National Academic Foundation (Studienstiftung des deutschen Volkes e.V.): *"Multistage rock-slope failures revealed in lake sediments (Lake Oeschinen, CH)",* 26.04.2016, Berlin. *„Tsunamis bei uns in den Alpen? Von brechenden Bergen und fliegenden Flutwellen",* 14.11.2016, Düsseldorf. ,,*Wenn Felsen ins Wasser stürzen – Tsunamis in den Bergen",* 21.03.2017, Bad Homburg. ,,*Auf den Spuren von Naturkatastrophen – Detektivarbeit in den Alpen",* 10.11.2017, Heidelberg.

Conference proceedings (poster presentations):

Knapp, S., Mamot, P., Krautblatter, M. (2015): The mobility of rock avalanches: disintegration, entrainment and deposition - a conceptual approach. EGU General Assembly 2015, Vol. 17, EGU2015-12496, Vienna, Austria.

Knapp, S., Gilli, A., Anselmetti, F.S., Krautblatter, M., Hajdas, I. (2016): Large Rock-Slope Failures Impacting on Lakes – Event Reconstruction and Interaction Analysis in Two Alpine Regions Using Sedimentology and Geophysics. AGU Fall Meeting 2016, NH43C-1885, San Francisco, California, USA.

Knapp, S., Gilli, A., Anselmetti, F.S., Krautblatter, M., Hajdas, I. (2017): Large rock-slope failures impacting on lakes - Reconstruction of events and deciphering mobility processes at Lake Oeschinen (CH) and Lake Eibsee (D). EGU General Assembly 2017, Vol. 19, EGU2017-15712, 2017, Vienna, Austria.

Knapp, S. (2017): Large Rock-slope Failures Impacting on Lakes – Event Reconstruction and Mobility Processes. Young Geomorphologists´ Conference 2017, Herrsching.

Knapp, S., Schwenk, M., Krautblatter, M. (2018): Evolution of the Toma hills and transport of flood deposits in a propagating Flims rock avalanche (Grisons, Switzerland). EGU General Assembly 2018, Vol. 20, EGU2018-10046, Vienna, Austria.

Scholz, D., Krautblatter, M., **Knapp, S.**, Poschinger, A., Clague, J. (2019): Sedimentological reconstruction of an outburst flood in response to the Flims Rock Slide into the potential Lake Bonaduz. EGU General Assembly 2019, Vol. 21, EGU2019-18773, Vienna, Austria.

The following (unpublished) master thesis has been incorporated in this thesis:

Knapp, S. (2012): The Sedimentary Archive of Lake Oeschinen (Bernese Alps, Switzerland): Reconstruction of the Rockfall History. Department of Earth Sciences, Institute of Climate Geology, ETH Zurich, Zurich, Switzerland. Unpublished master thesis, 73 p.

Acknowledgments

First of all, I want to thank my supervisor Prof. Dr. Michael Krautblatter for the chance to study rock-slope failures over many years, giving me the freedom to further develop my own research ideas, thereby inspiring me on field trips and mapping courses and giving me trust in my work. One of the best "side-products" of our co-work is that he introduced me to the lovely *Rotflügelige Schnarrschrecke* at the Tschirgant rock avalanche.

Special thanks goes to Prof. Dr. Flavio Anselmetti, who was quasi my second supervisor and worked with me on all questions regarding the lakes. Thank you, Flavio, for your support, reliability and encouragement during all our projects, even in harsh coring conditions with rock-avalanche material crushing our drill bit. ☺

Thanks to my mentor Dr. Bernhard Lempe for our long-lasting discussions on complex geo-fantasy, teaching me to think as an engineer while assessing an outcrop, and giving me advice in difficult times.

Further I want to thank Dr. Ulrich Haas for introducing me to the Eibsee rock avalanche with long discussions in the field and proofreading my Eibsee articles. Also, I want to thank Dr. Andreas von Poschinger for his support during our studies at the Flims rockslide, where he showed us new outcrops and accompanied our sedimentological analyses. Also John Clague supported fieldwork at the Flims rockslide, where we had lots of fun doing ERT with sheep, deer and an eagle. Thanks to Dr. Anja Dufresne for showing me around the Tschirgant rock avalanche at the beginning of my studies, where I learned a lot about entrainment processes at the base of rock avalanches, and for providing me with valuable literature from volcanologists.

I also acknowledge support from Michael Schwenk, Verena Stammberger, Mathias Schimpfle, Joel Achenbach, David Scholz and Julia Gottfriedsen, who contributed to collecting and analysing data at the Eibsee and Flims rock avalanche during their diploma theses. Thanks also to all further co-authors and helpers in the lab and the field, as well as the TUM Landslide Research Group for excellent field trips with coffees and beers in the aftermath, as well as the secretaries Astrid Merling and Stephanie Schaidhammer.

Last but not least, my parents, my sister, Falko, Jenny and Laura accompanied me on this long journey with all ups and downs. Your patience, your love and everlasting belief in my work make me proud and very grateful.

Finally, I acknowledge in total 8 years of financial and ideational support from the Studienstiftung des deutschen Volkes. During this time, I profited by numerous seminars and contacts to other fellows, which shaped my personality to a high extent. Some of them became friends for life.

Table of Contents

Index of Figures

Index of Tables

Abstract

Natural hazards and catastrophes like earthquakes, floods, avalanches or landslides are worldwide known phenomena. Large landslides belong to the most dangerous natural hazards in alpine environments. Among single-event landslide disasters, massive rock-slope failures account for 75% of disasters with more than 1000 casualties per occurrence. Rock avalanches destroy and reshape landscapes within only a few minutes. Water within the travel path often causes high impact waves and exceptional runouts. Moreover, recent studies show that mountain flanks do not collapse in a single event, but rather through multistage progressive failures, often detaching from identical scarps or neighbouring niches. As younger event deposits superimpose, partially cover and hide older ones, deciphering the multistage character of rock-slope failures is a challenging task. Thus, the frequency of rock-slope failures is often highly underestimated and their magnitudes misinterpreted. Especially Lateglacial and Holocene rock-slope failures often occur as multistage failures, where paraglacial adjustment and stress adaptation are hypothesized to control phases of detachment. It often takes hundreds of years for the catchment to stabilize again. For hazard assessment, it is essential to refine recurrence rates and to better understand progressive-failure evolution as well as multistage reshaping of the geomorphology in the impact zone.

Lake Oeschinen, situated in the Bernese Alps, Switzerland, reveals a unique inventory covering ~2.5 kyrs of rock-slope failure history. The lake sediments have been investigated using sediment-core analysis, radiocarbon dating and seismic-to-core and core-to-core correlations, which were linked to (pre-) historic and meteorological records. The results imply that the lake in its present extent is significantly younger than the ~9.5 kyrs old Kandersteg rock avalanche in the close vicinity. Up to eleven rock-slope failure events could be identified and related to specific detachment scarps, which provided information for energy considerations. Four events likely coincided with (pre-) historic earthquakes. At least six events detached from the same area. The data imply unexpected high recurrence rates (~1/300 yrs) and additionally help to understand the generation of a historical lake-outburst flood.

The ~0.2 km³ Eibsee rock avalanche in the Bavarian Alps detached from Mount Zugspitze and presumably impacted Paleolake Eibsee, which in turn became completely displaced. The studies on the lacustrine and terrestrial archives analyse the catchment response to the large failure and the effects of the lake impact. In the lake, a quasi-3D reflection seismic survey, four sediment cores from modern Lake Eibsee, nine radiocarbon dates from event deposits, and geomorphological analysis make it possible to distinguish the main rock-avalanche event from a debris avalanche and sturzstrom in the aftermath. The highly fluidized debris avalanche formed a megaturbidite and multiple swashes captured in the lake sediments. The newly calibrated age shows a coincidence with other megaevents in the Fernpass cluster, especially in the neighbouring Lake Plansee and Lake Piburg, which makes an earthquake as regional trigger more likely. On land, 9.5 km of Electrical Resistivity Tomography (ERT) profiles with up to 120 m penetration depth and more than 34,000 datum points allow to decipher multiple interactive processes caused by the impact. Finally, this study enable to reconstruct both position and dimension of the paleolake prior to the catastrophic event.

The ~10-12 km³ Flims rockslide in the eastern Swiss Alps is the largest known rock-slope failure in the Alps and has fascinated researchers with its complex and diverse features ever since. Here we focus on the hypothesized impact of the Flims rockslide on Lake Bonaduz, which caused intensely fluidized rock material, known as Bonaduz gravels, and Toma hills. Geophysical investigation with ERT to a sediment depth of up to 160 m and sedimentological analyses answer long-debated questions on the stratigraphic relation between the Flims and Tamins rockslide deposits. There is new field evidence that the Bonaduz gravels build an onlap on the Ils Aults and were therefore formed after the Tamins rockslide. We further consider a simultaneous transport of the Toma within the Bonaduz gravels. Finally, this study helps to decipher water-rich entrainment in rock avalanches, the genesis and transport of outburst-flood deposits, in particular of Toma hills resp. hummocks.

In this dissertation, the attention is mainly centralized on large rock-slope failures impacting lakes with a focus on refining recurrence rates and deciphering effects of the impact and the consequences for the mobility of the propagating rock mass. Complementary method application at three test sites, namely Lake Oeschinen (Bernese Alps, Switzerland), Lake Eibsee / Eibsee rock avalanche (Bavarian Alps, Germany) and Flims rockslide (Grisons Alps, Switzerland), yields novel results for the reconstruction of rock-slope failure in time and space and their secondary effects when impacting a lake. At Lake Oeschinen und Lake Eibsee, reflection seismology, radiocarbon dating, sedimentology on cores and geomorphology are used to reconstruct multistage rock-slope failure recorded in lake sediments. Here we show how polymethodical analysis of lake sediments can help to decipher multistage rock-slope failures, which are often camouflaged in subaerial settings. At Lake Eibsee, the complex history of erosion and sedimentation can thus be disclosed, and the catchment response and the "rebirth" of the lake after the catastrophic impact can be revealed. Furthermore, the studies on terrestrial deposits applying electrical resistivity tomography (ERT), geomorphology and sedimentology in outcrops at the Eibsee and Flims rock avalanches decipher multiple effects of a rock avalanche impacting a lake. The reconstruction and close-up of subsequent impact phases with bulldozing, fluidization of the rock mass, the entrainment of lake sediments and valley infill, and the transport of outburst-flood deposits such as Toma hills, are valuable contributions to understanding processes, future modelling and hazard assessment.

Zusammenfassung

Naturgefahren und Naturkatastrophen wie Erdbeben, Hochwasser, Lawinen oder Hangbewegungen sind weltweit bekannte Phänomene. Große Hangbewegungen gehören zu den gefährlichsten Naturgefahren in alpinen Gebieten. Betrachtet man einzelne Katastrophenereignisse mit mehr als 1000 Toten, machen massive Felsabbrüche davon etwa 75% aus. Bergstürze verwandeln beziehungsweise zerstören Landschaften binnen weniger Minuten. Die Anwesenheit von Wasser in der Auslaufzone führt oft zu hohen Flutwellen und großen Reichweiten. Neuere Studien haben außerdem gezeigt, dass Bergflanken nicht auf einmal kollabieren, sondern dass es sich vielmehr um multiple Felsabbrüche handelt, die oft aus derselben oder aus benachbarten Ausbruchsnischen stammen. Das führt dazu, dass die Ablagerungen älterer Ereignisse von jüngeren überlagert und dabei teilweise bedeckt oder gar versteckt werden. Die Entschlüsselung mehrerer Ereignisse wird dadurch zur Herausforderung. Dadurch werden vor allem die Häufigkeit von Felsabbrüchen unterschätzt, und deren Magnituden fehlinterpretiert. Insbesondere spätglaziale und holozäne Ereignisse treten als multiple Felsabbrüche auf. Dabei beeinflussen die Umweltveränderungen in der unmittelbaren Umgebung von Gletschern auch die mechanischen Spannungsverhältnisse im Fels und stehen somit in Verdacht, die Felsabbrüche zu kontrollieren. Es dauert oft Hunderte von Jahren, bis sich das Einzugsgebiet wieder stabilisiert. Für die Gefahrenanalyse ist es wesentlich die Wiederkehrraten genauer zu bestimmen und besser zu verstehen, wie es zu dem stufenweisen Felsversagen kommt, und wie sich die Landschaft in der Auslaufzone mit jedem weiteren Ereignis verändert.

Der Öschinensee im Berner Oberland, Schweiz, offenbart ein einzigartiges Archiv der seit über ~2500 Jahre andauernden Bergsturzgeschichte. Die Seesedimente wurden anhand von Bohrkernen, Radiokarbondatierungen und Reflektionsseismik untersucht, und die daraus abgeleiteten Resultate wurden mit meteorologischen Daten verglichen. Der heutige See ist deutlich jünger als der ~9500 Jahre alte Kandersteg-Bergsturz in der unmittelbaren Umgebung. Bis zu elf Felsabbrüche konnten identifiziert und bestimmten Ausbruchsnischen zugeordnet werden. Die Analyse der Ausbruchsnischen liefert außerdem Erkenntnisse über die Energiebilanzen der Felsablösungen. Vier Ereignisse können mit (prä-) historischen Erdbeben in Zusammenhang gebracht werden. Mindestens sechs Events stammen von derselben Bergflanke. Die Ergebnisse implizieren unerwartet hohe Wiederkehrraten (~1 Event alle 300 Jahre) und helfen darüber hinaus, die Entstehung einer historischen Ausbruchsflut nachzuvollziehen.

Der ~0,2 km³ große Eibsee-Bergsturz in den Bayerischen Alpen löste sich von der Zugspitze und stürzte in einen vermuteten Paläo-Eibsee. Dieser wurde durch den Impakt zerstört. Die Studien der lakustrinen und terrestrischen Archive untersuchen die Auswirkungen auf das Einzugsgebiet infolge des Felsversagens und Impakts auf den See. Hierfür kamen im See quasi-3D Reflektionsseismik, vier Sedimentbohrkerne aus dem heutigen See, neun Radiokarbondatierungen aus Eventlagen und geomorphologische Analyse zum Einsatz. So ist es gelungen das Großereignis des Eibsee-Bergsturzes von zwei aufeinanderfolgenden Fels- bzw. Bergstürzen zu unterscheiden. Das zweite Event war hochfluidisiert und hinterließ einen Megaturbidit sowie Spuren mehrerer Schwappwellen in den Seesedimenten. Das neu kalibrierte Alter von ~4000 cal BP zeigt einen zeitlichen Zusammenhang mit anderen Großereignissen im sogenannten Fernpass-Cluster auf, insbesondere mit dem benachbarten Plansee. Diese Erkenntnisse machen ein Erdbeben als regionalen Trigger wahrscheinlicher. An Land ermöglichen 9,5

km ERT-Profile mit bis zu 120 m Eindringtiefe und mehr als 34.000 Datenpunkten die Unterscheidung von diversen interaktiven Prozessen, die durch den Impakt des Bergsturzes auf den See ausgelöst wurden. Letztlich kann der Paläo-Eibsee anhand der Ergebnisse nachgewiesen und in seiner Position und Dimension bestimmt werden.

Der ~10-12 km³ große Flimser Bergsturz in den östlichen Schweizer Alpen ist der größte bekannte Bergsturz in den Alpen und fasziniert die Forscher mit seinen komplexen und diversen Merkmalen seit jeher. Hier fokussieren wir uns auf den vermeintlichen Impakt des Flimser Bergsturzes auf den Bonaduzer See. Dies führte zur Bildung einer hochfluidisierten Geröllmasse, auch bekannt als Bonaduzer Kiese, sowie zur Ausformung von Tomahügeln. Geophysikalische ERT-Messungen bis zu einer Eindringtiefe von 160 m und sedimentologische Analysen beantworten langwährende Diskussionen über den stratigraphischen Zusammenhang zwischen den Ablagerungen des Flimser und Taminser Bergsturzes. Es gibt nun neue Hinweise, dass die Bonaduzer Kiese einen Onlap auf den Ils Aults bilden, d. h. sie wurden nach dem Taminser Bergsturzereignis abgelagert. Außerdem nehmen wir einen simultanen Transport der Tomahügel in den Bonaduzer Kiesen an. In dieser Studie werden außerdem die Aufnahme von Substrat unter dem Einfluss großer Mengen an Wasser sowie die Genese und der Transport von Ausbruchsflutsedimenten, insbesondere von Tomahügeln, entschlüsselt.

Diese Dissertation behandelt vornehmlich große Felsabbrüche, die in einen See gestürzt sind. Dabei liegt der Fokus auf der genaueren Bestimmung von Wiederkehrraten, der Entschlüsselung der Folgen des Impakts und den Konsequenzen für die Mobilität der weiter fließenden Felsmasse. In drei Untersuchungsgebieten, nämlich am Öschinensee (Berner Alpen, Schweiz), am Eibsee beziehungsweise Eibsee-Bergsturz (Bayerische Alpen, Deutschland) und am Flimser Bergsturz (Graubündner Alpen, Schweiz) werden durch den Einsatz komplementärer, d.h. sich ergänzender Methoden neuartige Ergebnisse erzielt. Dabei werden die Felsabbrüche in Zeit und Raum rekonstruiert, sowie deren Auswirkungen bei einem Impakt auf einen See ermittelt. Am Öschinensee und Eibsee kommen die Methoden der Reflektionsseismik, Radiokarbondatierung, Sedimentologie an Bohrkernen und Geomorphologie zum Einsatz, um multiples Felsversagen anhand von Seesedimenten zu rekonstruieren. Damit wird deutlich, wie die Untersuchung von Seesedimenten unter dem Einsatz verschiedener Methoden dabei helfen kann, stufenweises Felsversagen zu entschlüsseln, wo es doch an Land so oft unentdeckt bleibt. So kann die komplexe Landschaftsgeschichte vom Eibsee inklusive der Veränderungen im Einzugsgebiet und der „Wiedergeburt“ des Sees nach dem katastrophalen Impaktereignis nachvollzogen werden. Weiterhin werden die Auswirkungen des Impakts auf einen See auch an terrestrischen Sedimenten am Eibsee- und Flimser Bergsturz untersucht. Dabei werden die Methoden der Widerstandstomographie (ERT), Geomorphologie und Sedimentologie in Geländeaufschlüssen angewandt. Aufeinanderfolgende Phasen des Impakts, angefangen bei Bulldozing, Fluidisierung der Felsmasse, Aufnahme und Einarbeitung von Seesedimenten und Talfüllungen in die Felsmasse, sowie letztlich dem Transport von Sedimenten in der Ausbruchsflut, wie zum Beispiel Tomahügel, werden auf diese Weise detailliert betrachtet. Diese Ergebnisse wiederum tragen entscheidend zum allgemeinen Prozessverständnis, zur zukünftigen Modellierung und Gefahrenanalyse bei.

1 Introduction

1.1 Research Motivation

Natural hazards and catastrophes like earthquakes, floods, avalanches and landslides are worldwide known phenomena. In the perspective of advancing climate change and numerous disastrous events being spreading by the media, human kind is gradually realizing the threat to modern society and the economy, fascinated and feeling threatened at the same time. Nobody really knows how much climate change will affect our lives. Therefore, research in the field of natural hazards can be substantially important to us all. This way, our knowledge of the frequency and severity of catastrophic events in the past will be improved, and the key mechanisms and triggers will be encoded. Finally, a detailed hazard assessment and risk management, combined with the establishment of early warning and monitoring systems will in future protect lives and infrastructure from damage and destruction to a highest possible extent.

Large landslides belong to the most dangerous natural hazards in all alpine environments. A very high percentage of people affected by a landslide lose their lives, and this is a notable fact when compared to other catastrophes. The hazard potential is impressively illustrated by the most deadly landslide disaster in history with more than 100,000 fatalities, triggered on a widespread and gigantic scale by the M 7.8 Gansu Earthquake of December, 1920 in China (e.g. Zhang and Wang, 1995; Havenith and Bourdeau, 2010; Wang *et al.*, 2014).

Among single-event landslide disasters, massive rock-slope failures account for 75% with more than 1000 casualties (Evans, 2006). Massive rock-slope failures are defined by Evans *et al.* (2006) as extremely rapid movements of failed rock mass such as rockslides, rock avalanches and catastrophic rockfalls with a high socio-economic impact potential. Although large rock failures are relatively rare in space and time (Abele, 1974), they are extremely destructive compared to other types of smaller landslides like rockfalls, debris flows etc. (Plafker and Ericksen, 1978; Evans, 2006; Hermanns *et al.*, 2006). Large rock-slope failures are generally characterized by a highly pulverized mass, which moves like a slurry. The geometry of the moving rock material is highly influenced by the valley topography and determines runout behaviour. Large rock-slope failures often occur in sedimentary rocks, where the dip of the sedimentary strata seems to determine the volume of the rock-slope failure. Steep dips of strata correspond with less volume and vice versa (Ekström and Stark, 2013).

1.2 Problem Statement and Research Needs

In this dissertation, the attention is mainly turned to large rock-slope failures impacting lakes with a focus on refining recurrence rates, and deciphering effects of the impact and the consequences for the mobility of the propagating rock mass. Moreover, the case studies aim at deciphering the event history at the specific test sites.

Frequency and Magnitude of Rock-Slope Failures

Massive rock-slope failures can reduce rather than increase slope stability (Hermanns *et al.*, 2006), i.e. large rock failures tend to produce even more events in the aftermath. We hypothesize that the multistage character of massive rock-slope failure is often not deciphered, and

therefore magnitude and frequency are highly misestimated. This is because single event deposits are camouflaged on land under massive piles of debris deposits, which makes it hard to identify multiple events. Knowing the magnitude and frequency of rock-slope failures at a specific site, however, is essential for future hazard assessment at certain rock slopes. Therefore, studies on multistage rock-slope failures with the goal of refining recurrence rates and magnitudes are in great demand and subject of this dissertation.

Effects of Lake Impact on Mobility Processes in Rock Avalanches
Climate warming leads to a drastic change of the high-mountainous landscape with permafrost degradation and glacier retreat (Haeberli *et al.*, 2017). As a result, more destabilized mountain flanks will be exposed above newly formed (meltwater-) lakes. Large rock-slope failures impacting lakes have a very high hazard potential due to secondary effects such as impact waves, dam failures and highly fluidized rock material. Lubrication due to the entrainment of water and fine-grained sediments is hypothesized to play a major role for rock avalanches to reach long distances.

Site-Specific Event History and Paleotopography
Knowing from a specific mountain flank and its surroundings, how many, when and from which scarp niche rock-slope failures have actually occurred and how lakes and dams have developed during the last few thousands of years, improves the preconditions for future hazard assessment at this specific site to a substantial degree. Being confronted with a rapidly increasing risk from destabilized mountain flanks due to deglaciation and permafrost degradation and newly formed meltwater lakes, many Alpine communities are asked for resolute action and the installation of an early warning system and prevention measures (e.g. Lake Oeschinen and Grindelwald Glacier; Werder *et al.*, 2010; Huggel *et al.*, 2013; Haeberli *et al.*, 2017). Where possible, potential (regional) triggers such as seismic tremors are discussed in the case studies.

In conclusion, investigating lake sediment archives may play a key role in this research field and is a main subject of this dissertation. The lacustrine basin acts as the final sink for incoming sediment and is a natural chronometer, which records both long-term environmental changes and short-term catastrophic events. Revealed in lake sediments, rock-slope failures may be deciphered in time and space. Hence, there is a high need of fieldwork-based case studies with a complementary method application on terrestrial and lacustrine sediments for a better understanding of these interactive processes. These factors were taken into account when choosing three suitable test sites for this dissertation.

1.3 Thesis Outline

This thesis is structured in 7 chapters and an Appendix with supporting figures and tables. Chapter 2 describes the three test sites of Lake Oeschinen, Lake Eibsee and Flims, with a focus on the characteristics that make them suitable for the research approach. Chapter 3 is an extensive overview of the state of knowledge, including well established concepts, as well as recent developments in the research fields of rock-slope stability and failures, lake systems, and their combination in alpine environment. A short review paper on the energy budget of rock avalanches is included here. In Chapter 4, a detailed methodology is illustrated. All ap-

plied methods are described with regards to their general function, their potential and limitations for our research approach, and the applied setup. Chapter 5 continues with the case studies, consisting of three embedded publications on Lake Oeschinen and Lake Eibsee, and the preliminary results of a paper in preparation on the Flims deposits. Chapter 6 contains the synopsis and discussion of the major outcomes of this dissertation, including the evaluation of the applied method set, as well as further research needs and suitable methods, which might be applicable in future studies on this subject. Finally, in Chapter 7, an outlook is given with future perspectives on the reaction to atmospheric warming and the contribution of the research results to the research communities and society. At the end of the document, an Appendix provides ten supporting Figures S1-S10 and five supporting Tables S1-S5.

2 Test Sites and Research Questions

Most and the largest massive rock-slope failures in the Alps detach from limestone headwalls (Abele, 1972). Thus, we aim to compare three test sites with rock-slope failures of different magnitudes, but generally similar geotechnical properties of the limestone host rock (Table 1).

Table 1: Key parameters of the test sites Lake Oeschinen, Lake Eibsee and Flims.

Test site	**Size** of rock-slope failures	**Lithology**	**Unique characteristics**
Lake Oeschinen, Bernese Alps, Switzerland	Varying between 10,000 m³ and ~40 mio. m³ (Köpfli *et al.*, 2018)	Helvetic Limestone	Rockslide-dammed lake; multiple rock-slope failures documented since lake formation, partially multistage; different types and varying volumes of rock-slope failures; historical outburst flood
Lake Eibsee, Bavarian Alps, Germany	150-200 mio. m³ (Haas *et al.*, 2014; Leith *et al.*, 2016) 300-400 mio. m³ (Jerz and Poschinger, 1995)	Wetterstein Limestone	Assumed paleolake displaced by rock avalanche, phases of lake "rebirth" revealed in modern lake; multiple detachments from Mount Zugspitze and surroundings
Flims, Grisons Alps, Switzerland	12,000 mio. m³	Triassic and Jurassic limestone, dolomite, Helvetic shale	Largest rockslide/ rock avalanche in the European Alps; rockslide-dammed paleolake displaced by rock avalanche, dam breakage; water-rich entrainment (Bonaduz gravels) and Toma type locality

2.1 Lake Oeschinen, Bernese Alps, Switzerland

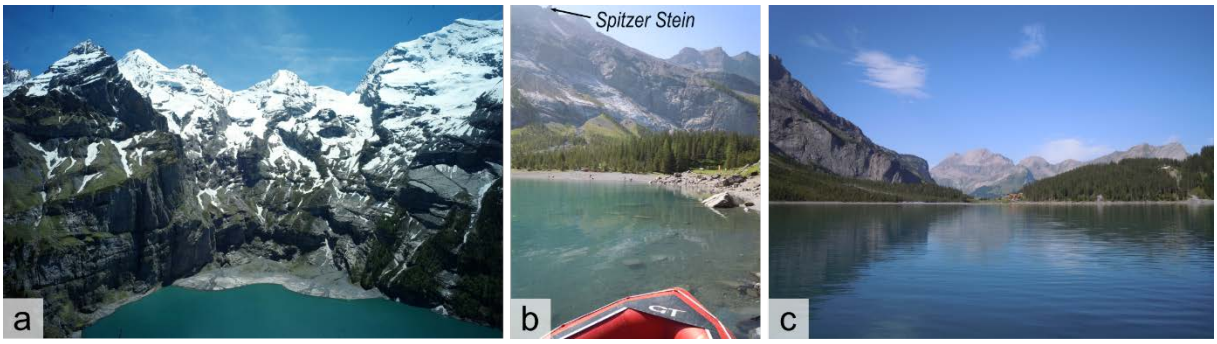

Figure 1: Impressions of Lake Oeschinen showing a) steep rock walls and melting glaciers surrounding the lake, b) scarp niches at Mount Spitzstein ("Spitzer Stein") with rockslide deposits below, and c) a western view towards the rockslide dam.

Surrounded by steep, nearly vertical slopes and several active glaciers (Figure 1a), Lake Oeschinen is situated in an area prone to rock-slope failures (Figure 1b) and related natural hazards. The lake is part of the Jungfrau-Aletsch-Bietschhorn UNESCO World Heritage Site, and is therefore of high touristic interest, so it is necessary to assess the hazard potential properly. For limnogeological research, Lake Oeschinen is an ideal place, as it is the largest naturally formed alpine lake in the northern Swiss Alps at an elevation between 1,000 and 2,000 m a.s.l. without any surficial outflows (Niklaus, 1967). Thus, any incoming sediment is recorded at the lake bottom and can be used to decipher the history of rock-slope failures impacting the lake and the related effects. It is worth noting that there is a handed down outburst flood of the lake in 1846 AD, which overtopped the rockslide dam (Figure 1c) and demonstrates the possible severity of hazards around the lake and the downstream valley of Kandersteg.

Research Questions

Deciphering Multistage Rock-Slope Failures

- How can continuous lake sedimentation contribute to a better understanding of multistage rock-slope failures?
- How accurate can the recurrence rates of repeated massive rock-slope failures be determined?
- Can the single event deposits be deciphered and how far did the rock mass(es) reach?

Effects of Impact on the Lake

- How does the impact of a rock-slope failure alter the lake and its sedimentation?

Event History

- How and when was the lake formed? Was there more than one rock-slope failure that dammed the lake to its recent size? What can we learn about the paleotopography? Can we decipher potential (regional) triggers?

2.2 Lake Eibsee, Bavarian Alps, Germany

Figure 2: Impressions of Mount Zugspitze and Lake Eibsee depicting a) Lake Eibsee at the foot of the Wetterstein Mountains, b) the scarp niche "Bayerisches Schneekar" below the summit, and c) a northwestern view of Lake Eibsee with its numerous islands containing rock-avalanche material.

The Zugspitze area is part of the Wetterstein mountains (Figure 2a) in the Bavarian Alps, Germany, near Garmisch-Partenkirchen. Situated at the edge of the Northern Calcareous Alps and consisting mainly of limestone, the area is prone to rock-slope failures at varying scales (Krautblatter *et al.*, 2012b). Especially Mount Zugspitze is affected by destabilization due to permafrost degradation (Krautblatter *et al.*, 2010; Schroeder *et al.*, 2020). The Holocene Eibsee rock avalanche detached from the scarp of the “Bayerisches Schneekar” (Figure 2b), had a volume of ~200 mio m³ and a remarkable runout of ~9-10 km (Jerz and Poschinger, 1995). The deposits reaching the village Grainau and the town of Garmisch-Partenkirchen demonstrate clearly how dangerous rock-slope failures can be in this region and that detailed hazard assessment in the close vicinity is essential. The assumed impact on a paleolake, which was presumably displaced by the rock avalanche, makes the area around Lake Eibsee (Figure 2c) a unique large-scale study site, where event phases including lake impact and interactive processes with the fine-grained lake sediments and water can be analysed. Also, the complex interaction with an obstacle in the main flow direction (Mount Zirmerskopf) after crossing the paleolake is of high research interest. Furthermore, the formation of modern day Lake Eibsee on top of the rock-avalanche deposits make it possible to combine geophysical and sedimentological methods, both on terrestrial and lacustrine sediments.

Research Questions

Deciphering Multistage Rock-Slope Failures

- Can we find evidence of multiple collapses from the rock walls around Mount Zugspitze? Can we decipher them in magnitude and frequency, and classify them accordingly?

Paleolake Eibsee

- Can we prove the existence of the assumed paleolake? Can we further reconstruct the dimensions of this paleolake? What can we learn about the paleotopography? Can we decipher phases of the lake´s “rebirth”?

Effects of Impact on the Lake

- Can we decipher interactive processes related to the impact, the entrainment of water and fines, and the collision with obstacles in a confined setting?

2.3 Flims, Grisons Alps, Switzerland

Figure 3: Impressions of the area around the Flims rockslide/rock avalanche showing a) the landscape formed by the rockslide deposits at the foot of Mount Flimserstein, b) large outcrops of the rock-avalanche deposits in the Rhein river gorge (Ruinaulta), and c) view of the Toma hill Tum`Arsa from the Tuma Tschelli.

The Flims rockslide/rock avalanche (Figure 3a) had a volume of ~8-12 km³ and is the largest rock-slope failure known in the European Alps (Poschinger *et al.*, 2006), as well as one of the largest on Earth. The deposits provide the researchers with outstanding options of analyzing the sediments due to the incision of the river Rhine (Figure 3b). The rock-slope failure started as a rockslide and transformed into a rock avalanche. For reasons of simplification, it will be here termed rockslide, only. The Flims rockslide is supposed to have impacted a paleolake (Lake Bonaduz) that was dammed by the deposits of the Tamins rockslide, which presumably occurred only short time earlier. The exceptional outcrop conditions allow for investigation of processes related to disintegration, water-rich entrainment, and transport and deposition of rock-avalanche deposits. Especially the formation of the famous Bonaduz gravel deposits and the so-called Toma (or *Tuma*; Figure 3c), i.e. rock-avalanche hills containing Helvetic rock material, are of high research interest and give insights into mobility processes of large fluidized mass flows (Calhoun and Clague, 2018). How enormous the outburst flood due to the failure of the Tamins rockslide dam was, can be shown by two clastic layers in the Upper Lake Constance, which were ascribed to the downstream influence of the Flims rockslide and should be mentioned here (Schneider *et al.*, 2004).

Research Questions

Paleolake Bonaduz

- Can we find evidence of the Tamins rockslide deposits damming Paleolake Bonaduz?

Effects of Impact on the Lake

- How did the impact of the rockslide affect the paleolake sediments and the valley infill? Can we decipher different modes of fluidized transport and ascribe them to distinct deposit types?

Event History

- Can we conclusively establish a geological timeline of event phases and related transport and sedimentation processes?

3 State of Knowledge

3.1 Rock-Slope Stability and Failure in Alpine Environment

3.1.1 Development of Rock-Slope Stability due to Atmospheric Warming

Rock slopes in high-mountainous regions are often associated with ice and permafrost, and indeed, permafrost is detected in many mountain ranges characterized by rugged topography (Gruber, 2012a; b). The long-term stability of rock slopes containing ice is defined by three primary factors: geology, topography and ice distribution/temperature (Haeberli *et al.*, 2017). The relation between permafrost degradation and rock-slope stability in cold mountains remained unclear for a long time, but as we now know, it is the ice conditions that are affected most rapidly by climate change and are therefore especially crucial (Haeberli *et al.*, 2017). Much research was done in the last two decades in order to provide concepts and models on this topic (e.g. Fischer *et al.*, 2006; Gruber and Haeberli, 2007; Krautblatter *et al.*, 2012a; Krautblatter *et al.*, 2013; Deline *et al.*, 2015b; Schroeder *et al.*, 2020; Stoll *et al.*, 2020). Laboratory tests on the stability of rock slopes with ice-filled joints show that these rock slopes already become unstable just below 0° C (e.g. Davies *et al.*, 2001; Mamot *et al.*, 2018), i.e. critical conditions can already arise before melting. Then short-term effects of e.g. heavy rainstorms, earthquakes or warm summer temperatures could be strong enough to trigger large rock/ice avalanches (Huggel *et al.*, 2010; Huggel *et al.*, 2012), which can be shown by several cases in the European Alps (e.g. Ravanel and Deline, 2011; Fischer *et al.*, 2012).

In general, permafrost distribution depends on the mean annual air-temperature, the altitude, and the incoming solar radiation, the latter of which varies widely during the year in mid-latitude mountain ranges. Here, permafrost is often distributed in complex patterns (Boeckli *et al.*, 2012; Haeberli *et al.*, 2017). Beside air-temperature and solar activity, snow cover variability is an important player concerning the evolution of permafrost in time and space at a specific site (Haberkorn *et al.*, 2015; Draebing *et al.*, 2017; Magnin *et al.*, 2017). When intact water-saturated rocks thaw, fracture toughness and tensile/compressive strength are intensely reduced. Thereby, rock-mechanical characteristics on the one hand are related to destabilizing processes that come along with high normal stresses and correspond with larger event magnitudes due to greater depths affected. On the other hand, smaller affected depths and magnitudes as well as accelerating deformation are ascribed to ice-mechanical properties (Mellor, 1973; Krautblatter *et al.*, 2013; Haeberli *et al.*, 2017). In steep mountains, permafrost degradation progresses rapidly, because the melting effect of the warming air temperatures affects a mountain in several places and can penetrate to great depths (Noetzli and Gruber, 2009). This causes heat flow anomalies, which already reach up to several tens of meters into permafrost-holding summits in Europe (e.g. Harris *et al.*, 2009; Krautblatter *et al.*, 2010; Magnin *et al.*, 2015; Ravanel *et al.*, 2017; Krautblatter *et al.*, 2018; Magnin *et al.*, 2019; Scandroglio and Krautblatter, 2020; Schroeder *et al.*, 2020). Debuttressing by glacier retreat will further decrease rock-slope stability and lead to crack propagation in exhumed bedrock (e.g. Leith *et al.*, 2014).

With global warming continuing, the presented results suggest a long-term destabilization of permafrost peaks in all regions on Earth. Thereby, the destabilization tends to increase from

lower to higher altitudes and warmer to colder rock walls (Hewitt *et al.*, 2011; Haeberli *et al.*, 2017).

3.1.2 Classification of Rock-Slope Failures Based on Movement Types

In the following, definitions are given for the most important mass movements discussed in this dissertation. The following landslide types are classified after Hungr *et al.* (2014) with respect to the original classification by Varnes (1978) and Cruden and Varnes (1996). This modified classification includes 32 landslide types and is mainly based on the type of material, mechanism of failure and type of movement. Thereby, the failure stage is key to post-failure performance, i.e. a sliding movement may transform into a flow or a fall, which consequently influences the runout and hazard potential of the mass movement. The authors propose to use the classification as a flexible system, in which the term assigned to the landslide type reflects the particular focus of the research. For example, a "debris flow" can also be termed "debris slide" or "slope deformation" if the focus is more on the pre-failure stage. In the context of the presented studies in this thesis, the most general term "landslides" is in most cases specified as "rock-slope failures". Rock-slope failures are in the first order referred to from a mechanical point of view, i.e. as failed solid rock mass, which detached from a mountain flank. Also, this term stresses the focus of the material, which is failed ice/rock mass and not soil, earth or other weak substrate. Hewitt *et al.* (2011) define "catastrophic rock slope failure" as the sudden failure and downslope movement of a large mass of intact rock. Rapid disintegration and long-runout flows with acceleration of up to 100 m/s and lengths of up to several kilometers are common. Especially in high, glaciated areas with eroded and unstable, steep rock slopes, catastrophic rock-slope failures are numerous and often show enhanced mobility.

Fall Movement

Rock/ice fall

"Detachment, fall, rolling, and bouncing of rock or ice fragments. May occur singly or in clusters, but there is little dynamic interaction between the most mobile moving fragments, which interact mainly with the substrate (path). Fragment deformation is unimportant, although fragments can break during impacts. Usually of limited volume." (type 1; Hungr *et al.*, 2014)

Important about the distinction of a "fragmental" rock fall is that single fragments move independently as rigid bodies and episodically impact the substrate (Evans and Hungr, 1993), whereas e.g. rock or debris avalanches move as a flow of masses of fragments.

Slide Movement

Rock (planar) slide

"Sliding of a mass of rock on a planar rupture surface. The surface may be stepped forward. Little or no internal deformation. The slide head may be separating from stable rock along a deep, vertical tension crack. Usually extremely rapid." (type 7; Hungr *et al.*, 2014)

Also referred to as "translational slides", some of the largest and most dangerous landslides belong to this type. Examples include the 1248 Mt. Granier rock avalanche in the Savoy Alps, which killed ~5,000 people and is regarded the deadliest landslide in European history (Cruden and Antoine, 1984; Hungr *et al.*, 2014), and the Seimareh slide in the Zagros Mountains of Iran (Roberts and Evans, 2013), with a debris volume of ~44 km³ the largest known subaerial non-

volcanic landslide on Earth. Planar rock slides usually occur at all scales in bedded and folded sedimentary as well as metamorphic and intrusive rocks. A dominant preparing factor is often the undercutting of dip slopes during erosion or excavation. Usually, the entire rock body is actively sliding.

Flow Movement

Rock/ice avalanche

"Extremely rapid, massive, flow-like motion of fragmented rock from a large rock slide or rock fall." (type 18; Hungr *et al.*, 2014)

Heim (1932) defined rock avalanches as sturzstroms with volumes > 10^6 m³. There is often a transition between rock fall or slide and rock avalanche, due to dynamic disintegration. Famous examples from the European Alps are the Flims rock avalanche in the eastern Swiss Alps (e.g. Poschinger 2006) and the Tschirgant rock avalanche in the Austrian Alps (e.g. Dufresne *et al.*, 2016b). The deadliest known single landslide event is the earthquake-triggered 1970 Huascarán rock/ice avalanche, which killed ~ 15,000 people (Plafker and Ericksen, 1978). In chapter 3.1.4, the enhanced mobility of such large rock-slope failures is described in detail.

Debris flow

"Very rapid to extremely rapid surging flow of saturated debris in a steep channel. Strong entrainment of material and water from the flow path." (type 22; Hungr *et al.*, 2014)

Debris flows ("Murgang" in German) are common hazardous phenomena in mountain areas. The term refers to periodical landslides in established channel paths, often triggered by heavy rainfalls, and with hazard potential related to a specific site/path (e.g. Dietrich and Krautblatter, 2017). Debris flows often evolve from other types, for example rock avalanches. "Debris flowslide" (type 20; Hungr *et al.*, 2014) is an alteration of this term and is reserved for failures with spontaneous or earthquake liquefaction.

Debris avalanche

"Very rapid to extremely rapid shallow flow of partially or fully saturated debris on a steep slope, without confinement in an established channel. Occurs at all scales." (type 25; Hungr *et al.*, 2014)

At a specific site, debris avalanches are usually unique events, in contrast to debris flows. Debris avalanches may enter established debris-flow paths on their way and might transform into debris flows. Clusters of debris avalanches and debris flows, which might occur during heavy rainstorms or earthquakes, belong to the most hazardous regional landslide disasters, for example the 1999 Vargas State disaster of Northern Venezuela, where ~15,000 people lost their lives (Larsen *et al.*, 2006).

Complex Types

Transformations between the presented landslide types are possible and common. Rock slides often transform into rock avalanches or can trigger further debris flows or debris avalanches (Sassa and Wang, 2005; Dufresne and Geertsema, 2020). It is therefore sometimes essential to combine two or three types when describing a case, and it is down to the researcher to find appropriate compounds for the specific case (Hungr *et al.*, 2014). Hungr and Evans (2004) for

example, describe several cases with transformations from rock slides to debris avalanches, and use the term “rock slide – debris avalanche”. In another instance, Walter *et al.* (2020) document the 2017 Piz Cengalo rock-slope collapse with ensuing debris flows.

The attempt to classify based on a maximum volume with a fixed boundary (e.g. Heim, 1932; Whalley, 1984) proved as being challenging or even problematic (Hungr *et al.*, 2014). In the German language, the terms “Felssturz” and “Bergsturz” are differentiated by the volume boundary of 10^6 m³.

3.1.3 Multistage and Progressive Rock-Slope Failures

Massive rock-slope failures can reduce rather than increase slope stability (Evans *et al.*, 2006). They produce post-failure slopes, which are prone to fail again and again, because they often result in (i) irregular slopes, which might be as steep or even steeper than the pre-failure slope, and (ii) zones of weakness due to sudden unloading, which causes slope deformation and tensional cracks to open. Such “repeated, non-random rock-slope failure along the same mountain slope” (Hermanns *et al.*, 2006) are referred to as *“multistage”* in the presented studies of this thesis.

Famous examples of multiple rock collapses from one single mountain flank can be found in all parts on Earth. First, Plafker and Ericksen (1978) interpreted an older lobe of rock avalanche deposits, which was found below the 1970 Huascarán rock avalanche (Cordillera Blanca, Peru), to be of prehistoric origin. In British Columbia, Canada, Mathews and McTaggart (1978) also detected prehistoric deposits beside the 1965 Hope rockslide, which was supported by seismic analysis by Weichert *et al.* (1994). In New Zealand two rock avalanches happened at Mt. Cook within 118 years, and at Mt. Flechter within only 88 days (McSaveney, 2002). In Taiwan, four rockslides were documented at Mt. Tsao-Ling between 1862 and 1979, three of which detached from the same slope (Hung *et al.*, 2002). In Norway, two rock avalanches occurred in in Loen in 1905 and 1936, which killed 61 and 73 people, respectively, due to the impact wave from Lake Loenvatnet, with another rockfall occurring in 1950 (Hermanns *et al.*, 2006). More recent cases are also known, for example, from the Swiss Alps, the famous Randa rockslides in 1991 detached within only 3 weeks of another (Eberhardt *et al.*, 2002), and the Piz Cengalo rock/ice avalanche in 2017 was followed by multiple debris flows within subsequent hours and days (Mergili *et al.*, 2020; Walter *et al.*, 2020).

These examples demonstrate that unless historic sources like chronicles or eyewitnesses document multiple failures from one single slope, it is hard to distinguish between single events of one series. The failure deposits interpreted as prehistoric in Huascarán or at the Hope rockslide, could neither be deciphered in time nor in space so far. In these cases, the researchers could only determine the two-event character without age determination. Only by applying geomorphological and dating methods, like cosmogenic nuclide dating (Martin *et al.*, 2014; Ivy-Ochs *et al.*, 2017; Hilger *et al.*, 2018; Von Wartburg *et al.*, 2020), a distinction between single events becomes possible. The presented studies within this thesis will even show refined recurrence rates and classification of multistage rock-slope failures at Lake Oeschinen and Lake Eibsee by using lake sediments and radiocarbon dating (chapters 5.1 and 5.3).

Progressive failure is likely to occur in the context of multistage rock-slope failures, e.g. proved by numerical modelling at Tafjord in western Norway (Hermanns *et al.*, 2006) or at Randa (Eberhardt *et al.*, 2004).

The term *"progressive"* describes the case when different parts of a failure surface reach failure at different times. If joints or pre-existing failure surfaces are pre-sent in the potential failure surface, the rock often first breaks along existing cracks/fissures, where the peak shear strength is reached before other places (e.g. Voigtländer *et al.*, 2018). The term is mostly used in relation to failure in stability and deformation analyses (Hungr *et al.*, 2014).

3.1.4 Mobility of Rock Avalanches

Large rock-slope failures tend to show a higher mobility than small ones. Thereby, the mobility increases systematically with topographic confinement, e.g. in narrow valleys (Nicoletti and Sorriso-Valvo, 1991), and with the volume of the event (Hungr *et al.*, 2014). There are several effects which control the motion of rock avalanches. The main acting forces are linked to disintegration including fragmentation, and the entrainment of water and/or soft substrate combined with fluidization and/or lubrication. All these processes alter the grain size distribution and modulate the physical properties of the flow (Pudasaini and Krautblatter, 2014; Pudasaini and Mergili, 2019). As a result, these factors define the velocity and mobility, and provide the most striking questions for the researchers.

Rock avalanches have longer runouts than can be derived from the internal angle of friction of loose debris, which is 32° (Hsü, 1975). Long runouts are ascribed to a large involved volume of rock, to a pervasive, intense fragmentation of the debris (McSaveney and Davies, 2007), and to the entrainment of material, which reduces basal friction (Aaron *et al.*, 2017; Aaron and McDougall, 2019). When grains fragment quickly during disintegration, then very high local pressures occur, and the frictional resistance to shear can be reduced (Bowman *et al.*, 2012). The rock avalanche velocity and travel distance are therefore increased. Velocities may rise to several 100 km/h (Plafker and Ericksen, 1978).

When it comes to entrainment and the affected substrate is water-saturated, the rock avalanche is likely to spread further than it would without water (Imre *et al.*, 2010). In water-saturated debris, the intergranular direct stress between the single grains is reduced by the pore-water pressure. The pore-water pressure increases with depth below the surface due to the effect of undrained loading (e.g. Hungr and Evans, 2004). Increasing pore pressure leads to fluidization at the front and enhances mobility (Abele, 1997). Fluidized lobes can travel far beyond the main deposit. The 2000 Yigong rock avalanche in Tibet, China, received worldwide attention as one of the largest non-seismic landslides in recent years, with a volume of ~100 mio. m³ (Xu *et al.*, 2012; Delaney and Evans, 2015). Very high basal pore pressure due to steam production led to much higher erosional power than expected and yielded a runout of ~10 km.

How much sediment can be entrained, depends on the momentum and impact energy of the rock mass, and on the strength and geometry of the basal surface. In order to make a statement of the properties of the substrate, one needs to know about the presence of ice or water (Pudasaini and Krautblatter, 2014). Rock avalanches involving glacier ice either as part of the moving mass or as the substrate, often show "excessive mobility", like the recent 2016 Lamplugh Glacier rock avalanche with ~10 km runout (Bessette-Kirton *et al.*, 2018), the 2012 Lituya rock/ice avalanche in Alaska with ~9 km runout (Geertsema, 2012), or the 2002 Karmadon-Kolka event in the Caucasus Mountains (Haeberli *et al.*, 2004). It is worth noting that long

runouts are also possible without water (Legros, 2006; Weidinger *et al.*, 2014) and that there is still a large need to research how entrainment changes flow behaviour.

3.1.5 Energy Considerations of Rock Avalanches

This chapter has been published in the Journal Frontiers in Earth Science under the title "Conceptual Framework of Energy Dissipation during Disintegration in Rock Avalanches" by Sibylle Knapp and Michael Krautblatter (2020).

Abstract

Rock avalanches usually progress through three consecutive phases: Detachment (Phase 1), Disintegration (Phase 2) and Flow (Phase 3). While significant advances have been achieved in modelling Rock Avalanche Phase 1 (Detachment) and Phase 3 (Flow), the crucial link between both during Phase 2 (Disintegration) is still poorly understood. Disintegration of the detached rock mass is often initiated as soon as sliding starts, and in-situ measurements are impossible due to the excessive energy release equivalent to multiple nuclear explosions. Better understanding the energy dissipation during Phase 2, and the resulting residual kinetic energy that propels the rock avalanche in Phase 3, is one of the keys to defining the mechanical properties of the avalanche in the runout zone and thus also the resisting force within the avalanche. This paper is a review of our knowledge of energy dissipation in rock avalanches with a focus on processes like friction, collision, fragmentation, comminution, entrainment and explosion during the phase of disintegration. We distinguish between energy sources and sinks and consider not only physical processes, but also chemical alterations that might occur at high temperatures. With that, we make a contribution to improve our understanding of Phase 2 "Disintegration", which is needed for accurately modelling rock avalanches and assessing their hazard potential.

Introduction

Rock avalanches are defined as "extremely rapid, massive, flow-like motion of fragmented rock from a large rock slide or rock fall" (Hungr *et al.*, 2014). Due to their high velocity, volume and runout distance, rock avalanches have a significant impact on human activities in mountain areas, can seriously damage infrastructure and settlements and can cause high numbers of casualties (Evans *et al.*, 2006; Legros, 2006; Hewitt *et al.*, 2008). Landslides resulting from large-scale rock-slope failures are especially hazardous; in the 20th century, disasters of this type have killed more than 50,000 people globally (Evans *et al.*, 2006). As a consequence of increasing population density and the development of infrastructure in mountain areas, the number of elements at risk is growing and accelerating the vulnerability to landslide hazards (Fischer, 1999; Korup, 2005; Hungr, 2006; Legros, 2006). At the same time, the number of massive rock failures from permafrost warming appears to be increasing with potentially disastrous consequences especially when causing rock-ice avalanches with high mobility (Haeberli *et al.*, 2004; Huggel, 2009; Huggel *et al.*, 2012; Krautblatter *et al.*, 2013; Krautblatter and Leith, 2015) or causing flooding after impacting lakes (Haeberli *et al.*, 2016b; Knapp *et al.*, 2018).

Better understanding the disintegration (Phase 2; Figure 4) is key to defining mechanical properties like grain size composition and content of large blocks in the runout zone and therefore

the hazard potential of rock avalanches. Current approaches based on Mohr-Coulomb friction models adequately describe the detachment processes (Phase 1; Figure 4) and its energy dissipation (Maddock, 1986) or the rock avalanche flow (Phase 3; Figure 4) utilizing fluid (Bingham) or snow avalanche (Voellmy) analogues with adequate parameterisation (Hungr, 2006; Christen *et al.*, 2010; Preuth *et al.*, 2010; Pudasaini and Krautblatter, 2014; Pudasaini and Mergili, 2019). For Phase 2, some models on dynamic fragmentation were just developed (e.g. Zhao *et al.*, 2017; Ghaffari *et al.*, 2019), whereas other disintegration processes, e.g. heat transfer and phase transitions still represent major research gaps. This situation is mainly related to insufficient understanding of energy dissipation during Phase 2, and the resulting residual kinetic energy that propels the ensuing rock avalanche (Phase 3). The material properties of the avalanche result from these energetic processes and from the material being overrun. Only by understanding disintegration, will more precise modelling of rock avalanches and their hazard potential be possible. In this paper, we are going to primarily concentrate on the intrinsic properties of rock avalanches that influence disintegration, and we are going to focus on disintegration and energy dissipation in Phase 2, that is directly after the detachment.

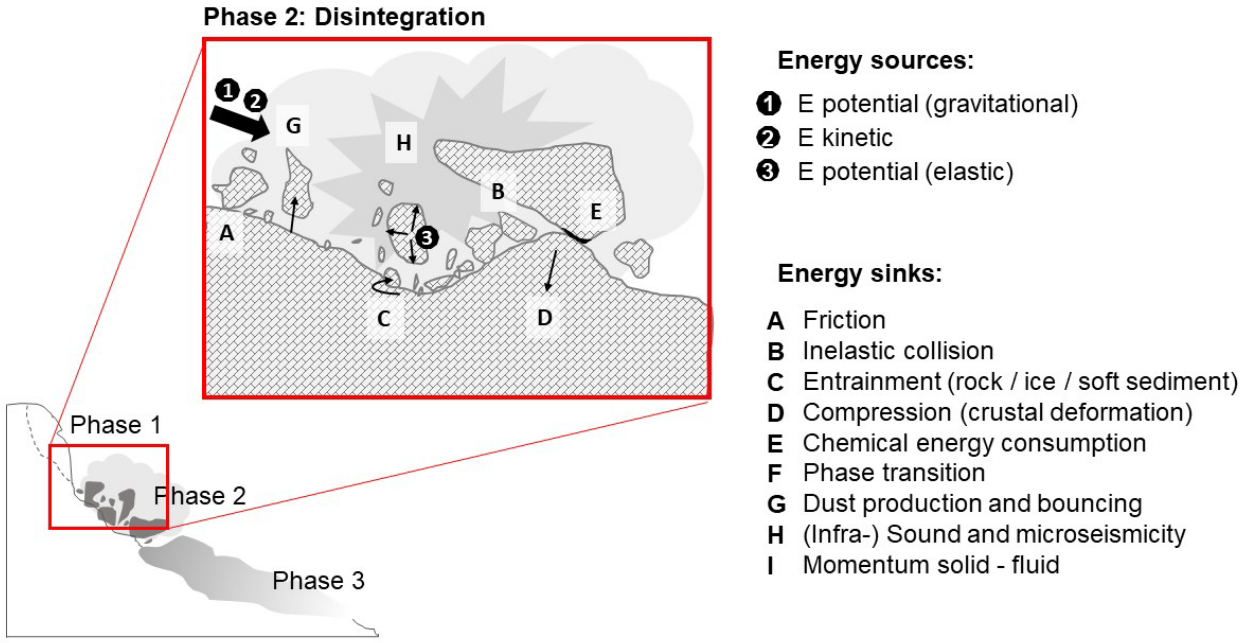

Figure 4: Energy dissipation in Rock Avalanche Phase 2 (Disintegration). The primary energy input to the system is mostly derived from the potential/kinetic energy of the moving rock mass ("Energy sources"). "Energy sinks" cover different types of energy transformation, the majority of which involve heating. (A) Friction. (B) Inelastic collision: breaking at bonds stretching and friction. (C) Entrainment: ploughing, scouring. (D) Compression: crustal deformation. (E) Chemical energy consumption: e.g. mineral transformation. (F) Phase transition: solid – fluid – gas, needs latent energy. (G) Dust production and bouncing. (H) Sound and microseismicity. (I) Momentum exchange between solid and fluid phase: energy dissipates to shock wave. The sediment record theoretically shows transitions linked to (A)-(F). (F) and (I) may be present, but cannot be illustrated in the figure. Small arrows indicate direction of energy transfer.

Energy dissipation during disintegration

Disintegration processes

Large rock-slope failures usually undergo different stages of downhill movement which may occur consecutively (Abele, 1974): i) The rock mass moves as a coherent block, and translational shearing occurs along the contact of the bottom of the rock avalanche and the ground

surface. ii) Subsequently, differential movement of individual blocks initiates crushing of the original rock mass. iii) If the coherent rock mass loses its internal cohesion and disintegrates intensely (shattering) it can evolve into a rapid granular flow (Pollet and Schneider, 2004), which is defined as the distributed shear motion of a group of clasts where individual grains interact with each other and with the boundaries of the moving flow (Dufresne and Davies, 2009). The result can be a highly fragmented (pulverized) rock mass which consists of angular grains of all sizes down to < 1 micrometre (Figure 5A-D; e.g. Davies and McSaveney, 2012).

To decipher individual processes during disintegration, two types of disintegration can be distinguished: (i*) static disintegration*, a collision-free process driven mainly by gravity, and (ii) *dynamic disintegration,* referring to particle comminution by grain-to-grain collisions driven by motion. Disintegration refers to fracturing by rapid changes in stress coupled with sudden (un-)loading caused by bending, transverse shearing or delamination of the rock mass creating large blocks, thin vertical slabs or, horizontal sheets, respectively (Erismann and Abele, 2001). Static disintegration is an essential precursor for dynamic disintegration as it creates fractures along which further relative shearing and fragmentation can occur. Shearing along predefined bedding and foliation planes induces shear crushing and the creation of a granular layer.

Energy sources and sinks

Energy dissipation in rock avalanches occurs by transformation of the total energy into thermal energy, acoustic energy or inelastic deformation energy (Nicoletti and Sorriso-Valvo, 1991), where due to the law of energy conservation, the final energy available for mechanical work is less than the initial amount. The energy release is often in the range of dozens to more than a thousand Hiroshima bombs (~15 kt TNT or 63 TJ each) for large rock avalanches. Recent work also emphasizes the energy transfer into chemical reactions and phase transitions (Anders *et al.*, 2010; Mitchell *et al.*, 2015). Energy “release” and “consumption” describe the transfer of energy into a different form. Energy in rock avalanches is released by friction, collision and fracturing. Far from a continuous process, energy release is concentrated at points of impact with the ground surface and obstacles where major friction and disintegration of the rock mass is initiated (Erismann and Abele, 2001).

Field conditions constraining energy dissipation can be derived from i) paleotopography (Nicoletti and Sorriso-Valvo, 1991), ii) compressive and extensional flow structures in the rock-avalanche deposits (Hewitt, 2006; Dufresne and Davies, 2009; Dufresne *et al.*, 2015), iii) positions inside the flow recording differences between intact rock and major shear zones (Pollet *et al.*, 2005), iv) the sedimentological record (Yarnold, 1993; Weidinger *et al.*, 2014) with v) fine-sediment signatures (Reznichenko *et al.*, 2012), and vi) melting mineral formation (Weidinger and Korup, 2009). Referring to i), Nicoletti and Sorriso-Valvo (1991) differentiate dissipation types and rates dependent on geomorphic controls along the runout path: The low-energy dissipative type refers to rock avalanches which are, for example, channelized in narrow valleys. Here, little potential energy is dissipated to other processes than kinetic energy, and mobility is enhanced. The moderate-energy dissipative type refers to radial spreading “free from lateral constraints”, resulting in moderate mobility. Finally, the high-energy dissipative type describes running across a narrow valley and impacting against the opposite, at best perpendicular slope, which results in low mobility. Here, most initial energy is dissipated to energy sinks, and only little is left for the transfer into kinetic energy.

During disintegration, ~20-50 % of the potential energy is consumed (Locat *et al.*, 2006; Haug *et al.*, 2016). Considering multiple energy sinks in Figure 4, A-D (friction, inelastic collision, entrainment, crustal deformation) cause heating to some degree, E-F (chemical energy consumption, phase transition) require latent energy for phase transitions, and G-I (dust production and bouncing, sound and microseismicity, momentum exchange) act to export energy outside the impact/disintegration zone. The relative importance of D, G, H and I (compression, dust production and bouncing, sound and microseismicity, and momentum exchange) has yet to be determined, but Erismann and Abele (2001) assumed that they are of minor importance. If A-C (friction, inelastic collision and entrainment) have a major share in the energy dissipation and cause a mean frictional shear resistance whereas E-F (chemical energy consumption, phase transformation and dust production) consume energy for phase transitions, the rate of frictional heat generation per unit area Q is

$$\dot{Q} = \tau v - \phi = \mu_k \sigma_n v - \phi$$

where $\boldsymbol{\tau}$ is the average frictional shear resistance, v is the average velocity, $\boldsymbol{\phi}$ is the heat sink-rate due to latent heat, μ_k is the kinetic coefficient of friction and σ_n is the normal stress across the sliding plane (Maddock, 1986). Effective latent heat sinks could be from decarbonation of dolomite and calcite in sedimentary rock failures (Mitchell *et al.*, 2015) or from phase transitions of water during melting and vaporisation (De Blasio and Medici, 2017). The heat flow away from a source (e.g. a sliding plane) can be calculated by 1D-heat diffusion (Carslaw and Jaeger, 1959; Mitchell *et al.*, 2015), where the temperature increase ΔT within the observed slip zone is

$$\Delta T(x,t) = \frac{1}{2\rho c\sqrt{\kappa\pi}} \int_0^t \frac{\tau(t')v(t') - \phi(t')}{\sqrt{t-t'}} e^{\frac{-x^2}{4\kappa(t-t')}} dt'$$

where x is the distance from the slip zone, t is time, ρ is mass density, $\boldsymbol{\kappa}$ is thermal diffusivity, c is heat capacity.

Physical processes

Fragmentation / Collision / Comminution

Fragmentation describes the initiation and propagation of fractures and breaking apart and movement of grains (Turcotte, 1997). The related process energy is both linked to the length of the crack extension within existing grains (microcracking) and to the surface energy of the new created grains during comminution (Bieniawski, 1967; Hamdi *et al.*, 2008). Fragmentation occurs as a *static* (Eberhardt *et al.*, 2004; Wang *et al.*, 2011; Zhang, 2016) or *dynamic* process (Pollet and Schneider, 2004; Crosta *et al.*, 2007; Imre *et al.*, 2010; Zhang *et al.*, 2019). *Static fracture* occurs before any collision triggers the disintegration of a mass, whereas *dynamic fragmentation* shows more intense disintegration, e.g. in shear zones at the base of rock avalanches.

Grains fragment quickly under high local pressures and, thus, general intergranular effective stress and the frictional resistance to shear are reduced (Bowman *et al.*, 2012). In laboratory experiments, the overburden strain-rate is directly related to the fragmentation process. If load is applied sufficiently quickly, particles will dynamically fragment and the kinetic energy of the resulting fragments will cause collisions with surrounding particles. Under dynamic dis-

integration, kinetic energy is dispersed through the system as colliding particles undergo further fragmentation (Rait and Bowman, 2010). The higher the spatial concentration of simultaneously-fragmenting grains, the lower the effective direct stress on the grain flow (Davies and McSaveney, 2009b). Thereby, the basal sliding friction dissipates upwards and laterally through the mass, which causes the slabs at the bottom to come to rest first. Thus, slabs higher in the moving mass travel further than the ones lower down (Erismann and Abele, 2001; Pollet and Schneider, 2004). Grain-to-grain collisions require an unconfined environment, in which particles can move freely. In such a case the highest levels of friction, crushing and collision occur in the lower part of a rock avalanche due to high compressing forces and large differences in velocity between the moving particles and the ground (Erismann and Abele, 2001). Running on dry rock substrates, it is mainly fragmentation that leads to an increased travel length of the rock avalanche (Pollet and Schneider, 2004; McSaveney and Davies, 2007; Davies and McSaveney, 2009b). After Haug *et al.* (2016), increased fragmentation mostly affects the front of a rock avalanche travelling further, whereas the center of mass crucial for energy considerations, is hardly displaced or decelerates. In comparison to previous papers stating that fragmentation accelerates the flow (Bowman *et al.*, 2012; Langlois *et al.*, 2015), Haug *et al.* (2016) confirmed that high fragmentation rather favours a more energy-efficient transport mode yielding longer runouts without acceleration.

In either case, fragmentation is considered an 'energy sink' (Locat *et al.*, 2006; Crosta *et al.*, 2007; Haug *et al.*, 2016). Haug *et al.* (2016) propose that static fragmentation may use up to 50% of the potential energy. Also, Ghaffari *et al.* (2019) postulate that the kinetic energy is only a small portion of dissipated energy during fragmentation, and the energy rather transfers into intergranular collision and friction. Thereby, it is important to note that the energy input for grain-internal 'micro-cracking' weighs far more than for 'macro-fragmentation', i.e. the formation of new grains (Ouchterlony *et al.*, 2004; Hamdi *et al.*, 2008). Zhao *et al.* (2017) quantify the energy dissipation by friction and plastic deformation to ~ 90 %, and the energy needed by bond breakage to < 5 %. Plus, the smaller the grain size becomes, the more energy is needed for comminution (Locat *et al.*, 2006). The process of dynamic rock pulverization (Figure 5A-D) consumes massive amounts of energy, e.g. in gouge formation it sums up to 50% of earthquake energy (Wilson *et al.*, 2005). During grinding, most energy (~ 97 %) is converted to heat, with only a small portion (< 1 %) actually contributing to fracturing (Spray, 1992).

Friction / Heat

Near the base of the moving rock mass, confining forces are largest and so the majority of frictional energy dissipation occurs in this zone (Pollet and Schneider, 2004). Disintegration and heating of the rock mass mainly arise (i) along well-defined persistent shear planes, or (ii) as a total disintegration of the whole mass. Shearing may be localized to a thin, discrete layer and frictional heating of bedrock may reduce basal strength (Hu *et al.*, 2018; Hu and McSaveney, 2018; Hu *et al.*, 2019). For (i), a high proportion of the energy release is focused on only a small proportion of the whole mass and will cause significant heating up to a partial melting of clasts, called *frictionite* (Heuberger *et al.*, 1984; Erismann and Abele, 2001).

Figure 5: Examples of energy-related features in deposits of the Flims Rock Avalanche (Switzerland): (A) Shattering into cube-like, sharp-angled fragments of different size (cm-dm) in dark grey Helvetic limestone, secondar-ily cemented with white matrix of rock powder. (B) 'Snapshot' of pulverization with multiple grain-internal layers of micro-shearing. (C) and (D) Grinding within a shear zone. (E) Entrained lump of lake sediment in the Bonaduz gravel deposits. (F) Vertical Pavoni pipes indicate rapid water discharge after deposition (person for scale).

As soon as particles are ~1 micron and below, the amount of heat produced by their elastic and plastic deformation leads to their melting (Spray, 2005). In rare cases (i) this heating can cause centimetre-thick melting of rock and formation of frictionites at temperatures of 1700

°C (Erismann *et al.*, 1977; Weidinger *et al.*, 2014). Discrete layers of more intense fragmentation contain *micro-breccias* and traces of partial melting (frictionite along shear planes; Schramm *et al.*, 1998; Weidinger and Korup, 2009). For phase transitions, latent energy is absorbed. Besides, frictional shearing is controlled by the production and decay of random kinetic energy during gravitational work (Preuth *et al.*, 2010). Random kinetic energy is referred to the random motion and inelastic interaction between the fragments; it is irreversible because it cannot perform mechanical work (Bartelt *et al.*, 2006; Buser and Bartelt, 2009; Christen *et al.*, 2010). For quantification, Schneider *et al.* (2010) argue that the total frictional work best correlates with the seismic signal of a rock (-ice) avalanche. The seismograph represents a small, but proportional fraction of this energy loss.

Erosion / Entrainment / Role of Water

There is an apparent increase in rock-avalanche mobility with volume (e.g. Heim, 1932; Scheidegger, 1973). The volume can be increased either by fragmentation up to 25-30 % (Hungr and Evans, 2004; Crosta *et al.*, 2007) or by the entrainment of substrate material. How enormous the effect of entrainment is, can be shown by the 2000 Tsing Shan event (Hong Kong), where a small volume of 150 m^3 of material grew to 1620 m^3 because of the strong erosion along the slope. Entrainment strongly depends on the character of the path material (Hungr and Evans, 2004; Crosta *et al.*, 2009; Aaron and McDougall, 2019) and, for example, may cause high basal shear resistance and momentum loss, when overrunning bedrock or dry bed material (Iverson *et al.*, 2011; Aaron *et al.*, 2017; Whittall *et al.*, 2017; Aaron and McDougall, 2019). In other cases, basal friction is reduced and mobility enhanced (Hungr and Evans, 2004; Aaron and Hungr, 2016; Coe *et al.*, 2016). On the one hand, entrainment is an energy sink because the erosion, uptake and incorporation of material along the travel path by ploughing, scouring or even surficial scratching (Hu and McSaveney, 2018) is mechanical work, accompanied by heating. On the other hand, the gain in weight increases the energy budget by acting as an energy source and must not be neglected. Water plays an important role for the amount and rate of entrainment and erosion (Iverson and Ouyang, 2015). Especially for rock avalanches travelling on ice (Huggel *et al.*, 2008; Deline *et al.*, 2015a; Bessette-Kirton *et al.*, 2018; Walter *et al.*, 2020) or wet, soft sediments (e.g. lake sediments, Figure 5E), the increased pore pressure enhances the scour of the bed, reduces basal friction and causes velocity, mass and momentum to increase (Iverson *et al.*, 2011; Iverson, 2016; Johnson *et al.*, 2016). Pure ice has a basal friction which is about 75 % lower than that of pure rock. Hence, in rock-ice avalanches, a ~12.5 % reduction of basal friction angle is observed for every 10 % increase in ice content (Sosio *et al.*, 2012). The intergranular direct stress between single grains is reduced by pore-water pressure, i.e. in initially wet sediment more overburden is necessary to start fragmentation than in dry sediment (Abele, 1997). Water may escape quickly after deposition like at the Flims Rock Avalanche (Figure 5F; Pavoni, 1968b; Calhoun and Clague, 2018) but increasing temperature may cause water to be pressurized (Voight and Faust, 1982) and / or vaporized, as it is proposed for the Vajont Rockslide (Habib, 1975) or the Köfels Rockslide (De Blasio and Medici, 2017). For the melting of ice, a specific latent heat of 334 kJ/kg is needed, and for vaporization ~2265 kJ/kg, which is almost 7 times as much. There is a momentum exchange that consumes energy (Pudasaini and Krautblatter, 2014), and

steam explosions are present, but probably camouflaged in the other energy dissipative processes. We have yet to understand the sedimentological imprint of steam explosions in the sediments.

Chemical processes

Chemical processes are often neglected in the energy balance of rock avalanches. Novel friction experiments on carbonate rocks, for example, show that at velocities of several meters per second carbon dioxide starts to degas due to thermal decomposition induced by flash heating after only a few hundred microns of slip (Mitchell *et al.*, 2015). This process creates vesicular degassing rims in dolomite clasts and crystalline calcite cement (Anders *et al.*, 2010; Mitchell *et al.*, 2015) and may allow the upper rock mass to slide over a 'cushion' of pressurized material. Around 800-850°C, talc and dolomite start to decompose (Hu *et al.*, 2018) and to produce high-pressure live steam and carbon dioxide (Habib, 1975; Hu *et al.*, 2019). De Blasio and Medici (2017) found bubbles grown in the frictionites of the Köfels Rockslide, which they ascribe to water vapor, either due to seeping of vadose water through rock fissures prior to the rock-slope failure, or due to dehydroxylation of the mica, which occurs at ~ 700°C (Alexiades and Jackson, 1967). Also, the existence and relative increase of pyrophyllite on sliding surfaces indicate hydrothermal alteration around 450 °C (Schäbitz *et al.*, 2015). The accumulation of pyrophyllite at the sliding surface results in reduced shear strength. Also, graphitization (crystallization of amorphous carbon) was recognized in slip zones as phase transformation, which implies frictional heating due to rapid sliding (Oohashi *et al.*, 2011). Graphite is well known as an effective solid lubricant in fault zones with a friction coefficient as low as that of smectite, $\mu = 0.1$ (Oohashi *et al.*, 2014).

Discussion of research needs

Processes during the disintegration phases of rock avalanches are beyond observation, and we have very few analogues that show pressure and temperature conditions inside rock avalanches. Thus, it is likely that we neglect important processes such as steam explosions, partial melting, chemical transitions and material explosion processes at high pressures.

To systematically decipher relevant processes in rock avalanches, we propose that the energy balance needs to be considered more seriously, since it will help us to reveal energy-relevant processes that we would otherwise neglect. Here we propose to balance the primary energy input to the system constrained by the potential/kinetic energy of the moving rock masses ("Energy sources"). "Energy sinks" include heating, friction, inelastic collision, entrainment, compression during crustal deformation, chemical energy consumption, phase transition solid - fluid – gas, dust production and bouncing as well as sound and microseismicity, and momentum exchange between solid and fluid.

Using an energy balance approach, we can attribute proportions of the energy transmission to certain processes and we can rule out others. However, for this approach, we have to find ways to accurately constrain the 3D deposition temperature of the rock avalanche by new methods as has been exemplified in a few cases in this paper. The influence of the substrate on types and rates of energy dissipation during disintegration and during the flow represent major research gaps and ask for more studies. For the hazard assessment of rock avalanches, it makes sense not only to differentiate between energy sources and sinks, but also to sepa-

rate processes that favour mobility and runout length from those which may consume or release energy but do not essentially contribute to the hazard potential. Furthermore, we need to transfer the achievements gained in qualitative assessment towards a more quantitative approach.

Future research in the field should focus on analysing spatial patterns of disintegration using surface mapping and 3D subsurface reconnaissance of rock slide/avalanche deposits using geophysical methods at varying scales. Sedimentological analyses reveal abundant information on internal processes, for instance high-stress comminution preserved in fine-sediment signatures (Reznichenko *et al.*, 2012). There is a great demand for study cases with petrographic analysis at microscopic scale (Weidinger *et al.*, 2014), and for such with cross sections through the debris (Locat *et al.*, 2006).

Future research in the laboratory should focus on the implementation of disintegration scenarios in large-scale analogue models to help better understand the impact of disintegration and heating on runout length. This way, a conceptual physical (and chemical) model of rock-avalanche disintegration in time and space may be set up in a first step, followed by the implementation in benchmark one- and two-phase runout models.

Conclusions

1. Due to the law of energy conservation we have a superior tool to decipher processes we have yet neglected in rock avalanches: heating, friction, inelastic collision, entrainment, compression crustal deformation, chemical energy consumption, phase transformation solid - fluid – gas, dust production and bouncing as well as sound and microseismicity generation and momentum exchange.
2. Energy dissipation is concentrated in the disintegration zone where energy estimations indicate considerable heating above 100°C of significant portions of the rock mass.
3. The spatial pattern of heating is characteristic for individual types of movement ranging from concentrated heating by friction along defined sliding planes to diffuse clustered heating in crushing zones near to obstacles.
4. Massive entrainment where large rockslides drive into, or override, valley sediments also evidently causes crushing and very likely significant heating.
5. Massive energy dissipation may leave a distinct sedimentological signal detectable in compressive and extensional flow structures, melting or new mineral formation, rock-avalanche structure, material composition, brecciation and fine-sediment signature.

Acknowledgments

The authors want to thank Dr. Andreas von Poschinger (Bavarian Environmental Agency, Germany), Prof. John Clague (Simon Fraser University, British Columbia, Canada) and Dr. Anja Dufresne (RWTH Aachen, Germany) for longtime and intense discussions on rock avalanches in general, and the Flims Rock Avalanche and Tschirgant Rock Avalanche in particular. We also acknowledge the contributions by three reviewers that helped to improve this manuscript.

3.2 Lake Sediment Archives

3.2.1 Potential of Lake Sediments

Lake sediments provide researchers with archives of earth and ecosystem history that are highly resolved in time and of long duration. Thus, at best, it is possible to decipher annual events and environmental changes over the whole life cycle of a lake, for example over Lake Tanganyika´s 10-million-year history (Central Africa, e.g. Rosendahl *et al.*, 1986; Cohen, 2003; O'Reilly *et al.*, 2003; Tierney *et al.*, 2010). What makes lakes such ideal archives, are (i) the special properties of their depositional environment that turn lakes into a final sediment sink and chronometer, (ii) the enormous range of questions that can be examined with lake sediments, and (iii) the numerous sampling techniques for the retrieval of the rather easily accessible, unconsolidated sediments (Cohen, 2003; Ariztegui and Wildi, 2013; Gilli *et al.*, 2013).

Thus it is not surprising that paleolimnologists work with lake sediments in all regions on Earth in order to constrain the timing of past climate change (e.g. Hajdas *et al.*, 1993; Brauer *et al.*, 1999; Amann *et al.*, 2014; Amann *et al.*, 2015), flood frequencies (e.g. Arnaud *et al.*, 2005; Bøe *et al.*, 2006; Wolfe *et al.*, 2006; Glur *et al.*, 2013; Wirth *et al.*, 2013), anthropogenic impact (e.g. Blegen *et al.*, 2015; Süfke *et al.*, 2019), and changes in sea and lake levels (e.g. Van Daele *et al.*, 2011).

Lakes also enjoy a high reputation for studying seismic tremors. Lakes situated close to active faults are sensitive recorders of seismic activity (Howarth *et al.*, 2012; Moernaut *et al.*, 2014) and thus contribute to a qualitative and quantitative earthquake assessment in a specific region (Monecke *et al.*, 2006; Strasser *et al.*, 2013; Kremer *et al.*, 2017; Praet *et al.*, 2017; Van Daele *et al.*, 2020).

In the studies presented in this thesis, an alternative approach is applied. The lake sediments of Lake Oeschinen and Lake Eibsee are used to date and reconstruct the rock-slope history in the catchment area, as well as decipher the spatial extent of the distinct deposits, which is especially valuable for identifying multistage rock-slope failures.

3.2.2 Lake Sedimentation Processes

Sediments in a lake system are characterized on the basis of (i) their origin and genesis, (ii) climatic conditions, (iii) transport mechanisms, and (iv) processes within the lake, just to name the most important factors (Glew *et al.*, 2002). Consequently, lake sediments vary widely in density and consistency. According to Sturm (1979), five different sources of sediment can be deciphered, each of which supplies suspended matter to the lake basin: (i) *River sediment,* respectively all kinds of subaerial runoff, (ii) *Aerial sediment,* respectively all kinds of dust particles, (iii) *Autochthonous sediment,* i.e. (bio-) chemically produced within the water column, (iv) *(Re-)Suspended sediment,* i.e. through processes like bioturbation, degassing and bottom currents, and (v) *Upwelling sediment,* i.e. through groundwater flow or subaqueous springs. In the following, the sources and processes that are most important in the presented studies at Lake Oeschinen and Lake Eibsee, are described in detail.

River Input / Subaerial Runoff

River tributaries supply the lake with suspended matter. Differences in density occur due to gradients of temperature, salt concentration and the amount of supplied suspended matter.

This supply may follow a seasonal and/or discontinuous pattern, and may favour, combined with a stratification of the lake, the formation of laminated sediments. In this case, varves can be formed. The term “varve” is of Swedish origin and was first introduced by De Geer (1912). It is defined as a rhythmic sequence that represents the deposition of sediments or growth of a precipitate over one single year. Clastic varves and nonglacial organic or biogenic varves need to be distinguished (Zolitschka *et al.*, 2015). In proglacial and periglacial environments, clastic varves predominate (e.g. Amann *et al.*, 2014; Boes *et al.*, 2018) and show a high influence of intense physical weathering and sparse vegetation in the catchment. Clastic varves contain a clayey winter unit, which represents the slow setting of suspended matter, and a silty to sandy summer unit, which is highly influenced by glacial melting (Mörner, 2014).

It is worth noting that subaerial mass movements in the catchment, like debris flows, also alter the sediment supply and related elemental concentrations in the water (e.g. Kiefer *et al.*, 2020).

Aerial Sediment

Dust particles can be transported by air over huge distances. Lake surfaces may trap these sediments, which in most cases are of clay to silt size. Settling down through the water column, they may build distinct, slightly graded layers, which can be distinguished from the (autochthounuos) background sediment. Examples of dust particles captured in lake sediments are (i) volcanic tephra layers, which may be used for setting up chronologies (e.g. Hajdas *et al.*, 1993; Blegen *et al.*, 2015; Moernaut *et al.*, 2019), (ii) pollen, often used for climate reconstruction (e.g. Wick *et al.*, 2003; Peyron *et al.*, 2005), and (iii) dust particles derived from rock-slope failures, e.g. rock-avalanche dust from the Flims rockslide (Deplazes *et al.*, 2007).

Resuspension and Redeposition

As soon as the bottom shear stress exceeds the critical state for the sediment, the deposits are resuspended. Thereby, the mechanical properties of the respective lake sediment, for example grain size and pore volume, determine critical shear stress. For resuspension, the forces of gravity and cohesion need to be overcome. The periodical mixing process in stratified lakes involves the whole water column and leads to resuspension at the water-sediment-interface (Bloesch 1995). The morphology of the lake basin and the surroundings, the exposure to wind, and the river input are important factors, which influence the degree of disturbance in the water column and therefore determine sediment resuspension (Wetzel, 2001). Hence, shallow deposits are more easily affected by (wind-driven) waves compared to sediments in the deeper parts of the basin.

Turbidity Currents

Turbidity currents are a type of sediment gravity flow, in which suspensions flow along the bottom of a standing water body (Hsü and Kelts, 1985). These suspensions show differences in concentrations of salts and materials, and thus occur as overflows, interflows and underflows – depending on the density difference between suspension and lake water (Sturm and Matter, 1978; Middleton, 1993). During the flow, bed friction causes an overhanging lobe at the front with turbulent mixing at the back of the head (Middleton, 1993). High-density turbidity currents deposit thick, graded sand layers and are usually linked to catastrophic events like floods, earthquakes or subaerial landslides. These impact the water body and supply high amounts of terrestrial sediment. Overflows and interflows, however, have lower densities,

usually occur seasonally during periods of high river discharge and transport fine-grained sediment, which settles down continuously during summer thermal stratification.

Deposits from turbidity currents, turbidites, are common in lacustrine and marine realms and are of high research interest due to their material content, amount and grain size distribution, as well as their distribution in the water basin and their stratigraphic position (e.g. Wynn and Masson, 2003; Girardclos *et al.*, 2007; Moernaut *et al.*, 2014; Vandekerkhove *et al.*, 2020).

Methanogenesis

Organic matter is either transported to the lake from terrestrial sources (allochthounous) or produced in the water column (autochthonous). Due to low redox conditions in the water column and the surface sediment, some of the buried organic matter degrades through methanogenesis (Wetzel, 2001). Anaerobic bacteria and methane-producing bacteria convert acetate into carbon dioxide and methane, as well as reducing carbon dioxide to methane. These degassing processes lead to turbation of overlying sediments and strongly influence reflection seismology (Vanneste *et al.*, 2001).

3.2.3 Development of Lakes in Deglaciating Alpine Areas

Glacial ice is one of the most important agents in cold, alpine environments. In most high-mountainous regions on Earth, mountain glaciers are shrinking rapidly due to atmospheric warming (Kaser *et al.*, 2006; Zemp, 2008; Gardner *et al.*, 2013). For example, in the European Alps, the glaciers are decreasing in volume by ~2-3 % per year (Haeberli *et al.*, 2007). From modelling there is evidence that many mountain ranges are likely to lose their glacier cover within the next decades (Zemp *et al.*, 2006; Radić *et al.*, 2014) and will develop into new alpine landscapes characterized by bare bedrock, loose debris, stinted vegetation and newly formed lakes. Glacial ice-scour lakes emerge in over-deepened glacier beds, which become exposed as the glacier retreats (e.g. Farinotti *et al.*, 2009). The water is then held in cirque depressions with steep rock walls by a rock lip or moraine deposits (e.g. Clague and Evans, 2000; Hubbard *et al.*, 2005; Werder *et al.*, 2010). These new landscapes will show a strong disequilibrium for a long time, mainly affecting the evolution of the ecosystem, the erosion-sedimentation-cycle and slope stability (Haeberli *et al.*, 2017). Based on quantitative approaches for the Swiss Alps, the future lakes built after deglaciation in the entire Alps will contain about a few km³ volume, i.e. a few percent of the presently remaining glacier volume (Haeberli and Linsbauer, 2013). Many of these lakes – not only in the European Alps but also in other cold mountain areas – will likely form right at the foot of steep rock walls, which are being destabilized by degrading permafrost and de-buttressing by glacier retreat (Oppikofer *et al.*, 2008; Haeberli *et al.*, 2017). Hence, the hazard conditions will fundamentally change in regions of glacier retreat/disappearance and it is therefore necessary to model potential future lake outbursts (Frey *et al.*, 2010).

3.3 Alpine Rock-Slope Failures and Lakes – Secondary Effects and Hazards

The most important secondary effects of rock-slope failures and lakes in alpine environment include the formation and failure of rockslide dams and impact waves of landslides which enter these lake basins. Important for the hazard assessment are the damming potential of a

future rock-slope failure dependent on the valley geometry and runout direction of the landslide (Hermanns *et al.*, 2011), the size of the dam, and the possible size of the dammed lake. Further, the outburst hazard and the downstream risk include the potentially new damming and lake formation after the first dam breakage, like in the case of the Tangjiawan landslide after the 2008 Wenchuan earthquake, Sichuan, China (Fan *et al.*, 2018).

3.3.1 Formation and Failure of Dams

As outlined above, new lakes form due to the immense erosional and depositional influence of glacier retreat on the geomorphology. However, spontaneous mass movements may also lead to a damming of valleys and cirques with material of rock, ice or any other substrate. Rockslide dams are formed in bedrock landscapes as a result of landslides blocking drainage, thus they are natural dams (Evans *et al.*, 2011). Often, lakes created by such dams only persist for a short time because the unconsolidated deposits are quickly eroded by the outflows of the lake. The Dadu River in Sichuan, China, for example, was dammed by an earthquake-triggered rockslide in 1786 (Dai *et al.*, 2005). The dam breached after only 10 days, killed 100,000 people downstream, and is still the most destructive single-event landslide disaster in history.

If the dam is large enough and contains sufficient non- or semipermeable material, the lake can become permanent. Consequently, the whole flow regime in the closer environment is subject to change (Wetzel, 2001). Lake Sarez, Tajikistan, was formed in 1911 by the earthquake-triggered Usoi rockslide (Schuster and Alford, 2004), and is presently the largest landslide-dammed lake on Earth, with a volume of 17 km³ (Evans *et al.*, 2011). As the examples demonstrate, these dammed lakes are not restricted to deglaciating areas, but are common in all mountainous regions, and are often linked to earthquake-triggered rock-slope failures and landslides. Therefore, they are sometimes referred to as “Quake Lakes” and are formed in high numbers after major earthquakes. After the 2008 M7.9 Wenchuan Earthquake in Sichuan, China, for example, about 200 “quake lakes” were dammed by landslides. (Evans *et al.*, 2011)

The outburst hazard potential of a rockslide-dammed lake mainly depends on the stability of the dam. Many rockslide dams do not fail at once, but rather gradually degrade as soon as the dammed lake has run full and the dam is overtopped (Hermanns *et al.*, 2011). In the worst case, the whole volume of the stored water drains after a dam breakage (e.g. Hermanns *et al.*, 2004). If they breach suddenly, for example triggered by another rock-slope failure impacting the lake, catastrophic flooding may devastate downstream valleys. Thus, formation and failure of dams resulting in massive outburst floods are to be taken into account when assessing the hazard potential of rock-slope failures (Evans *et al.*, 2011).

3.3.2 Lake Impact – Triggering Waves, Outburst Floods and Fluidized Mass Flows

The newly forming lakes in deglaciating areas (chapter 3.2.3), in addition to existing alpine lakes, may on the one hand be attractive for tourism and hydropower generation, but can also represent a major hazard for humans and infrastructure (Frey *et al.*, 2010; Schaub *et al.*, 2013; Haeberli *et al.*, 2017). Due to the close proximity to now unsupported, destabilized rock slopes, the potential of a rock-slope failure impacting a lake is highly increased. Rock avalanches may trigger large outburst floods with impact waves of tens to hundreds of meters high, as exemplified by the 1905/1936 Loen rockslides in Norway (Grimstad and Nesdal, 1990),

the 1958 Lituya Bay landslide in Alaska (Fritz *et al.*, 2009), the 1963 Vajont rockslide in Italy (Crosta *et al.*, 2016) and the 2015 Taan Fjord landslide in Alaska (Higman *et al.*, 2018). Also glacier surges during deglaciation or ice avalanches from upper glacier slopes may reach and impact a lake and lead to flooding, e.g. Lake Nostetuko, British Columbia, Canada (Clague and O'Connor, 2015) or Laguna Safuna Alta, Cordillera Blanca, Peru (Hubbard *et al.*, 2005).

In the worst case, the impact waves can affect the whole water column and develop into landslide tsunamis with far-reaching runups. These can extend to areas well above the shoreline and endanger infrastructure and human life. This was shown dramatically in the case of the 1963 Vajont rockslide, when the downstream town of Longarone was completely devastated and almost all ~2000 inhabitants were killed by the wave (e.g. Genevois and Tecca, 2013; Wolter *et al.*, 2014). Landslide tsunamis in lakes need to be distinguished from tsunamis at sea, usually linked to earthquakes, due to three main reasons: (i) the affected areas of the wave(s) are close to the wave source, (ii) the highest runups occur without a time lapse, i.e. the tsunami hazard is directly linked to the catastrophic landslide event, and (iii) the often enclosed lake geometry keeps the energy within the basin and the near field around it, which leads to tremendous impacts at the shoreline and beyond (Couston *et al.*, 2015). Due to the high hazard potential of landslide tsunamis, much research has been recently done on physical modelling (e.g. Miller *et al.*, 2017) as well as numerical modelling (Fine *et al.*, 2003; Fritz *et al.*, 2009; Couston *et al.*, 2015). Concerning multistage rock-slope failures, it is worth noting that lakes might fill successively with each further rock-slope failure deposit, and thus only small landslide tsunamis occur during subsequent events of a series (Hermanns *et al.*, 2006).

The impact on the lake may not only result in impact waves and outburst floods, but may also trigger debris flows or debris avalanches, if the sediment load has enough momentum to overcome the lake barrier, which was the case in the 2013 Kedarnath disaster, Indian Himalaya (Allen *et al.*, 2016). For high-energetic impacts with large volumes of rock mass and water involved, hyperconcentrated mass flows can be formed, which is, for example, postulated for the Flims rock avalanche, Switzerland (Calhoun and Clague, 2018). Furthermore, the energy transferred to the lake basin may lead to a dam breakage and the formation and long-distance transport of characteristic outburst-flood deposits such as Toma hills (e.g. Poschinger *et al.*, 2006; Calhoun and Clague, 2018).

4 Methodology

The method application combines geophysical, sedimentological, geomorphological and dating techniques, which enable an analysis bridging scales (Figure 6). Both direct and indirect measurements are used for investigation.

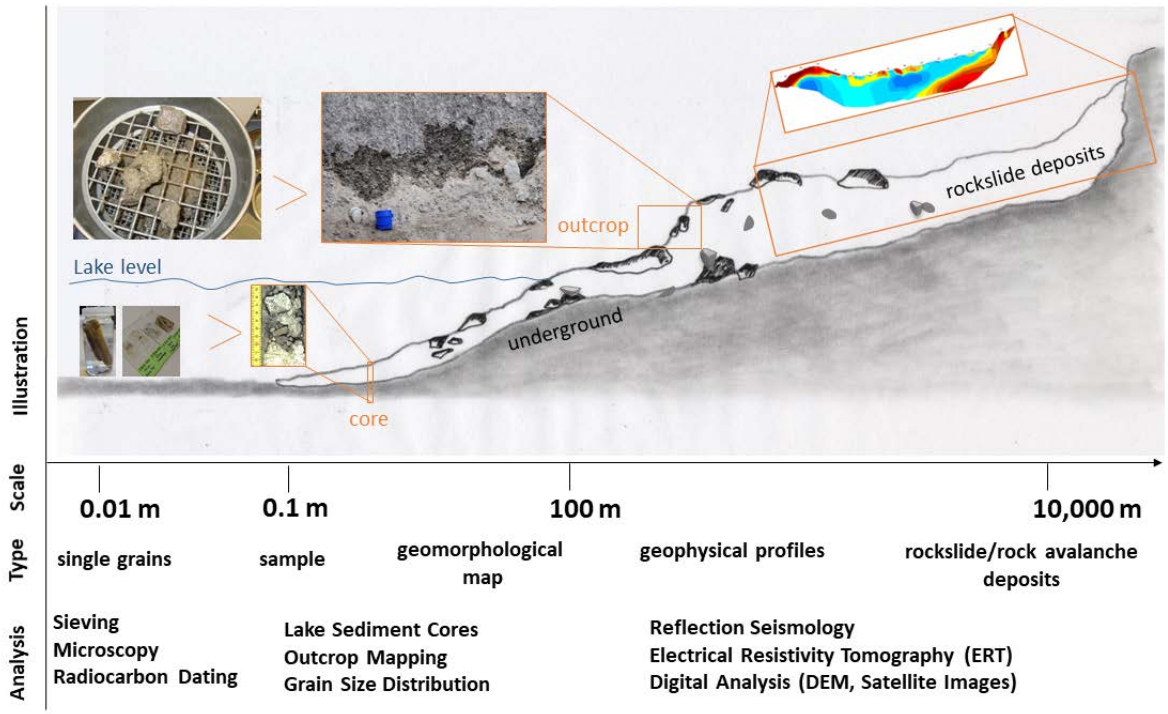

Figure 6: Overview of applied methods with respect to the covered scales and the systematical approach.

4.1 Geophysical Methods

The geophysical investigation aims to image the subsurface, either on land or under water. For this, rock and /or sediment structures are analyzed in terms of stratigraphic sequence, thickness and volumes of geological strata, their mechanical characteristics and insights into paleotopography. The techniques are indirect, i.e. the imaging needs some computing, and therefore it is important to correlate the results with independent analyses, e.g. in outcrops or drillings.

4.1.1 Reflection Seismology

General Function

Reflection seismology is an applied geophysical method which is based on seismic waves. Natural seismic waves travel through the Earth at different velocities through the Earth´s layers. The velocity depends on the physical properties of the geological strata. When they encounter an interface, some portion of the wave energy will reflect off, and some portion will refract through. An interface in this context is usually a tectonically or geologically relevant layer, e.g. the interface between two different lithologies. However, this means not only the change in petrological content, but also an abrupt change in grain size, for example between loosely packed lake background sediments and coarse rockfall deposits.

For the measurement, elastic waves are generated artificially by a pinger source at a certain frequency. It is then recorded how long the waves travel through a layer, are reflected by an interface, and travel back to the surface, there being detected by a receiver or geophone, respectively (Sheriff and Geldart, 1995). Knowing the two-way traveltime from the source to the receiver and the velocity of the seismic waves, a seismic profile can be computed in order to image the subsurface. Seismic profiles are distance-travel time curves, where usually the distance is plotted on the x-axis and the travel time on the y-axis. The depth of the recorded seismic reflection can be calculated based on the measured travel time. The resolution of sedimentary features in the seismic profiles may be as fine as 0.1-0.2 m if systems with high-frequency transducers are used. They are able to penetrate from a few tens of metres up to a few hundred metres into the subsurface, with source bandwidth ranges from 1 kHz to 6-12 kHz, accordingly (Scholz, 2002). The seismic profiles are interpreted by tracing and correlating along continuous reflectors throughout the 2D or 3D dataset. This way, seismic units can be identified and build the basis for further geological interpretation.

Potential and Limitations

The system is easily transported and installed on location, which makes it ideal for the application in an alpine environment. The high-resolution seismic data provides accurate information on the subsurface, which can then be used to assign suitable coring locations, and to link core features directly to seismic data. It is ideal for locating coring sites in fine-grained and unlithified sediment in a Holocene or late-Pleistocene context (Scholz, 2002). The correlation to lake sediment cores and measurements of physical parameters like γ-ray density constrain the seismic interpretation and represent a powerful combination of independent, complementary methods.

The quality of the results may be limited, for example, by i) the difficulty of distinguishing between primary reflections and noise, ii) interbed multiples, and iii) degassing sediments. Noise and processing may lower the quality of the picture, and multiple reflections are also recorded. Therefore, a seismic profile must be carefully evaluated. Often an indication of multiple reflections is a two-way traveltime that is exactly half of another reflection horizon above. Multiple reflections are more common in shallow water, as the water surface is close to the reflected horizons in the sediment (Gilli *et al.*, 2013). Furthermore, gas sources in or underneath the sediment may cause artefacts in the seismic images (Vanneste *et al.*, 2001; Gilli *et al.*, 2013). Better data can only be acquired using multichannel methods (Scholz, 2002).

Applied Setup

In the presented lake studies, a catamaran is attached to a boat and equipped with a seismic source and receiver (Figure 7a). The source and receiver positions are very close to each other (Figure 7b). This setup of single channel seismic profiling assures that a normal pathway is described by both the source signal and the reflected signal back to the receiver (Scholz, 2002). The 3.5 kHz seismic system contains four piezo crystals (Figure 7c). By contraction, these crystals release a pressure wave. The electrical impulse is transformed into a mechanical impulse, whereby the seismic wave is released into the water. During the survey (Figure 7d,e).

Figure 7: Setup for a reflection seismic survey showing a) the boat and the catamaran, b) equipped with a seismic source (red), which c) contains four piezo crystals (black / white). During operation, d) the catamaran is navigated in front of the boat, with e) the pinger positioned directly below the water surface.

Every half a second a signal is shot. The velocity of the seismic wave in the water is ~1500 m/s, and thus a vertical resolution of ~0.4 m can be gained. The seismic signals, received by the apparatus on the catamaran, are then recorded and transmitted by the *OCTOPUS 360 sub-bottom processor™,* which is installed on the boat. For the study on Lake Eibsee, the *OCTOPUS 760 Geophysical Acquisition System™* is operated. The research boat is navigated by GPS with the *Fugawi Global Navigator™*, ideally combined with bathymetric maps. The seismic lines are recorded perpendicularly to the objects of interest (cross sections) and are analysed by the *KingdomSuite™* interpretation software.

4.1.2 Electrical Resistivity Tomography

General Function

The electrical resistivity tomography (ERT) is a geophysical method based on electric currents. As the current is induced directly into the ground via electrodes, it is a direct current (DC) method (Milsom, 2003). It is based on the varying electrical conductivity or resistivity, i.e. 1/conductivity, of different ground materials (Hauck and Kneisel, 2008). The current is mostly transported in the liquid phase of rocks or other ground materials, as rock-forming minerals usually have a low conductivity. If ionized salts are present in the pore water, the electrical conductivity is positively influenced by these ions (Milsom, 2003). Archie´s law (1942) describes the resistivity of a rock, which contains a liquid and solid (rock) phase, as follows:

$\rho e = a\varphi - mS - n\rho w$

ρe = resistivity of damp rocks; φ = porosity of rock; S = pore space occupied by liquid water; ρw = resistivity of water; a, m, n = constants (Krautblatter and Hauck, 2007).

According to this law, the resistivity of damp rocks depends on porosity, the pore space filled with water and the resistivity of the pore water. At its most basic, a measurement needs four electrodes with two current electrodes inducing the electrical current into the ground, and two potential electrodes measuring the voltage difference (Figure 8; Hauck and Kneisel, 2008). Ohm´s law describes the basic physical principle:

$V = IR$

V = voltage [V]; I = current [A]; R = resistance [Ω] (Milsom, 2003).
This formula states that the current in a conductor is proportional to the voltage which runs across it. From that, the apparent resistivity ρ can be calculated:

$$\rho = \mathrm{K}\frac{\Delta \mathrm{V}}{\mathrm{I}}$$

ΔV = voltage difference; K= geometric factor (depends on configuration) (Kneisel and Hauck, 2008). Applied to the basic principle of four electrodes, the formula is:

$$\rho = \frac{\Delta V}{I} 2\pi \left(\frac{1}{\left(\frac{1}{C1P1} - \frac{1}{C1P2}\right) - \left(\frac{1}{P1C2} - \frac{1}{P2C2}\right)} \right)$$

ΔV = voltage difference between electrodes P_1 and P_2; I = durrent between C_1 and C_2; $C_X P_Y$ = distance between the electrodes C_X and P_Y (Milsom, 2003).

The *Wenner*, *Schlumberger-Wenner* and *Dipole-Dipole* configurations are most common. For the presented studies, the Wenner and Schlumberger arrays are used, and are described in the following. The Wenner array, with a constant distance *a* between the electrodes (Figure 8a), yields relatively short measuring times (Hauck and Kneisel, 2008) and a better resolution for horizontally layered structures in comparison with the Schlumberger array (Milsom, 2003). However, the Wenner array only investigates the ground to a moderate depth. Therefore, a combination of Wenner and Schlumberger is the best choice for most applications. For this, the terrameter starts to measure in the Wenner configuration, and then stepwise increases the spacings of the current electrodes while keeping the spacing of the potential electrodes constant, which describes the Schlumberger array (Figure 8a). This way the Wenner and Schlumberger arrays complement each other and yield a good vertical and horizontal resolution with a reasonable measuring time (Hauck and Kneisel, 2008).

Potential and Limitations

ERT has been proven to be a powerful tool for a wide variety of permafrost landforms and purposes (e.g. Krautblatter and Hauck, 2007; Hauck and Kneisel, 2008; Hilbich *et al.*, 2008; Kneisel *et al.*, 2014; Draebing and Eichel, 2018) and has also been applied to rock-avalanche deposits (e.g. Socco *et al.*, 2010; Ostermann *et al.*, 2012). The method can even be used in difficult terrain, as long as sufficient electrical contact between electrodes and the ground is provided. It has the broadest potential of all terrestrial geophysical methods. With the TUM

equipment, ERT can reach up to ~160 m depth. With that, it becomes possible to i) detect and map rock-avalanche deposits, ii) distinguish coarse rock avalanche material from finer-grained underlying material, iii) determine mixing with comminuted or entrained material, and iv) help to detect the paleotopography and bedrock obstacles. This makes ERT suitable to alluvial and lake sediment materials that can be or were entrained. Even meter to decameter large lumps of entrained lake deposits can be assessed with ERT profiles. This helps to i) find fine-grained sediment which is in-situ or displaced by entrainment, and to ii) estimate how much material has been entrained in the rock avalanche material subsequent to the take-up.

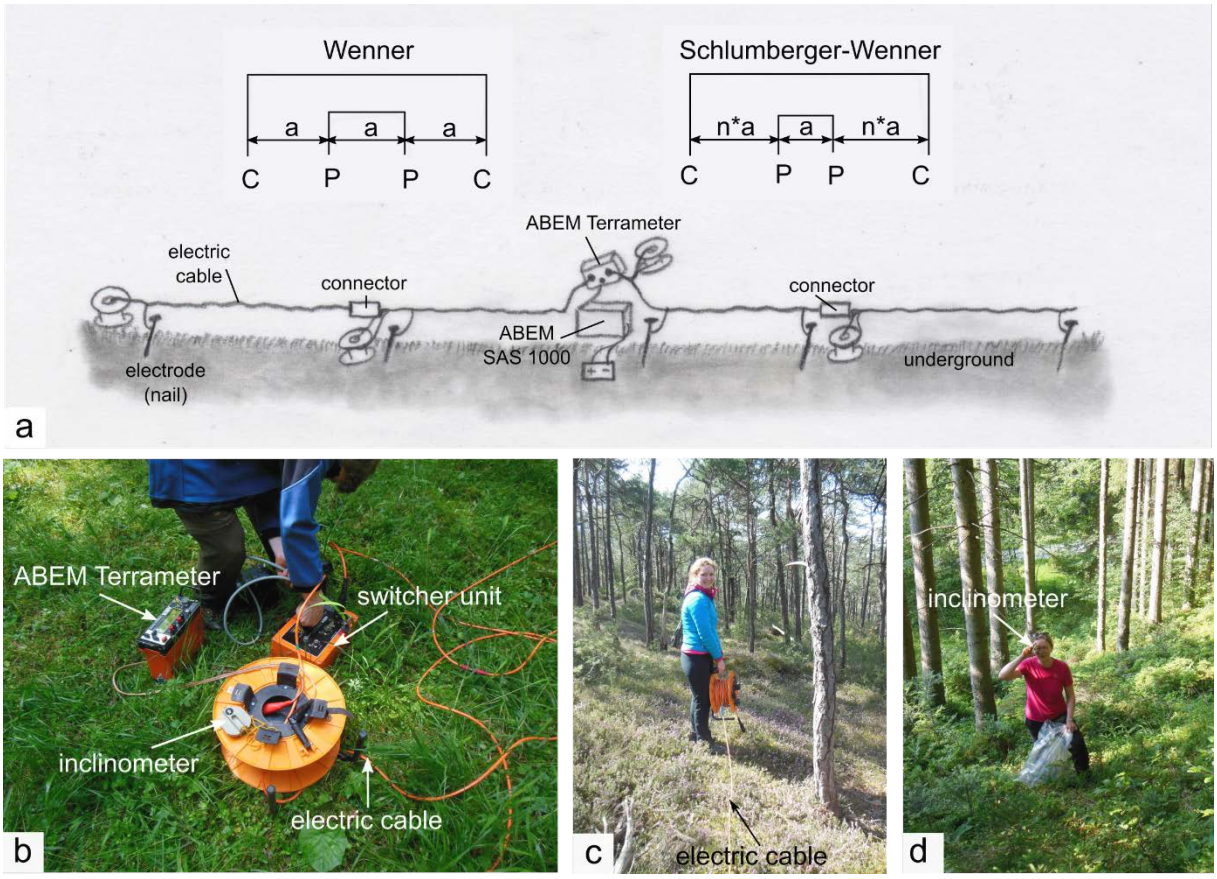

Figure 8: a) Schematic sketch of the Wenner and Schlumberger-Wenner arrays according to Hauck and Kneisel (2008) and the ERT setup in the field with b) the TUM equipment used in the presented studies, c) rolling out the electric cables, and d) measuring local topography with an inclinometer.

However, depending on the equipment and the spacing of the measurement, there is a limited vertical resolution. Moreover, the differentiation between ice/water, air and specific rock types can sometimes be challenging and often needs correlation with independent methods. The method is only applicable on either free of or at least only lightly covered ground with snow as galvanic contact between electrodes and ground is required. Also, good electrical contact between the electrodes and the ground is essential. The method is quite sensitive to noise, which can be metal-covered pipes and cables in the ground, electric fences, mobile phones or power lines (Reynolds, 2011).

Applied Setup

For the surveys in the presented studies, an *ABEM Terrameter System SAS 1000™* is connected to a battery and an *Electrode Switcher Unit* (Figure 8b). Here, the electric cables are plugged

in and then rolled out (Figure 8c). With this equipment, up to four highly durable multi-conductor cables can be used in a “roll along”, reaching a maximum investigation depth of approximately 0.2*total length of the cables. The cables are interlinked with each other by connectors (Figure 8a). Each cable has 21 contacts, which are distributed every 5 or 10 m along the cable. Here, the electrodes are connected to the cable with cable jumpers. Depending on the set of cables used, spacings of up to 10 m can be reached. The ABEM Terrameter induces the current according to the selected array at the current electrodes, and measures the voltage difference at the potential electrodes. From that, the apparent resistivity is calculated according to the configuration – Wenner and/or Schlumberger. The local topography influences the current and is therefore recorded by measuring slope gradients with an inclinometer (Figure 8d). The interpretation of the measured apparent resistivity datum points is based on a Gauss-Newton inversion, processed by applying the *RES2DINV™* (v. 3.5) software.

4.2 Sedimentological Methods

Sediments in general and rock-slope failure deposits in particular can be assessed in depth directly through drillings and outcrops. Sediments of any kind, i.e. terrestrial and subaquatic, reveal information related to their origin, transport and deposition, and moreover, document involved processes over time and space. Sedimentological techniques are direct and yield important complementary data for the correlation with geophysical methods.

4.2.1 Coring of Lake Sediments

General Function

Coring locations are specified on the basis of the reflection seismic profiles and the research questions. The more stratigraphic units are cored, the more information on the evolution of the lake (sediments) and the environment can be gained. Different sampling depths and different types of sediment require different coring techniques (Glew *et al.*, 2002; Glew and Smol, 2016). There are samplers that recover “short cores” of the soft and watery material at the sediment-water interface, sampling down to only about one meter. Usually, gravity corers come into operation, which ram an empty plastic tube vertically into the sediment by a lead weight (only using gravity). For deeper parts of the sediment record and more compact sediment, there are samplers with greater penetration depth. Here, piston corers are suitable for “long cores” of several meters in length (Figure 9; Glew *et al.*, 2002). When driving down to the requested sampling depth, the piston closes the sampling tube at the front and keeps the penetrated sediment out. Once there, the piston is fixed in position via a piston cable that is operated from the surface. Then a driving weight is moved up and down in order to drive the sampling tube over the piston into the sediment until the piston reaches the top end of the tube (Glew *et al.*, 2002). The full plastic tube is then lifted and covered on the bottom by a plastic cap as soon as it reaches the water surface (Figure 9b).

Potential and Limitations

The sediment cores provide directly accessible structures which can be assessed with different techniques in the laboratory (see chapter 4.2.2) and used for lithostratigraphy. In a steady lake without outflows, the sediments are archived without destruction or erosion and reveal insights into the environmental and event history, which cannot be accessed by other means in such detail. The cores can further be correlated with the reflection seismic profiles. Moreover,

there is a chance of age dating, e.g. radiocarbon dating of terrestrial organic material, or varve chronology (see chapter 4.4).

On the other hand, there is a high risk of destroying fine sediment structures during the coring procedure, for example by deformational forces due to the penetration of the tube, or by frictional forces at the tube walls, and cohesion (Glew *et al.*, 2002). For long cores, a coring platform is usually needed. In such cases, the coring can be expensive, and the equipment difficult to transport.

Figure 9: Drilling lake sediment cores applying a) a piston coring device installed on a swimming platform, from where b) lake sediments are retrieved; c) after recovery, the core catcher is being removed, d)-e) allowing to see the lowermost cored sediment.

Applied Setup

In the presented studies, an *UWITEC™* percussion piston coring device is used for the long cores. This system can be applied in water depths up to 140 m. From a coring platform (Figure 9a) the three meter long PVC tubes with a diameter of 63 mm are drilled into the sediment. The UWITEC system is equipped with a core catcher, which is positioned at the bottom of the plastic sleeve and prevents the sediment from falling out of the tube while retrieving the coring device back to the platform (Figure 9b). After recovery, the core catcher is removed (Figure

9c-e) and the long core is cut into 1m sections. For the short cores, a gravity corer and a modified gravity corer with a hammering device, a so-called “bob corer”, come into operation. The bob corer allows recovery of longer short cores up to ~1.5 m.

4.2.2 Lake Sediment Analysis

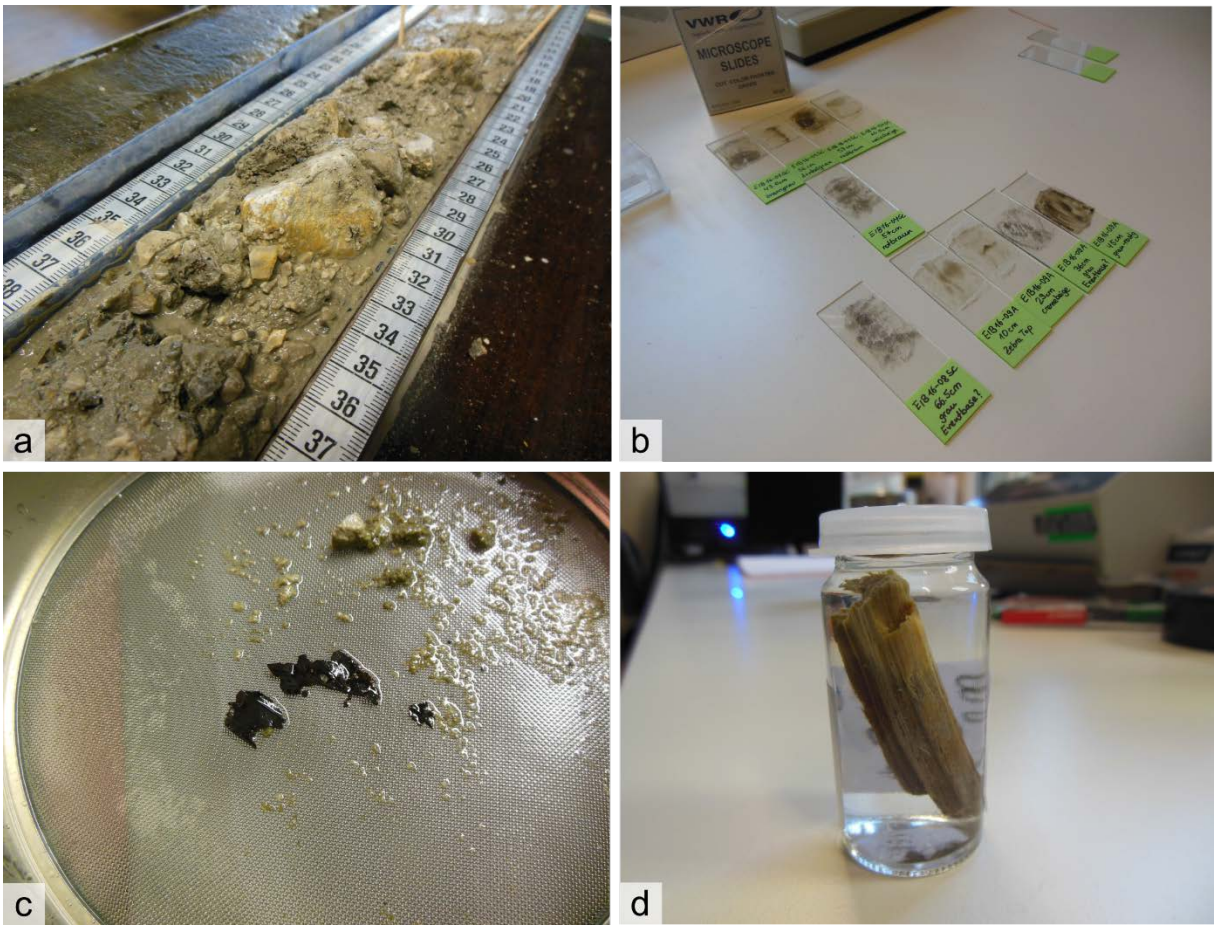

Figure 10: Working in the laboratory on a) a core half filled with rock-avalanche clasts embedded in a fine-grained matrix and b) smear slides for microscopic analysis; c) wet sieving helps to find appropriate samples for radiocarbon dating, which d) are stored in distilled water for further treatment.

In the laboratory, the sampled sediment cores are refrigerated at 4°C. Before the cores are opened, they are analysed by a multi-sensor core logger, which can measure density (attenuated γ-counts), p-wave velocity and magnetic susceptibility by whole-core logging, usually at small intervals of 0.5 cm (Weber, 1997; Nowaczyk, 2002; Bøe *et al.*, 2006). The logger used in the presented studies is produced by *GEOTEK™ Ltd* (Geotek, 2000). After the scan, the cores are opened by splitting them into two halves. This is done by pushing two copper plates lengthwise into the sediment. Where rockfall deposits have been retrieved, the plastic sleeve is filled with clasts and matrix (Figure 10a), and the copper plates need to be pushed apart slightly by hand. In order to scatter the coarse material as equally as possible on both core halves, a knife helps to distribute the gravel.

For visual analysis and photographing, the sediment cores are usually dried for only a few hours, so that the colour contrast between the layers is improved. However, if glacial influence on the lake sediment leads to dark grey clay blooming on the surface of the core halves, as it is the case in Lake Oeschinen, the sediment surface needs to be dried for several days and

then abraded slightly. This way, the colour contrast is reinforced, and the sediment layers can be visually differentiated. The core pictures in the presented studies are taken by applying an *AVAATECH™* XRF core scanner that features a Color Line Scan Camera.

For petrographic microscopic analysis, smear slides can be produced. For this, tiny quantities of loose sediment are embedded on a glass slide (Figure 10b) and can then be evaluated under the microscope referring to mineralogy, grain size, microfossil content etc. Coarse sandy layers, eye-catching bright layers and general changes in deposition mode serve as prominent tie points for the definition of the composite core. Please see Figure S1 (Appendix) for the working principle.

For radiocarbon sampling, in the retrieved sediment is searched for terrestrial organic matter with sample sizes of at least a few milligrams. Either suitable material can be detected macroscopically, or small amounts of sediment are washed and sieved through a mesh size of 0.25 mm (Figure 10c) and may finally be analysed under a binocular. Stored in distilled water (Figure 10d), the samples are ready for transport to the dating laboratory.

4.2.3 Terrestrial Sediment Analysis

Figure 11: Analysis of terrestrial sediments includes a) taking samples in outcrops along a distinct sediment horizon, b) dissecting the outcrop (left of Figure) in order to make sediment structures visible and ready for photo documentation, and c) wet sieving for obtaining grain size distributions. Photo courtesy: B. Lempe.

In the presented studies, the terrestrial sediment is mainly analysed in outcrops. These can be natural ones, which develop due to rapid erosion (e.g. small landslides, debris flows, changing river beds etc.). Outcrops allow 2D-, and often 3D investigation of the sediments, and samples can be taken at a much broader scale than in cores (Figure 11a). Thus, the variation in the sediment deposits can be assessed much better than in cores. The outcrop needs to be fresh for proper study of the sediments, but they are rarely assessed systematically in the first few days. More often, older outcrops are detected by chance and need to be dissected manually at the surface for refreshing. This work requires sensitivity and is often a time-consuming process. Slight scratching with a geologist´s hammer and a spar helps to remove the uppermost few centimeters of sediment in order to clear an older outcrop (Figure 11b). After that, key features become visible and can be described in a detailed profile. For photo documentation (Figure 11b), it is advisable to return to the outcrop several times at different daytimes and weather conditions. After heavy rainfalls, the older sediment surface is often washed away, revealing new insights. The same is true for artificial outcrops, like gravel pits or quarries. In an active pit, there is a chance to document new surfaces each time visiting, especially when

the researcher knows the mining schedule. In either case, the classical geologist´s field equipment including hammer and pocket lens, combined with sieves of different mesh size, water in a spray bottle and some sampling devices help to thoroughly study the terrestrial sediment in an outcrop, that is lithologically, petrographically, and stratigraphically. In the lab, wet sieving (Figure 11c) and microscopic analysis of thin sections accomplish further interpretation.

4.3 Geomorphological Methods

With proliferation of high-resolution ground data and the improvement of appropriate software for digital analysis, geomorphology has become inevitable as a cross-cutting discipline.

4.3.1 Geomorphological Mapping

Geomorphological mapping is regarded as a fundamental method for geomorphological and environmental research, which is applied to produce valuable, reliable base data on landforms, surface features and subsurface materials (Otto and Smith, 2013). Purely manual approaches with schematic sketches and basic maps of landscapes and landforms (e.g. Dykes, 2008) can be combined with digital analysis for further interpretation (see chapter 4.3.2). Basic geomorphological maps either focus on a full view of a landscape with certain landforms or depict distinct elements referring to a research question, for example the morphology of landslide-related processes (Knight *et al.*, 2011). Mapping scale varies between 1:3000 to 1:25,000 for detailed field maps, and 1:5000 to 1:50,000 for geomorphological maps with generalized field data (Dramis *et al.*, 2011).

4.3.2 Digital Analysis

General Function

Digital processing of data includes the visualisation, interpretation and quantification of landforms. Geographical information systems (GIS), satellite imagery and digital elevation models (DEM) are by now widely used tools and provide many options for the digitalization and analysis of manually derived data from the field (Smith, 2011). Before mapping, the study of aerial imagery or DEMs may already support the researcher with planning the field trip and becoming familiar with the project area. In the field, the use of digital devices such as field computers equipped with appropriate software and GPS, makes it possible to collect, sort, categorize and store field data in quasi one step (Otto and Smith, 2013). For satellite imagery, there are three main controls on the quality of the representation of the landform: i) relative size, i.e. landform compared to resolution; ii) azimuth biasing, i.e. landform orientation related to solar azimuth; and iii) landform signal strength, i.e. how well can the landform be recognized (Smith and Wise, 2007; Otto and Smith, 2013). DEM processing, for example with GIS application, is called *geomorphometry* and is rapidly becoming a central aspect of geomorphological research (Hengl and Reuter, 2008; Bishop and Houser, 2016). In the presented study at Lake Eibsee (chapter 5.3), for example, the geomorphometric method *gradient* is used to measure the steepness of the slope, i.e. the rate of change of elevation.

Potential and Limitations

Geomorphic work can greatly improve our understanding of landforms and processes, also in the context of natural hazards. Thereby, multiscale morphometric parameters characterize mesoscale properties of the morphology. The high resolution of DEMs allows for quantification of the shape and contextual characteristics of the morphology (Bishop and Houser, 2016).

In the context of the presented studies, not only the detection and characterization of landforms is essential for the assessment of rock-slope failure deposits, but also the analysis of satellite imagery with focus on potential travel paths, volume estimations and energy considerations (e.g. at Lake Oeschinen, chapter 5.1). Furthermore, there is great potential of the complementary application of methods for subsurface reconnaissance, such as ERT (chapter 4.1.2), which provide information on the paleotopography and the stepwise overprinting of the morphology (Bishop and Houser, 2016).

However, the quality of geomorphometry strongly correlates with the quality of the source data. Therefore, the primary data sources should be carefully checked for scale, sufficient coverage of the study area and resolution (Otto and Smith, 2013). Also, the high amount of easily accessible digital spatial data may seduce to interpret landforms without visiting the field. . Nevertheless, the visual learning from observation in the field is highly valuable, as it provides the researcher with the most direct way of understanding the morphology (Otto and Smith, 2013).

4.4 Dating Methods

For the interpretation of sediment archives accurate chronologies are essential, especially for the correlation between multiple sites (Appleby, 2002). There are a bunch of radiometric dating methods available, e.g. based on the isotopes ^{210}Pb, ^{137}Cs, ^{230}Th/^{234}U, ^{36}Cl or ^{14}C, just to name a few. In the presented studies, radiocarbon dating and varve chronologies play an important role.

4.4.1 Radiocarbon Dating

General Function

Radiocarbon dating is a radiometric dating method that uses the naturally occurring radioactive isotope ^{14}C to estimate the age of carbon-bearing materials up to about 55,000 years (Bowman, 1990). The basic process is radioactivity. Some elements have several isotopes that all have the same atomic number (protons), but different amounts of neutrons. Some of these isotopes are radioactive (e.g. ^{3}H and ^{14}C), i.e. they are unstable and decay with a certain velocity that is determined by the half time $t_{1/2}$. For ^{14}C, that is used for radiocarbon dating, $t_{1/2}$ = 5568 yrs. During photosynthesis, plants fix almost the same amount of ^{14}C (in CO_2) as there is in the atmosphere. The radiocarbon dating method was first introduced by Arnold and Libby (1949) and can be applied to plants (wood), charcoal, textiles, bones, shells (e.g. ostracodes, foraminifers), corals (carbonate), macrofossils etc., and also to wine, vanillin and wax.

In the traditional method, several grams of carbon are necessary, whereas applying Accelerator mass spectrometry (AMS), only a few milligrams of carbon are needed for one measurement. First, pure carbon is extracted from the sample, then the ^{14}C decay (conventional) or ^{14}C atoms (AMS measurements) are counted. Bowman (1990) states that the age is calculated by the ^{14}C/^{12}C ratio of the sample (A_t) and the known sample (A_0):

$$t = -8033 \ln \frac{At}{A0}$$

Raw, i.e. uncalibrated, radiocarbon ages are given in BP (''before present'' = 1950), calibrated ages in cal BP or cal BC (''before Christ''). On a historic scale, ages can also be given in AD (“Anno Domini”), which effectively means calendar years.

Due to changing A_0, there are wiggles and plateaus in the atmospheric curve over time. This is due to changes in the ^{14}C production rate (depending on solar activity and the geomagnetic field) as well as atmosphere-ocean exchange rate and anthropogenic impact. The conventional (Libby) ^{14}C age, which assumes a constant A_0, is therefore not the calendar age. The calendar age is obtained via calibration. For this, *OxCal* is used, an online calibration tool with a tree-ring calibration curve, developed at the University of Oxford (Ramsey, 1995; Bronk Ramsey, 2013).

Potential and Limitations

In general, traditional measurement is relatively insensitive and there are high statistical errors for small samples; AMS is more precise. Due to nuclear tests in the 1950/60ies, the atmosphere became "too old" because of > 100 % increase in ^{14}C content. The resulting `bomb peak' in 1963 allows for precise dating of modern samples (e.g. Goslar *et al.*, 2005). Moreover, fossil fuel burning leads to a difference from $A_0$, which is measured in $\Delta^{14}C$. This so-called `Suess effect' documents the industrial revolution with a negative $\Delta^{14}C$. All these mentioned uncertainties are corrected for by applying dendro-based calibration like IntCal09, which extends back to 12,600 cal BP, and combined with marine records back to ~50,000 cal BP (Reimer *et al.*, 2009) and the updated version IntCal13 (Reimer *et al.*, 2013), respectively. Radiocarbon-based age models can also be supported by tephra layers from volcanic eruptions (e.g. Hajdas *et al.*, 1993; Schnellmann *et al.*, 2006) or varve chronology (see chapter 4.4.2; e.g. Hajdas and Michczyński, 2010).

Radiocarbon ages obtained from lake sediments need to be corrected for the so-called reservoir effect. In hard water, the material has not achieved isotopic exchange equilibrium with the atmospheric CO_2, maybe caused by fixation during photosynthesis or precipitation of $CaCO_3$ (Deevey *et al.*, 1954). The reservoir effect can be avoided when using AMS-^{14}C ages of terrestrial macrofossils (e.g. seeds, flowers, tree needles, twigs, leaves).

4.4.2 Varve Chronology

General Function

Varves are annually laminated sediments that can be dated by counting layers back to 14,000 years (Lamoureux, 2002; Mörner, 2014). In clastic varves, beside the grain size, also colouring helps to differentiate winter and summer layers; often, winter layers are dark brown or grey, and summer layers are bright. Varves are often compared to tree-rings, which are also counted year by year and are measured as to thickness. From that, site-specific long-term chronologies can be established, for example at Lake Van, Turkey, spanning over 13,000 years (Wick *et al.*, 2003), the Hector Lake, Alberta, Canada (Leonard, 1997), the Meerfelder Maar, Germany (Brauer *et al.*, 1999), or Lake Oeschinen, Switzerland (Leemann and Niessen, 1994; Amann *et al.*, 2014; Amann *et al.*, 2015).

Potential and Limitations

Varve chronology is regarded as highly accurate. If various people count the layers, the errors can be reduced to a minimum by building an average. This way, varved lake sediments are ideal for environmental reconstruction, as they provide continuous dating without interpolation, which often cannot be ensured by other methods (Zolitschka *et al.*, 2015).

However, certain internal lake processes may destroy varve structures, like bioturbation, sediment resuspension or erosive turbidity currents, so that most sediment records only show discontinuous varve structures. Especially large rock-slope failures impacting a lake can lead to long-term alteration of the lake system. Therefore, varve counting should be better referred to as relative rather than absolute (Gilli *et al.*, 2013).

5 Case Studies

5.1 Lake Oeschinen: Multistage Rock-Slope Failures Revealed in Lake Sediments

This chapter has been published in the Journal of Geophysical Research: Earth Surface under the title "Multistage Rock-Slope Failures Revealed in Lake Sediments in a Seismically Active Alpine Region (Lake Oeschinen, Switzerland)" by Sibylle Knapp, Adrian Gilli, Flavio S. Anselmetti, Michael Krautblatter and Irka Hajdas (2018). This chapter contains results of my unpublished master thesis (Knapp, 2012), which has been fully revised and extended. The data sets presented in this paper are available at https://doi.org/10.14459/2018md1432577.

Abstract

Lateglacial and Holocene rock-slope failures occur often as multistage failures where paraglacial adjustment and stress adaptation are hypothesized to control phases of detachment. However, only limited datasets are available to decipher large multistage rock-slope failures in detail. Here we apply sedimentology, radiocarbon dating and geophysics to reconstruct multistage rock-slope failure recorded in lake sediments. We present a unique inventory from Lake Oeschinen (Bernese Alps, Switzerland) covering ~2.5 kyrs of rock-slope failure history. The lake sediments have been investigated using sediment-core analysis, radiocarbon dating and seismic-to-core and core-to-core correlations, which were linked to (pre-) historic and meteorological records. The results imply that the lake in its present extent is significantly younger than the ~9.5 kyrs old Kandersteg rock avalanche in the close vicinity. Up to eleven rock-slope failure events could be identified and related to specific detachment scarps, which provided information for energy considerations. Four events likely coincided with (pre-) historic earthquakes. At least six events detached from the same area, potentially initiated by prehistoric seismicity and later from stress-relaxation processes. The data imply unexpected high recurrence rates (~1/300 yrs) and also help to understand the generation of a historical lake-outburst flood. Here we show how polymethodical analysis of lake sediments can help to decipher massive multistage rock-slope failures, which are often camouflaged in subaerial settings.

Plain Language Summary

Rock-slope failures account for two thirds of the most catastrophic landslide events in the last millennium. A key question is how often catastrophic rock-slope failures happen, but single rock-slope failure deposits can hardly be distinguished because failed rock material may fall onto and partially cover older deposits. Hence, the frequency of rock-slope failures is often highly underestimated. Preserved in a lake, the event deposits can be deciphered in time and space because the lake consistently records environmental changes and events and acts as a natural chronometer. This study at Lake Oeschinen in Switzerland shows that at least eleven rock-slope failures occurred around the lake over the last ~2.5 thousand years. The results imply that the lake is much younger and that the dam is built by at least six rock-slope failure deposits rather than by one or two, as previously thought. We also calculated the seismic trigger potential of well-known earthquakes in the region and found four earthquakes which

might have prepared or triggered rock-slope failures around Lake Oeschinen. Here we demonstrate that the analysis of lake sediment archives can help to improve recurrence rates of rock-slope failures and to show that they occur much more often than previously expected.

Introduction

Climate warming forces us to face a continuous environmental change in high-mountain landscape settings. The accelerating melting of glaciers (e.g. Paul *et al.*, 2004; Schiefer *et al.*, 2007) will form an increasing number of proglacial lakes (Haeberli *et al.*, 2016a). In combination with enhanced failures from recently deglaciated rock slopes (Leith *et al.*, 2014), moraine walls and proglacial sediments, this landscape change will lead to new hazardous situations (Paul and Haeberli, 2008; Huggel *et al.*, 2013). Pronounced in permafrost areas, increasing rock-slope instability following stress adaptation can lead to multistage rock-slope failures, which are prone to even evoke outburst floods from lakes dammed in the forefield. To better anticipate multistage rock-slope failures and related flood waves in the foreseeable future, we need to improve our process understanding of rock-slope failures (Scheidegger, 1973; Moore *et al.*, 2009; Krautblatter and Moore, 2014) and their interactions with water bodies located in their runout path (e.g. Legros, 2006; Pudasaini and Krautblatter, 2014).

Lake inventories have been explored in numerous studies on general lake sedimentology and geochemistry, turbidites and sediment-deformation structures related to climate and environmental change as well as earthquakes. Lakes provide continuous sediment archives for assessing the frequencies of flood events (Arnaud *et al.*, 2005; Wolfe *et al.*, 2006; Gilli *et al.*, 2013) and/or earthquakes (Strasser *et al.*, 2013; Moernaut *et al.*, 2014; Reusch *et al.*, 2016), as well as for studies on paleoclimate changes (Eden and Page, 1998; Brauer *et al.*, 1999; Stockhecke *et al.*, 2016). Recent studies have also used lakes to assess the natural hazard potential of lake tsunamis (Kremer *et al.*, 2012; Hilbe and Anselmetti, 2015; Beigt *et al.*, 2016). However, they have rarely been investigated to reconstruct multistage rock-slope failures. This is especially important as the older deposits of multistage rock-slope failures on land are often covered and hidden underneath the latest event deposits and, thus, recurrence rates are misestimated (Sass and Krautblatter, 2007; Sass *et al.*, 2007; Krautblatter *et al.*, 2012b). In this context, lakes provide a key source of information because they act as the final sink for incoming sediment and can produce a complete sediment record that reaches back in time for thousands of years (e.g. Hodell *et al.*, 1999; Kremer *et al.*, 2015).

Most lake-based mass-movement studies deal with mass movements triggered subaquatically, but lakes can also be useful for studying subaerial mass movements. Subaerial mass movements, like rock falls, may reach the lake basin and are often detected but rarely analyzed in terms of depositional characteristics (Hermanns *et al.*, 2004; Schnellmann *et al.*, 2006). While short-term (months-years) frequency and magnitude information has boosted due to LiDAR monitoring and other methods (Perret *et al.*, 2006; Stoffel, 2006; Sass *et al.*, 2007; Ravanel *et al.*, 2010; Krautblatter *et al.*, 2012b), long-term information on rock-slope failure recurrence rates is still only available for single well-dated sites (e.g. Martin *et al.*, 2014). Here, analyzing the depositional characteristics of rock fall in a lake basin may allow for a more complete understanding of rock-slope failures and their mobility processes (Bussmann and Anselmetti, 2010). This is also important in the context of glacier- and permafrost-related instabilities, stress adaptation and paraglacial adjustment (Krautblatter and Moore, 2014;

Leith *et al.*, 2014; Deline *et al.*, 2015b; Huggel *et al.*, 2015), especially in the context of this study site, which has undergone rapid glacial and permafrost fluctuations in the Holocene, combined with seismic tremors.

The study of rock-slope failures in lakes provide presumably the most accurate method for ascribing stratigraphic positions to certain rock-slope failure events because the lake acts as a natural chronometer, usually represented by annual varve layers, which allow to estimate the elapsed time between the single events. Moreover, erosion is usually absent in the deep depot centers of the lacustrine systems so that these archives are perfectly preserved. This is especially valuable for deciphering the multistage character of massive rock-slope failures that occur at one single mountain flank, i.e. events, which stack on each other due to the same detachment direction and trajectory in the lake. The recurrence period between the single events may differ a lot and is subject to diverse triggers and process and stress relaxation chains. In this study, we employ high-resolution quasi-3D reflection seismic profiles correlated with lake-sediment cores to answer the following questions: 1) How can continuous lake sedimentation contribute to a better understanding of multistage rock-slope failures? 2) How accurate can the recurrence rates of repeated massive rock-slope failures be determined? 3) How does the impact of a massive rock-slope failure alter a lake and its sedimentation?

Geological and Geographical Setting – Lake Oeschinen

Lake Oeschinen (46°29'53.2"N 7°43'40.2"E) is a proglacial, landslide-dammed lake located ~60 km southeast of Bern, in the Bernese Oberland in Switzerland at an elevation of 1578 m a. s. l. (Figure 12a). The lake is ~56 m deep and embedded in a deep circular valley, which was formed due to glacial erosion. It is surrounded by steeply inclined, partly vertical rock walls and hanging glaciers that discharge into the lake from the South and Northeast. The W-E oriented Oeschinen valley is connected to the N-S oriented main Kander valley (1174 m a. s. l.). In terms of Alpine geology, the area is part of the Helvetic nappes, particularly of the Doldenhorn nappe, and is only ~20 km northwestern of the Rawil depression, currently one of the seismically most active parts of the Alps (Kastrup *et al.*, 2004; Ustaszewski and Pfiffner, 2008; Pfiffner *et al.*, 2011; Cardello and Mancktelow, 2014).

The surrounding mountains consist of Upper Jurassic and Cretaceous, blackish limestone (Troesch, 1908; Niklaus, 1967). The geological strata dip to the Northwest with ~25-30°. It is obvious that the tectonic situation and the partially overhanging valley flanks around the lake favor landslides (Turnau, 1906). The lake does not have a surficial but only an underground outflow, which makes the lake an efficient sediment trap suitable for limnogeologic studies. Turnau (1906) and Groll (1903) postulated a postglacial age of both the Kandersteg rock avalanche (Figure 12b), and the Oeschinen rock avalanche. They could detect neither the age nor the sequence of the events, but interpreted them to be of a similar age. In a later study, the Kandersteg rock avalanche could be dated to ~9.5 cal kyrs BP (Tinner *et al.*, 2005). Recently, surface exposure dating results implied a much younger age of the Oeschinen rock avalanche, dated to 2.3 ± 0.2 kyr (Köpfli *et al.*, 2018).

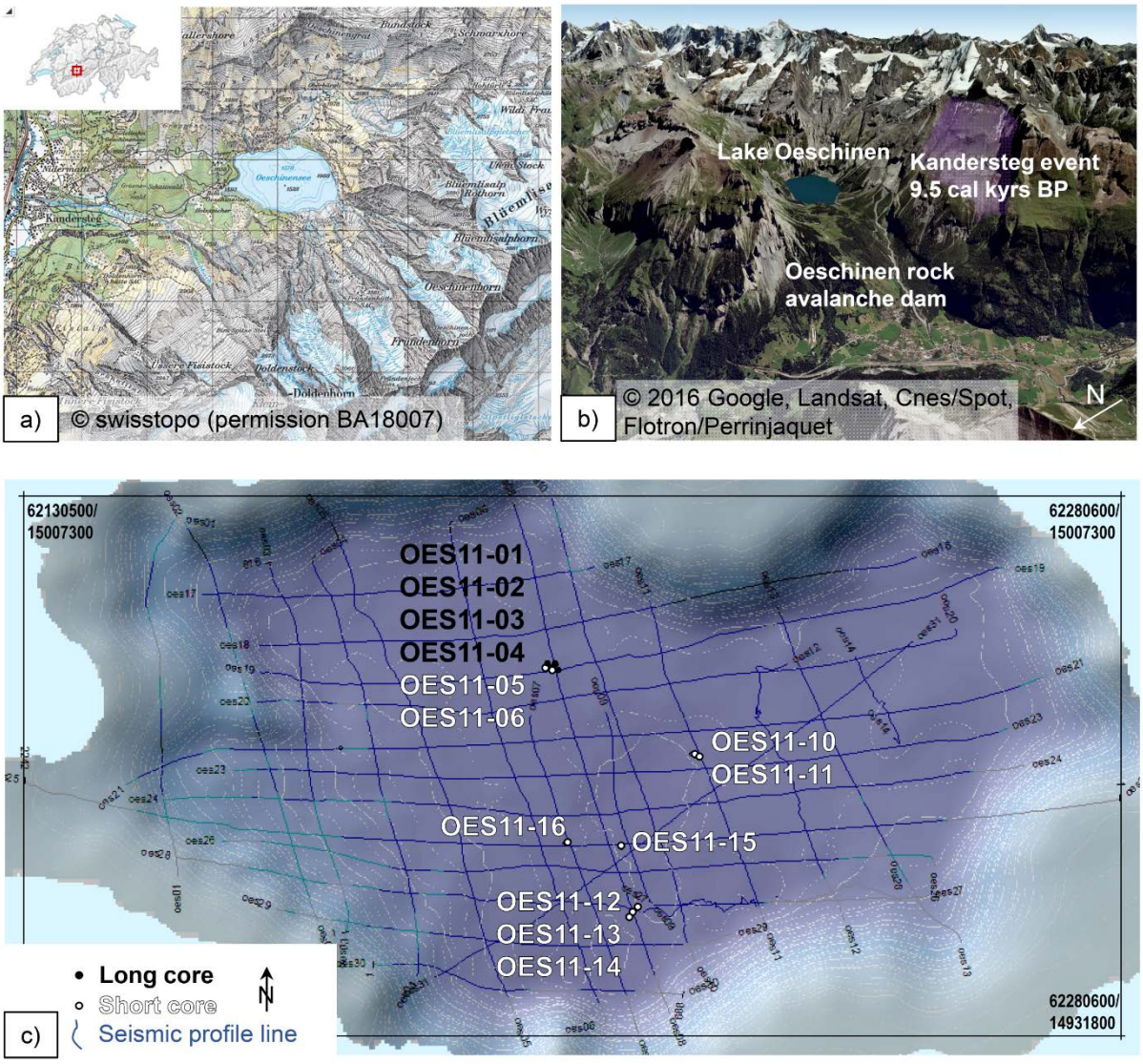

Figure 12: Overview of Lake Oeschinen in the Bernese Oberland in Switzerland. a) Topographical map showing Lake Oeschinen and the Kander valley. b) 3D-view showing Lake Oeschinen and the scarp of the ~9.5 cal kyrs BP rockslide event (Tinner et al., 2005). c) Bathymetric map of Lake Oeschinen with core locations and 3.5 kHz seismic survey grid. The cores OES11-02, -03 and -06 were used by Amann et al. (2014); Amann et al. (2015).

Methods

Seismic Survey and Sediment-Core Retrieval

Fieldwork on Lake Oeschinen was carried out in August 2011. We conducted a reflection seismic survey and obtained 31 seismic profiles across the lake. For the seismic survey, a 3.5 kHz pinger source was used with a boat speed of 5-6 kmh^{-1} to acquire a dense grid of high-resolution seismic lines (Figure 12c) by which the sedimentary subsurface of Lake Oeschinen could be reconstructed seismic-stratigraphically in quasi three dimensions. The seismic data was band-pass filtered using the SPW™ seismic processing software package, and afterwards analyzed using the KingdomSuite™ interpretation software. The two-way travel time to depth conversion is based on a P-wave velocity of 1500 ms^{-1} for both water and lake sediments. Based on the results of the seismic survey, appropriate coring locations were identified (Figure 12c and Table S1).

Coring was carried out from a coring platform with an UWITEC percussion piston-coring system. The PVC tubes used in this device had a diameter of 63 mm and a length of 3 m, which were cut into 1-m sections immediately after core recovery (for example, core OES11-01-A was cut into three 1-m pieces OES-11-01-A1, -A2 and -A3 ; Table S1 and Figure S1). Additionally, a gravity corer and a modified gravity corer with a hammering device were employed in order to recover the uppermost ~1 m of the sediment layers. The coring location was chosen as to i) recover the oldest rock-avalanche deposits in order to date the lake formation, ii) recover no younger rock-fall deposits on the way to avoid the risk of getting stuck in the coarse rock mass, and iii) coring outside the gas-blanked area where we had hardly any seismic penetration. Thus, it was intended that the events reached the coring site not through the rock-fall deposits but with their turbidites, allowing a much more robust and complete event chronology. Three separate cores were compiled to form the composite core using cores OES11-01, OES11-04, which were recovered with an overlap of 1.5 m, and short core OES11-05 for the uppermost sediment of this location, as this is usually destroyed when applying the piston coring system (Figure S1 and Table S2). The cores OES11-02, OES11-03 and OES11-06 provided a basis for the varve chronology (Amann *et al.*, 2014; Amann *et al.*, 2015). More hammer cores OES11-10 to OES11-14 were recovered in order to track the stratigraphic position of mass-movement-related turbidites at different locations, as well as the short cores OES11-15 and OES11-16. In total about 45 m of sediment in long and short cores were retrieved.

Core Analysis and Sediment Description

In the laboratory, the sediment cores were stored in a cold room at 4 °C. The gamma-ray density of all cores were determined by a GEOTEK Ltd. multi-sensor core logger (MSCL) with a sampling resolution of 0.5 cm. Subsequently, the cores were split lengthwise into two halves. As the sediment structures were covered by the smear of dark grey clay due to the high glacial influence, the cores needed to be dried for several days and abraded with a sharp knife on the uppermost surface layer before being photographed and sedimentologically described by visual analysis of grain-size and material. Color differences are due to differential drying in the lab (Figure S2). The composite core was constrained with nine tie points down to a total composite depth of ~14.6 m (Figures S1 and S2, Table S2).

Analysis of Rock-Slope Failure Events

Rock-slope failure deposits were first identified on the seismic data based on the detection of i) mound-shaped chaotic seismic facies and ii) transparent onlapping units, which were interpreted as i) deposits of rock-slope failures and ii) distinct event-related turbidites. In a second step, these obtained seismic stratigraphic horizons were correlated with distinct lithologic layers (e.g. prominent turbidites) in the cores. Not each individual turbidite in the sediment record was described and interpreted, even if it reached comparable thickness, but only those, which could clearly be correlated with the seismic data.

Rough guesses of fall height distance of center of gravity to lake level and associated potential/kinetic energy were determined based on aerial images of the scarp niches surrounding Lake Oeschinen. The calculations of the potential energy

$$E = V * \rho * g * h$$

were based on best approximations of i) the volumes *V* of failed rock/debris in the lake (derived from the chaotic mass in the seismic data), and ii) the average fall-height distances *h* of the center of gravity of the failed rock material to the present lake level. Paleolake levels cannot be inferred, but these would only change *E* by a few percent. The density of the rock material consisting of limestone is assumed to be ρ = 2.7 kgm-³.

Radiocarbon Dating and Age-Depth Model

Preparation, pretreatment and radiocarbon dating were carried out at the Institute of Particle Physics at the ETH Zurich. The radiocarbon ages of the wood samples were calibrated using the calibration program OxCal v.4.2.4 (Ramsey, 1995; Bronk Ramsey, 2013), including the IntCal13 calibration curve from Reimer *et al.* (2013). Turbidites in the seismic and sediment record were used for stratigraphic analysis of the single events (Schnellmann *et al.*, 2006). The radiocarbon ages were assigned to their stratigraphic level in the composite core. We did not account for the instantaneous depositional time of the turbidites because these event layers all were thin when compared to the thickness of the entire dated section. It was possible to define the age-depth model of the upper part of the sediment archive more precisely (down to ~5.5 m sediment depth). Here, we applied core-to-core-correlation using the short cores and the sediment chronology derived by varve counting and by a composite 210Pb CRS-model (Leemann and Niessen, 1994; Amann *et al.*, 2014; Amann *et al.*, 2015), in which the varve analysis was validated with flood documentation in the Kander region back to 1480 AD (Bütschi, 2008; Schmocker-Fackel and Naef, 2010).

Seismic Tremors

As Lake Oeschinen is very close to the assumed center of the reactivated alpine fault zone around the Rawil depression, the area is earthquake-prone so that seismic tremors need to be considered as a trigger for rock-slope failures (Keefer, 1984; Lavé *et al.*, 2005; Owen *et al.*, 2008). Rock falls and rockslides are amongst the most abundant types of earthquake-induced landslides (~80% of all reported), and especially weakly or moderately indurated sedimentary rocks are prone to failure (Keefer, 1984; 2000). The Newmark`s (1965) sliding-block model is used to estimate the co-seismic slope deformation at Lake Oeschinen. In order to calculate the theoretically expected impact of different earthquakes, we used well-introduced regression models (Jibson, 1993; Jibson *et al.*, 2000; Miles, 2001; Jibson, 2007). The theoretical Newmark displacement D_n in centimeters

$$log\, D_n = 2.401\, log\, I_a - 3.481\, log\, a_c - 3.230 \pm 0.656$$

can be derived from the Arias Intensity I_a and Newmark's critical yield acceleration a_c. The attenuation of the Arias Intensity I_a with distance

$$log\, I_a = M - 2\, log \sqrt[2]{r^2 + h^2} - 4.1$$

can be calculated using the moment magnitude *M*, the distance of the examination site from the epicenter *r* and the focal depth *h* (Arias, 1970; Wilson, 1993). This attenuation relation applies for active tectonic environments, respectively (Stewart *et al.*, 2002). Newmark's critical yield acceleration

$$a_c = (FS - 1)\, g \sin \alpha$$

uses the Factor of Safety *FS* and the ground acceleration *g* in terms of the Earth´s gravity to calculate a threshold for the acceleration that is needed for a sliding block on a plane (inclined at an angle of α) to overcome shear resistance. For comparison of different events, we inferred the residual stability of pre-sliding carbonate blocks with a factor of safety of 1.1 based on the evaluation of other pre-sliding carbonate blocks with few remaining rock bridges (Heckmann *et al.*, 2012).

Results

Seismic Facies

The high-resolution seismic data depict the morphology and the seismic facies of the subaqueous slopes and the basin of Lake Oeschinen, which we interpret in accordance to previous studies (Schnellmann *et al.*, 2006). Deep seismic penetration down to the acoustic basement at ~13-14 m seismic depth is only given in the most central part of the lake basin, where we retrieved the composite core (Figure 13). Near the deltas and other shallow areas, the seismic signal could not penetrate the subsurface sufficiently due to coarser grains and high gas content in the sediments (e.g. Gilli *et al.*, 2013). In most parts of the subsurface, the seismic profiles show an acoustically well-stratified seismic facies with high lateral coherence, which is interpreted as lake background sediments.

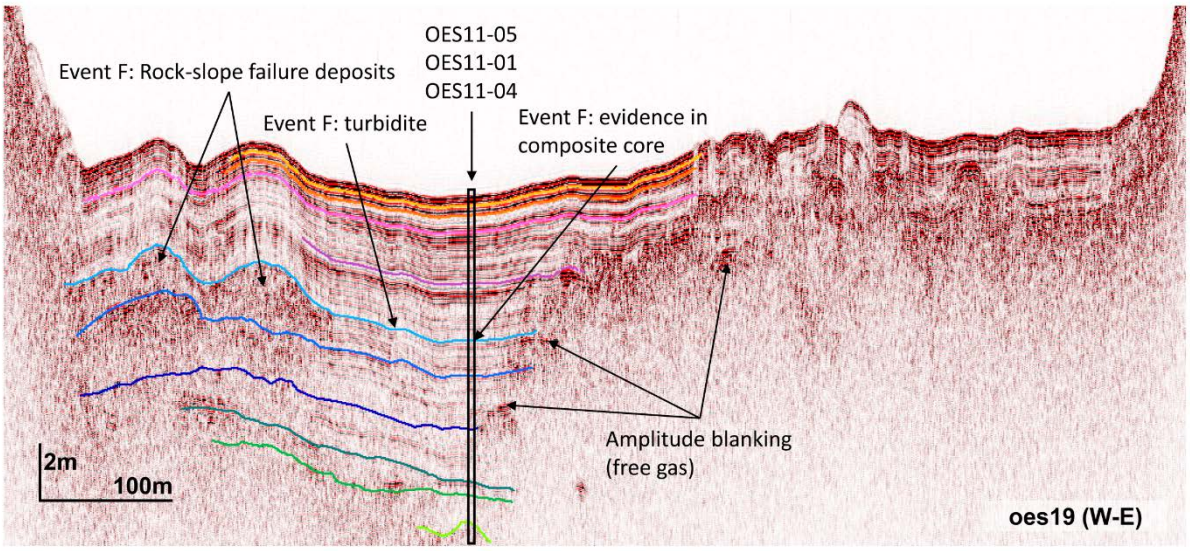

Figure 13: Seismic profile oes19 showing rock-slope failure deposits (chaotic-to-transparent units, e.g. Event F) and related turbidites as seismic stratigraphic horizons and time markers in the composite core. The composite core contains all event-related turbidites and includes the oldest, the lake damming deposits of the Oeschinen rock avalanche. The subsurface from the eastern basin is blanked by free gas.

In close vicinity to the slopes, they are intermitted by mound-shaped chaotic-to-transparent units. This seismic facies is here in Lake Oeschinen interpreted as rock-slope failure deposits, which will be elaborated in more detail below. High-amplitude diffractions (seismic artifacts, Figure S3a) appearing along the top surface of this facies indicate outstanding boulders, which are partially covered by a sediment drape. Onlapping transparent facies, which is interpreted as mass-movement related turbidites, occurs towards the lake center. These units show strong seismic reflections can be used as seismic stratigraphic positions for rock-slope failure

deposits (Figure S3b,c). In the eastern basin, however, the seismic penetration is limited to only the upper few meters because free gas is blanking the seismic image (Figure 13).

Sedimentology of the Cores

The sediment record of Lake Oeschinen, as constructed in our composite core, consists in total of ~14.6 meters of i) dark grey limestone clast deposits, overlain by ii) high-energy-event-related megaturbidites, and iii) clastically dominated, proglacial background sediments with iv) intercalated flood and matrix-supported turbidites. Eleven mass-movement event deposits, named A-K, could be detected (Figure 14a,c).

Rock-avalanche deposits were discovered at the bottom of the sediment record at ~13.4 m depth in the composite-core sections OES11-04-D3 and OES11-01-E1. When the Oeschinen rock avalanche dammed the Oeschinen valley, the basin of the modern lake was formed. The initial trough exhibits a bumpy, blocky surface (light green horizon in line oes08, Figure 14a). The rock-avalanche deposits mainly consist of sharp-edged, dark grey, almost black Helvetic limestone gravels with a sandy to silty matrix (Figure 14d).

Two *graded turbidites,* each with a thickness of ~0.3 m, overlie the rock deposits. These "megaturbidites" show dark grey, normally graded coarse sand at the base, overlain by homogeneous bright beige clay, which probably derived from rock-avalanche dust-cloud particles (Figure 14b,d). Its thickness exceeds 0.5 m but cannot be exactly measured because of a small gap between OES11-04-D3 and OES11-01-E1, which likely not exceeds a few centimeters.

The initial filling of the trough flattened the topography of the lake basin (line oes08 in Figure 14a). The first layered sediments occur at a depth of ~12.2 m marking the onset of the newly formed lake system with background sedimentation and varve formation. All stages of this single high-energy event are detected in the sediment core, showing from the bottom rock-avalanche deposits, two graded subsequent megaturbidites and particularly bright-yellowish colored, fine-grained dust deposits (Figure 14d).

Background sediments in Lake Oeschinen show various characteristics of the proglacial environment. The laminated silts and clays show diverse hues of grey and beige color. The laminae are interpreted as varves (Amann *et al.*, 2014) and depict the continuous lake sedimentation processes between event-related deposits. The sediments were heavily deformed during core retrieval due to stiffness and adhesive power (Figure 14b).

Flood-related turbidites derive from river floods ending up as high-density currents containing in Lake Oeschinen mostly dark brown to reddish, fine sandy to silty sediments with a high amount of terrestrial organic matter (Figure 14b).

During subaqueous mass-movement events, turbidity currents usually erode and resuspend fine-grained lake sediment on the lake slopes (e.g. Gilli *et al.*, 2013), which then settles out on top of the event deposits. Turbidites generated by subaerial mass movements entering a lake differ in terms of incoming material and available energy. Here, turbidity currents are either caused by the impact of the landslide on the lake floor causing resuspension, or from disaggregation of landslide material into more dilute sediment suspension (Hunt *et al.*, 2015).

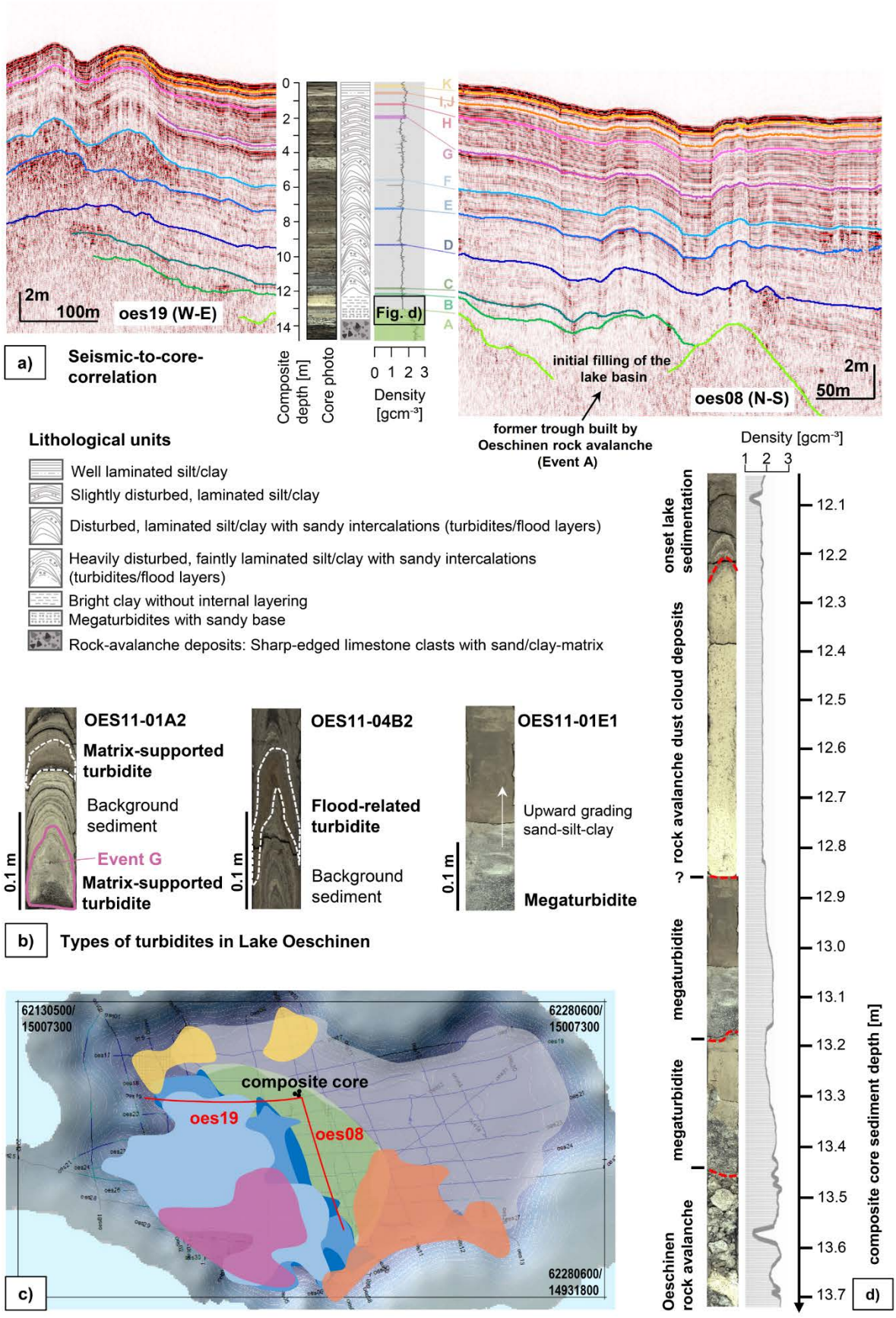

Figure 14: Overview of seismic and sediment record in Lake Oeschinen. a) Seismic-to-core-correlation with oes19 and oes08 showing the composite core reaching down into Event A. b) Types of turbidites detected in the

sediment cores. c) Distribution and location map. d) Lowermost part of composite core (sections 04-D3 and 01-E1) with massive clay cap, representing one event A.

The ability of subaerial mass movements to resuspend sediment when entering the water body mostly depends on (i) the potential energy, i.e. fall height and volume of the rock material, (ii) the subaerial and subaqueous slope gradient (falling/bouncing or sliding), (iii) the character of the rock-slope failure and composition of rock material (debris flow, debris slide, rock fall, rock slide, rock avalanche), (iv) the height of the water column / lake volume, and (v) the presence of rock material in the subaqueous runout-path, which derived from earlier multistage events. Usually, multistage rock-slope failures generate thicker turbidites at the beginning of a sequence than during following events.

Subaerial rock-slope failures continuing in Lake Oeschinen generate *matrix-supported turbidites* and show sections of various thickness (up to 18 cm) with a coarse sandy base of dark grey, blackish limestone (Figure 14b). We interpret those poorly sorted and normally graded matrix-supported layers as rockfall-event related, as they show significant characteristics like high amounts of sharp-edged clasts of black Helvetic limestone in silt to sand size with hardly any organic material (e.g. like LT2 in Van Daele *et al.*, 2015; Wilhelm *et al.*, 2016). The black color derives from the natural color of the Helvetic limestone and not from organic content.

Event Chronology

The event chronology was set up by radiocarbon dating of well-preserved wood samples (Table 2), supported by core-to-core-correlation (Figure 15) and the varve chronology (Amann *et al.*, 2015), collated in an age-depth model for the whole sediment record (Figure 16).

Table 2: Results of radiocarbon dating. OxCal v. 4.2.4 and IntCal13 were used for calibration (BP = 1950 AD).

Section	sample lab code	Sediment depth [m]	Material	C14 age [BP]	Cal age [BP] (2 sigma range)	Cal age [BP]
OES 11-04-B2	ETH-46470	6.30	twig (~0.3 cm^3)	1270 ± 30	1288 to 1091	1190 ± 98
OES 11-01-D3	ETH-46471	11.99	twig (~1.0 cm^3)	2265 ± 30	2348 to 2158	2253 ± 95
OES 11-01-E1	ETH-46472	13.64	wood (~0.8 cm^3)	2465 ± 30	2713 to 2379	2546 ± 167

We checked coincidences with chronicles (Bach, 1935) and historical and prehistorical earthquake events (Earthquake Catalogue of Switzerland ECOS-09, Strasser *et al.*, 2006; Fäh *et al.*, 2011) to refine our results within the uncertainties of the obtained event ages in the independent age model. The age of Lake Oeschinen was determined by radiocarbon dating of a piece of wood from a depth of 13.64 m, situated in the Oeschinen rock avalanche deposits (Figure 14d). The lake formation is dated to ~2550 cal yrs BP and is thus in its present-day extent much younger than expected and not linked to the Kandersteg event ~9.5 cal kyrs BP. Two more wood samples yielded ages of ~2250 cal yrs BP for Event B, and ~1200 cal yrs BP for a turbidite between the events E and F, respectively. The latter sample could not be correlated to a discrete event, but supports the age-depth model in the middle part of the sequence for the interpolation of the dating downwards (events E and D). These data represent maximum ages because the wood had grown before the event happened, and was then entrained and deposited during the mass movement. According to the OxCal age-depth model in Figure 16a, Event E might be a bit younger than suggested in the graphical solution (Figure 16b).

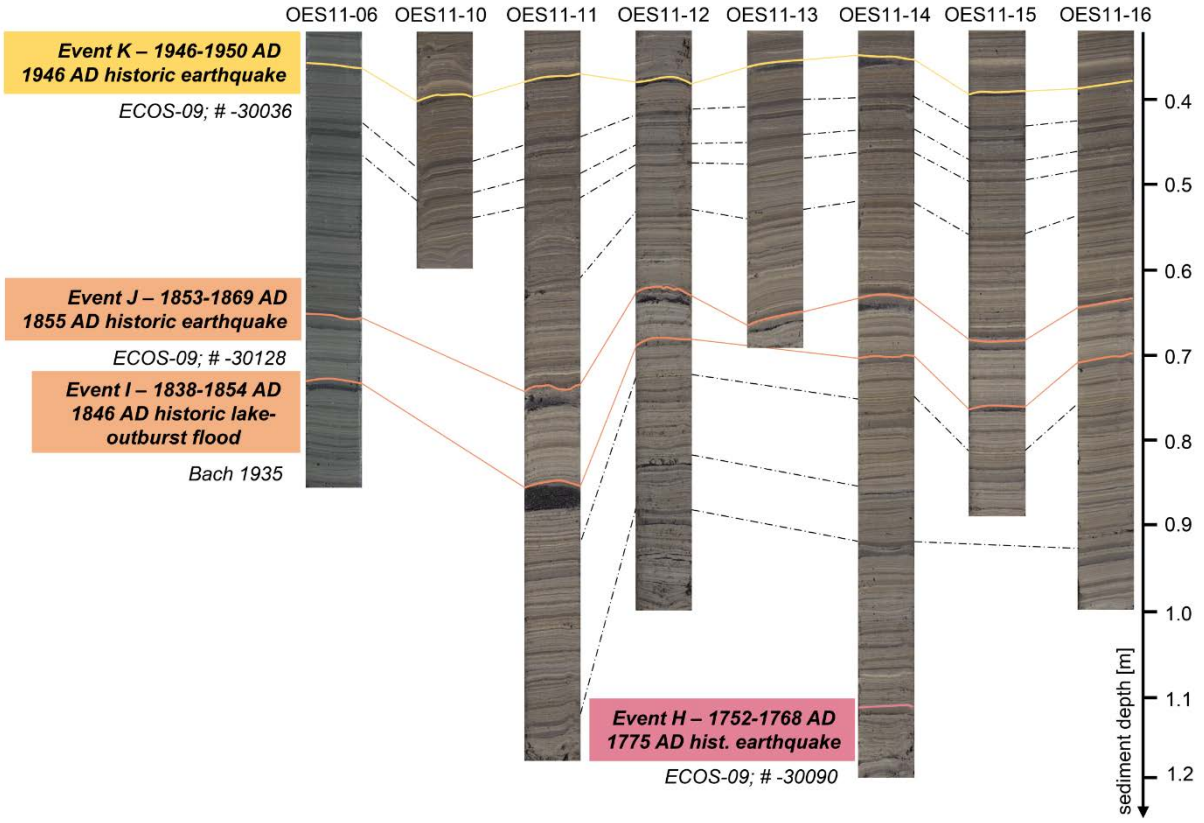

Figure 15: Core-to-core-correlation for short and percussion cores for dating the uppermost event horizons H-K. The turbidite related to Event H is contained in core OES11-14 only, but could be correlated to the composite core and the varve chronology (Amann et al., 2015). Cores OES11-11 and OES11-15 are located in local depressions. Black-dashed horizons act as offset calibration.

The short sediment cores used for core-to-core-correlation (Figure 15) show much less coring artefacts than the composite piston-core sections and are, therefore, better for finding the exact stratigraphic position of an event. Thus, we could even distinguish the two events I and J, which occurred within a time span of only a few years.

Inventory of the Detected Mass-Movement Deposits

The sedimentary record of Lake Oeschinen reaches back to ~2.5 cal kyrs BP. The determined events indicate mass-movement deposits, which derive from subaerial rock-slope failure events that reached the lake and were deposited on the lake floor. The polymethodical approach made it possible to decipher multistage events detaching from the same mountain flank (A-F and I-J, respectively). In the following section, an overview of all detected mass-movement events is given, where each event is presented with its main characteristics. Energy considerations were made after analyzing the seismic profiles and aerial images (Table 3**,** Figure 17 and S4).

Events A, B and C: The lowermost event deposits A, B and C and their turbidites can seismically only be determined in a small "window" with deep seismic penetration. Event A is located at ~13.4 m sediment depth and occurred ~2550 cal yrs BP. These deposits cannot be tracked further to the East because the seismic stratigraphy is masked by free gas in the sediments (Vanneste *et al.*, 2001; Figure 13 and Figure 17b).

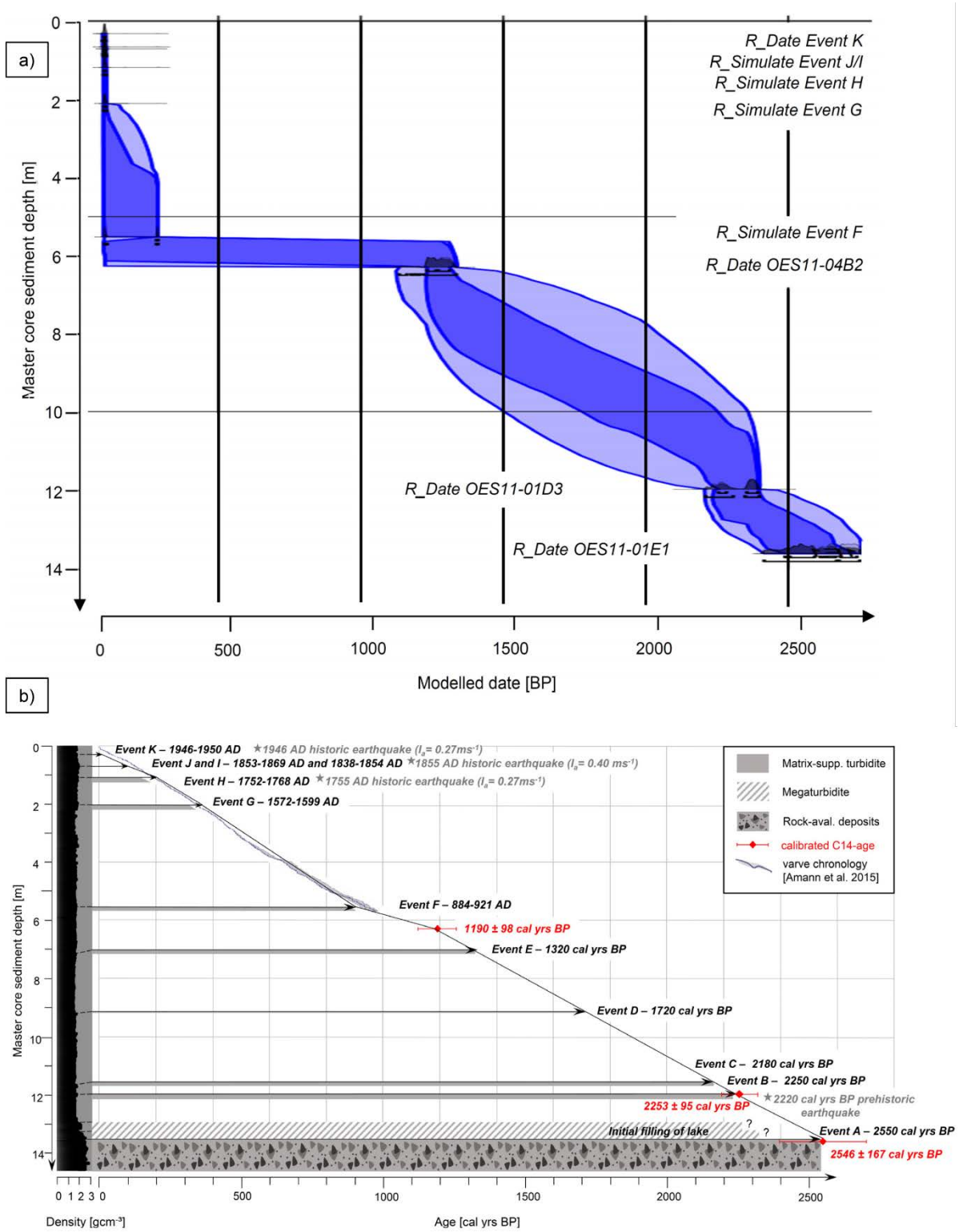

Figure 16: Age-depth models of all events A-K. a) Modelling with OxCal v.4.2.4 and IntCal13 (Bronk Ramsey, 2013; Reimer et al., 2013); light blue depicts the 2-sigma probability range. b) Constructed model with turbidites representing events detected in the composite core and the density values measured with the multi-sensor core logger (left of Figure), plotted with the varve curve by Amann et al. (2015).

The deposits of the events B and C are located at a sediment depth of 11.9 m and ~11.5 m and are dated to ~2250 and ~2180 cal yrs BP, respectively. The events A-C are covered to the western lake basin by the overlying deposits of events D-F and cannot be unequivocally linked to one of the two scarps at the northern flank of Mount Spitzstein. The events had fall heights of

~800 m and a potential energy in the range of 101 GJ (≙24 tons TNT) detaching from the upper scarp, and ~450 m and ~48 GJ (≙11 tons TNT) coming off the lower scarp.

Table 3: Rock-slope failure energies vs. sediment/seismic record.

Event	Age model	Sediment/seismic depth [m]	Volume [m³]	Fall height [m]	Potential energy [GJ]	TNT equivalent [t]
K	1946-1950 AD	0.31 / 0.5	15000	500	20	5
J	1853-1869 AD	0.65 / 0.8	14000 total	750	28 total	7 total
I	1838-1854 AD	0.70 / 0.8				
H	1752-1768 AD	1.18 / 1.1	15000	370	15	4
G	1572-1599 AD	2.10 / ~2.5	n.a.	n.a.	n.a.	n.a.
F	884-921 AD	5.52 / 5				
E	~1320 cal yrs BP	7.05 / ~7				
D	~1720 cal yrs BP	9.12 / 9	~45000 each	400 (low) / 850 (high)	48 (low) / 101 (high)	11 (low) / 24 (high)
C	~2180 cal yrs BP	11.5 / ~11.6				
B	~2250 cal yrs BP	11.9				
A	~2550 cal yrs BP	13.4 / ~13.5				

Events D, E and F: The mass-movement deposits of events D, E and F are detected in the western lake basin and show quite similar distribution patterns, yielding ~1.5 m thick deposits for each event. Their stratigraphic positions occur at a sediment depth of 5.5, 7.1 and 9.1 m, respectively. The deposits of Event F cover and hide the underlying deposits of E and D, which can be only detected in their most distal parts. The event ages are calibrated to 884-921 AD, ~1320 and ~1720 cal yrs BP, respectively. These three event deposits detached from the same mountain flank of Mount Spitzstein, where two large scarp niches lie on top of each other. The event deposits raised the lake dam sequentially, and only parts of the rock material ran into the lake basin.

Event G: This event is identified in the seismic and sedimentary record by a prominent turbidite at ~2.5 / ~2.1 m depth. The distribution of the event deposits, however, cannot be mapped seismically, and the scarp cannot be determined either. Therefore, Event G is not listed in Figure 17 and the related energies could not be calculated in Table 3. The age of this event is calibrated to 1572-1599 AD.

Event H: This is the youngest event in the Southwestern lake basin and marks the last multistage rock-slope failure detaching from Mount Spitzstein. The event deposits are ~1 m thick and lie at a sediment depth of ~1.1 m. Event H is calibrated to 1752-1768 AD and potentially coincides with an earthquake in 1775 AD (ECOS-# -30090). The rock-slope failure occurred at a height of ~370 m above Lake Oeschinen with a potential energy of ~15 GJ (≙4 tons TNT).

Events I and J: In the Southeastern lake, the multistage rock-fall deposits occur in the seismic data at ~0.8 m depth with a thickness of ~0.7 m (Figure 18a). We find the event-related turbidites in the cores at 0.6-0.7 m sediment depth (Figure S2, Figure 14 and Figure 18b). With a temporal separation of only a few years, the two event-related turbidites almost coincide in the seismic record and can only be separated from each other by the detection of onlap structures (Figure 18f). We can also observe an offset between the event deposits and the lake slope with a small turbidite running up against the slope (Figure 18d) – and not only towards the lake center as usual. The sediment core OES11-11 (Figure 18b) shows two turbidites, the first, i.e. the lower of which is slightly thicker than the second (~2.5 vs. ~2.0 cm) and contains

more coarse sand. More fine-grained material was resuspended during the second event, observed in the short cores in Figure 15. Their accurate stratigraphic position could be determined by applying core-to-core-correlation. Considering the varve chronology of Lake Oeschinen (Amann *et al.*, 2015), we calibrated the first event to 1838-1854 AD. With respect to the chronicle of Frutigenland (Bach, 1935), there might be a coincidence with a lake-outburst flood from Lake Oeschinen in 1846 AD, which destroyed arable land in the region around Kandersteg.

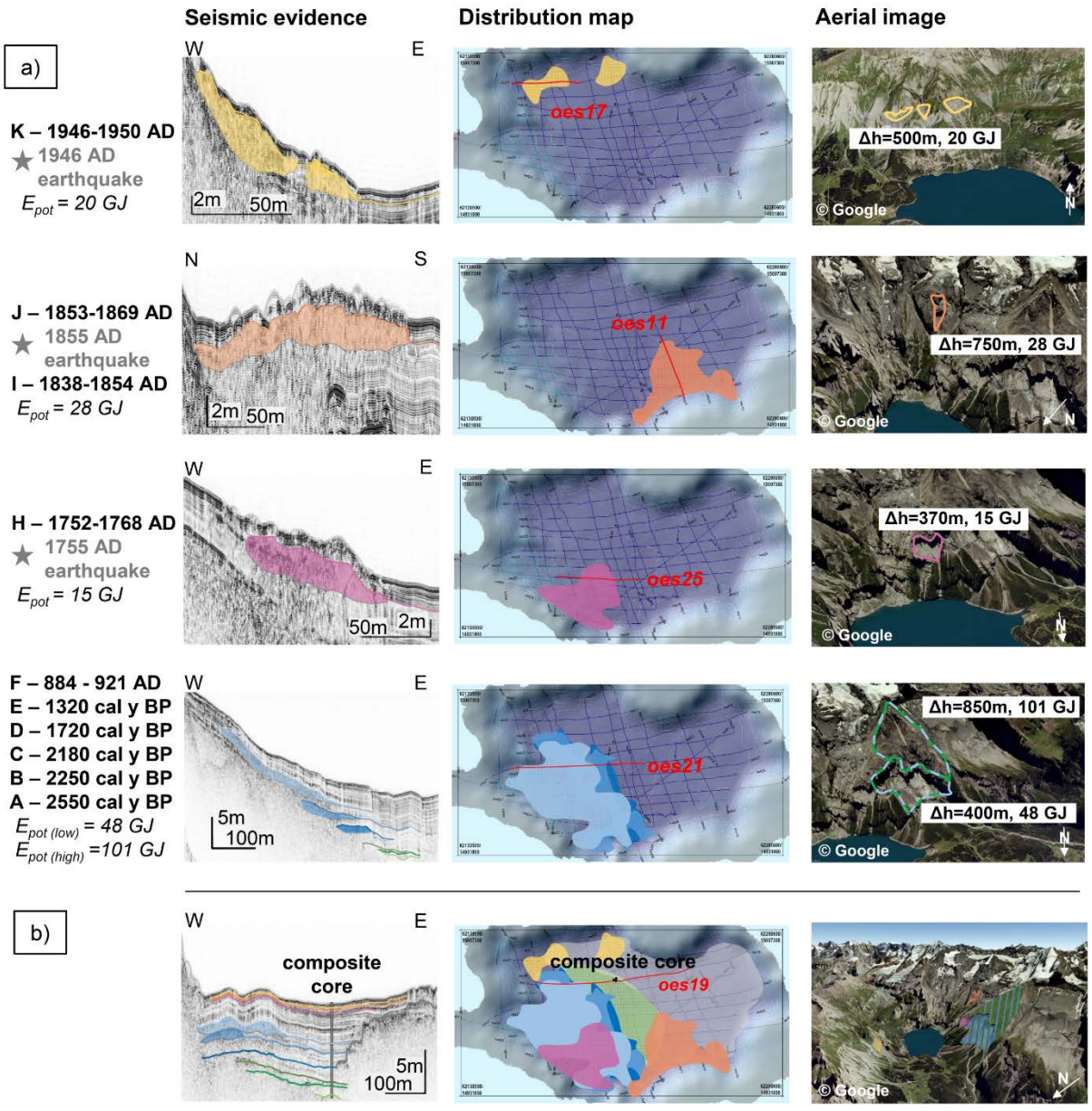

Figure 17: Overview of observed rock-slope failure and debris-flow events A-K (except G). a) Seismic evidence with distribution maps and potential scarps indicated on aerial images with energy assumptions, b) all events and the gas distribution (grey) collated in one map next to the core, and a 3D-view of all scarp niches (image © 2016 Google, Landsat, Cnes/Spot, Flotron/Perrinjaquet). See Figure S4 for detailed aerial images.

The second event is calibrated to 1853-1869 AD, and potentially coincided with a strong historic earthquake in 1855 AD (ECOS-# -30128). The aerial images depict at least five potential scarp niches between an elevation of ~2540 m a.s.l. and the toe of the lowermost scarp niche

at ~2110 m a.s.l resulting in a fall height between 530 m and 960 m (Figure 18c). It is not possible to ascribe the scarps and the deposits to the single events. For our qualitative approach, an average fall height of 750 m was chosen - which is also the minimum fall height for the uppermost 4 out of 5 potential scarp niches - yielding a total potential energy in the range of ~28 GJ (≙7 tons TNT) for both events.

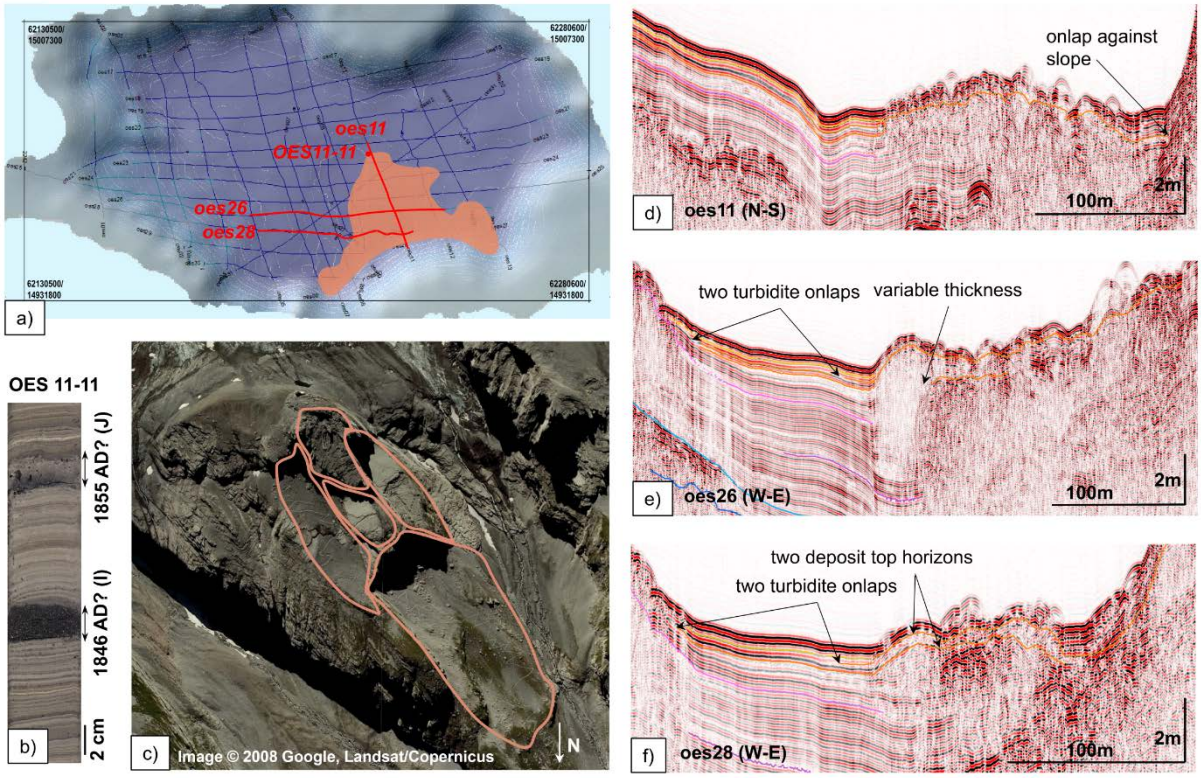

Figure 18: Multistage events I and J. a) Overview of seismic profile lines, core location and event deposits. b) Short core OES11-11 with distinct matrix-supported turbidites. c) Aerial image with a 3D-view of five potential scarps. Seismic profiles oes11 (d) with onlap against slope, and oes26 (e) and oes28 (f) showing complex rock-fall deposits with variable thickness and multiple events along same transect.

Event K: The youngest event can be detected in the Northwest of the lake basin in ~0.3 m sediment depth with an estimated thickness of the deposits of 1 m. This event entered the lake at the northern shore. The deposits are widely spread, flat and comparatively thin. In contrast to the other events, Event K shows a seismic horizon that can be tracked all over the lake basin. According to the age model, this rock-slope failure is dated to 1946-1950 AD and potentially relates to a historic earthquake in 1946 AD (ECOS-# -30036). Three potential scarp niches can be identified at 500 m height above the lake level. The potential energy related to this event is ~20 GJ (≙5 tons TNT).

Discussion

Limitations of Analysis

In the sedimentary subsurface of Lake Oeschinen, eleven rock-slope failure event deposits were detected. The mean recurrence rate of 200-300 years between the single events allow for an identification of the events on the seismic lines because the turbidites are separated by a sufficiently thick section of laminated background sediment. Some of the event-related tur-

bidites are very small (e.g. Event D with ~2 cm), which makes it challenging to trace the stratigraphic positions in the seismic record. Thus, the event catalogue might be incomplete as more multistage events might have occurred without generating prominent turbidites as between the events C and D. If two or more matrix-supported turbidites occur in close stratigraphical vicinity, we chose the thickest and/or the lithologically most 'prominent' for the event layer. For example, Event G was defined at a seismic depth of ~2.5 m and correlated with a turbidite at ~2.2 m composite depth in core section OES11-01-A2 (and not to those at ~2.4 m in OES11-01-A3 or the one at ~2.1 m composite depth in OES11-01-A2; see Figure S2 for composite core pictures). The chosen layer contains the highest amount of blackish sand, which implies a rock-slope source and high transport energy. Other matrix-supported turbidites in the sediment record may indicate reworked event material, e.g. after heavy rainstorms, or more rock-slope failures of smaller magnitude. They may vary due to (i) channelized flow vs. surface runoff during heavy precipitation events and (ii) different source areas (vegetated areas vs. bare rocky slopes). Those were excluded from our inventory due to the lack of seismic evidence. In the eastern basin, free gas inhibits seismic penetration and detection of potentially further event deposits.

Energy considerations are important for a better understanding of the mobility processes of multistage rock-slope failures. Such calculations are only based on order-of-magnitude estimates of the deposit volumes and the positions of the center of gravity of the failed rock mass. The volume is estimated on the seismic data in respect to the with rock/debris material covered lake-floor area and the deposit thickness, the latter of which is hardly detectable for superimposed multistage event deposits. Turbidites are excluded from volume estimation, as it remains unclear how much sediment is reworked. The older multistage event deposits can only be mapped at their distal parts (events B-E). The volume of the deposits outside the lake (concerning the lake-damming event deposits A-F) cannot be taken into account for the calculation of the potential energies. In general, we rather underestimated fall heights (assumed mid center of gravity often lies below average fall height) and deposit thicknesses in order to avoid exaggerated statements and rounded the volumes to 1000´s of m^3 so that we consider the energy considerations as a first-order estimate.

Concerning the age-depth model, we are confident of the ages of the events F-K based on the varve chronology down to a sediment depth of ~5.6 m. The error of the varve counting sums up to ~32 years for Event F in the last 1100 years (i.e. only ~3%). The uncertainties of the lowermost events B and A are given by the radiocarbon-dating supported calibration (Figure 16a).

The Rock-Slope Failure – Lake Interaction Inventory

The Oeschinen rock avalanche has been described and connected to the scarp niches at Mount Spitzstein since the last century (Groll, 1903; Turnau, 1906; Penck and Brückner, 1909). Turnau (1906) interpreted talus cones on the lake dam as repeated rock-slope failures. Groll (1903) noticed talus cones, deriving from the upper scarp and covering parts of the lower scarp. He also detected the scarp niches referring to the events I and J “in den Fründen”. This study shows that Mount Spitzstein is affected by at least six multistage failure events (A-F, maybe G) deriving from two main scarp niches (Figure 17). For facilitating the allocation of potential

niches, we analyzed the event-related turbidites in the lake, which respond to impact energies (see Table 3 for energy calculations, and Figure 16b for relative turbidite thickness).

The multistage rock-slope failure events at Mount Spitzstein provided massive amounts of rock debris and fragmented sediments over time, covering subaqueous slopes and increasingly filling up the basin. The deposits show a specific emplacement pattern, entering the lake from South and running out in the southwestern part of the lake basin. Newly incoming rock material falls onto the rocky surface of boulders that were deposited earlier, and most of the kinetic energy is horizontally diverted into wave propagation, or ice breakthrough during winter, at the first impact on the lake surface. The more initial energy is transferred to the wave generation, the less velocity and energy remains in the subaqueous movement after the impact (Fine *et al.*, 2003; Hunt *et al.*, 2011). Subaquatically, lots of the remaining kinetic energy is then transferred into friction so that the rock fall stalls in between the older boulders, causing a high roughness. The velocity of the mass movement decreases, and so the runout distance.

Younger event deposits superimpose, partially cover and hide older ones, but they do not reach the frontal limits of the earlier event deposits (Figure 17). Every successive failure of the over-steepened and unstable rock slope leads to more rock material either sliding/flowing or falling/bouncing downslope. A sliding or flowing movement causes the landslide material to displace previous deposits and to push them forward onto the undisturbed lake floor, generating a further turbidity current (Masson *et al.*, 2006). Here, resulting deformation structures should develop in front of the pushed event deposits apparent in the seismic record. In Lake Oeschinen, however, deformation structures are missing so that we rather expect a steep impact of bouncing and falling blocky rock fragments.

For the scarp niches at Mount Spitzstein, two scenarios need to be considered: (i) a detachment from the lower of the two eligible scarp niches on the southern mountain flank with potential energies in the range of 48 GJ, and (ii) an active upper scarp, with event energies of 101 GJ (Table 3). Event A (Oeschinen rock avalanche) raised the lake dam significantly and generated the two thickest turbidites of the sediment record (~32 and ~28 cm) on top of each other at a depth of ~13.5-13.0 m, indicating an initial filling of the lake basin. This high-energy event might have detached from several scarps, and marks the start of a multistage series. It has been observed that subsequent failures generate thinner turbidites, which seems to reflect reduced event energy and velocity (Wynn and Masson, 2003; Masson *et al.*, 2006; Hunt *et al.*, 2011; Hunt *et al.*, 2013; Hunt *et al.*, 2015). In fact, the first three events A-C show a significant difference in thickness and content of coarse material. The thick turbidites of A-C contain much more coarse material than the turbidites of the events D, E and F (Figure S2), which might also suggest a higher energy level due to detachment from the upper scarp. The turbidite of Event D stands out because its thickness (~2 cm) is similar to those of the events H-K (~1-2 cm), and much smaller than the turbidites of B, C, E and F (~15-18 cm), even if thicknesses are potentially overestimated due to deformed sediment laminae (Figure S2). Therefore Event D is interpreted to imply a lower potential energy and to have detached from the lower scarp with a smaller volume.

The turbidites related to the multistage events B-G are observed to be significantly thicker than those of events H-K, which corresponds to the 3-6 times higher event energy compared

to Event H (see Table 3). With a fall height of ~370 m, Event H had the smallest potential energy compared to all other events. The rock slope and the runout-path towards the lake are quite flat and the rock material slid on a delta and onto earlier event deposits (B-G). These characteristics explain the lack of a prominent turbidite. The multistage events I and J had a potential energy in the range of 28 GJ and a fall height of ~750 m with a slope steepness of ~80 %. Here not only the multistage character influences the sedimentation process, but also the type of movement. The rock material rather bounced than slid into the water body. The free fall of the boulders resulted in a massive impact on the lake surface and generated impulse waves. Only little kinetic energy was left, when the rock material dropped on the lake floor. The generated turbidites can only be conclusively determined as event layers at the close core location OES11-11 (Figure 18b and Figure 15). Paris *et al.* (2011) postulated that the impulse wave is reduced by 75% when debris is released over 300 seconds rather than in one block. This supports the assumption that Event I consisted of large single blocks falling simultaneously or rapidly after each other into the lake and causing high impulse waves with short travel times (Freundt *et al.*, 2007). Finally, Event K, with a potential energy of ~20 GJ, generated a thin, yet prominent turbidite that can be traced throughout the lake basin, indicating a high amount of incoming or resuspended fine-grained material. The aerial images show large talus cones below the scarp niches and lots of debris lying on the runout-paths. Therefore, Event K could be interpreted as debris slide/flow, which entered the lake on a shallow delta distributing the fine-grained material over a wide range of the basin.

Potential Triggers

The events in Lake Oeschinen show surprisingly high recurrence rates. Separating tectonic from climatic causes and triggers for rock falls/slides is a major challenge and has been studied on shorter time scales in order to exclude the potential control of earthquakes (Huggel *et al.*, 2013). The events H, J and K potentially coincide with historic earthquakes that are intense enough to potentially trigger rock falls at Lake Oeschinen (Table 4). There is a remarkable coincidence of three events with earthquakes with high Arias Intensities, namely Event J in 1855 AD (I_a=0.4 ms^{-1}), Event K in 1946 AD and Event H in 1755 AD (both with I_a=0.27 ms^{-1}). Also the prehistoric Event B, dated to 2250 cal yrs BP, might be linked to the well documented ~2200 cal yrs BP earthquake (Monecke *et al.*, 2006; Strasser *et al.*, 2006; Kremer *et al.*, 2017). This study at Lake Oeschinen shows that it might have had the potential to trigger rock falls in the Bernese Oberland, which is also supported by (Köpfli *et al.*, 2018). The link between seismic triggering and rock-slope failure is often difficult to pinpoint since i) seismic shaking might prepare but not directly trigger rock-slope failure, ii) seismic attenuation is anomalous in the intraplate region and in addition influenced by topographic effects, and iii) lithological strata may provide weak layers sensitive especially to low seismicity (Keefer, 2002).

Moreover, heavy rainfalls need to be considered as trigger of rock-slope failures (Chen and Hawkins, 2009) and debris flows (maybe Event K). A lake-outburst flood in 1846 AD (Bach, 1935) was potentiallycaused by Event I. Releasing the high potential energy and the enclosed lake surroundings could have favored the generation of large water waves and an overtopping of the lake dam (Slingerland and Voight, 1982; Vischer *et al.*, 1998). The flood was thought to be linked to the heavy rainfalls that occurred in the summer of 1846 AD, and nobody observed the rock fall (Bach, 1935).

Table 4: Calculation of Arias Intensity (Ia) and Newmark displacement (DN) related to historic earthquakes coinciding with the events K, J and H. Earthquake data taken from the SED Earthquake Catalogue of Switzerland (ECOS-09).

Event	Age model	Earthquake	M_w	Epicenter (coordinates CH1903/LV03)	r [km]	α [°]	I_a [ms^{-1}]	$D_{N,\ min\text{-}max}$ [cm]
K	1946-1950 AD	25 Jan 1946	5.8	Wildhorn (597000/133200)	30.1	40	0.27	0.1-2.8
J	1853-1869 AD	25 Jul 1855	6.2	Stalden-Visp (631700/119900)	30.3	42 27	0.40	0.3-6.7 0.5-12.1
H	1752-1768 AD	09 Dec 1755	5.7	Brig-Naters (641700/130000)	27.3	35	0.27	0.1-3.1

The high recurrence rates and the multistage character of the rock-slope failures in a proglacial environment also support the role of triggers like stress adaptation and altered rock-mass strength due to erosion (Moore *et al.*, 2009; Krautblatter and Moore, 2014; Leith *et al.*, 2014). The Oeschinen rock avalanche (Event A) happened during the early Subatlantic when the retreat of glaciers and presumably permafrost weakened the mountain flanks (Joerin *et al.*, 2006). Also in the present warming period of the late Subatlantic, massive permafrost ice is found close to the failure scarps at the Doldenhorn at very low altitudes of ~2500 m a.s.l. (C. Hilbich, personal communication, 2017) and is exposed to degradation. The warm and humid climate during the Atlantic might have favored chemical weathering presumably on limestone surfaces, prone to karst formation, and also weakened mountain flanks. During the period of the Little Ice Age, unusual glacier activity and environmental changes may have weakened the slopes. Finally, rather spontaneous failure due to repeated freeze-thaw weakening has to be considered.

Early History of Oeschinen Valley – Reconstruction of Paleotopography

Analyzing the seismic and sediment record of Lake Oeschinen allows to reconstruct the paleotopography of the Oeschinen valley (Figure 19). Free gas occurs in the eastern basin (Figure 13 and Figure 17b) and supports the reconstruction of the dimensions of the Oeschinen rock-avalanche deposits. The topography (Figure 12) indicates that the Kandersteg rock avalanche descended slightly into the Oeschinen valley, considering a radial spreading of rock-avalanche deposits in a non-confined valley, as observed at the Tschirgant in Austria (Dufresne *et al.*, 2016a). The deposits probably built a first low dam at the valley entrance forming a shallow basin with a paleolake producing sediments with abundant organic material. This paleolake probably remained at a shallow lake level until ~2.5 cal kyrs ago, when the Oeschinen rock avalanche detached from Mount Spitzstein and raised the lake dam significantly. The generation of the fine-grained and graded sediments in the two megaturbidites and their clay caps of Event A deposits (Figure 14d) support the presence of such a paleolake providing sediments prone to resuspension and settling in an already existing water body. The dust produced by the rock avalanche forms the subsequently deposited clay layer (Deplazes *et al.*, 2007). Events B-F acted to increase the dam height. In the growing lake, organic material from the original lake was buried and started to decompose, thereby producing free gas which blanks the seismic record in the eastern lake. Whereas in the eastern lake the free gas likely rises in the overlying strata, the event deposits in the western lake seal the gas. From their distributional

pattern (Figure 17b) and the springs at the top of the western side of the dam (Niklaus, 1967), we speculate that the deposits of the events A-C are less permeable than those of the events D-F.

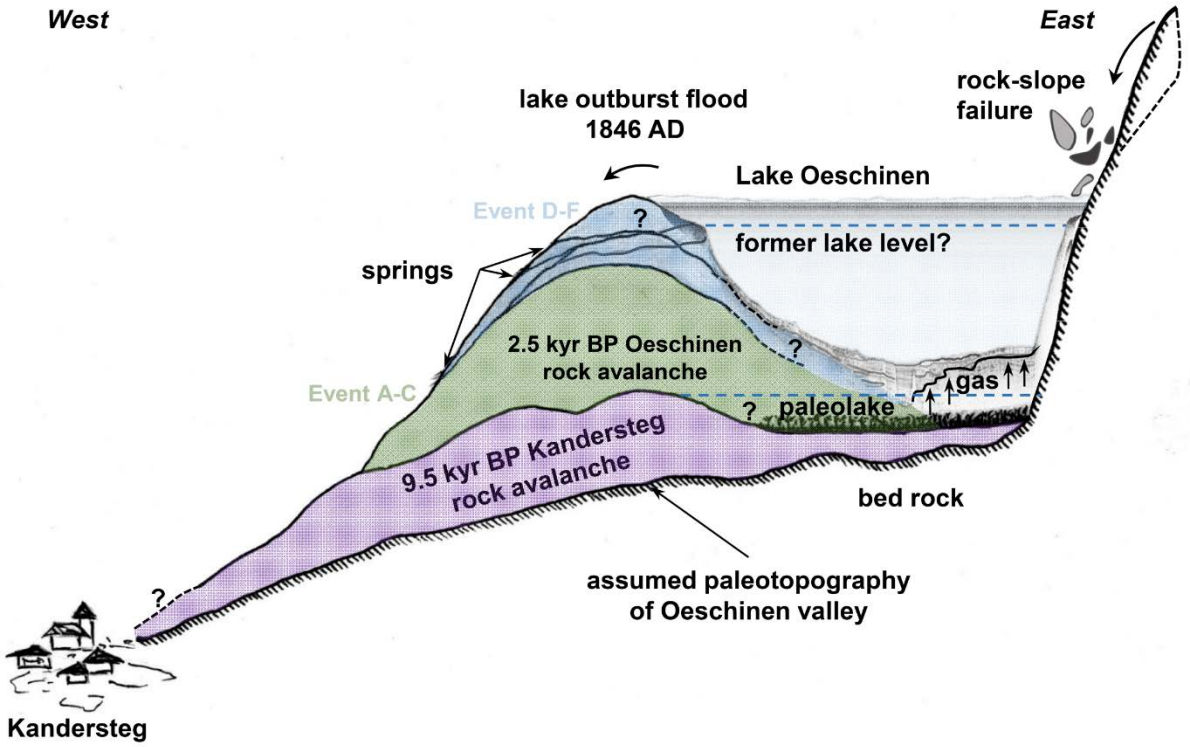

Figure 19: Synthetic sketch highlighting the polyphase development of modern Lake Oeschinen. Assumed paleotopography of Oeschinen valley, covered with rock avalanche deposits from 9.5 cal kyrs BP Kandersteg event (Tinner et al., 2005) and the multistage events from Mount Spitzstein, A-C (green) and D-F (blue). Spatial limits of the single events remain unclear. Without scale.

We suppose that the lake dam reached its present-day height after the last multistage event F detaching from Mount Spitzstein, or possibly after Event G, whose trajectory is uncertain. Whereas (Köpfli *et al.*, 2018) ascribe the dam deposits to two events (possibly Kandersteg and Oeschinen rock avalanche), this study rather indicates at least six multistage rock-slope failures (events A-F) building the dam. The events H-K did not contribute to the evolution of the dam because they detached away from Mount Spitzstein. Event I, however, might have generated a hazardous outburst flood, which destroyed parts of the arable land in the Kander valley (Bach, 1935) and might have lowered the lake level to an unknown extent. The inhabitants of Kandersteg channelized the Oeschibach stream in 1847, shortly after the catastrophe.

Conclusions

Lake sediments act as a natural chronometer providing a powerful dateable record of discrete rock-slope failure events. Turbidites and event deposits on the lake floor deliver insights into the properties of the related rock-slope failures, which may include age, volume, affected area, subaerial or subaqueous origin of the mass movement, and multistage or single failure (Hunt *et al.*, 2015). Multistage subaerial rock-slope failures of the Lake Oeschinen area can be reconstructed by analyzing lake sediments with high-resolution seismic surveys and sediment

cores. Aerial images allowed the allocation of scarp niches to failure events, and were used for energy considerations. The sediment-based event stratigraphy is absolutely dated using radiocarbon dating, historic chronicles and a varve chronology in the upper ~5.6 m of the sediment record.

Lake Oeschinen provides a unique inventory of multistage rock-slope failures covering a history of ~2.5 cal kyrs BP. Eleven events could be distinguished, from which at least six detached from the same direction at Mount Spitzstein. The data imply surprisingly high recurrence rates (~1/300 yrs), and four events potentially coincided with (pre-) historic earthquakes. The lake in its present-day extent is thus much younger than expected and is not linked to the Kandersteg event ~9.5 cal kyrs BP.

We identified rock-slope failures having potential for triggering massive flood waves, and correlated a witnessed lake-outburst flood in 1846 AD (Bach, 1935) with a rock fall. Huggel *et al.* (2013) detected a similar remarkable coupling of hazardous processes at the Lower Grindelwald Glacier. These studies provide evidence that subaerial rock-slope failures impacting on glacial or moraine-/landslide-dammed lakes will become more common and relevant in high-mountainous regions due to future climate warming and glacier/permafrost retreat.

In conclusion, this study shows that temporal and spatial correlation of reflection seismic data and sediment cores from lake basins combined with aerial images provide a valuable approach for deciphering multistage subaerial rock-slope failures, constraining the event chronology and improving our knowledge of the rock-slope failure involved processes and related hazard.

Acknowledgments

The authors would like to thank Martin Grosjean and his team from the Oeschger Centre for Climate Change Research in Bern for the support during field work at Lake Oeschinen. A special thanks goes to Benjamin Amann who provided us with the varve age information. We further thank the Limnogeology Group at ETH Zurich for the help in the field, in the laboratory and with data processing. Sibylle Knapp acknowledges PhD funding from the German National Academic Foundation, which has enabled this study to be completed. We also want to thank the reviewers for their suggestions and remarks helping to improve this manuscript.

5.2 Lake Eibsee: Displaced Paleolake and Effects of Rock-Avalanche Impact Deciphered from Terrestrial Sediments

This chapter has been published in the Journal Earth Surface Processes and Landforms under the title "Impact of an 0.2 km³ Rock Avalanche on Paleolake Eibsee (Bavarian Alps, Germany) – Part I: Reconstruction of the Paleolake and Effects of the Impact" by Sibylle Knapp, Philipp Mamot, Bernhard Lempe and Michael Krautblatter (2020a).

Abstract

Rock avalanches destroy and reshape landscapes in only a few minutes and are among the most hazardous processes on Earth. The surface morphology of rock avalanche deposits and the interaction with the underlying material are crucial for runout properties and reach. Water within the travel path is displaced, producing large impact waves and reducing friction, leading to long runouts. We hypothesize that the 0.2 km³ Holocene Eibsee rock avalanche from Mount Zugspitze in the Bavarian Alps overran and destroyed Paleolake Eibsee and left a unique sedimentological legacy of processes active during the landslide. We captured 9.5 km of Electrical Resistivity Tomography (ERT) profiles across the rock avalanche deposits, with up to 120 m penetration depth and more than 34,000 datum points. The ERT profiles reveal up to ~50 m thick landslide debris, locally covering up to ~30 m of rock debris with entrained fine-grained sediments on top of isolated remnants of decameter-wide paleolake sediments. The ERT profiles allow us to infer processes involved in the interaction of the rock avalanche with bedrock, lake sediments, and morainal sediments, including shearing, bulging, and bulldozing. Complementary data from drilling, a gravel pit exposure, laboratory tests, and geomorphic features were used for ERT calibration. Sediments overrun by the rock avalanche show water-escape structures. Based on all of these datasets, we reconstructed both position and size of the paleolake prior to the catastrophic event. Our reconstruction of the event contributes to process an understanding of the rock avalanche and future modelling and hazard assessment. Here we show how integrated geomorphic, geophysical, and sedimentological approaches can provide detailed insights into the impact of a rock avalanche on a lake.

Introduction

Massive rock-slope failures cause more than 60 % of all catastrophic landslide disasters (Evans *et al.*, 2006). The interaction of the rockslide and rock avalanche material with the substrate over which they travel strongly influences runout properties (e.g. Abele, 1994; Hungr and Evans, 2004; Dufresne *et al.*, 2010; Robinson *et al.*, 2015). Erodible and deformable substrates as well as obstacles may divide the rock avalanche into multiple lobes, and their deposits often show complex emplacement structures with longitudinal and transverse ridges (Hewitt, 2006; Dufresne *et al.*, 2015; Dufresne *et al.*, 2016a). Water reduces basal friction of the sliding mass, resulting in increased runout velocity and length (Abele, 1997; Erismann and Abele, 2001; Legros, 2006). Large landslides that enter lakes or other water bodies have generated disastrous waves up to several 100 m high (e.g. Lituya Bay; Fritz *et al.*, 2009). Landslide-triggered waves may also transform into debris avalanches or debris flows that endanger human lives and infrastructure over a wide area (Iverson *et al.*, 1997; Walter *et al.*, 2020). Researchers have analysed landslide-triggered impact waves in the laboratory (e.g. Evers and Hager, 2016;

Miller *et al.*, 2017), reconstructed displacement waves by numerical modelling (e.g. Kafle *et al.*, 2016; Gylfadóttir *et al.*, 2017), and provided insights into the sedimentology of impact-wave deposits (e.g. Roberts *et al.*, 2013; Dufresne *et al.*, 2018).

In spite of the scientific progress described above, the reconstruction and modelling of ancient events often remain challenging, and become speculative, as researchers are confronted with a lack of data on paleotopography, substrate characteristics, and the possible involvement of water. If the landslide mass is large relative to water depth, much of the water in a lake will be pushed out of the impact zone rather than entrained (e.g. Miller *et al.*, 2017). In such cases, the resulting landform may resemble that of dry rock avalanches, even though they ran out on water-saturated sediments or entered a lake (Shaller, 1991). Water-escape structures within sediments overrun by landslides may provide evidence of water (Pavoni, 1968a; Lowe, 1975; Yarnold, 1993), but the basal contact between the rock avalanche deposits and underlying substrates are rarely accessible (Dufresne *et al.*, 2015). Hence, geomorphic evidence is often used to infer the presence and role of water in massive rock-slope failures (Plafker and Ericksen, 1978; Shaller, 1991; Siebert, 2002). This approach, however, can be problematic for high-energy events because the water may not become fully incorporated into the streaming debris.

To date, no study has documented sedimentology that reveals the spatial and temporal reconstruction of a rock avalanche that has entered a lake and displaced its water. In this paper, we focus on this issue by presenting evidence for the existence and size of a paleolake in the German Alps that was overrun by a rock avalanche. We marry geomorphological mapping with a geoelectrical survey and sedimentological analysis of outcrops and drillhole data to prove the existence of this paleolake and to provide an estimation of its size. The geoelectrical profiles provide insights into the structure, thickness, and distribution of the rock avalanche deposits and their interaction with lake water and lake sediments. Our results offer an explanation for the exceptionally long runout of the rock avalanche (9-10 km; Jerz and Poschinger, 1995) and support our paleotopographic reconstruction, thus providing a valuable contribution to future modelling and hazard assessment.

Lake Eibsee and Mount Zugspitze

Geographical Setting and Geology

Lake Eibsee is located in the Wetterstein Mountains in the southernmost part of Bavaria at an elevation of 973 m a.s.l. It lies at the foot of Mount Zugspitze, the highest summit in Germany at 2962 m a.s.l. (Figure 20a). This area is of considerable research interest as it lies at the edge of the Northern Calcareous Alps and is prone to large rock-slope failures in carbonate rocks (Krautblatter *et al.*, 2012b). The rock avalanche that is the subject of this paper detached from the scarp niche ‘Bayerisches Schneekar’ on the north flank of Mount Zugspitze. The Zugspitze comprises Triassic limestones and dolostones of the dislocated and overthrust Wamberg Anticline (Rüffer, 1995; Haas *et al.*, 2014). The Eibsee Syncline, over which these rocks have been thrust, are Jurassic and Cretaceous limestones and dolostones with low permeability that favour the presence of a paleolake on the valley floor (Tollmann, 1976; Hornung and Haas, 2017).

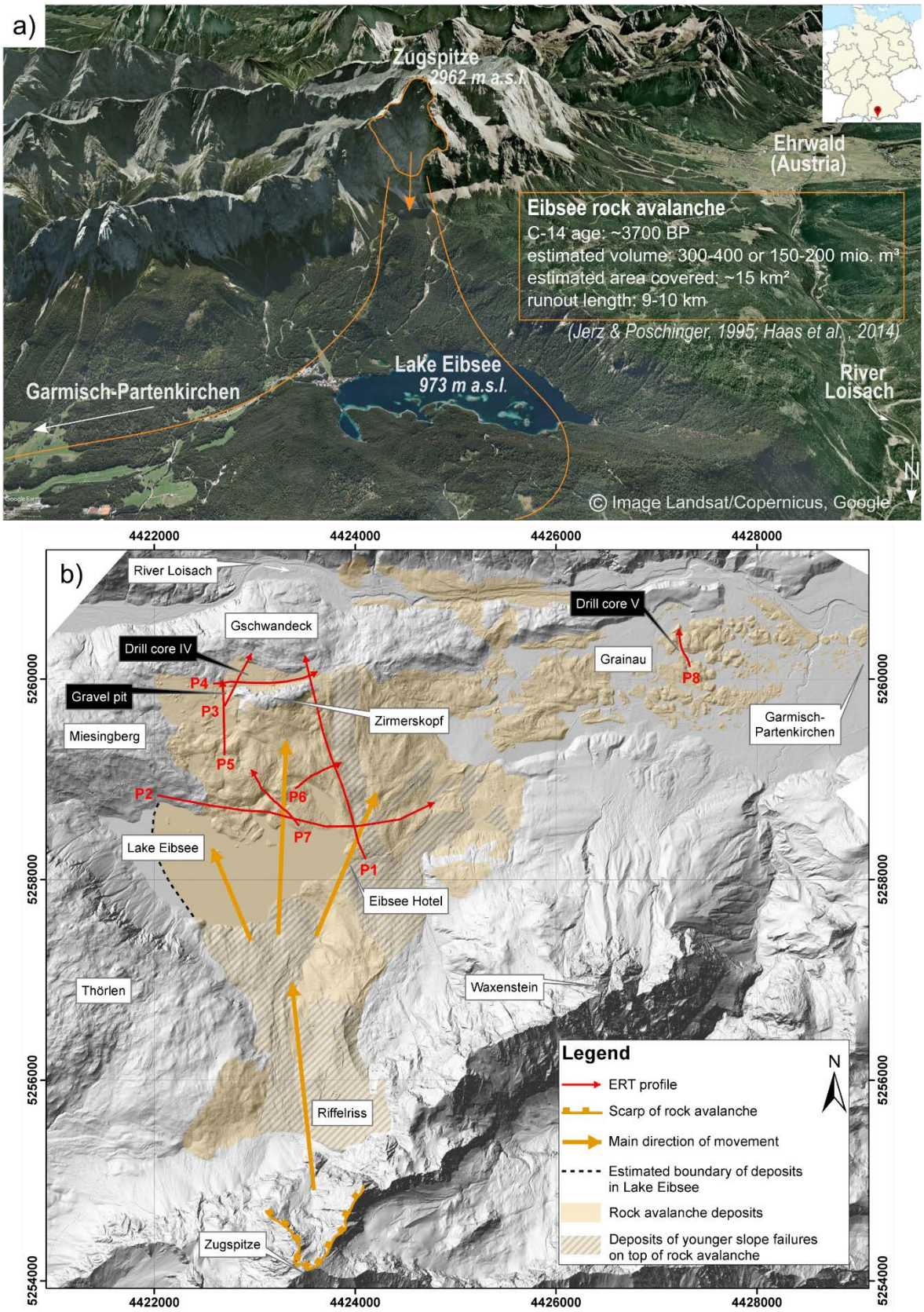

Figure 20: a) Satellite image with a 3D-view of the Wetterstein Mountains in southern Germany, showing Mount Zugspitze (2962 m a.s.l.) and the scarp of the Eibsee rock avalanche, modern Lake Eibsee and part of the runout zone towards Garmisch-Partenkirchen. b) Lidar image (hillshade) with overview of the scarp niche Bayerisches Schneekar at Mount Zugspitze and the area covered with rock-slope failure deposits. The locations of ERT profiles

P1-P8 are shown as red lines. Coordinates are given in Gauss-Krüger Zone 4 (Bavarian Surveying and Mapping Authority, 2006).

Eibsee Rock Avalanche

The Eibsee rock avalanche is the largest rock-slope failure in Bavaria (Abele, 1974). The landslide deposit covers an area of ~15 km² and has a runout length of 9-10 km and a maximum vertical travel distance of ~2.3 km (Jerz and Poschinger, 1995; Haas *et al.*, 2014). Volume estimates range from 400-600 million m³ (Abele, 1974; Prager *et al.*, 2008) and 300-400 million m³ (Jerz and Poschinger, 1995) to 150-200 million m³ (Haas *et al.*, 2014; Leith *et al.*, 2016). Vidal (1953) initially interpreted the debris to be glacial, but Abele (1974) recognized them to be rock avalanche deposits. The main flow direction is to the north, but a large lobe extends to the east towards Garmisch-Partenkirchen (Figure 20). Jerz and Poschinger (1995) obtained a radiocarbon age that dates the event to ~3700 BP (Part II, the companion to this article, Knapp *et al.*, 2020b). They inferred that the landslide had overridden a lake based on the presence of displaced lake clay in a drillcore, and accordingly suggested that the long runout resulted from the involvement of the lake waters. Haas *et al.* (2014) proposed a paleolake situated at the same location as modern Lake Eibsee. However the displaced clay site is far from the modern lake, and the existence and size of a paleolake remained speculative.

Methods

Geomorphological Mapping

Geomorphological mapping was performed at a scale of 1:10,000 on airborne laser-scan images and topographic maps. A bare-earth digital elevation model (DEM) with 1-m resolution was provided by the Bavarian Surveying and Mapping Authority (2006). We mapped characteristic landforms of the rock avalanche deposits, distinguishing between longitudinal and transverse ridges and valleys. To evaluate landslide flow directions, we covered the study area with a grid of 200-m-wide cells. The 200-m cells divided ridges and valleys into smaller segments. A ridge or valley was classified as ‘longitudinal’ if it diverges no more than 30° from the mean flow direction of the segment, and ‘transverse’ if it diverges no more than 30° from the orthogonal to that direction. An ‘undefined’ orientation refers if the angle relative to the mean flow direction is 30-60°.

Electrical Resistivity Tomography (ERT)

We performed an ERT survey with an ABEM SAS 1000 Terrameter with 81 electrodes. The roll-along method was employed along eight two-dimensional profiles (Figure 20b, Table S3) with electrode spacings of 5 m and 4 m using 100-m-long cables, as well as one profile with a 10 m electrode spacing using 200-m-long cables. All measurements were made with Wenner and Schlumberger arrays and the same current settings (up to 200 mA and 400 V, respectively). The contact resistance of each electrode was tested before measurements were started.

Data were processed with the inversion software RES2DInv (Loke, 2006) in three steps: (i) bad datum points (few outliers) were eliminated; (ii) the data were inverted using robust inversion to avoid smoothing the resistivity gradients (Sass, 2004); and (iii) in the case of profile P8, we used a finer mesh size to cope with high-resistivity contrasts (Krautblatter and Hauck, 2007) and inverted the data with a half electrode spacing of 2.5 m.

The ERT profiles were calibrated in the field where data from drillings and outcrops are available, and the measured values of apparent resistivity were cross-checked with laboratory data on the different rock types (Plattenkalk Limestone, Wetterstein Limestone and Hauptdolomite).

Sedimentological Analysis

A detailed sedimentological analysis was undertaken in a gravel pit northwest of Mount Zirmerskopf to facilitate the recognition and characterization of distal rock avalanche deposits. Two sediment samples of matrix-rich bands were analysed by wet sieving using the Euronorm DIN EN ISO 17892-4 (2017-04) protocol and classified based on their fractal dimension (Xu *et al.*, 2001; Dufresne and Dunning, 2017). The results are presented using *DCSIEVE* software.

Results and Interpretation

The results of the complex flow behaviour of the Eibsee rock avalanche can be seen in deposit morphology, bulk material composition related to mixing or entrainment of substrate material and water (ERT), and rock avalanche lithofacies (sedimentology).

Rock Avalanche Landforms and Interpretation

Geomorphic mapping revealed several features characteristic of rock avalanches (Figure 21). Parallel or radiating ridges with small valleys or depressions in between can be found throughout the study area. The longitudinal ridges, oriented towards the north, are common. The ridge surfaces are covered with limestone mega-blocks that derived from the scarp niche (Wetterstein Limestone), many of them exceeding 10 m in diameter. The largest blocks, with diameters of 20 m, lie along the main flow path. All ridges consist entirely of rock avalanche debris. Debris flows and sturzstrom-like debris flow deposits are present locally on top of the rock avalanche deposits (Hornung and Haas, 2017). Swamps are present at the west margin of the rock avalanche adjacent to bedrock slopes and north of Mount Zirmerskopf.

Topographic interference leads to longitudinal and transverse confinement of a rock avalanche (Hewitt, 2006; Dufresne *et al.*, 2015). Longitudinal and transverse ridges can be interpreted to be pressure ridges (Hewitt, 2006) and record the deflection of debris by valley walls and obstacles as defined by Heim (1932) and related ‘caroming’ flow (Hewitt, 2006). The western half of the deposit has a chaotic orientation of ridges, indicating a complex interaction with topography, whereas ridges in the eastern half are mostly longitudinal and are parallel to the flow direction, probably because there were few obstacles along their path. The sturzstrom-like debris flow ran straight to the north without spreading, thus forming longitudinal ridges only.

Geophysical Insights into the Pre-Failure Landscape and the Rock Avalanche Impact on a Paleolake

Eight ERT profiles (location in Figure 20b) totalling ~9.5 km in length and with 34,000 resistivity datum points provide unprecedented insights into the rock avalanche deposits and the surface on which the deposits lie. The profiles, shown in Figure 22 and Figure 23, are depicted with the same colour ramp for ease of comparison. Min and Max-Plots of all profiles are included

in the Appendix (Figures S5 and S6) to show the uncertainties in the ERT measurements. Resistivity calibrations based on data from the literature, field, and laboratory tests are given in Table S4.

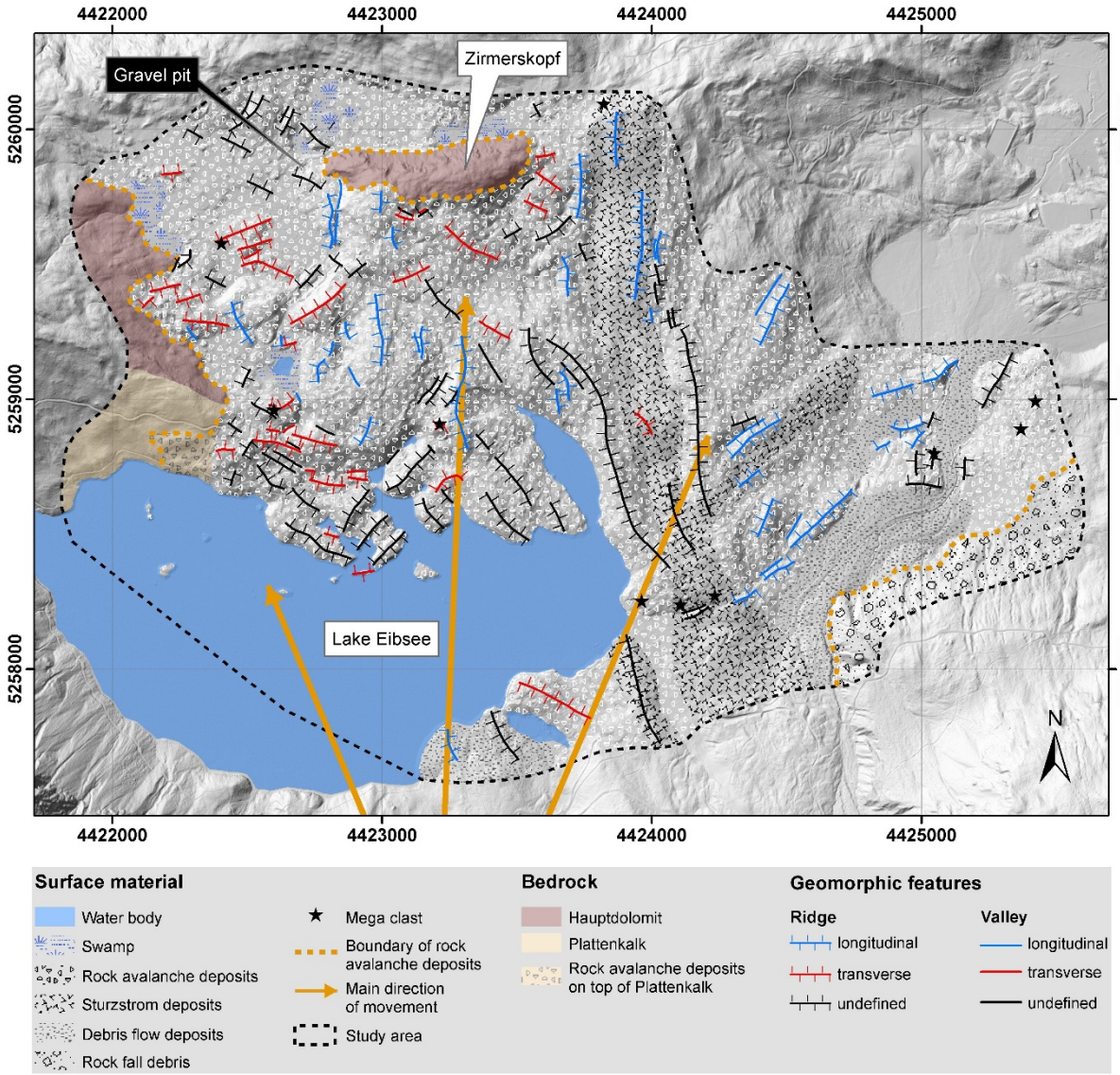

Figure 21: Geomorphic map of rock avalanche, rock fall, and debris flow deposits, showing the main direction of movement and longitudinal and transverse ridges and valleys. Lidar image: Bavarian Surveying and Mapping Authority (2006); coordinates given in Gauss-Krüger Zone 4.

Four resistivity zones can be distinguished in Figure 22 and Figure 23:

1. High resistivity zones (>2000 Ωm, dark red): bedrock, either limestone (Plattenkalk or Wetterstein Formation) or dolomite (Hauptdolomite Formation). The rock avalanche carapace is highly resistive because of the large size and proximity of boulders.
2. Mid-range resistivity zone (~500-2000 Ωm, orange-red): mixed fine- and coarse-grained materials with a high proportion of boulders; interpreted to be moraine material covering bedrock. Mid-range resistivity is also encountered at the transition between high and low resistivity zones.

3. Low resistivity zone (~100-500 Ωm, yellow-blue): mixed fine- and coarse-grained materials with a high proportion of fines; interpreted to be highly fragmented rock avalanche debris mixed with entrained fine-grained (paleolake) sediments.
4. Extremely low resistivity zone (<100 Ωm, dark blue): clay- or silt-size sediment, perhaps, mixed with small amounts of sand and small gravel; interpreted to be paleolake sediments.

Eight types of materials and processes detected with ERT could be calibrated in the field (Table S4): i) rock avalanche body, ii) bedrock (pk and hd), iii) lake clay/silt and iv) mixed sediments as materials, as well as processes like v) bulldozing with vi) overriding of secondary lobes, vii) bulging, and viii) splashing of single boulders. For these, calibration sites have been introduced in Figure 22 and Figure 23. Moreover, morainal sediments, and upward injection of lake sediments are identified.

P1 (Figure 22a) is a profile oriented from south to north, in the direction of the incoming rock avalanche. At the south end of the profile, the surficial layer with mega-blocks can be calibrated at the Eibsee Hotel (Table S4; Socco *et al.*, 2010). Here, the rock avalanche deposits are ~50 m thick and lie on top of material with mid-range resistivity (brown-red colour). We interpret the latter material to be morainal deposits (Table S4; Samouëlian *et al.*, 2005) and/or bedrock that impound a paleolake towards the east. In the middle part of the profile are near-vertical shear zones with material of very low resistivity (<100 Ωm, dark blue colour). This material is interpreted to be lake sediment squeezed into and partially mixed with rock avalanche (~100-400 Ωm, light blue colour; interpretation follows Bader, 1979; 1981; Kneisel, 2003; Samouëlian *et al.*, 2005).

There is shearing due to compression (pressure ridges in Figure 21) during collision of the rock avalanche with bedrock at Mount Zirmerskopf (dark red colour). The ~30 m deep northern basin of the paleolake is seen at the north end of the profile with a thin cover of rock avalanche debris.

P2 (Figure 22b) extends in an easterly direction across the northern basin. The profile starts on the west on Plattenkalk Limestone bedrock (Table S4). Farther east, fine-grained material (~100 Ωm, blue colour) has been carried to the surface along shear zones, as is seen in P1. In the middle of the profile, rock avalanche debris overlies mixed sediments (~500 Ωm, yellow colour). The brown-red spots near the base of the profile in this area may delineate paleotopography shaped by glaciers (drumlins or flutings). At the east end, the profile extends across the paleodam observed in P1 (red colour), beyond which the surface elevation drops rapidly.

P3 (Figure 22c) and P4 (Figure 22d) provide views of the northern part of the paleolake. P3 passes the drilling site 'Grainau IV' (Jerz and Poschinger, 1995), where rock avalanche material is mixed with paleolake sediments and where the resistivity of Plattenkalk Limestone was calibrated. Large boulders at the surface are sparse and not connected to the main rock avalanche deposit farther south.

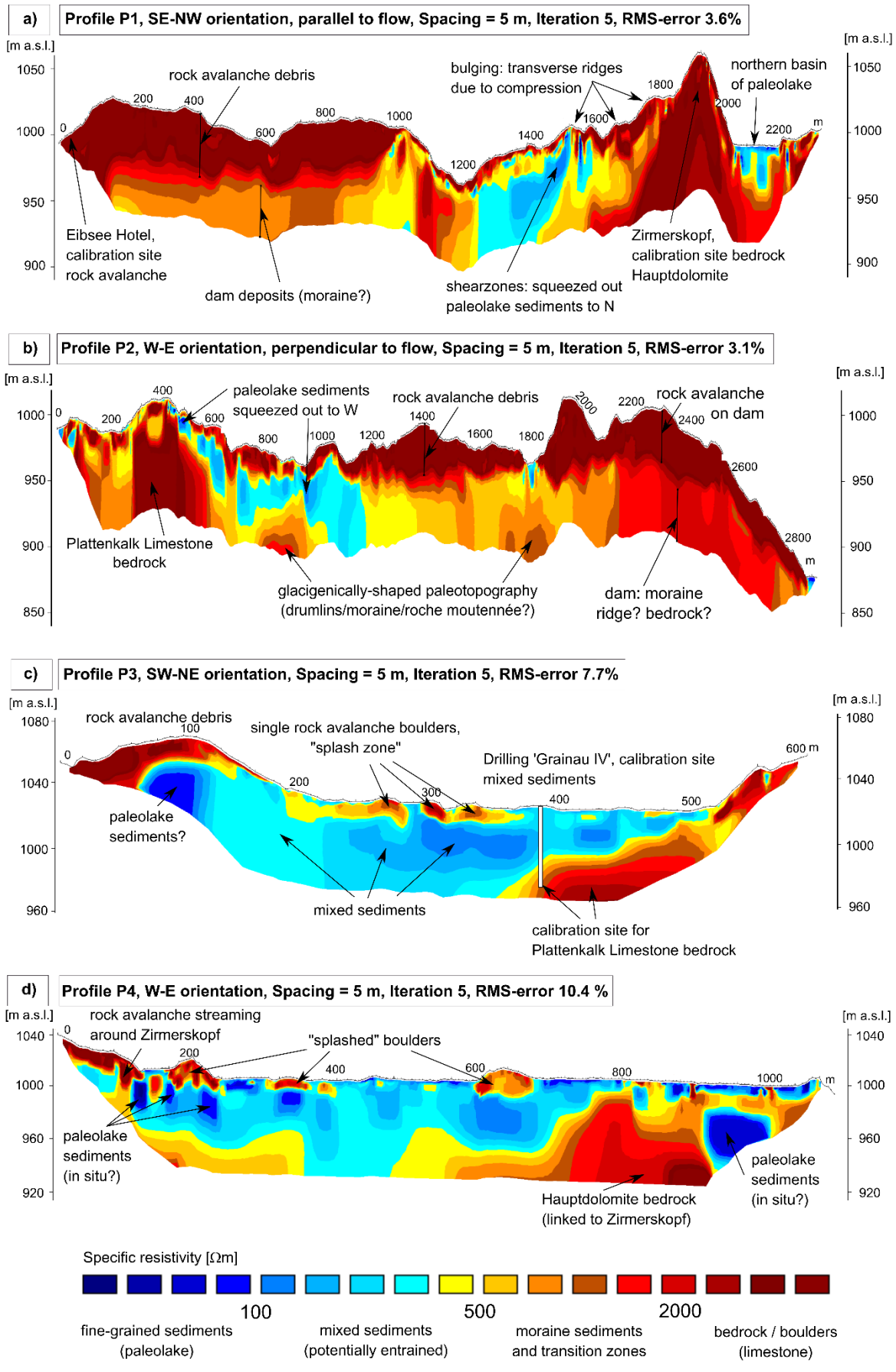

Figure 22: ERT profiles P1-P4. a) P1: SE-NW profile (in flow direction) of main deposits and bedrock at Mount Zirmerskopf. b) P2: W-E profile (perpendicular to flow direction) of main deposit between bedrock (W) and dam

(E), showing shearing and squeezing out of paleolake sediments. c) and d) P3 and P4 showing the northern basin with "splash zone", water-saturated mixed sediments and assumed in-situ paleolake clays.

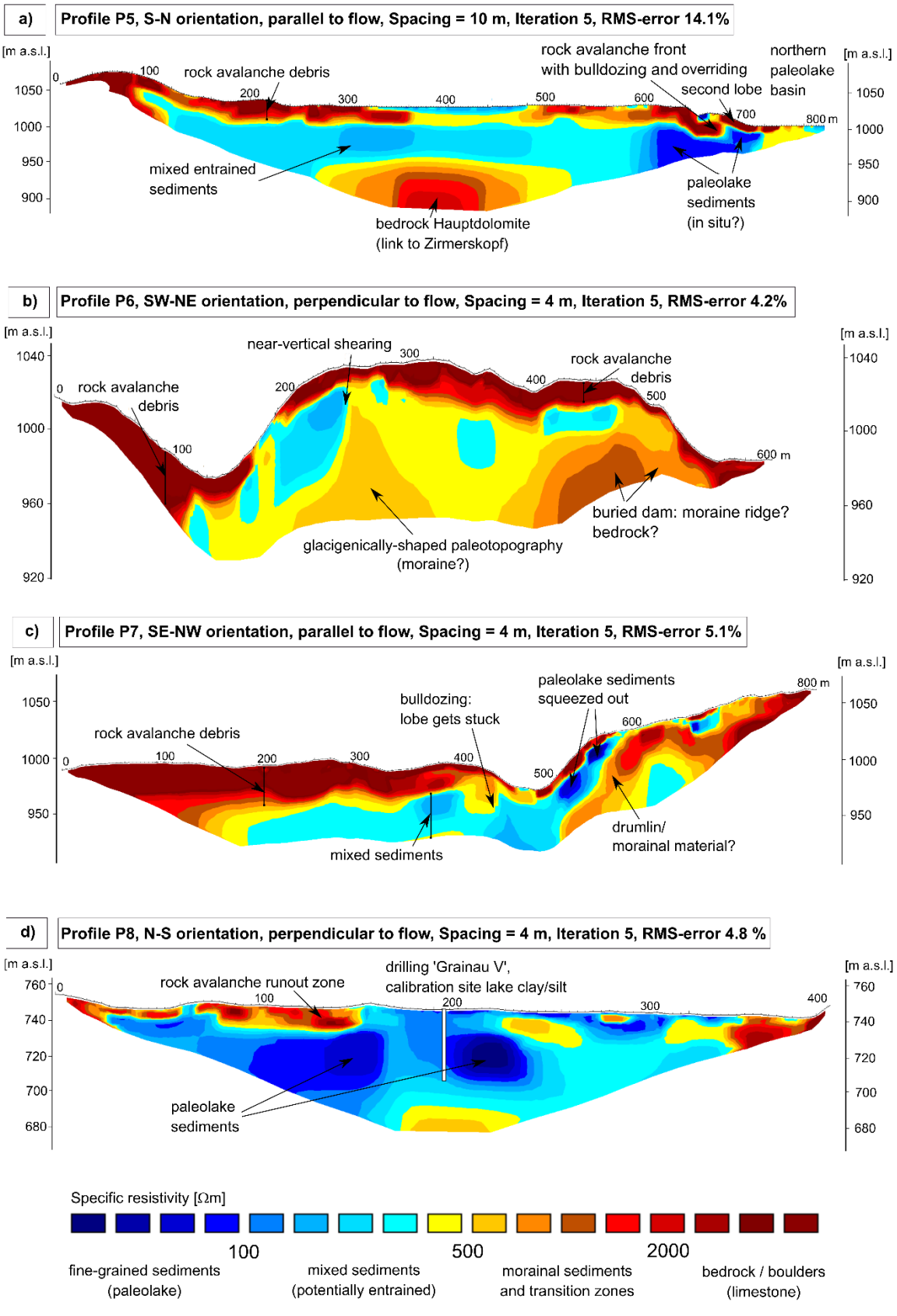

Figure 23: ERT-profiles P5-P8. a) P5: ~120 m deep paleolake basin. b) and c) P6 and P7: details of shearing processes and paleotopography. d) P8: the calibration site for lake clays with extremely low resisitivity values (<100 Ωm, dark blue).

In P4, large boulders are stacked atop one another and extend upward without any indication of flowing motion. This area may rather be a "splash zone" (e.g. Plafker and Ericksen, 1978; Cruden and Hungr, 1986) where boulders overtopped Mount Zirmerskopf at high speed and came to rest in the northern paleolake basin while rock avalanche material streamed around the ridge on both its west and east sides (homogenous debris; interpretation follows Ostermann *et al.*, 2012). The stacked boulders overlie dark blue (<100 Ωm) in-situ paleolake sediments.

P5 (Figure 23a) is another northerly oriented profile parallel to flow that ends at the distal margin of the rock avalanche, with evidence of bulldozing at the front. In the middle part of the profile, we identify Hauptdolomite bedrock at ~100-120 m depth, suggesting that the basin was ~100 m deep at this locality after deglaciation.

P6 (Figure 23b) provides insight into the structure of the paleodam and translational shearing resulting from collision of the rock avalanche with the dam. Two near-vertical obstacles (red colour), which may be moraine material, are covered by ~20-30 m of rock avalanche debris with entrained fine-grained sediments (~100-500 Ωm, blue-yellow colour).

P7 (Figure 23c) is a short NW-profile through ~30-m-thick rock avalanche deposits. One debris lobe has been overridden by a second lobe. Paleolake sediments (<100 Ωm, dark blue) have been injected upward as the debris ran up a former hill (moraine ridge or drumlin).

P8 (Figure 23d) is located near the east end of the rock avalanche deposit at the 'Grainau V' drillsite (Jerz and Poschinger, 1995), where we calibrated ERT measurements in lake sediments (<100 Ωm, dark blue). Thin rock avalanche deposits are registered in red.

Shear Zones and Water-Escape Structures Revealed in Sediments

A gravel pit is located in a distal facies of the rock avalanche deposit west of Mount Zirmerskopf (Figure 20). The gravel pit provides a panoramic view ~30 m wide and ~10 m high of a blocky carapace and main body of the rock avalanche deposit with a paleoflow direction towards the observer (Figure 24). The base of the deposit is not visible. In the eastern half of the outcrop, the body of the rock avalanche deposit is covered by large boulders of Wetterstein Limestone. To the west, however, there are two sheets of diamictic rock avalanche deposits separated by a matrix-rich band, but without a distinct carapace (Figure 24a, b). Both sheets of rock avalanche debris have the same composition, but the lower sheet contains larger boulders than the upper one. The smaller fragments are angular to subangular and intensely fractured. The matrix-rich band is at the surface at the west end of the exposure, dips eastward down to ~3-4 m depth, then rises again and reaches the surface in the middle of the exposure (Figure 24a, b; for original photos see Figure S7 in the Appendix). The matrix-rich band consists of matrix-supported gravel, and is up to ~1.0 m thick (Figure 25). It has a reddish-orange tint that differentiates it from the light grey diamictic rock avalanche deposits.

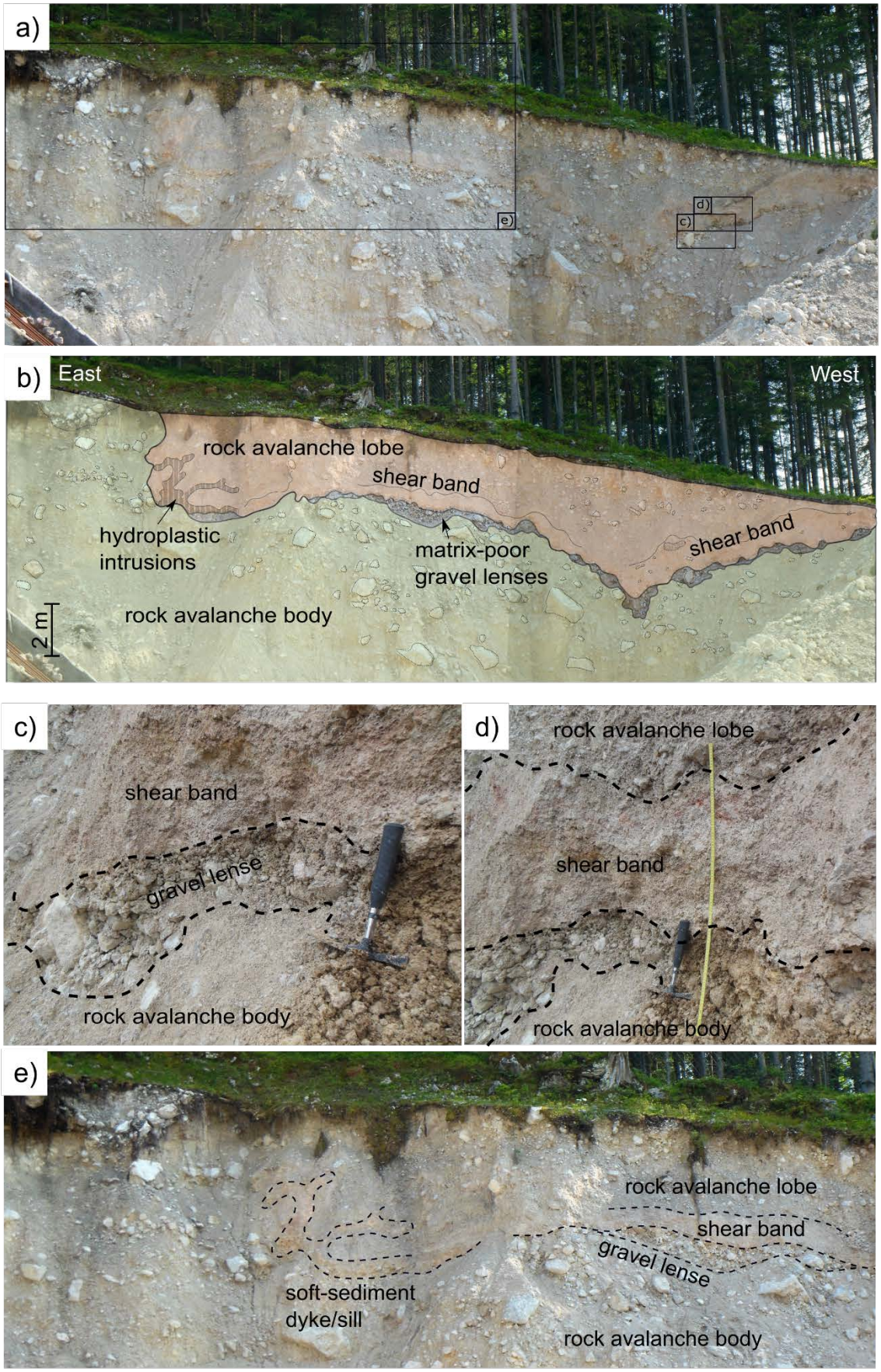

Figure 24: Gravel pit exposure at Mount Zirmerskopf: a) and b) Two lobes of rock avalanche debris separated by c) and d) reddish shear bands and gravel lenses. e) Convoluted structures in the shear band. (Original photos are provided in Figure S7 in the Appendix.)

Contorted sill- and dyke-like structures are evident at the eastern termination of the band (Figure 24e). Here, the matrix-rich band shows complicated folding and penetration of the overlying rock avalanche material in multiple flame, diapir and injection structures. Matrix-free and matrix-poor gravel lenses locally sharply separate the matrix-rich band from the underlying rock avalanche deposits (Figure 24). The lenses are only few decimeters thick, are structureless, and contain stones that are more rounded than those in the body facies (Figure 24c, d).

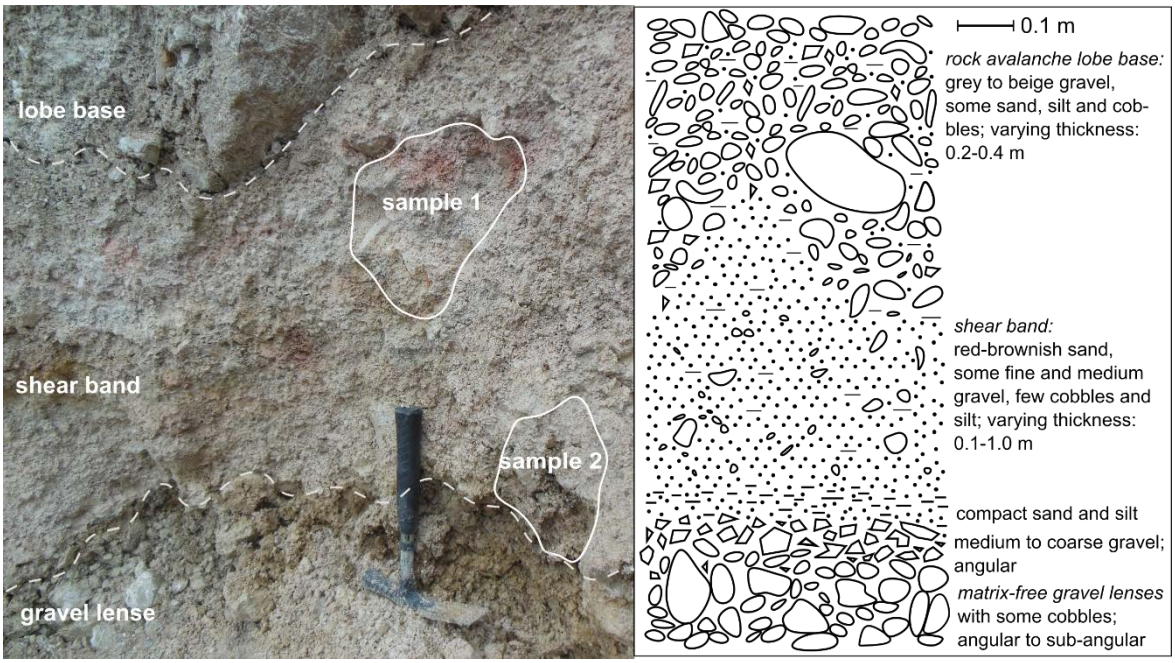

Figure 25: Sampling locations within shear band between two rock avalanche lobes. Sieving results are provided in Figure S8 in the Appendix.

The two rock avalanche bodies are interpreted to be the deposits of two, nearly simultaneous lobes. This interpretation is supported by ERT profile P5 (Figure 23a), where the outcrop is depicted at ~650 m length with up to ~30 m of rock avalanche deposits that have been bulldozed at the front of the rock avalanche. A thin front lobe overlies and presumably overran an initial thicker lobe. This happened when the first lobe slowed down while bulldozing as it entered the northern basin of the paleolake. The matrix band is interpreted to be a zone of shearing between these two lobes. Two sieved samples from the shear band (Figure 25 and Figure S8) have fractal dimension factors of ~2.59 and ~2.72, typical of shear bands according to Dufresne and Dunning (2017). The fine-grained matrix is likely a product of comminution during fragmentation (Yarnold, 1993; Davies and McSaveney, 2009a), but it might also contain entrained fines.

The convoluted sill- and dyke-like structures at the east edge of the shear band are interpreted to be soft-sediment deformation structures that formed due to water escape (Hewitt, 2006) and can be considered hydroplastic intrusions (Lowe, 1975). We attribute the convolution to shear-induced liquefaction as the flow decelerates (Bennett *et al.*, 2000; Carling, 2013). The gravel lenses are likely wedges of debris bulldozed and washed out close to the front of the upper rock avalanche lobe as it ran out, when great hydraulic pressures were generated in the

trapped moisture (Krieger, 1977; Yarnold, 1993). They can only form when water under high pressure entrains and removes fines, not by pore-water escape from wet substrates.

Discussion

ERT Error Sources

For the ERT survey, we used Wenner and Schlumberger arrays, which provides the best compromise between measurement precision and time investment (Rödder and Kneisel, 2012). The electrode arrangement provides high resistivity resolution in the vertical direction, but there is uncertainty in precision in the horizontal direction (Aizebeokhai, 2010). Additional uncertainties relate to (i) bad connections between the electrodes and substrate material, (ii) dryness of the sediment or (iii) large air-filled cavities, for example around rock avalanche boulders in the carapace (Supper *et al.*, 2014). With regard to the first cause of uncertainty, it is important to push the nails thoroughly into the ground and remove loose sediment or plant cover prior to making measurement. We obtained sharp resistivity contrasts between rock avalanche material (~500-2000 Ωm, red), fine-grained lake sediments (<100 Ωm, dark blue) and the mixed sediments (~100-500 Ωm, blue-yellow) in between.

The deviation between the measured values and the final tomography is indicated by the root mean square error (RMS). Small errors do not necessarily indicate a realistic model (Hauck and Mühll, 2003), therefore we selected only five iterations of modelling rather than risking overfitting, while obtaining satisfying RMS errors between 3.1 % and 14.1 %. To further assess the reliability of the inversions, we created MinMax-Plots of the ERT uncertainty (Figures S5 and S6 in the Appendix) based on a model covariance matrix (Alumbaugh and Newman, 2000). These plots show negligible uncertainty with respect to the interpreted sections.

Evidence that the Rock Avalanche Impacted a Lake

Complex emplacement structures with longitudinal and transverse ridges point toward the Eibsee rock avalanche impacting a deformable substrate (interpretation follows Hewitt, 2006; Dufresne *et al.*, 2010; Dufresne *et al.*, 2015). Swamps on the west and north margins of the rock avalanche deposit indicate water-impermeable geological strata, which favour the existence of a lake at this position.

Extremely low resistivity values below the rock avalanche deposit in the ERT profiles are indicative of lake sediments, which we calibrated with similar sediments encountered in drilling at ‘Grainau V’ (Jerz and Poschinger, 1995) and with data from the literature (Table S4). Moreover, zones of mixed deposits are present in distal areas where the rock avalanche moved into an existing lake. This is also supported by water-escape structures in the gravel pit at Mount Zirmerskopf (Figure 24). The matrix-free gravel lenses below the matrix-rich zone in this exposure indicate that the lake was filled with water and not dry (Yarnold, 1993).

Paleolake Eibsee

During the Last Glacial Maximum, the study area was covered by the Inn glacier flowing from the crest of the Alps (Fernpass area). When the glacier retreated, it left behind a landscape shaped by glacial erosion and partly blanketed by till and meltwater deposits. Till and/or bedrock formed a dam that sealed off part of the Eibsee Syncline (P1, P2 and P6; Figure 22 and

Figure 23). A lake formed behind the dam, and fine-grained lake sediments began to accumulate in it.

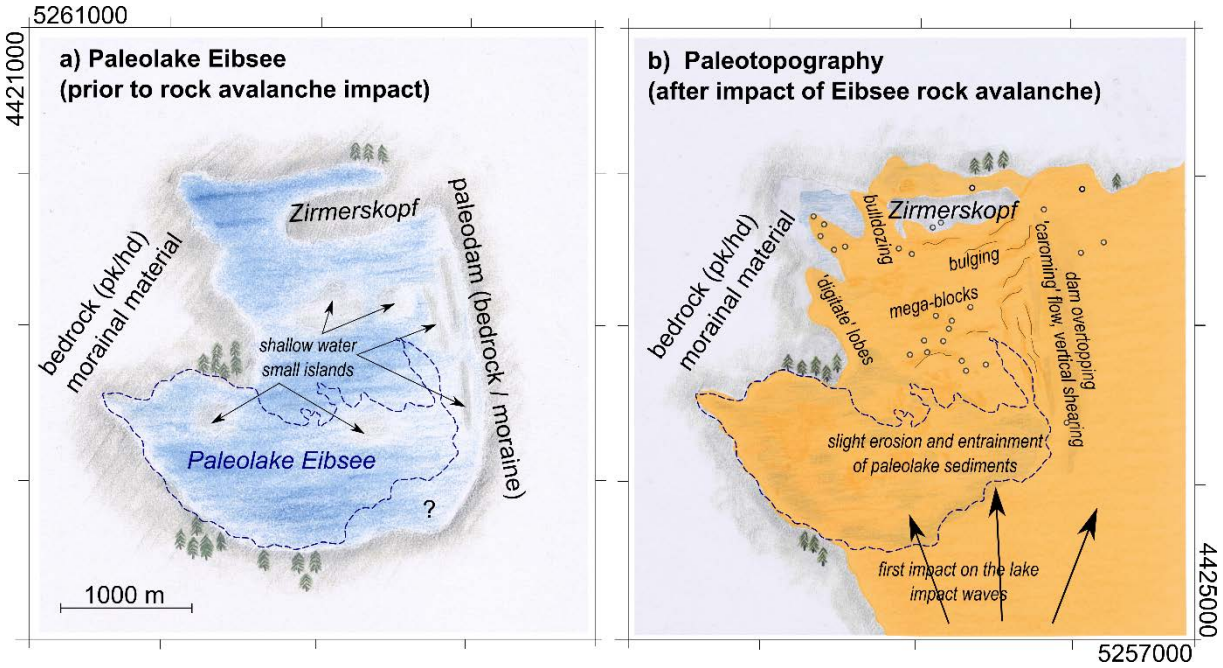

Figure 26: a) Schematic sketch of Paleolake Eibsee with assumed dimension and position of the paleodam and shallow water areas and small islands. b) Paleotopography after the rock avalanche impacts the lake, showing inferred processes. Dashed line indicates outline of modern Lake Eibsee. Coordinates are given in Gauss-Krüger Zone 4.

The lake formed adjacent to the roche moutonnée Zirmerskopf (Figure 26a) near where late-glacial lake sediments, mobilized and redeposited by the rock avalanche, were found during the drilling at 'Grainau IV' (Jerz and Poschinger, 1995). To the west, the lake presumably reached the rising slope of Plattenkalk Limestone bedrock. At the south, the modern Lake Eibsee basin was also part of the paleolake, again dammed to the west and south by Plattenkalk Limestone. The paleolake existed and continued to accumulate silt and clay up to the moment of the Eibsee rock avalanche (Figure 26b; see Part II, Knapp *et al.*, 2020b).

Interaction of the Rock Avalanche with the Lake

Upon impact with the valley floor, the rock avalanche split into several lobes radiating fanwise across the valley floor. The center of the rock avalanche impacted the paleolake and probably generated a displacement wave that moved north, east, and west.

The streaming rock mass eroded the floor of the lake but then slid on the fine-grained lake sediments. The basal friction was reduced due to lubrication or partial fluidisation, probably causing the rock avalanche to accelerate. The eastern part of the rock avalanche decelerated as it crossed the rough and hilly terrain of the paleolake dam, and continued down the valley towards Garmisch-Partenkirchen. Lake sediments were entrained and mixed into the coarser, diamictic rock avalanche material (yellow and blue mid-range ERT values, Figure 22 and Figure 23).

Due to collision with obstacles the rock avalanche split into several smaller lobes along its distal margins (Figure 23a, c, and Figure 24). Bulldozing, squeezing, and shearing are recorded

in the deposits at the margins of the paleolake. Here, multiple shear planes developed as successive lobes ran into one another with little time between them (P1 and P2; Figure 22). Also, soft-sediment deformation structures and water-escape structures formed where the rock avalanche ran over water-saturated fine-grained sediment.

Conclusions

The Eibsee rock avalanche overran Paleolake Eibsee. The entire body of water in the lake was displaced by the rock avalanche, presumably causing a large impact wave.

Fine-grained paleolake sediments were eroded and entrained by the rock avalanche. Water-escape structures, soft-sediment deformation structures, and matrix-free gravel lenses provide additional evidence for the existence of Paleolake Eibsee.

The paleolake was larger than modern Lake Eibsee. The main deposits of the rock avalanche cover the northern half of the paleolake. Today, swamps along the north and northwest sides of Lake Eibsee hint at the existence of the paleolake.

The long runout of the rock avalanche is attributed to low basal friction induced by entrainment of water and fine-grained sediments.

The rock avalanche deposits show evidence of complex runout and emplacement processes. Geomorphic mapping and an electrical resistivity tomography survey provide detailed insights into interactive processes of the rock avalanche and the lake: separation into lobes, bulldozing, and formation of multiple shear planes at the lake margins with upward injection of fine-grained lake sediments.

We reconstructed the paleotopography of the valley before the rock avalanche. Resistivity values typical of morainal sediments were measured at the paleodam and along ridges and hilly landforms in the former basin of the proglacial paleolake.

Acknowledgments

Sibylle Knapp acknowledges PhD funding awarded by the German National Academic Foundation (Studienstiftung des deutschen Volkes e.V.). We thank Andreas von Poschinger for providing detailed information on the drillhole logs, and Ulrich Haas for discussions drawing from his lengthy experience in the Werdenfels region, particularly around Lake Eibsee. The authors also thank Christoph Wichert, Tobias Kriesmair, Julia Gottfriedsen, and Mathias Schimpfle for their help with the ERT field survey and laboratory work in context of their diploma theses at the TUM. Finally, we thank Simone Herrmann (forest ranger), Jonas Kiesel and Falk Lempe for their support with fieldwork.

5.3 Lake Eibsee: 3-Stage Progressive Rock-Slope Failure and Formation of Modern Lake Deciphered from Lacustrine and Terrestrial Deposits

This chapter has been published in the Journal Earth Surface Processes and Landforms under the title "Impact of an 0.2 km³ Rock Avalanche on Paleolake Eibsee (Bavarian Alps, Germany) – Part II: Catchment Response to Consecutive Debris Avalanche and Debris Flow" by Sibylle Knapp, Flavio S. Anselmetti, Bernhard Lempe and Michael Krautblatter (2020b).

Abstract

The ~0.2 km³ Eibsee rock avalanche impacted Paleolake Eibsee and completely displaced its waters. This study analyses the lake impact and the consequences, and the catchment response to the landslide. A quasi-3D seismic reflection survey, four sediment cores from modern Lake Eibsee, reaching far down into the rock avalanche mass, nine radiocarbon ages, and geomorphic analysis allow us to distinguish the main rock avalanche event from a secondary debris avalanche and debris flow. The highly fluidized debris avalanche formed a megaturbidite and multiple swashes that are recorded in the lake sediments. The new calibrated age for the Eibsee rock avalanche of ~4080-3970 cal yr BP indicates a coincidence with rockslides in the Fernpass cluster and subaquatic landslides in Lake Piburg and Lake Plansee, and raises the possibility that a large regional earthquake triggered these events. We document a complex history of erosion and sedimentation in Lake Eibsee, and demonstrate how the catchment response and the rebirth of the lake are revealed through the complementary application of geophysics, sedimentology, radiocarbon dating, and geomorphology.

Introduction

Massive rock-slope failures often occur progressively in multiple stages from the same scarps or nearby scarps. Recent examples show that after an initial massive failure, a mountain flank may collapse again after few days (e.g. Randa 1991, Switzerland; Eberhardt *et al.*, 2004), few years (e.g. Tangjiawan 2008 and 2016, China; Fan *et al.*, 2018), or tens to hundreds of years (e.g. Mount Spitzstein, Switzerland, now active again after events at ~2550 cal yr BP, ~2250 cal yr BP, ~2180 cal yr BP, ~1720 cal yr BP, and ~1320 cal yr BP; Knapp *et al.*, 2018). Yet, it is not possible to predict when and how often a scarp might be reactivated, and it is unclear what role the trigger and predisposing factors play in the catchment response. Clearly, however, refining recurrence rates and magnitudes is essential for future hazard assessment, and improving our understanding of progressive failure and catchment response after such catastrophic events.

The so-called 'Fernpass rockslide cluster' is a group of large rock-slope failures in the Northern Calcareous Alps and Central Eastern Alps (Figure 27a; Prager *et al.*, 2008). Many of these landslides occurred at or after the end of the Holocene climate optimum during the Subboreal (~4800 to ~3800 yr BP; Wanner *et al.*, 2008; Wanner *et al.*, 2011). Researchers have made a lot of effort to bracket the ages of these landslides with different dating techniques to refine recurrence rates. Well-known examples are the rockslides at Fernpass (~4200-4100 cal yr BP; Prager *et al.*, 2009) and Tschirgant (~3010 cal yr BP; Ostermann *et al.*, 2017). However, all dating techniques carry uncertainties, and dating is sometimes too imprecise to recognize separate events, even though the deposit morphology suggests multistage failure (e.g. the

Pletzachkogel and Köfels rockslides; Ivy-Ochs *et al.*, 1998; Hermanns *et al.*, 2006; Prager *et al.*, 2008; Patzelt, 2012b). Consequently a new complementary approach is required to decipher the multistage character of ancient events.

The Eibsee rock avalanche, sourced at Mount Zugspitze in the Bavarian Alps, is part of the Fernpass rockslide cluster and has until now been considered a single failure dated at ~3700 yr BP (Jerz and Poschinger, 1995). In this paper, we present the results of geophysical and sedimentological investigations of Lake Eibsee, new radiocarbon ages from event deposits in the lake, and geomorphic observations. The data not only document three rock-slope failure events that we presume are related to each other, but also help to improve our understanding of how and under which circumstances a fragmenting rock mass may transform into or trigger a highly mobile debris avalanche or debris flow. The importance of this learning is highlighted by the massive rock-slope failure at Piz Cengalo in 2017 (Walter *et al.*, 2020), where secondary debris flows reached and destroyed settlements and other infrastructure, causing fatalities far beyond the reach of the original rock avalanche.

Our study addresses five research questions: Is the Eibsee rock avalanche a single failure, or can we decipher multistage events? What happens during and after the impact of the rock avalanche on the lake? Does a new lake form, and if so, how and where? Can we find evidence of a displaced paleolake in the modern lake? And, finally, what can we learn about progressive scarp evolution and repeated rock-slope failures that feature consecutive rock avalanche and debris flow events?

Study Site

Lake Eibsee (973 m a.s.l.) is located at the foot of Mount Zugspitze (2962 m a.s.l.), the highest summit in Germany, in the Loisach-Fernpass fault zone (Figure 27a). The lake has a surface area of ~1.8 km² and a maximum depth of ~36 m. It is mostly fed by groundwater; there are small surface water inflows from the west (Kotbach and Markgraben), and there is no out-flowing stream. The lake shoreline is undulatory, and there are several small islands (Figure 27b), mainly in the western and middle parts of the lake, that consist of rock avalanche material (Wetterstein Limestone and some limestones and marlstones of the Alpine Muschelkalk, mostly Reifling Formation). Plattenkalk Limestone and Hauptdolomite bedrock are exposed north of the lake. A Paleolake Eibsee, larger than the modern one, existed at this site until the Eibsee rock avalanche impacted and destroyed it (see Part I, the companion to this article, Knapp *et al.*, 2020a).

Methods

Seismic-Reflection Survey

Seismic surveys were carried out on Lake Eibsee in May 2015. The surveys were performed with an Octopus 760^{TM} Geophysical Acquisition System with a single-channel 3.5 kHz pinger source/receiver. We operated the system with an inflatable boat travelling at a mean speed of 5-6 kmh^{-1} to acquire a dense, quasi-three-dimensional grid of seismic profiles in the lake (Figure 27b). The seismic profiles were analysed with the KingdomSuite^{TM} interpretation software. The conversion of two-way travel time to depth assumes a *P*-wave velocity of 1500 ms^{-1} for both water and lake sediments.

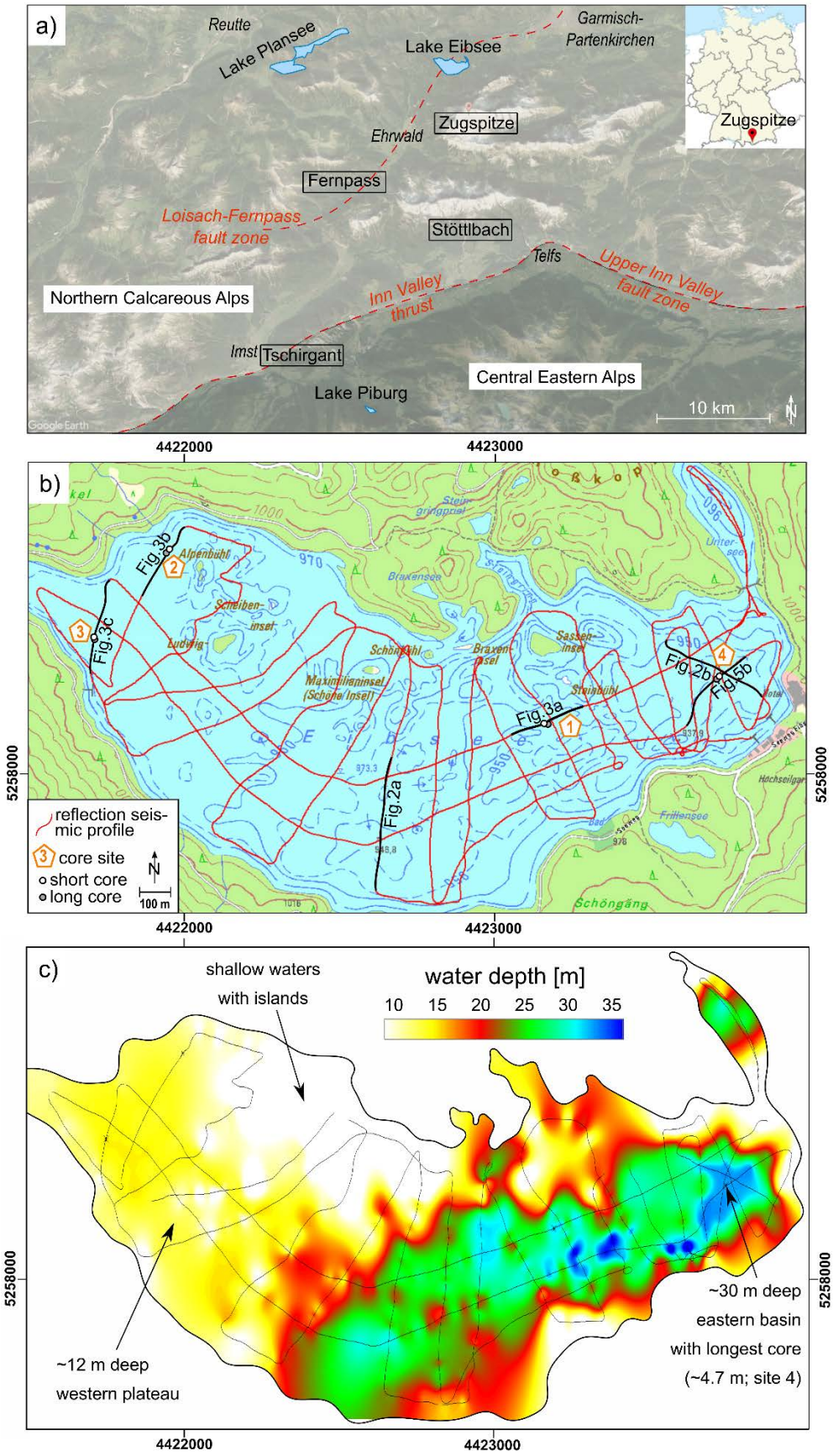

Figure 27: a) Map of the region including Mount Zugspitze and Lake Eibsee in the Northern Calcareous Alps; landslides and fault zones related to the 'Fernpass cluster' are shown. Image © 2020 Maxar Technologies/Google Earth. b) Map of Lake Eibsee and surroundings showing seismic reflection survey lines and core locations. Source

of topographic map: Bavarian Surveying and Mapping Authority (2006). c) Bathymetry of Lake Eibsee, interpolated from seismic data. Coordinates are given in Gauss-Krüger Zone 4.

Lake-Sediment Coring

We cored lake sediments from a platform with an UWITEC percussion piston-coring system in October 2016. Long cores were recovered in 3-m-long, 63-mm-diameter PVC tubes. The cores were cut into three 1-m-long sections immediately after core recovery (e.g., core EIB16-02 was cut into three 1-m pieces EIB16-02A, -B, and -C; Table S5 in the Appendix). A gravity corer was used to sample the uppermost ~1 m of sediment (short cores). Coring locations (Figure 27, Table S5 in the Appendix) were chosen on the basis of the seismic data to (i) find paleolake sediments beyond the reach of the Eibsee rock avalanche (in the west), (ii) recover Eibsee rock avalanche material with entrained organic matter for radiocarbon dating, and (iii) track multiple stages of catchment response in the aftermath of the catastrophic event, including possible further events, stages of lake rebirth, and basin-wide environmental processes. The long cores EIB16-09A-C, EIB16-09D-F, and EIB16-09G-H at location 4 were recovered with an overlap of ~1.5 m to compile a composite core. This composite core includes a gravity core at the same site to secure the sediment-water interface (Table S5). Coring was stopped, when the corer head reached rock material (locations 1, 2, and 4) or a log (location 3).

Lake-Sediment Analysis

Sediment cores were refrigerated at 4°C in the lacustrine core-storage facilities at the University of Bern. A GEOTEK Ltd. multisensor core logger measured the gamma-ray density, magnetic susceptibility, and *P*-wave velocity with a sampling resolution of 0.5 cm. The PVC tubes were then split lengthwise into two halves, photographed (Geotek Linescan camera), and described by macro- and microscopic analyses of grain size and material. The composite cores were constrained with tie points (marker horizons), where possible (Table S5). The final composite sections at the four locations range in length from 1.05 m to 4.71 m. The lowermost sections EIB16-09E, -F, and –H were scanned using computer tomography (CT) at the Institute of Forensic Medicine at the University of Bern to highlight differences in density at high resolution and in 3D.

Radiocarbon Dating

Accelerator mass spectrometer (AMS) radiocarbon dating was done at the Laboratory for the Analysis of Radiocarbon with AMS (LARA) of the University of Bern. Radiocarbon ages were reported by the laboratory with one-sigma uncertainty. For calibration, we applied OxCal v.4.3.2 (Ramsey, 2017), using the IntCal13 calibration curve from Reimer *et al.* (2013), and the 2-sigma-range.

Geomorphic Interpretation

A hillshade 3D digital elevation model (DEM; Bavarian Surveying and Mapping Authority, 2006) of the main depositional area north of Lake Eibsee was used for geomorphic interpretation (see also Part I, Knapp *et al.*, 2020a). Field investigation and a geological map (Hornung and Haas, 2017) provided further information. Satellite images were used to detect potential scarps and to assume travel paths of the landslides.

Results and Interpretation

Seismic Stratigraphy

The seismic signal penetrated to depths of up to 5 m below the lake floor, except in the easternmost part of the lake where gas masked the stratigraphy. We defined four seismic sequences (seismic units I-IV) on the basis of their geometries and seismic characteristics (Figure 28 and Figure 29).

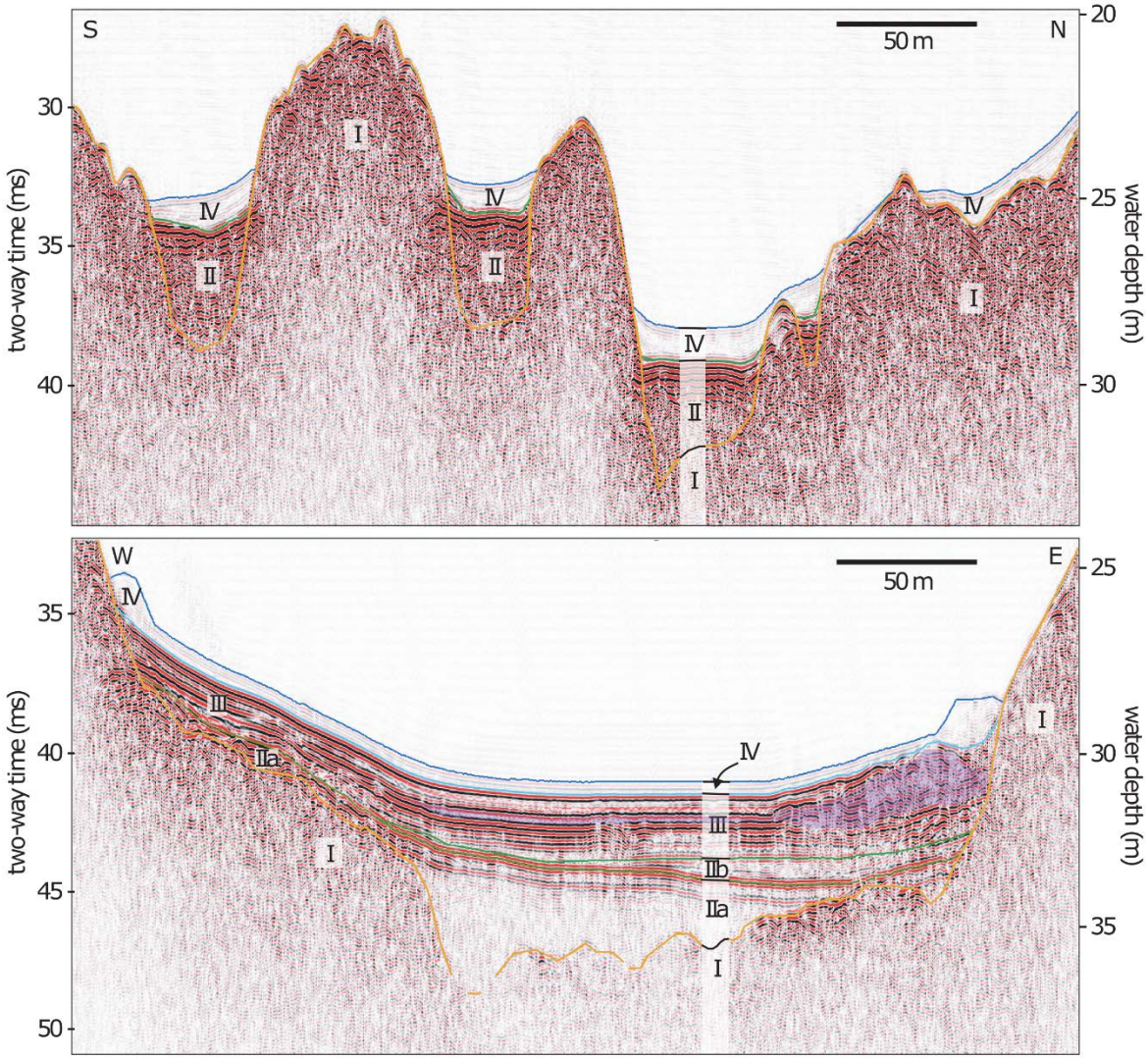

Figure 28: Two seismic profiles from the western (a) and eastern (b) parts of Lake Eibsee (see Figure 27b for locations). The seismic stratigraphy comprises four seismic sequences labelled I-IV. Seismic unit III occurs only in the eastern, deep basin and contains a mass-movement deposit marked with purple color.

Seismic Unit I

Seismic unit I is the lowermost sequence. Its upper surface scatters all seismic energy and thus forms the acoustic basement. This surface is highly irregular and bumpy (Figure 28a, b and Figure 29a), and has local relief of 10 m or more.

Seismic Unit II (a, b)

Seismic unit II fills the depressions at the top of unit I topography and has generally a flat upper surface. It is up to 5 m thick and shows at the top parallel high-amplitude reflections resulting from its very strong impedance relative to overlying low-impedance sediments (Figure 28a).

In the eastern basin, unit II can be subdivided in lower (IIa) and upper (IIb) subunits (Figure 28b). Subunit IIa occurs in sediment pockets on top of unit I characterized by chaotic or transparent seismic facies and has, when compared to the western basins (Figure 28a and Figure 29a), lower amplitudes on top. It is overlain by a topography-filling, onlapping unit with low-amplitude reflections (subunit IIb) that further flattens out the relief (Figure 28b).

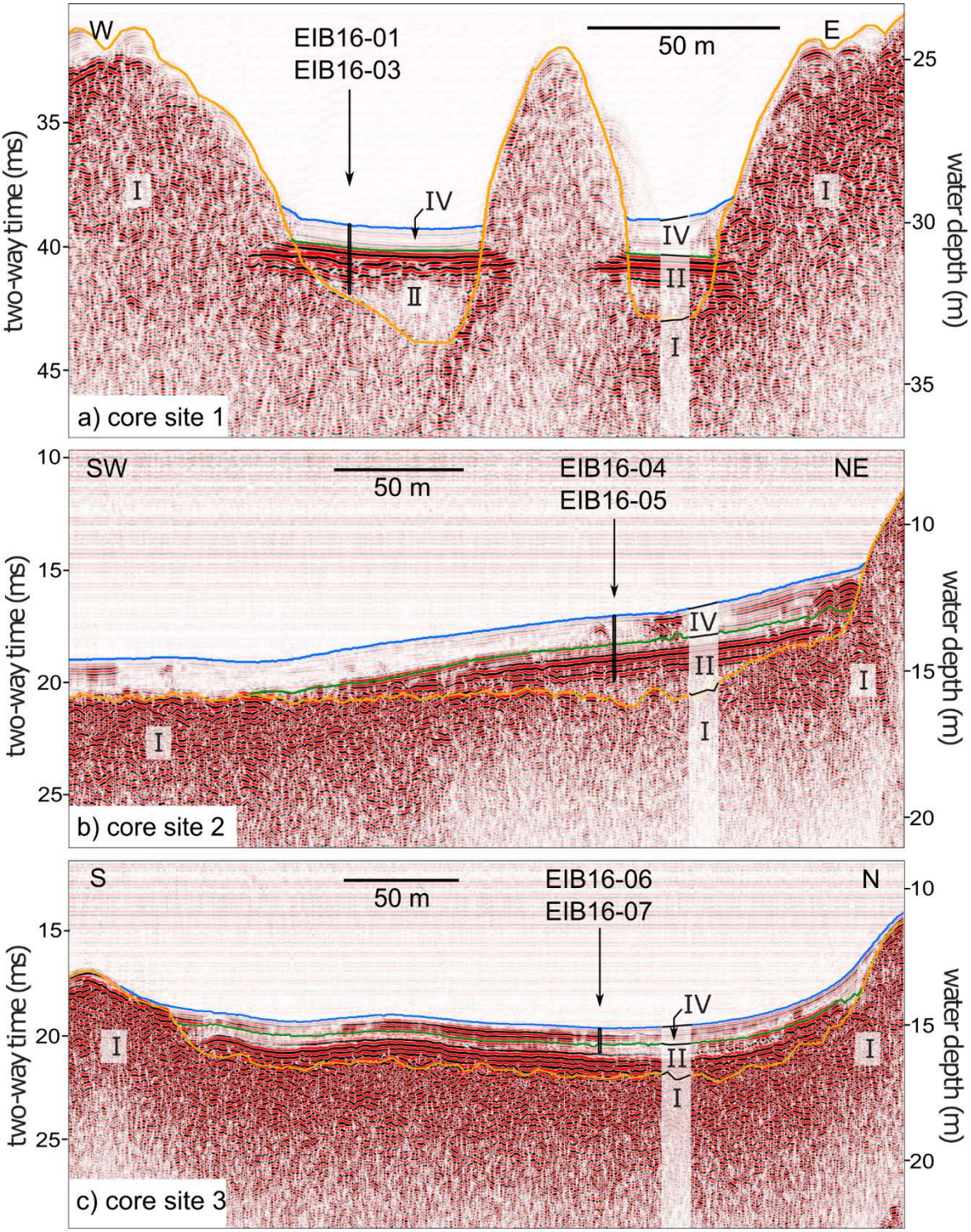

Figure 29: Seismic profiles at core sites 1, 2, and 3 (see Figure 27b for locations). Seismic units as in Figure 28.

Seismic Unit III

Unit III is found only in the eastern, deep basin (Figure 28b). It is up to 3 m thick and is characterized by horizontal medium-to-high-amplitude reflections. A chaotic convex-shaped mound occurs at the toe of the slope at the east side of the deep basin and is interpreted to be a mass-movement deposit originating from the slope to the east (purple colour on Figure 28b).

Seismic Unit IV

The uppermost seismic unit is characterized by very low amplitude reflections, indicating water-rich low-impedance sediments (Figure 28 and Figure 29). It has a maximum thickness of 1.5 m and occurs in the same depressions as units I and II. Unit IV has geometries with slightly curved edges that onlap onto the acoustic basement (unit I). In the deep, eastern basin, these edges have prominent mound structures indicating downslope movement of sediment at the toe of slopes (Figure 28b).

Core Lithostratigraphy

About 15 m of lake sediments were retrieved from the four core sites (2.11, 2.17, 1.05 and 4.71 m at locations 1, 2, 3, and 4, respectively; Figure 30 and Figure 31 and Table S5). We subdivided the sediment sequences into four lithostratigraphic units.

Lithostratigraphic Unit A

Lithology: Unit A is the lowest unit and was retrieved only at location 4, at a composite depth of ~4.5-4.71 m. Its base is marked by large boulders of light-beige Wetterstein Limestone, only a few centimeters of which were penetrated. Core images and CT data indicate that these pieces of limestones are overlain by a layer of cobble-sized clasts with a greyish, silty to sandy matrix (Figure 31).

Correlation and interpretation: Lithostratigraphic unit A correlates with seismic unit I, hence comprises the acoustic basement (Figure 28b). The rugged surface of seismic unit I, the lack of penetration of the 3.5 kHz signal, and an inability to core unit A with the exception of the single large block at the base of the core at location 4, indicates that this unit is the carapace of a rock avalanche comprising massive boulders underlying the entire modern lake bed. We name this largest and highest-energy event 'rock-slope failure event 1'.

Lithostratigraphic Unit B

Lithology: This unit is present at all four core sites (Figure 30 and Figure 31) at composite depths of ~0.6-2.1 m (site 1), ~1.0-2.2 m (site 2), ~0.9-1.1 m (site 3), and ~1.7-4.5 m (site 4). It comprises angular gravel- to cobble-sized fragments of Wetterstein Limestone and Alpine Muschelkalk embedded in a grey, silty to sandy matrix. Dark grey-brown limestones and marlstones of the Reifling Formation contrast markedly with light grey clasts of Wetterstein Limestone (Figure 31; composite depth ~4.1-4.2 m). Unit B has high density CT scan values and exhibits normal grading over a vertical distance of many decimeters (~0.8 m at site 1, Figure 30a; ~0.5 m at site 2, Figure 30b; ~1.0 m in the main lake basin at site 4; Figure 31). Two or more graded sections are present, and, fragments of wood are common in a cap of fine sediments at the top of the unit.

At site 4, the base of unit B (~4.3-4.5 m composite depth) consists of clay and silt (Figure 31) with low density values. The measured density values and visual observations indicate upward

coarsening of this interval, with an increase in amounts of sand, granules, and small pebbles (composite depth ~4.20-4.45 m). The fine-grained upper part of unit B (composite depth ~1.7-2.1 m) is characterized by four normally graded layers with stepwise up-core decrease in layer thickness (18, 12, 8, 4 cm) and a decrease in basal grain size (Figure 31).

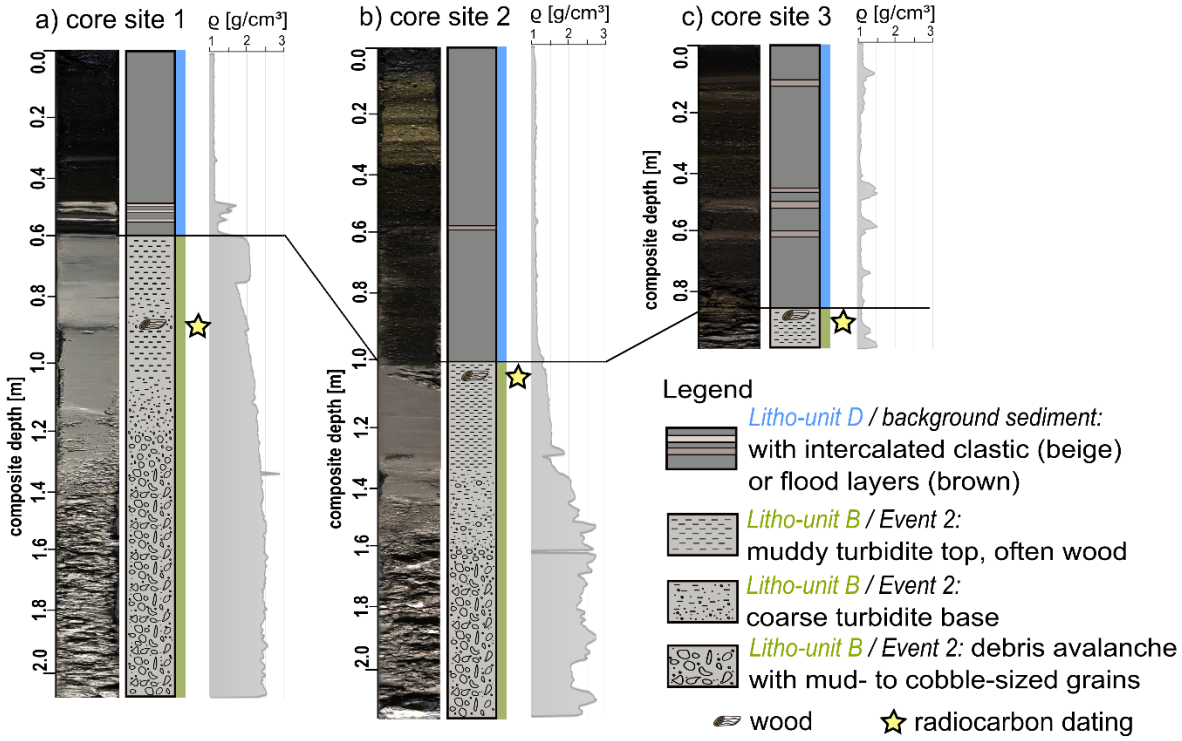

Figure 30: Core-to-core correlation with photographs, sedimentological descriptions, and density profiles at locations 1, 2, and 3 in the western and middle parts of the lake.

Correlation and interpretation: Unit B coincides with seismic unit II. The overall normal grading indicates deposition during a single event; we term this event 'rock-slope failure event 2'. We interpret the fine layer capping unit B to be a megaturbidite related to a highly fluidized slurry wave that crossed the rock avalanche material, with fine gravel in suspension.

At site 4, the four graded, subsequent and stacked sediment sections indicated as ‘swashes’ in Figure 31c are interpreted to be the deposits of a seiche. The seiche is an oscillating wave moving back and forward, which affects the whole lake basin and produces stacked turbidites with up-core fining basal grain sizes, as the basal flow velocity decreases with every passage; they correlate to the seismic subunit IIb. The coarser, graded deposits at the base of Litho-unit B here at site 4 coincide with the lower seismic subunit IIa and are interpreted to be debris infilling depressions on the Event 1 deposits. The sharp contact to the underlying lithostratigraphic unit A (seismic unit I) is interpreted as marked by a hiatus, the erosive boundary between rock-slope failure events 1 and 2. The very fine sediment and low density at the very bottom of lithostratigraphic unit B (composite depth ~4.3-4.5 m) indicate dust-cloud deposits of Event 1, which are partially reworked due to the entrainment during Event 2.

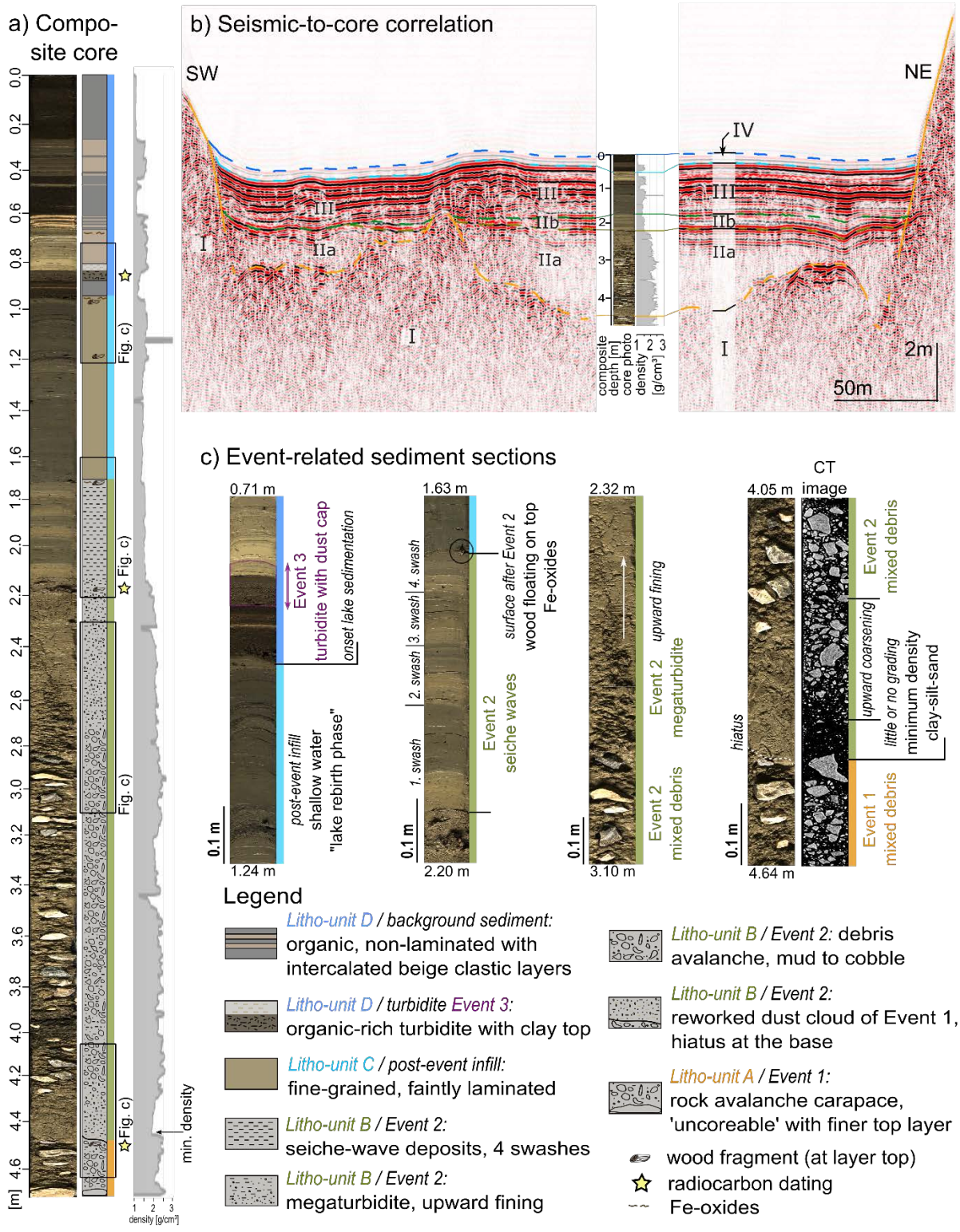

Figure 31: Photographs, sedimentological descriptions, and density profile of composite core from the eastern lake basin. a) Complete composite core with lithology and density values. b) Correlation of seismic units and lithologic units. c) Details of important event-related sediment sections and CT-image of the core base.

Lithostratigraphic Unit C

Lithology: This unit occurs only at site 4 in the deepest basin, at a composite depth of ~0.9-1.7 m (Figure 31). The fine-grained grey sediment has an overall medium density and is generally

structureless, with only a few laminations and intercalated coarser layers with wood and leaf fragments, and Fe-oxides.

Correlation and interpretation: Unit C correlates with seismic unit III and is interpreted to be post-event 2 infill. Reworked, shallow-water, marshy sediment was deposited in the flattest and deepest part of the lake basin.

Lithostratigraphic Unit D

Lithology: This unit consists of generally dark, jelly-like, low-density sediment rich in organic matter with a few intercalated clastic layers and rare small molluscs.

Its thickness is ~0.6 m at site 1, ~0.8 m at site 3, ~0.9 m at site 4, and ~1.0 m at site 2. At site 4, a normally graded, low-density layer consisting mainly of terrestrial organic matter capped by light-grey silt and clay occurs at ~0.8-0.9 m composite depth.

At sites 1 and 4, several higher density, centimeter-scale, normally graded, white-beige silt/clay layers occur at composite depths of ~0.5 and ~0.6 m, respectively. Also present in unit B are reddish-brown layers with higher density values that contain abundant terrestrial organic matter (Figure 30; location 2 at ~0.6m; location 3 at 0.1, ~0.5, and 0.6 m).

Correlation and interpretation: Lithologic unit D correlates with seismic unit IV and records the normal, background organic-rich deposition in the lake (gyttja). The edge-draping geometry reflects redeposition of low-density jelly-like material during storm events. The lower part of the lithologic unit D is dominated by light-colored clastic layers with down-core increasing density values (Figure 30a and Figure 31a). We interpret these layers to cause the strong acoustic reflection between seismic units III and IV and a slight mismatch between the lithologic C-D and the seismic III-IV boundaries, as the clastic layers belong to unit D, not unit C. We interpret the clastic layer at ~0.8-0.9 m depth to be a turbidite capped by dust-cloud deposits, produced by a third event that we term 'rock-slope failure event 3'. This event likely was of smaller magnitude than events 1 and 2. Other intercalated clastic layers in unit D in the cores at sites 2 and 3 may record rainstorms with heavy runoff that flush into the western part of the lake. Ephemeral streams enter the lake near these two coring sites at the west margin of the lake.

Age of Rock-Slope Failures

Radiocarbon ages of nine wood samples recovered from cores at four coring sites are presented in Table 5. The oldest sample BE-6932.1.1 (10,122 ± 55 yr BP) was collected from the megaturbidite bed (EIB16-03A) at site 1. The calibrated age range is 12,012-11,405 cal yr BP. This sample is much older than was expected; we interpreted it to be reworked and thus removed it from further consideration. Figure 32 summarizes the dating results pertinent to the events we describe in this paper, with coloured rectangles showing overlaps of the 2-sigma ranges of calibrated ages for the three events. Event 1 dates to 4089-3876 cal yr BP. With six overlapping sample ages, Event 2 dates to 4082-3976 cal yr BP. The two events cannot be separated based on radiocarbon ages. However, because Event 1 is older than Event 2, the age of Event 1 can be refined to 4089-3976 cal yr BP. Sample BE-6935.1.1 from the turbidite bed in core EIB16-09A returned a radiocarbon age of 3459 ± 35 yr BP and thus provides a calibrated age range of 3830-3640 cal yr BP for Event 3.

Table 5: Radiocarbon ages.

Section	Sample lab code	Sediment depth [m]	Material	C14 age [BP]	Cal age [BP] (2σ-range)	Event
EIB16-09A	BE-6935.1.1	0.35-0.36	wood	3459 ± 35	3830-3640	3
EIB16-09B	BE-6936.1.1	0.80	wood	3630 ± 41	4083-3840	2
EIB16-07	BE-6934.1.1	1.02	wood	3660 ± 19	4082-3907	2
EIB16-07	BE-6934.2.1	1.02	wood	3675 ± 19	4085-3929	2
EIB16-09B	BE-6936.2.1	0.80	wood	3689 ± 47	4151-3896	2
EIB16-05AB	BE-6933.2.1	0.64-0.66	wood	3693 ± 34	4148-3926	2
EIB16-05AB	BE-6933.1.1	0.64-0.66	wood	3725 ± 34	4221-3976	2
EIB16-09H	BE-6937.1.1	0.66	wood	3655 ± 37	4089-3876	1
EIB16-03A	BE-6932.1.1	0.18	wood	10,122 ± 55	12,012-11,405	old

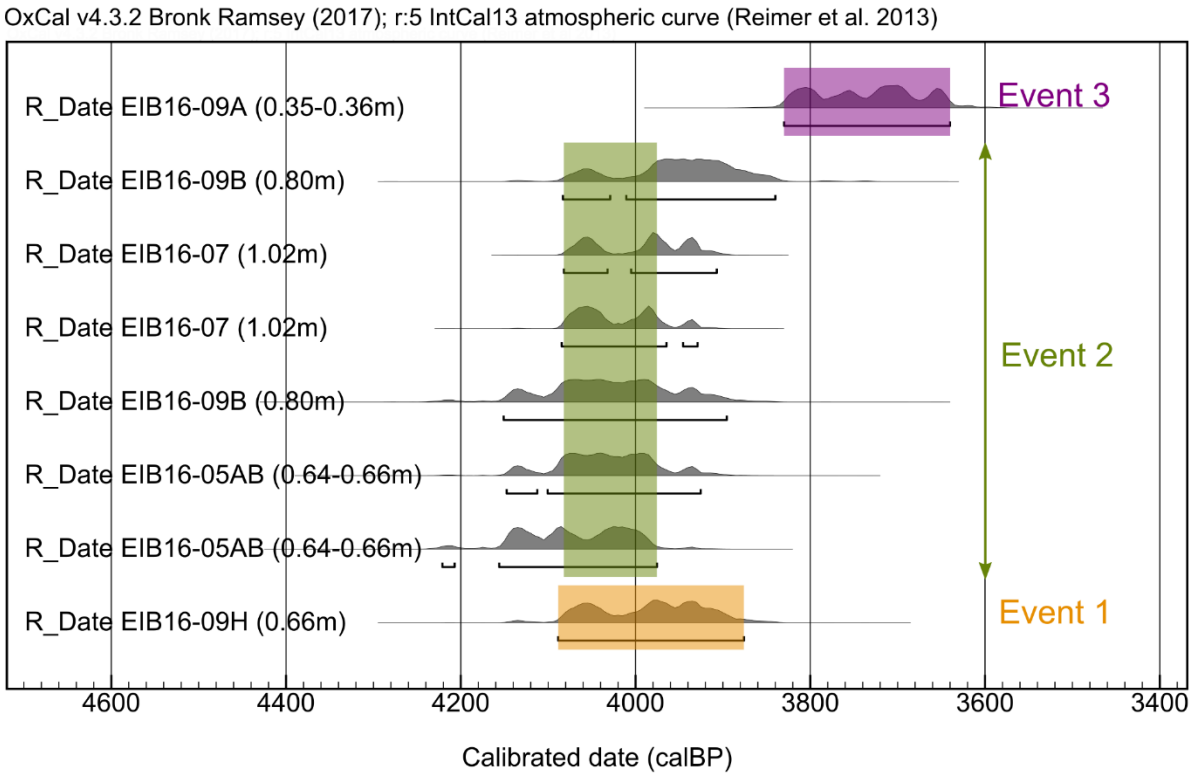

Figure 32: Radiocarbon ages of wood samples recovered from cores, calibrated with OxCal v.4.3.2. Events 1 and 2 are roughly 4000 years old and cannot be separated based on their calibrated age ranges. Event 3 occurred sometime between about 3830-3640 years ago.

Geomorphic Interpretation

In addition to the lake deposits, we also examined and mapped sediments and landforms around Lake Eibsee to distinguish different events. Slope analysis reveals flat plains north, west, and southwest of Zirmerskopf (Figure 33a). Sediments beneath these plains infill depressions within the Event 1 deposits. There are two plains, one at ~1000 m a.s.l. north of Zirmerskopf, and a second one at ~1030 m a.s.l. west of Zirmerskopf (Figure 33b). The latter slopes stepwise towards the east to ~1026 m a.s.l. and then ~1017 m a.s.l. We interpret these plains to be the result of water runoff towards the northeast during and after Event 2, which infilled the lower basin of the paleolake north of Zirmerskopf (see Figure 22b, c in Part I, Knapp *et al.*, 2020a). A 3D hillshade of the area (Figure 33c) displays our interpretation of how the highly fluidized mass of Event 2 entered and infilled the depressions beyond the Lake Eibsee shoreline. Flowing from the lake, it probably overran the Event 1 deposits at a nickpoint between Plattenkalk bedrock to the west, and the Event 1 deposits to the east. Figure 33c also shows Event 3 deposits to the east with levees to both sides.

Discussion

Here we discuss the three stages in Holocene evolution of the landscape at Lake Eibsee, potential triggers of the massive rock-slope failure from Mount Zugspitze, its impact on the paleolake, and the 'lake rebirth' phase.

The Rock Avalanche, Subsequent Mass Movements, and Rebirth of Lake Eibsee

The Eibsee rock avalanche (Event 1) occurred about 4000 years ago when 150-200 million m³ of limestone fell from the north flank of Mount Zugspitze (Haas *et al.*, 2014; Leith *et al.*, 2016). The seismic reflection survey showed that the rock avalanche deposits are distributed over the entire lake floor. A western lobe of the rock avalanche encountered a rising bedrock slope, and debris became stacked 10-20 m higher there than in the other parts of the lake (Figure 27c). An eastern lobe overtopped the paleodam and ran towards Garmisch-Partenkirchen. The main lobe, however, flowed directly to north through the paleolake (see Part I for details on interactive processes with the substrate). After deposition, the rock avalanche dust cloud presumably covered the whole area, and rainfall washed loose material into small valleys and depressions. Pools grew, merged, and started to build new small lakes with rock avalanche blocks and ridges between them (Figure 34a).

At this stage, a second rock-slope failure occurred (Figure 34b). The rock mass flowed into the shallow lake and entrained the water and dust of the Eibsee rock avalanche. In the distal facies, some centimeters of fine-grained sediment remained between the deposits of the first and second event (Figure 31a, at ~4.1- 4.2 m composite depth at core site 4). Therefore, we assume that Event 2 did not displace or entrain the underlying loose material, but rather first caused rapid loading (Hungr and Evans, 2004). Due to the loading, the fine sediment was compacted and consolidated, which is indicated by the up-core increase in density despite little or no change in grain size.

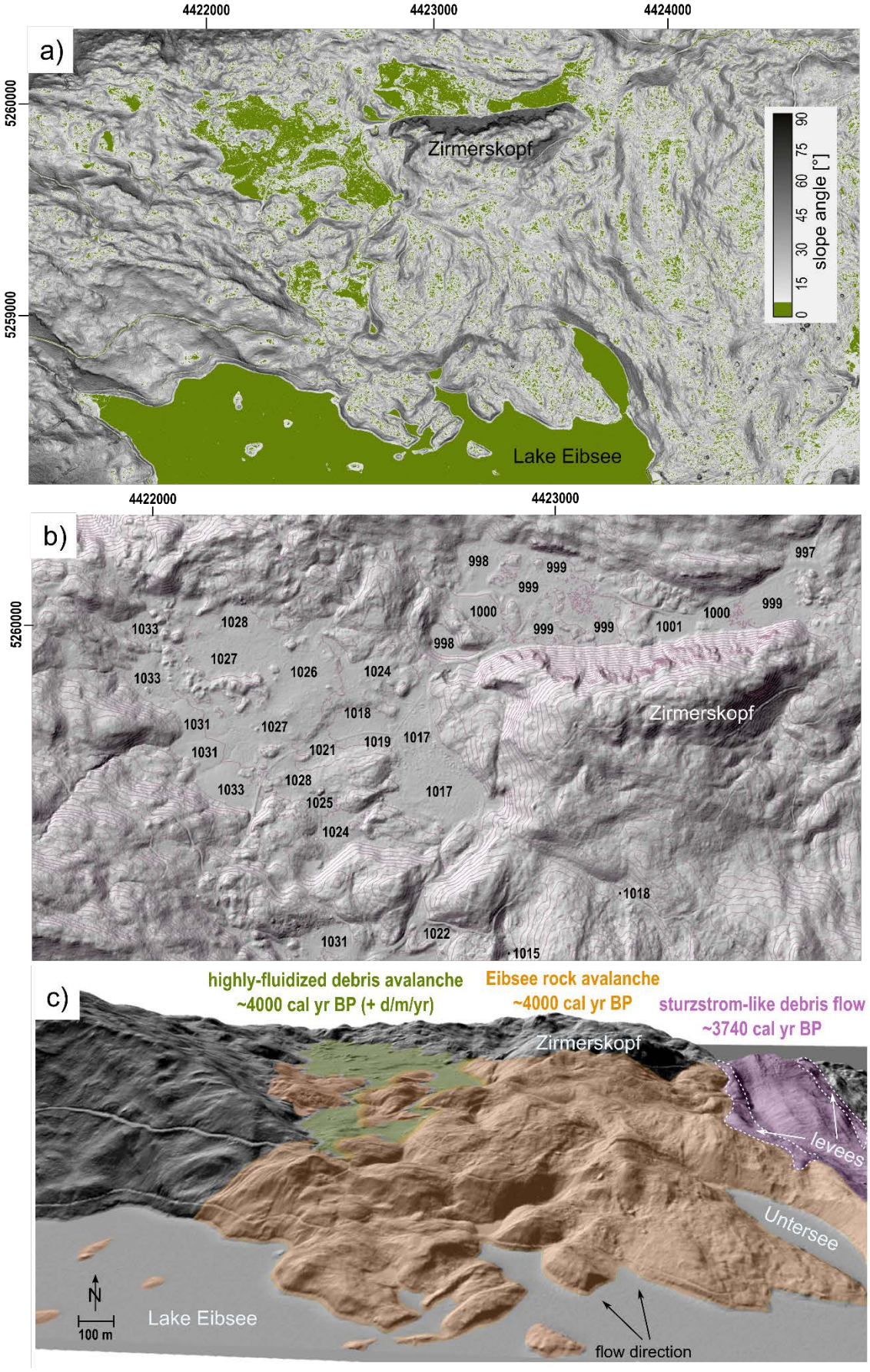

Figure 33: Geomorphology of the area north of Lake Eibsee. a) Slope angle map showing nearly horizontal plains within the hummocky rock avalanche deposits. b) Topographic map with 5 m contour lines showing the stepwise

southeastward decrease in the elevation of the plain west of Zirmerskopf, and the lower plain north of Zirmerskopf. c) Geomorphic interpretation in 3D view. All figures are based on a high-resolution 1-m-DEM hillshade (Bavarian Surveying and Mapping Authority, 2006). Coordinates are given in Gauss-Krüger Zone 4.

This process is interpreted to follow the conceptual model developed by Yarnold (1993; Figure 35), who hypothesized on the subaqueous runout of a rock avalanche. His conceptual model describes the interaction of the flowing rock mass with a lake floor and underlying fine-grained sediments. Three stages are differentiated, during which the rock avalanche debris (Figure 35a) entrains sediment, creating a 'contamination zone' at the base of the flow, and becomes more and more plastic (Figure 35b) and culminates with slip, but little scour before coming to rest (Figure 35c).

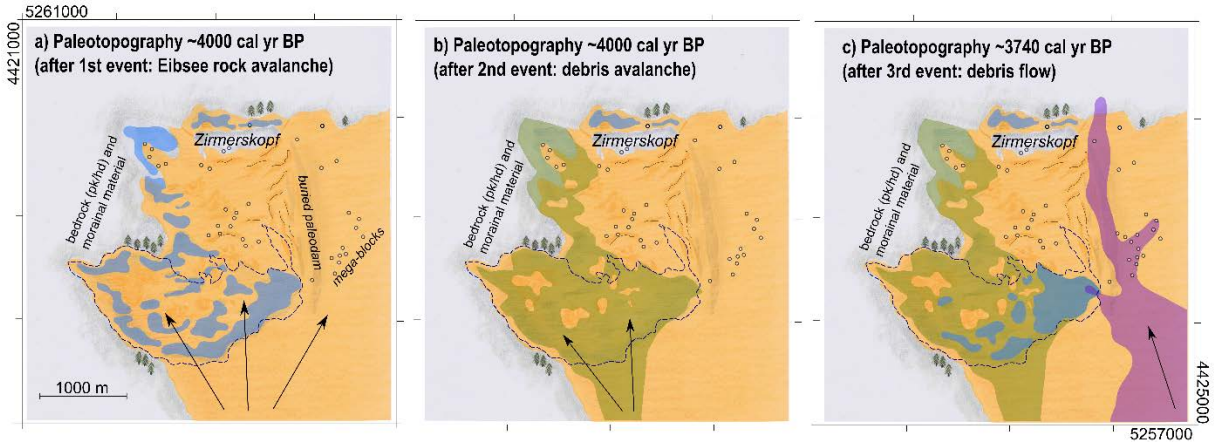

Figure 34: Synoptic sketch of landscape evolution around Lake Eibsee. a) Eibsee rock avalanche (orange). b) Debris avalanche (green) ~4000 cal yr BP. c) Debris flow ~3740 cal yr BP (purple). Dashed line delineates modern Lake Eibsee. hd = Hauptdolomite, pk = Plattenkalk Limestone. Coordinates are given in Gauss-Krüger Zone 4.

The highly fluidized debris infilled depressions on the rock avalanche deposits (Figures 28 and 29a; initial filling like in Lake Oeschinen, Knapp *et al.*, 2018), overtopped rock avalanche debris at the north shore and continued to the north until Zirmerskopf (Figure 33c). After the debris avalanche came to rest, coarse material settled down and finer and lighter material such as wood were deposited on top (Figure 30 and Figure 31). The deposits formed the plains described above (Figure 33a, b). Sediment from the adjacent slopes was washed in the newly formed Lake Eibsee (Litho-unit C).

Event 3 generated a large debris flow that travelled straight to the north, with a small western branch reaching the young "reborn" lake (Figure 34c), thereby generating a turbidite (Figure 28 and Figure 31) that interrupted the organic background sediments accumulating in the eastern basin. Fe-oxides and wood and leaf fragments in the sediment cores (Figure 31) indicate that the modern lake was shallow, which might explain the small amount of background sediment produced since Event 3, about 3700 years ago.

Today, Lake Eibsee drains to the north through the permeable rock avalanche deposits. Groundwater is retained by the clayey marlstones of the Allgäu Formation and flows around the Zirmerskopf. Here, the paleolake basin was not filled with rock avalanche deposits, and the ground surface is relatively low (~980 m a.s.l., Figure 33b). Swamps and wetlands in this

area are interpreted to be remnants of Paleolake Eibsee prior to the Eibsee rock avalanche (see Part I, Figure 26, Knapp *et al.*, 2020a).

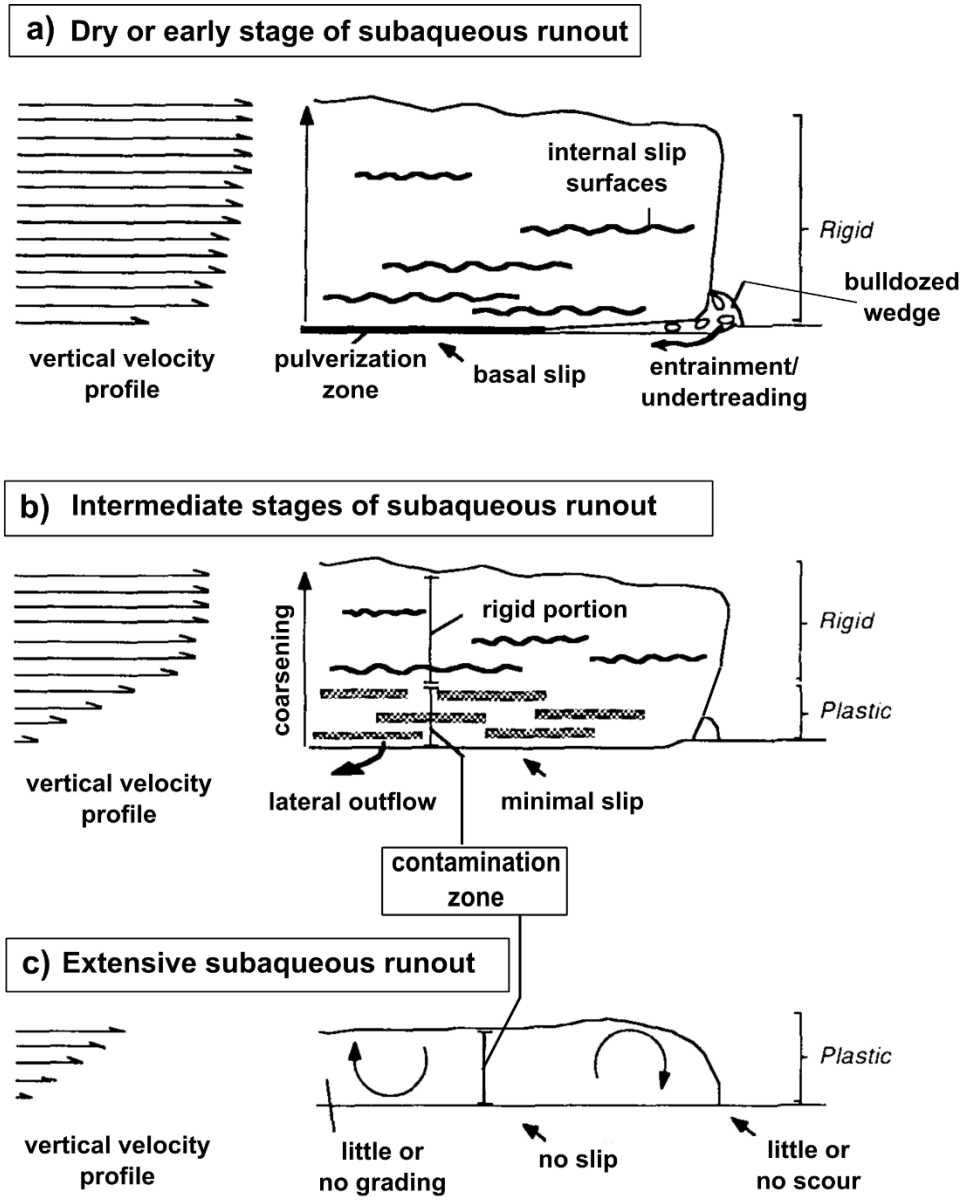

Figure 35: Modified conceptual model of subaqueous runout of a rock avalanche (redrawn from Yarnold, 1993).

Classification of Rock-Slope Failures

We recognize and characterize three large rock-slope failures. The classification of the landslides follows Hungr *et al.* (2014). Event 1, the Eibsee rock avalanche, was a massive rock-slope failure in carbonate rocks high on Mount Zugspitze (Abele, 1974; Jerz and Poschinger, 1995). The rock avalanche impacted Paleolake Eibsee and displaced its waters (Part I). The deposits show characteristics of dry rock avalanches with a carapace of mega-blocks (Krieger, 1977; Yarnold and Lombard, 1989; Shaller, 1991; Miller *et al.*, 2017).

Event 2 presumably started as a rock slide or rock avalanche similar to Event 1, but with much smaller volume and lacking mega-blocks. When entering the lake, we hypothesize that the rock mass entrained the available water. Partial or complete saturation of the sediments led

to fluidization of the mass (Iverson, 2005; McArdell *et al.*, 2007; Schneider *et al.*, 2011). Without confinement in an established channel but rather widespread shallow deposition, we interpret Event 2 to be a debris avalanche (type 25; Hungr *et al.*, 2014). Similar cases have been reported, for example, by Plafker and Ericksen (1978), Shaller (1991), Hungr and Evans (2004), and Hewitt (2006). The Event 2 rock mass may have detached from the Bayerisches Schneekar on Mount Zugspitze, thereby deepening the scarp niche of Event 1, or from a small scarp directly to the east (Figure 36).

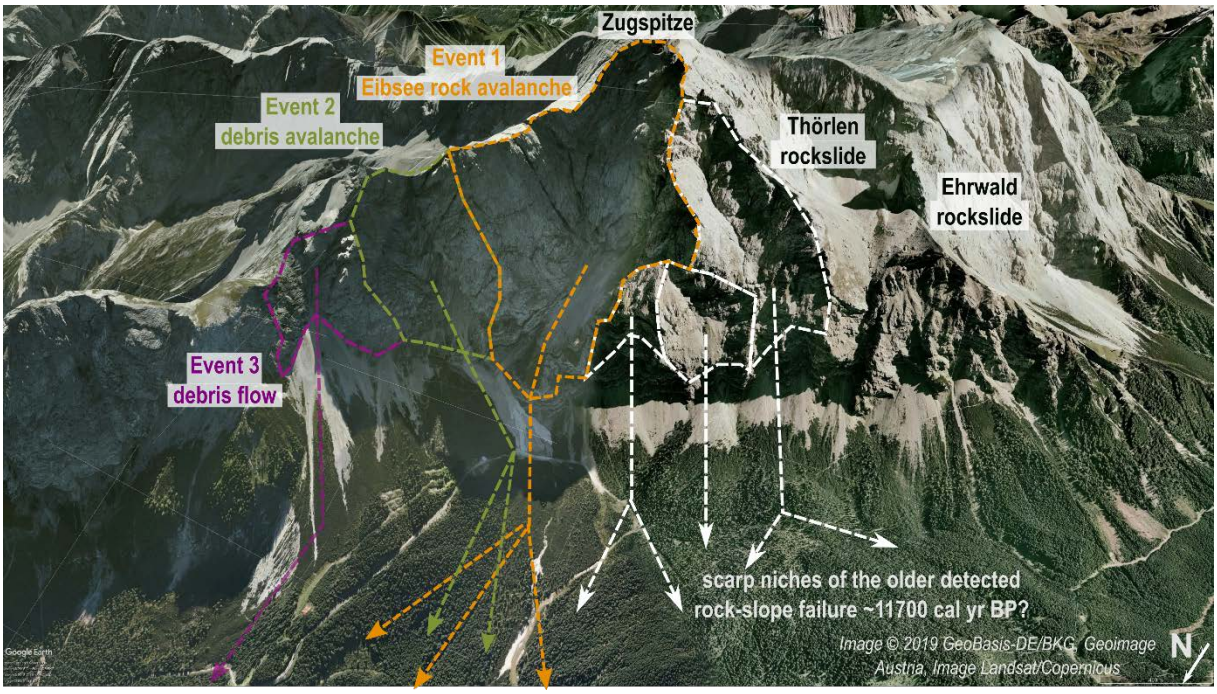

Figure 36: Potential scarps and travel paths of the mass movements documented in this paper. The scarp of Event 2 is oriented to the northwest. The neighbouring scarps may be related to older rock-slope failures (white polygons and arrows, see Table 5). Satellite image © 2019 GeoBasis-DE/BKG, Geoimage Austria, Image Landsat/Copernicus.

Event 3 is classified as a rock-slope failure, which transformed into a sturzstrom-like debris flow (type 19 or 22; Hungr *et al.*, 2014) that detached from Mount Hohe Riffel (Hornung and Haas, 2017) east of Mount Zugspitze. The debris ran ~4.5 km northward, leaving remarkable levees (Figure 33c). Possible scarp niches and travel paths are shown in Figure 36.

Re-dating of Events

Jerz and Poschinger (1995) obtained radiocarbon ages on seven wood samples recovered during drilling at Grainau IV and V (see Figure 20 in Part I for location). The ages range from 3615 ± 65 to 4915 ± 120 yr BP. They assumed that the Eibsee rock avalanche was ~3700 ^{14}C yr old.

Our samples from event deposits in Lake Eibsee yielded new chronological information. The Lake Eibsee sediments clearly do not record steady background deposition, as they are dominated by the event deposits: (i) large mass movements ran across the lake, displaced or entrained lake water, (ii) a turbidity current during a less energetic event might be trapped in one basin or trough, and (iii) some of the core sites may have been dry during the rebirth of the lake. Case (ii) happened at ~3740 cal yr BP when a mass movement entered the lake from the southeast; the related turbidite was found only at core site 4 (Figure 31). Thus, to establish

an event stratigraphy in Lake Eibsee is essential to recognize and correctly interpret superimposed event deposits. We compare our new radiocarbon ages with the previous ages from the Grainau drill cores, which we re-calibrated with OxCal v4.3.2 (Figure S9 in the Appendix).

Disregarding the outlier of samples 'BE-6932.1.1', which is probably reworked, and 'BE-6935.1.1', which marks the debris flow event at ~3740 cal yr BP, all other lake samples yielded ages ~4000 cal yr BP and date the Eibsee rock avalanche and the debris avalanche in its aftermath (events 1 and 2). All our ages overlap at 2σ to a period of 113 years, but is not possible to further refine the ages of events 1 and 2. The sediment between these two events, however, suggests an interval of at least some days or weeks to allow settling of dust and fine-grained sediment on top of the Eibsee rock avalanche mass and enough time to fill a shallow lake, but probably not more than few years or decades because there is no evidence of soil development.

Predisposing Factors and Potential Triggers

The Eibsee rock avalanche happened at the end of the second Holocene climate optimum (Wanner *et al.*, 2008). Climate cooled and became wetter ~4000-3700 cal yr BP (Heiri *et al.*, 2003), possibly gradually destabilizing the steep limestone rock slopes at Mount Zugspitze. Karst weathering favors the formation of cavities around the summits of the massive carbonate platform rocks in the Wetterstein Mountains (Hornung and Haas, 2017). In the case of events 2 and 3, the loss of rock mass in the headwall of the Bayerisches Schneekar during the Event 1 rock avalanche may have weakened the surrounding rock masses.

A possible earthquake trigger must also be considered, given that Mount Zugspitze is located in a seismically active region near the Loisach-Fernpass fault and the Inn Valley fault (Figure 27a; Linzer *et al.*, 2002; Lenhardt *et al.*, 2007; Nasir *et al.*, 2013). Our new dating results and re-calibration of the previously published ages enable a better evaluation of possible coincidences in the Fernpass rockslide cluster. The Fernpass rockslide has been dated at ~4150 ± 100 cal yr BP using the U/Th-method (Ostermann *et al.*, 2007). Other events in the Fernpass cluster include the Pletzachkogel landslide dated at ~3910 cal yr BP (Prager *et al.*, 2008; Patzelt, 2012b), the Stöttlbach landslide dated at 3800 ± 660 cal yr BP (Prager *et al.*, 2008), and megaturbidites generated by subaqueous landslides in Lake Piburg and Lake Plansee at ~4000 cal yr (Oswald *et al.*, 2020). The new results of the limnogeological studies at Lake Eibsee, Lake Piburg, and Lake Plansee, which are within a radius of 30 km, increase the likelihood that a large prehistoric earthquake triggered the Eibsee rock avalanche.

Conclusions

We identify and date three rock-slope failures at Lake Eibsee using a combination of lake core sedimentology and radiocarbon dating, geophysical surveys in the lake, and geomorphological analysis: (i) the Eibsee rock avalanche at ~4000 cal yr BP, (ii) a debris avalanche in the aftermath of the rock avalanche, presumably from the same scarp or a neighbor, and (iii) a sturzstrom-like debris flow from Riffelriss at ~3740 cal yr BP.

We radiocarbon dated the Eibsee rock avalanche at four sites in modern Lake Eibsee to 4089-3976 cal yr BP, which is about the same age as major rockslides in the Fernpass cluster. The possible coincidence in ages makes a large earthquake a possible trigger.

Age dating alone does not conclusively disclose the failure history. A multimethodological approach is important to refine recurrence rates. In contrast to the Tschirgant rock avalanche, where dating results first indicated two events (Patzelt, 2012a), but which Ostermann *et al.* (2017) later concluded was a single event, the Eibsee rock avalanche deposits suggest two events, the ages of which cannot be discriminated by radiocarbon dating.

The multiple events in the Lake Eibsee record provide evidence for successive failures of the Mount Zugspitze scarp niche.

There are three Eibsee lakes: (i) the original and largest one existed until the Eibsee rock avalanche (Event 1) about 4000 years ago (Paleolake 1; see Part I); (ii) several shallow ponds separated by islands that formed in the aftermath of the massive rock avalanche and lasted until the debris avalanche of Event 2 (Paleolake 2); and (iii) the modern Lake Eibsee, which started to form soon after Event 2.

Paleolake sediments were not retrieved at any of the coring sites because the piston corer could not penetrate the carapace of Event 1. However, geophysical data indicate that the entire lake floor is underlain by Event 1 deposits.

Acknowledgments

Sibylle Knapp acknowledges PhD funding from the German National Academic Foundation (Studienstiftung des deutschen Volkes e.V.). Radiocarbon dating was financially supported by the British Society for Geomorphology through a Postgraduate Research Grant to Sibylle Knapp. We thank the Rieppel family for allowing us to do fieldwork on Lake Eibsee. Verena Stammberger, Christoph Mayr, Ioannis Kouvatsis, and the Wasserwacht Garmisch-Partenkirchen supported fieldwork. Andreas von Poschinger provided drill-hole logs, and Ulrich Haas contributed to discussions during this study.

5.4 Flims: Sediment Transport after Rockslide Impacting Paleolake Bonaduz Revealed in Terrestrial Outburst-Flood Deposits

This chapter contains results of the unpublished master thesis by Schwenk (2017) and is a preliminary version of the following publication: Knapp, S., Schwenk, M., Krautblatter, M. (in preparation). New Geophysical Evidence for the Evolution of the Toma Hills and Bonaduz Gravels in the Flims Rockslide (Grisons Alps, Switzerland).

Abstract

Rock slides and rock avalanches are amongst the most destructive natural hazards in alpine environment. The Flims rockslide is the largest known rock-slope failure in the Alps and has fascinated researchers with its complex and diverse features, revealed in excellent outcrops, ever since. Here we focus on the hypothesized impact of the Flims rockslide on (Paleo-) Lake Bonaduz. This massive impact caused intensely fluidized rock material, which formed the famous Bonaduz gravels and Toma hills, probably accompanied by a catastrophic impact wave. Geophysical investigation with electrical resistivity tomography (ERT) combined with sedimentological mapping answers long-debated questions on the stratigraphic relation between the Flims and Tamins rockslide deposits. The distribution, thickness, and internal structure of the Bonaduz gravels, the Toma and Cresta hills, as well as other flood deposits around Ils Aults could be analysed to a sediment depth of up to 160 m. There is new field evidence that the Bonaduz gravels build an onlap on the Ils Aults and were therefore formed after the Tamins rockslide. The Toma/Cresta hills consist of blocky cores with an agglomeration of smaller mixed sediments, which drift and override the Toma core, building the smoothly shaped top. We consider a simultaneous transport within the Bonaduz gravels, yet a slightly slower movement at the front due to bulldozing effect. This study contributes to an improved understanding of the stratigraphical context of the Tamins and Flims deposits. Moreover, water-rich entrainment in rock avalanches, and the genesis and transport of outburst-flood deposits, in particular of Toma hills resp. hummocks are deciphered.

Introduction and Study Site

The Flims rockslide with a volume of 10-12 km³ is the largest known Alpine rock-slope failure and occurred in the Vorderrhein River valley, Eastern Switzerland. The broad, U-shaped valley tectonically separates Jurassic and Cretaceous limestone, dolomite, and schistose metasedimentary rocks of the Helvetic nappe to the North from metasedimentary Penninic rocks to the South (Pfiffner *et al.*, 2002). The rockslide occurred at the northern valley flank (Figure 37) in Triassic and Jurassic limestone, dolomite and shale of the Helvetic zone, and transformed into a rock avalanche. For reasons of simplification, the Flims rock-slope failure is in the following referred to as a rockslide. The deposits cover an area of ~52 km² (Heim, 1932; Abele, 1974; Poschinger *et al.*, 2006) and had originally been thought to be of Lateglacial age, but then could be dated in several studies by applying radiocarbon and cosmogenic nuclide dating to a mean age of ~9000 cal BP (Poschinger and Haas, 1997; Schneider *et al.*, 2004; Deplazes *et al.*, 2007; Ivy-Ochs *et al.*, 2009). The rockslide presumably impacted a lake (Poschinger *et al.*, 2006; Calhoun and Clague, 2018), which is in the following called (Paleo-) Lake Bonaduz. The mobilized sediment-water-mixture with a volume of several 100 million m³ must have had

gigantic capacities to transport such large units of rock slabs and to bring massive amounts of gravel into suspension, resulting in a hyperconcentrated mass flow (Calhoun and Clague, 2018). These slabs partially did not break apart during the transport and were deposited as 'Toma', i.e. isolated cone- to pyramidal- or roof-shaped hills composed of Helvetic rock material (Abele, 1974). The Toma and Cresta hills, i.e. Toma hills on the eastern side of the Ils Aults, are distributed over the Bonaduz gravels in certain places (Pavoni, 1968b; Poschinger *et al.*, 2006; Poschinger and Kippel, 2009; Poschinger and Ruegg, 2012), which are a characteristic graded but unstratified sediment (Figure 38a) and build a plain between the Flims and Tamins rockslide deposits. Toma in the European Alps are known also from the rock avalanches at Tschirgant (Dufresne *et al.*, 2016a), Eibsee (Ostermann and Prager, 2016), Fernpass (Prager *et al.*, 2006), and Obernberg valley (Ostermann *et al.*, 2012). They are also referred to as hummocks (e.g. Paguican *et al.*, 2014; Dufresne and Geertsema, 2020), although this is a more general term of rock-avalanche hill and does not necessarily show the typical shape of a cone.

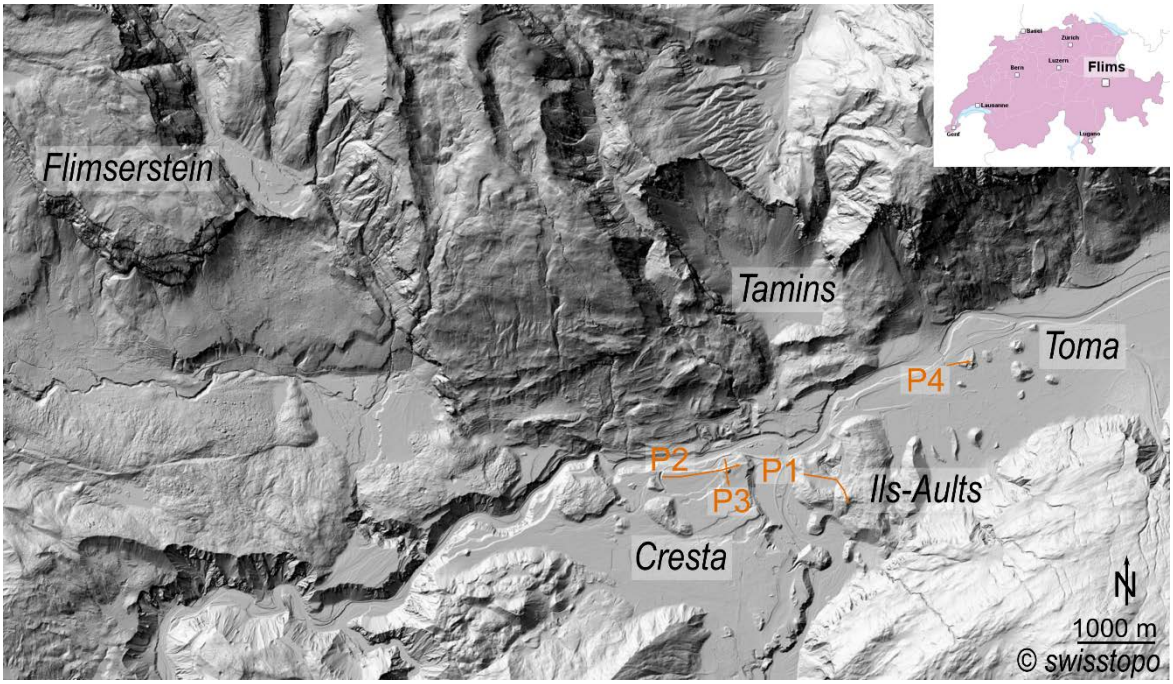

Figure 37: Overview of the Vorderrhein River valley depicting the Flimserstein, where the Flims rockslide detached from, the scarp of the Tamins rockslide, the Ils Aults consisting of Tamins deposits, and the Cresta and Toma hills. The ERT profiles P1-P4 are marked with orange colour. High-resolution DEM: swisstopo.

The evolution of the above described characteristic sediments of the Toma/Cresta and Bonaduz gravels, as well as the order of geological events related to the Flims and Tamins rockslides, including formation and failure of rockslide dams, formation and outburst of dammed lakes and the deposition of flood deposits, have been debated since the beginning of the 20th century. Assumed to be a key to understanding complex emplacement after water-rich entrainment, the internal structure of the Toma and Bonaduz gravels is important to study (Poschinger *et al.*, 2006). By applying geoelectrical measurements in this study, we aim to make the internal structure visible in a broad scale down to max. ~160 m sediment depth and, by this, contribute to a better understanding of the stratigraphic relationships.

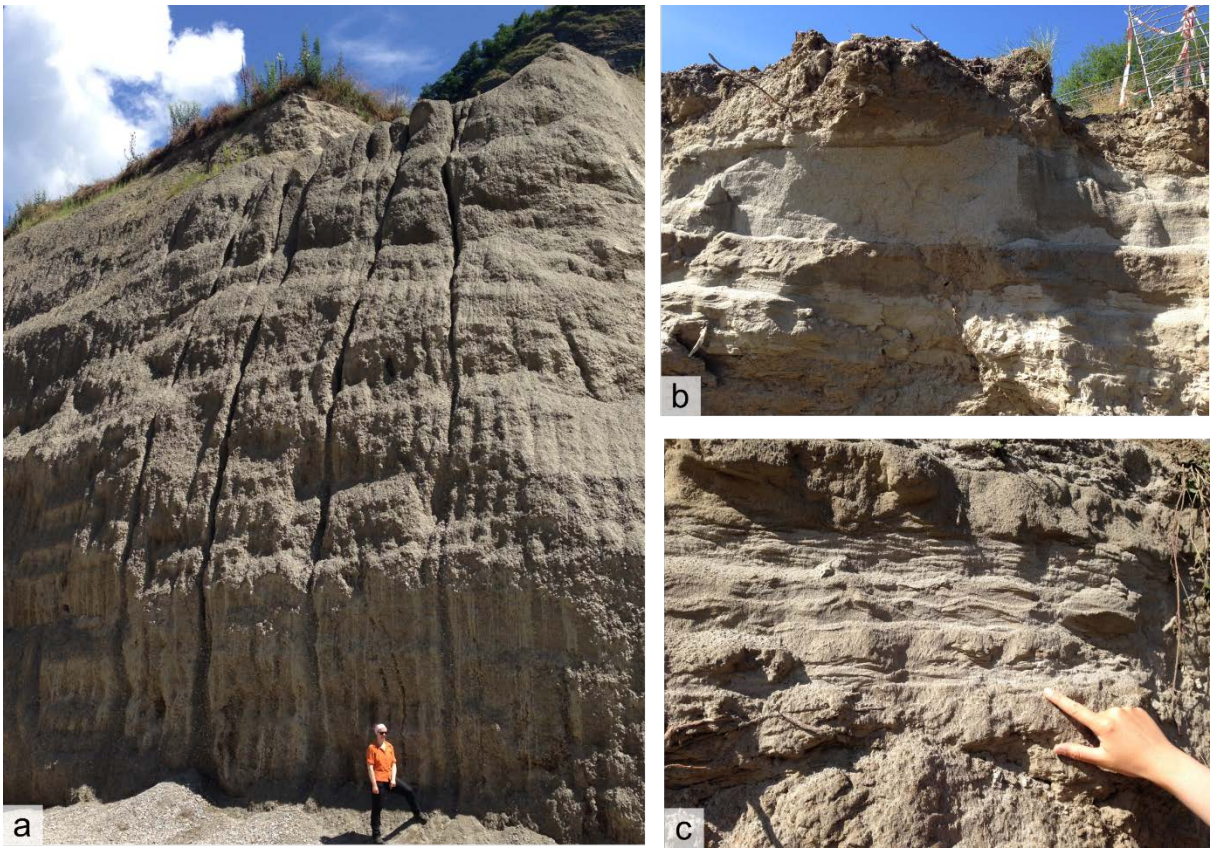

Figure 38: Outcrops of Bonaduz gravels showing a) unstratified, normally graded gravel deposits with fine-grained matrix, and b) and c) layered sands and silts at the top of the Bonaduz type locality at the gravel pit in Reichenau. Photo courtesy: M. Krautblatter.

Methods

Seven ERT surveys were conducted in the area around the Tamins deposits at Ils Aults. For the ERT measurements, an ABEM SAS 1000 Terrameter and four 100-m-long electric cables with an electrode spacing of 5 m, and four 200-m-long electric cables with an electrode spacing of 10 m came into operation. Roll alongs made it possible to increase the penetration depth over a broader distance covered with a profile (e.g. Figure 39a with one roll along yielding 1000 m profile length). A combination of Wenner and Schlumberger arrays was chosen. The local topography along the profiles was measured by an inclinometer and included in the ERT model, calculated with the RES2Dinv (ver. 3.5) software. The results were then interpreted on the basis of our field observations in the numerous outcrops close to the profiles.

Results and Interpretation

Profile P1 (Figure 39a) shows a NW-SE oriented transect modelled from two datasets. One data set was conducted in a 500 m roll along survey with 5 m electrode spacing, the second was generated from an 800 m long four-cable survey with 10 m electrode spacing. The transects are overlaid in order to provide a high spatial resolution in the upper 50-80 m sediment depth and a high penetration depth of up to ~160 m. The overall error of this combined model with 4.9 % is quite low, which can also be demonstrated by the similarity of the MinMax-models (Figure S10).

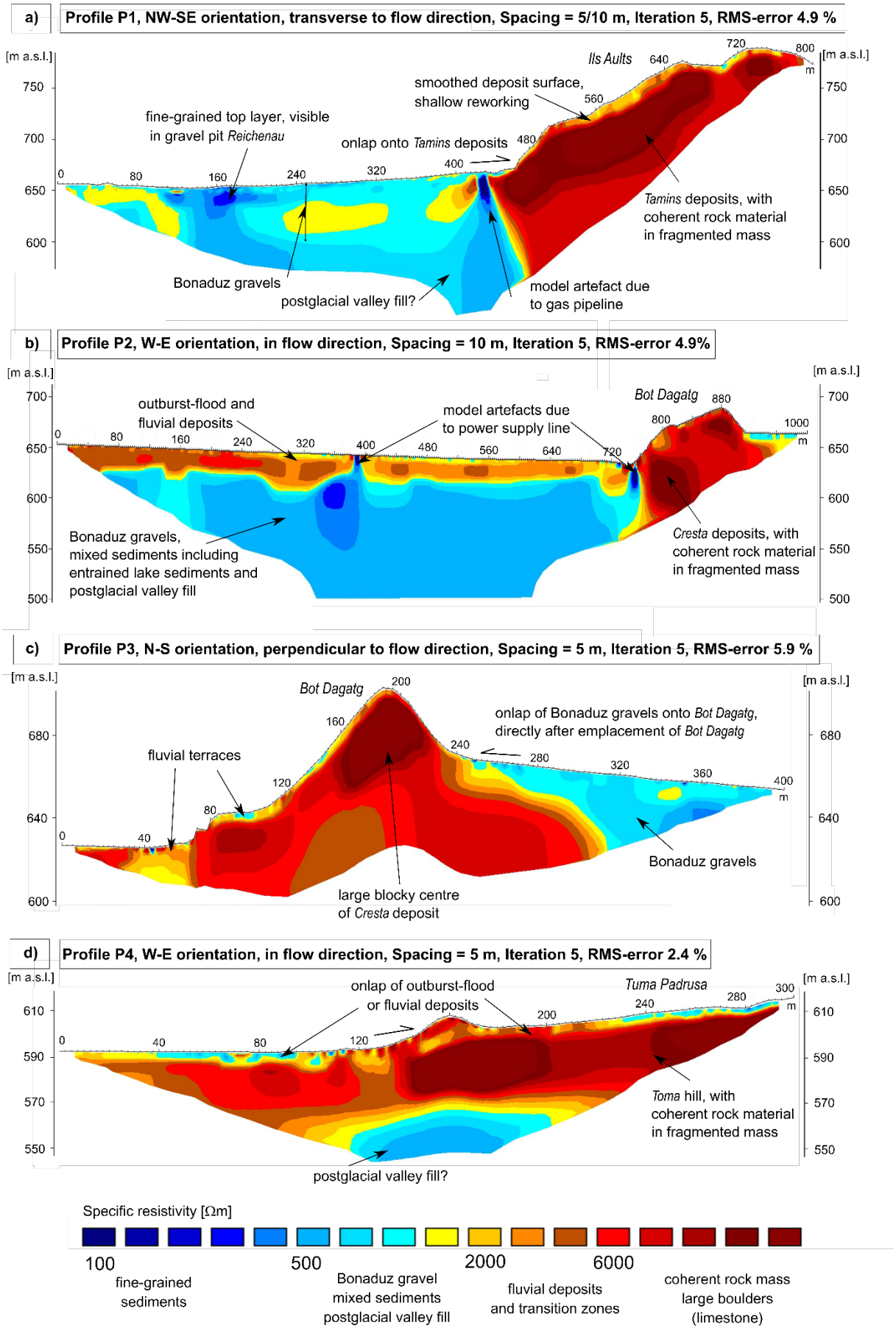
a) Profile P1, NW-SE orientation, transverse to flow direction, Spacing = 5/10 m, Iteration 5, RMS-error 4.9 %
[m a.s.l.]
Ils Aults
smoothed deposit surface, shallow reworking
fine-grained top layer, visible in gravel pit Reichenau
onlap onto Tamins deposits
Tamins deposits, with coherent rock material in fragmented mass
Bonaduz gravels
postglacial valley fill?
model artefact due to gas pipeline
b) Profile P2, W-E orientation, in flow direction, Spacing = 10 m, Iteration 5, RMS-error 4.9%
outburst-flood and fluvial deposits
model artefacts due to power supply line
Bot Dagatg
Bonaduz gravels, mixed sediments including entrained lake sediments and postglacial valley fill
Cresta deposits, with coherent rock material in fragmented mass
c) Profile P3, N-S orientation, perpendicular to flow direction, Spacing = 5 m, Iteration 5, RMS-error 5.9 %
Bot Dagatg
onlap of Bonaduz gravels onto Bot Dagatg, directly after emplacement of Bot Dagatg
fluvial terraces
Bonaduz gravels
large blocky centre of Cresta deposit
d) Profile P4, W-E orientation, in flow direction, Spacing = 5 m, Iteration 5, RMS-error 2.4 %
onlap of outburst-flood or fluvial deposits
Tuma Padrusa
Toma hill, with coherent rock material in fragmented mass
postglacial valley fill?
Specific resistivity [Ωm]
100
fine-grained sediments
500
Bonaduz gravel mixed sediments postglacial valley fill
2000
fluvial deposits and transition zones
6000
coherent rock mass large boulders (limestone)

Figure 39: ERT profiles P1-P4 indicating a) ~60 m thick Bonaduz gravels onlapping onto Ils Aults, b) Cresta Bot Dagatg transported within Bonaduz gravels, covered with some fluvial and/or outburst-flood deposits, c) onlapping Bonaduz gravels onto the Cresta Bot Dagatg, and d) Tuma Padrusa containing large slabs of coherent rock material in a fragmented rock mass.

It should be noted that at meter 430 a gas pipeline crosses perpendicular to the transect at unknown depth. Mainly two resistivity units can be deciphered. Coming from NW, mixed sediments reach far down to 50-60 m penetration depth, indicated in yellow and light blue colour in the model. These sediments are well accessible in the gravel pit of Reichenau for sedimentological correlation, and consist mainly of gravel with sandy to silty matrix, normally graded but unstratified, and partially covered with a sandy to silty top layer (Figure 38b,c). The Bonaduz gravels are ~60 m thick here. This location represents the type locality of the Bonaduz gravels. Despite the influence of the crossing gas pipeline causing a model artefact, the resistivity patterns to both sides of artefact appear to match, so the onlap of the Bonaduz gravels onto the rise of the Ils Aults at meter 400-450 is clearly visible. The Ils Aults is regarded as Tamins rockslide deposit, which is indicated by typical high resistivity values of coarse, blocky rock material. There is also a sediment cover visible on top of the Ils Aults rockslide deposits, which is indicated by mid-range resistivity values and marked with yellow colour in the model.

The Cresta Bot Dagatg is investigated in profiles P2 and P3 (Figure 39b,c). Profile P2 is a W-E oriented transect across Bot Dagatg, representing the highest point of the transect at an elevation of 690 m a.s.l. The survey reaches a maximum penetration depth of ~160 m on a total profile length of 1000 m. The overall error of the resistivity model with 4.9 % is low (for MinMax-models see Figure S10). It should be noted that at meters 390 and 740 power supply lines cross perpendicular to the transect. Profile P3 is the N-S oriented cross-cut section to Profile P2 and runs again across Bot Dagatg. This survey reaches a distance of 400 m with a maximum penetration depth of ~60 m. The overall error of the resistivity model is 5.9 % and shows highest uncertainties at locations with rapid changes in resistivity (for MinMax-models see Figure S10). In both profiles P2 and P3, the survey depth does not cover the “root”, i.e. the maximum depth of Bot Dagatg. However, we gain information on the contact of the Cresta hill and the surrounding sediment. There is a transition from highest resistivity values within Bot Dagatg to lower resistivity values around it. The contact is quite sharp. The centre of the Cresta shows blocky, coherent rock material. In profile P2, an onlap is indicated of the uppermost sediment onto the rise of Bot Dagatg. The Cresta, therefore, is interpreted to have been transported within the surrounding mixed sediments, which show smaller grain sizes, and has been slightly overrun during emplacement by the surrounding slurry, building an onlap.

Profile P4 (Figure 39d) is a W-E oriented survey crossing Tuma Padrusa on a length of 300 m. This survey reaches a maximum penetration depth of 60 m. The overall model error is 2.8 %. In the center of the Toma, coarse, blocky material is indicated by high resistivity values. The Toma is covered by a thin layer of mixed sediment, which seems to have overrun the coarse, coherent rock material in the centre, as already observed for Bot Dagatg in profiles P2 and P3, thereby forming the summit of the Toma at meter 160. The position of the summit is not directly in the middle of the Toma. The onlapping, overrunning material was probably decelerated during the uphill movement and came to stop “on the ramp”. The root of the Toma can be easily identified in ~30-40 m penetration depth.

Discussion

This study reveals geophysical insights into the internal structure and evolution of the Bonaduz gravels and Toma/Cresta hills. Our analysis of Bot Dagatg and Tuma Padrusa, shown in profiles P2-P4 (Figure 39b-d), confirm the observation by Staub (1910) that the Toma hills consist of large blocks of crushed and shattered mass movement deposits of presumably coherent limestone. Both Toma and Cresta hills show the same internal structure with sharp contacts to the surrounding resp. underlying sediment. As profile 4 clearly shows, the lateral boundaries of the Toma sediment are not restricted to the landform visible at the surface. The coarse material can be spread. This would support Calhoun and Clague (2018) in their theory that the Toma around Domat/Ems are remnants of Tamins rockslide deposits, which were torn apart during the catastrophic dam breakage. Our results of Tuma Padrusa at least indicate that the Tuma Padrusa was transported eastwards, indicated by the onlap and the overrunning sediment coming from West, and that the coarse rock material, which builds up the Toma hill, also occurs in the front and the back. Thus, a connection to neighboured Toma in the close vicinity seems possible, but needs more field research. The internal structure and content of the Toma/Cresta do not allow for a clear separation between Flims origin and remobilized Tamins material.

Concerning the general evolution and stratigraphical position of the Toma/Cresta hills, our results confirm the simultaneous transport within a highly fluidized mass movement (Prager *et al.*, 2006; Paguican *et al.*, 2014; Calhoun and Clague, 2018). The onlapping sediment units were also described by Prager *et al.* (2006), who investigated the Toma hills related to the Fernpass rockslide by applying ground-penetrating radar (GPR). They interpreted the onlapping sediments as post-rockslide fluvial clasts. In the Flims context, we suggest that the onlapping sediments could possibly derive from the Bonaduz gravels, where the uppermost transported, finer-grained portions of the hyperconcentrated flow (Figure 38b,c) were able to overrun the coarse material of a Toma/Cresta or the carapace of the Ils Aults (Figure 39a). This would rather imply a syn-depositional or late-depositional emplacement of the onlapping unit, clearly linked in time to the main event. We thereby assume that the coarse centre of a Toma/Cresta comes to stop first due to strong internal cohesive forces and resulting high friction to the surrounding sediment, so that the finer grained slurry can overtop in flow direction, building an onlap. It is possible that the Toma centre is slightly moved and maybe rotated during the overflow of and interaction with the finer sediment (Dufresne and Geertsema, 2020). Still, it remains unclear, whether the top deposits revealed in the outcrops and the geophysical data could also have been deposited during later outburst floods of Lake Ilanz (Schneider *et al.*, 2004; Poschinger *et al.*, 2006).

In the stratigraphical context of the Tamins deposits, the contact of the Bonaduz gravels with the deposits of the Ils Aults was investigated. Our results show an onlap of the Bonaduz gravels onto the Ils Aults deposits. Thus, the Ils Aults must have been deposited before the Bonaduz gravels were formed in the hyperconcentrated flow. This onlap is a novel piece of field evidence which further confirms the theories (Scheller, 1970; Abele, 1991; Poschinger *et al.*, 2006) that (i) the Tamins rockslide occurred before the Flims rockslide, (ii) the Tamins deposits formed a dam and probably created Paleolake Bonaduz, and (iii) the Flims rockslide impacted Paleolake Bonaduz, thereby triggering a hyperconcentrated mass flow with gravel in suspension (Calhoun and Clague, 2018), known as Bonaduz gravels (Figure 40).

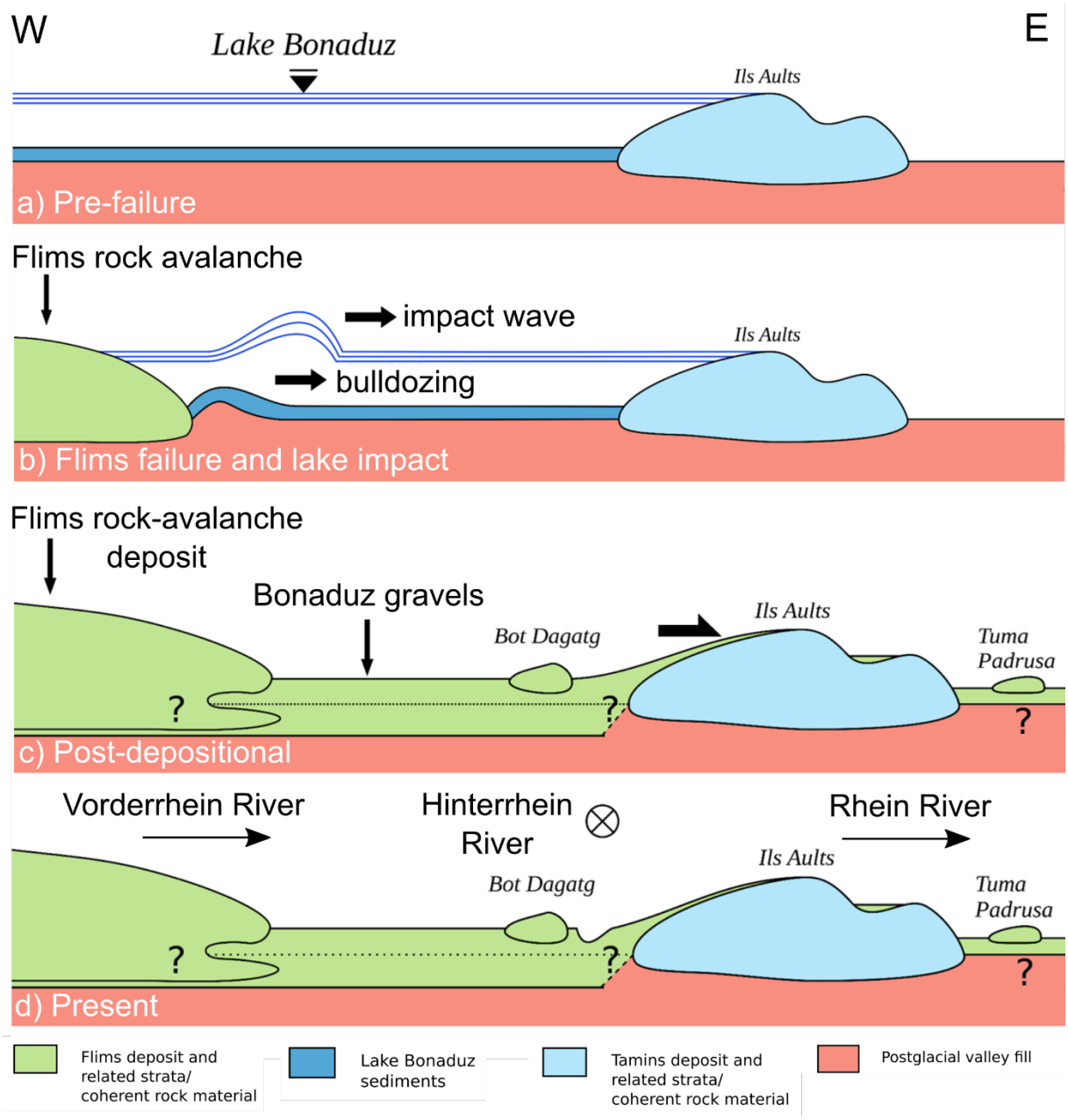

Figure 40: Geological timeline supporting the following theories: a) (Paleo-) Lake Bonaduz dammed by the Ils Aults, b) impact wave and bulldozing after impact of Flims rock avalanche, with c) and d) simultaneous formation of Bonaduz gravels, transporting Cresta hills, and maybe also Toma hills. Schematic sketch without scale modified after Schwenk (2017).

Conclusions

The *Toma/Cresta internal structure* shows a core of coherent, blocky rock material, embedded in a fragmented rock mass. Tuma Padrusa is ~30-40 m deep. The Ils Aults (Tamins rockslide deposits) contains numerous large boulders.

Concerning the *Toma morphology*, the results indicate that an agglomeration of mixed sediments with smaller grain size (gravel-sand-mixture) drift and override the Toma core, building an onlap in flow direction and a smoothly shaped top.

The *Toma transport* is regarded as simultaneous for the coherent rock slabs in the Toma core, but the onlapping and overriding slurry is assumed to be emplaced rather late-depositional,

while the Toma core has already stopped due to internal cohesion and resisting forces against the movement.

The *stratigraphic position of the Toma/Cresta hills* is related to the Flims rockslide/rock avalanche and the corresponding hyperconcentrated flow (Bonaduz gravels). Some of them might also be related to the previous Tamins rockslide. It is not possible to distinguish between Flims or Tamins origin based on the internal structure, material content, and flow direction.

In the Flims context, the *onlap of the Bonaduz gravels onto the Ils Aults* represents a novel piece field evidence in the debate of the geological timeline. The following theories are supported by this evidence: (i) the Tamins rockslide occurred before the Flims rockslide, (ii) the Tamins deposits formed a dam and probably created Paleolake Bonaduz, and (iii) the Flims rockslide impacted Lake Bonaduz, thereby triggering a hyperconcentrated mass flow with gravel in suspension (Calhoun and Clague, 2018), known as Bonaduz gravels.

6 Synopsis and Discussion

6.1 Major Outcomes from the Case Studies

6.1.1 Frequency and Magnitude of Rock-Slope Failures

- *Can we decipher multistage rock-slope failures in frequency and magnitude and classify them accordingly?*
- *How accurate can the recurrence rates of repeated massive rock-slope failures be determined?*
- *What role does continuous lake sedimentation play?*

In this thesis, two alpine lakes have been investigated in order to refine recurrence rates and magnitudes of rock-slope failures, which reached the lake. The data cover broad time spans, age ranges and detected volumes of the single rock-slope failures (Figure 41). In the sedimentary subsurface of Lake Oeschinen, the event deposits of at least eleven rock-slope failures, six of which have multistage character, are deciphered in time and space over the last ~2500 years. Thereby, the laminated background sediment in Lake Oeschinen plays a major role, as it separates the event-related turbidites by sediment sections, which are sufficiently thick for an identification on the seismic profiles. Here, the turbidity currents, caused by the mass movements, can be tracked throughout the lake and used for assigning stratigraphic positions by core-to-core-correlation and seismic-to-core-correlation. The presence of clastic varves and the varve chronology previously established by Amann *et al.* (2015) further enable an accurate dating of the last five events which have occurred in the last ~1000 years.

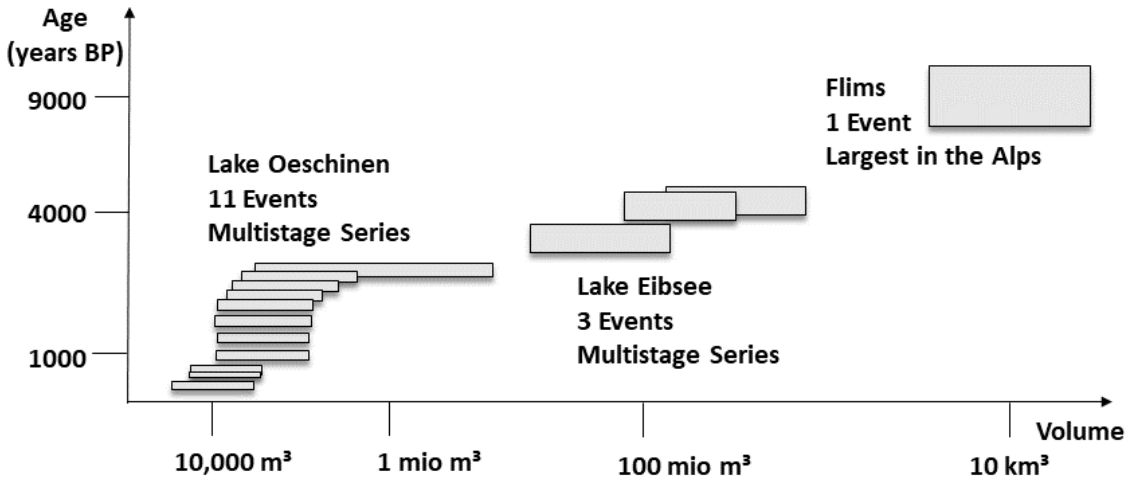

Figure 41: Synthetic graph with deciphered recurrence rates and volumes of rock-slope failure in the presented studies at Lake Oeschinen and Lake Eibsee, also related to the age and the volume of the investigated Flims rockslide.

At Lake Eibsee, two multistage rock-slope failures occurred ~4000 years ago. Although their impacts on the lake resulted in two completely devastating events and destroyed supposedly laminated lake sediments during erosion and entrainment, lake sedimentation is once again the major player for deciphering the multistage, superimposed event deposits of the two-stage failure. Rock-avalanche dust deposits had settled down gradually in the remaining, supposedly shallow water column after the first event. This sediment was then reworked during

the second event, but left a unique sequence of ~0.2 m between the coarse rock debris of Event 1 and 2, which is the field evidence to separate these two events. This small sediment sequence is especially important to note, as it was not possible to separate the two events by radiocarbon dating or varve chronology. The two events occurred shortly after each other, so that (i) there was hardly enough time for the production of background lake sediments such as varves, and (ii) not enough time between these two events for separating them within the age range of radiocarbon dates; finally these two events completely disturbed/destroyed the lake system, so that (iii) turbidites are lacking, which otherwise could be related to the two events and used for assigning stratigraphic positions like in Lake Oeschinen. Nevertheless, the third event formed a distinct turbidite in the midwhilst recovered lake system, which could be dated to ~3740 cal BP.

For the assessment of magnitudes, volumes are usually estimated based on the covered area and the thickness of event deposits. Other approaches analyse the potential scarp niche and calculate back the failed volume. Without knowing how many events actually contributed to the pile of rock debris and without the assessment of the thickness and amount of entrained material in numerous drillings, outcrops or by geophysical investigation (e.g. ERT), volume estimations of a supposedly single rock-slope failure event vary widely (e.g. Köpfli *et al.*, 2018). The studies of the lake sediments in Lake Oeschinen and Lake Eibsee cannot provide an accurate quantitative approach for assessing magnitudes, either. But, the sedimentological and geophysical information, both in the lakes and on land, combined with geomorphic analysis of potential scarp niches and energy considerations yield quite balanced qualitative results on magnitudes. Hence, as we now know, the volume of the Eibsee rock avalanche estimated to 300-400 mio. m³ by Jerz and Poschinger (1995) is distributed on three events. This further supports the volume estimations of 150-200 mio m³ by Haas *et al.* (2014) and 165 mio m³ by Leith *et al.* (2016) referring to one event only, namely Event 1 detaching from the scarp niche ”Bayerisches Schneekar”. Finally, including the information gained on the interactive processes of the failed rock mass with the lake sediments allows to classify the single event deposits.

6.1.2 Scenarios and Effects of Rock-Slope Failures Impacting Lakes

- *How does the impact of a rock-slope failure alter the lake?*
- *Can we decipher interactive processes related to the impact, the entrainment of water and fines, and the collision with obstacles in a confined setting?*
- *Can we decipher different modes of fluidized transport and ascribe them to distinct deposit types?*

While visible hazards and effects, i.e. happening at the surface, have recently been well documented and analysed (e.g. Evans *et al.*, 2011; Haeberli *et al.*, 2017; Fan *et al.*, 2020), subsurface effects lack detailed information because the base of large rock-slope failures are rarely accessible in outcrops. In this dissertation, diverse scenarios of a rock-slope failure impacting a lake have been investigated, both in the lakes (Lake Oeschinen and Lake Eibsee) and on land (Lake Eibsee and Flims).

The following synoptic sketch in Figure 42 and Table 6 are to summarize and visualize the most important deciphered scenarios and effects presented in the case studies. The type of the

rock-slope failure based on the movement, classified according to Hungr *et al.* (2014) and Hungr and Evans (2004), as well as the ratio of the assumed volumes of the rock-slope failure related to the lake are taken into account.

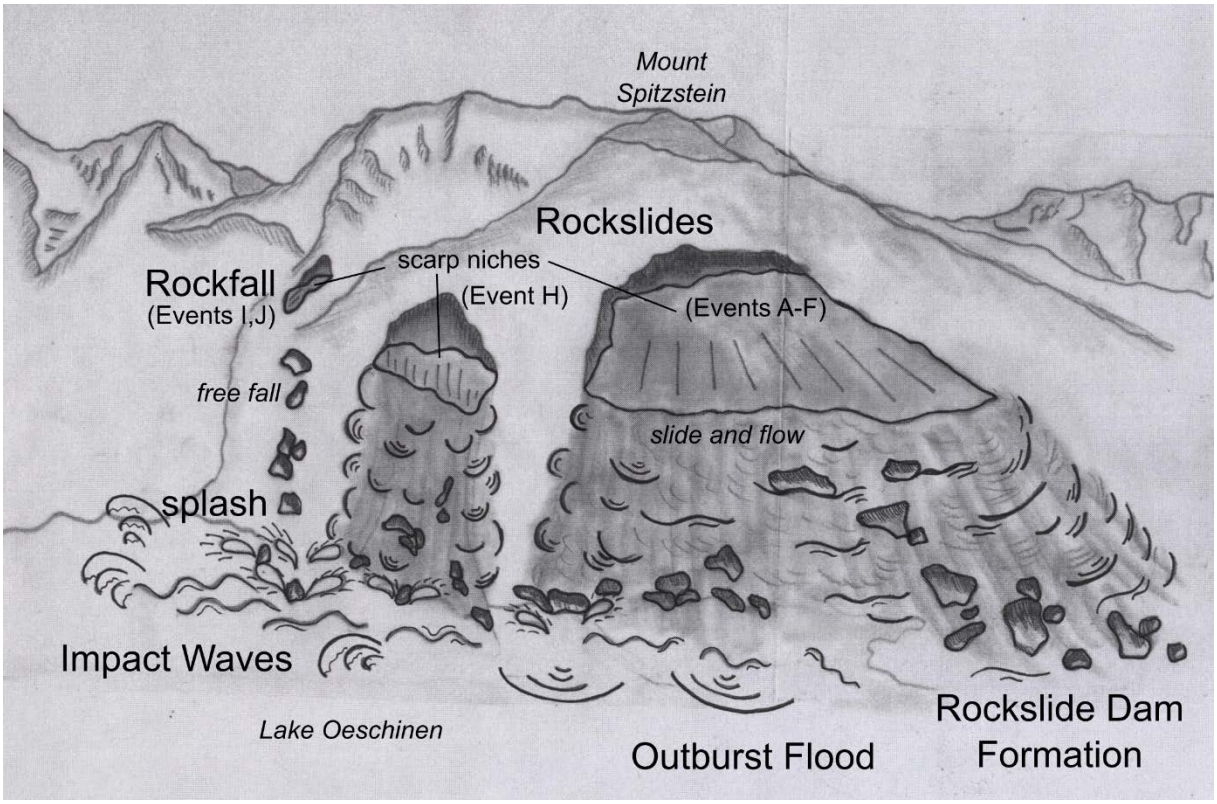

Figure 42: Scenarios of rock-slope failures at the southern shoreline of Lake Oeschinen illustrating rockfalls and rockslides, the latter of which formed or raised the lake dam. Schematic sketch without scale.

The hazards and interactive processes resulting from the impact on a lake mostly depend on (i) the type of the rock-slope failure and composition of rock material, (ii) the subaerial and subaqueous slope gradients, which determine the type of movement (falling/bouncing or sliding), (iii) the residual energy of the landslide when entering the water body, dependent on volume and mobility (Knapp and Krautblatter, 2020; chapter 3.1.5), (iv) the height of the water column/lake volume, and (v) the presence of rock material in the subaqueous runout path, which derived from earlier rock-slope failures.

At the Eibsee rock avalanche, ERT profiles disclose up to ~50 m thick rock-avalanche debris covering locally ~30 m mixed rock material. It is possible to distinguish between isolated remnants of paleolake sediments and mixed sediments, where path material such as postglacial valley infill has been entrained. At seven sites, materials including bedrock, rock avalanche, lake clay/silt and mixed sediments, as well as interactive processes of the rock avalanche with bedrock, lake and substrate can be deciphered. This way, extreme shearing, bulging, bulldozing and overriding of secondary lobes can be differentiated.

Table 6: Scenarios and effects of rock-slope failures impacting lakes, as detected in the presented studies. Some more examples from the literature are provided.

Size ratio landslide-lake	**Type of landslide**	**Propagation in the water**	**Effects of Impact**	**Possible Hazards**	**Examples from Case Studies**
landslide << or < lake Event deposits are stored in the lake.	**Rock fall**	(free) fall	offset between the event deposits and the lake slope, little resuspension, most impact energy transformed to wave propagation	Impact wave Outburst flood	**Lake Oeschinen (Knapp *et al.*, 2018)** Events I and J, historical outburst flood 1846 AD
	Debris flow	flow	high terrestrial sediment load, turbidites are widely spread over the lake basin, flat rock de-posits		**Lake Oeschinen (Knapp *et al.*, 2018)** Event K **Lake Plansee** (Kiefer *et al.*, 2020; Oswald *et al.*, 2020)
	Rock slide/ avalanche	slide/flow	much resuspension, might change lake system with in- and outflows, might build or raise a dam and the lake level or fill up the lake		**Lake Oeschinen (Knapp *et al.*, 2018)** Events B-F, Event H **Lake Lauerz** (Bussmann and Anselmetti, 2010), **Loen rock avalanches** (Hermanns *et al.*, 2006)
landslide ≈ lake	**Debris avalanche**	flow	complete mixing of debris and lake water, highly fluidized rock mass propagates on land	Impact wave Debris avalanche travels beyond the lake	**Lake Eibsee (Knapp *et al.*, 2020b)** Event 2
landslide > lake Lake displaced, dam stable.	**Rock avalanche**	flow	lake displaced by rock avalanche; dam is not affected, phases of lake "rebirth"	Impact wave Rock avalanche travels beyond the lake	**Lake Eibsee (Knapp *et al.*, 2020b)** Event 1 (Eibsee rock avalanche) **Vajont** (e.g. Genevois and Tecca, 2013)
landslide >> lake Lake displaced, dam failure.	**Rock slide/ avalanche**	slide/flow	lake displaced by rockslide; water-rich entrainment, long transport of flood deposits; dam breakage, no modern lake formation	Impact wave, outburst flood Debris flows, hyperconcentrated flows	**Flims (Knapp *et al.*, in preparation)** Bonaduz gravels and Toma hills

The Flims rockslide was much larger than the Eibsee rock avalanche. The impact on the assumed Paleolake Bonaduz not only resulted in the displacement of the lake, but also in a dam breakage. The dam probably failed because the Tamins rockslide deposits were not stable enough (Hermanns *et al.*, 2011) and the energy input during the impact and the bulldozing movement of the propagating rock mass was excessive. Nowadays, the Flims deposits are a terrestrial archive of diverse flood deposits, such as Toma hills and Bonaduz gravels.

Our improved understanding of the entrainment processes gained by sedimentological analysis and ERT measurements allows for a comparison of the Flims rockslide and the Eibsee rock avalanche. The very fine-grained deposits at the Eibsee rock avalanche, visible in the ERT profiles as decameter-wide zones with resistivity values < 100 Ωm, indicate coherent paleolake sediments (maybe at some locations in-situ), whereas the Flims impact was likely too strong to conserve clods of lake sediments large enough for ERT resolution (only clods of dm- to m-size were found, e.g. Figure 5). The conservation of large pieces of paleolake sediments in the Eibsee rock avalanche was maybe favoured by the complex valley paleotopography with higher friction at the sides and close to obstacles, where the rock avalanche was forced to decelerate, and the paleolake sediments were squeezed out, but still as large coherent slabs. The Flims rockslide, however, ran through the rather straight Vorderrhein valley, and completely disintegrated along an exceptional transport distance. The Bonaduz gravels in the ERT measurements at the Flims rockslide show similar patterns and resistivity values (blue to yellow colour, ~500 Ωm) as the mixed sediments in the Eibsee rock avalanche. Finally, Toma hills can also be found in the Eibsee rock avalanche close to Grainau (Ostermann and Prager, 2016), even though they are much smaller than in Domat/Ems.

6.1.3 Site-Specific Event History and Paleotopography

- *How and when was the modern lake formed? Can we prove the existence of a paleolake?*
- *What can we learn about the paleotopography? Can we establish a geological timeline of event phases?*
- *Can we finally decipher potential (regional) triggers?*

In Lake Oeschinen and Lake Eibsee, the seismic profiles were used to find the best-suited locations in the deepest lake basin to recover a composite core in order to get as much information about the history of the lake and the environment as possible.

Lake Oeschinen is dated to ~2500 cal BP and thus is found to be ~7000 years younger in its present-day extent than expected. The Oeschinen rock avalanche probably impacted a shallow paleolake, which had been dammed by the ~9500 cal BP Kandersteg rock avalanche (Tinner *et al.*, 2005; Köpfli *et al.*, 2018). Organic material from the original lake was buried and started to decompose, thereby producing free gas, which can be inferred from the blanking in the seismic profiles. This blanking also supported the reconstruction of the extent of the Oeschinen rock-avalanche deposits in the lake. The results further indicate at least six multistage rock-slope failures (events A-F) building the dam, whereas studies on land, mainly based on mapping and cosmogenic nuclide dating, propose only one or two events (Köpfli *et al.*, 2018). Finally, a hazardous outburst flood, documented in 1846 AD (Bach, 1935), can be linked to the rockfall event I.

The paleolake, which has been assumed to exist prior to the Eibsee rock avalanche, could only be tracked in the terrestrial deposits. This is because the impact of the Eibsee rock avalanche completely destroyed the paleolake and filled the former lake basin with decameter thick event deposits. Neither reflection seismology nor lake sediment cores are able to penetrate the carapace of such a massive rock-slope failure. On land, however, ERT measurements enable to disclose that the ~30-50 m thick deposits of the rock avalanche cover the northern half of the paleolake. Moreover, the ERT results provide insights of the paleotopography, which was typically shaped by glaciers. Resistivity values typical of moraine material were measured at the paleodam and along ridges and hilly landforms in the former basin of the proglacial lake.

Investigating modern Lake Eibsee yields evidence of a further paleolake, between Event 1 and 2. This second paleolake supposedly consisted of several shallow ponds with lots of islands and formed on top of Event 1 deposits. It lasted until the debris avalanche of Event 2. Since then, the modern lake has formed to its present-day state. These lake phases can only be deciphered in the lake sediment cores.

It is worth noting that in both investigated lakes Oeschinen and Eibsee, the generation of the fine-grained and graded megaturbidites and their dust-cloud clay cap in the uppermost section of the rock-slope failure deposits is a key to provide evidence of a preexisting lake, as such sediments are prone to resuspension and settling in an already existing water body. Furthermore, in Lake Oeschinen organic material from the original lake was buried and started to decompose, thereby producing free gas, which can be inferred from the blanking in the seismic profiles. This blanking also supported the reconstruction of the extent of the Oeschinen rock-avalanche deposits in the lake.

In the Flims context, the geophysical investigation of the Bonaduz gravels discloses an onlap on the Ils Aults, which represents a novel field evidence in the debate of the geological timeline. ERT measurements at the contact between the Bonaduz gravels and Toma hills also imply a simultaneous transport of the Toma hills in the hyperconcentrated mass flow (Calhoun and Clague, 2018), which deposited the Bonaduz gravels. These results further support the long-debated theory of Lake Bonaduz, a paleolake dammed by the Tamins rockslide deposits.

The new age data of the rock-slope failures offer the possibility to discuss potential (regional) triggers such as earthquakes. Historic rock-slope failures in Lake Oeschinen are cross-checked with the Swiss Earthquake Catalogue. Digital analysis of satellite images allow to detect potential scarp niches and calculate the co-seismic slope deformation according to Newmark (1965). In the case of the Eibsee rock avalanche, the comparison with large rock-slope failures in the close vicinity such as the Fernpass rockslide (Prager *et al.*, 2009) show coincidences, which might also hint at an earthquake as a regional trigger. It is challenging to assess prehistoric earthquakes (Kremer *et al.*, 2017) due to the lack of information, so the Eibsee failures and the older failures detected at Lake Oeschinen are hardly linkable to seismic tremors, although their age ranges are now refined.

6.2 Evaluation of Method Application

In the following, the applied methods and their combination are evaluated with respect to their suitability to yield information with which the research questions can be answered satisfyingly. Figure 43 illustrates the broad coverage of spatial scale on varying levels of abstraction.

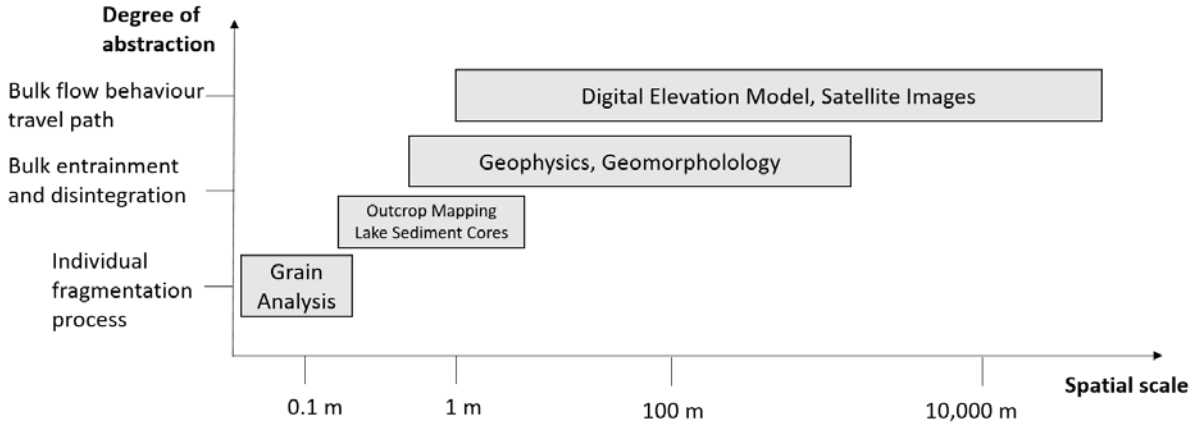

Figure 43: Schematic graph of the applied methods, which cover a broad range of spatial scales and degrees of abstraction.

Lacustrine Deposits

Reflection seismology at Lake Oeschinen and Lake Eibsee yield data of the lake sediment strata to a high resolution of ~0.4 m. In the lake basins of both lakes, the best suitable coring locations for the recovery of a composite core with the highest possible degree of information since lake formation, could be spotted based on the seismic profiles. This way, eleven rock-slope failures at Lake Oeschinen, instead of one or two as previously thought (Köpfli *et al.*, 2018), and three rock-slope failures at Lake Eibsee (instead of one (Jerz and Poschinger, 1995) or two (Haas *et al.*, 2014; Hornung and Haas, 2017)) could be deciphered in time and space, and classified. In both Lake Oeschinen and Lake Eibsee, however, the chaotic mass movements cannot be penetrated by the seismic waves. The rock-avalanche carapace of the Oeschinen or Eibsee rock avalanche, respectively, is the acoustic basement. Stacking deposits of multistage failures cannot be distinguished, either (e.g. events A-F in Lake Oeschinen). Consequently, rock-slope failure volumes can only be roughly estimated based on seismic data and sediment cores from the lakes. If the rock debris in multistage events differ highly in water content, they can be distinguished in the reflection seismic profiles, although both events show chaotic seismic facies. This is the case for the initial filling of the newly formed lake basins in both studied lakes: At Lake Eibsee, the highly fluidized debris avalanche, Event 2, on top of the dry rock avalanche, Event 1 (Figure 31), and at Lake Oeschinen, the fluidized initial filling of the lake basin by the events B and C on top of the Oeschinen rock avalanche, Event A, as visible in profile oes 19 (Figure 14a). Besides, if degassing processes are active in the sediment record, as in the case of Lake Oeschinen in the eastern lake basin, artefacts make seismic profiles unreliable.

In the transition from water to land, the geophysical information gained in the lake can be virtually complemented with the geophysical measurements on the terrestrial deposits. This way, the ERT profile close to the northern shoreline of Lake Eibsee (for location see Figure

20a) works as a “linking bridge” between the high-resolved reflection seismic data from the lake and the digital elevation model on land (Figure 44).

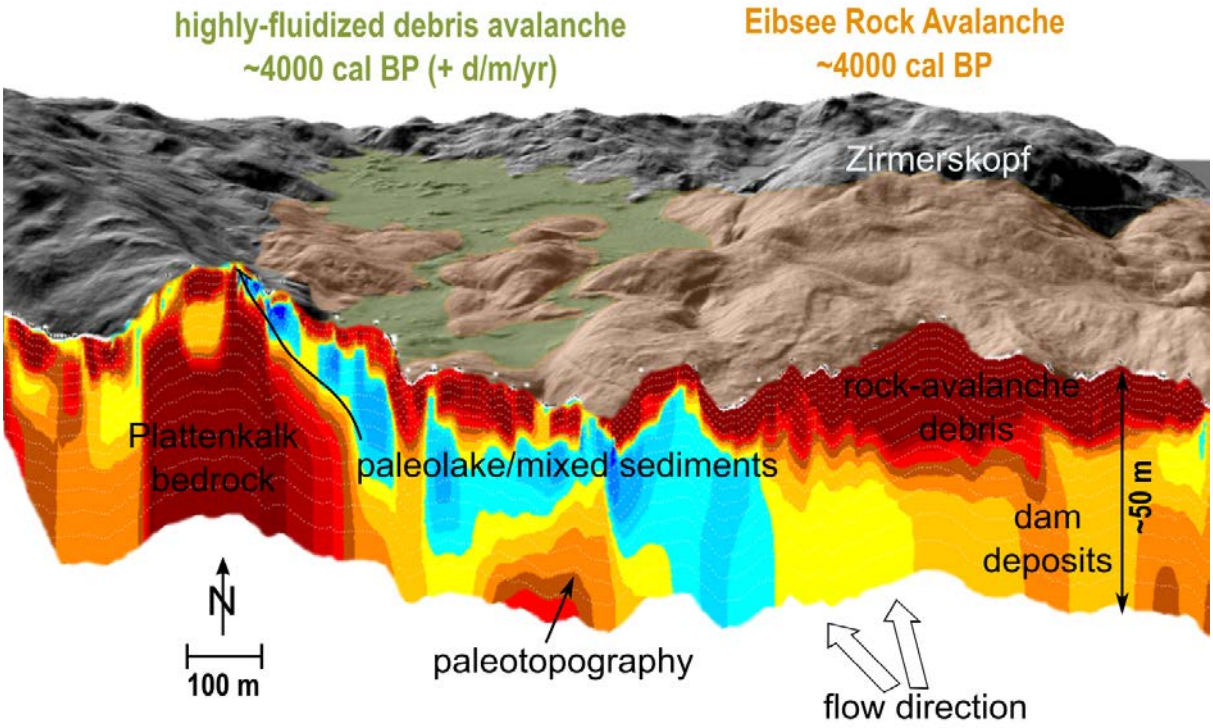

Figure 44: Digital elevation model of the Eibsee rock avalanche deposits in the North of Lake Eibsee, illustrated as a 3D-view with a projection of ERT measurements providing ~50m deep insights.

Terrestrial Deposits

The application of ERT in combination with sediment analysis in outcrops allows for studies on a broad scale. Outcrops like gravel pits at Mount Zirmerskopf (Eibsee rock avalanche) or at Reichenau (Flims rockslide) enable a broad 2D or even 3D assessment of the deposits and correlation with geophysical measurements. Samples can be taken at several spots along a stratigraphic horizon. ERT can reach up to 160 m penetration depth with the TUM equipment. Additionally, two or more datasets of surveys with different spacing can be combined to one model, so that a higher resolution of the uppermost sediments can be reached at the same time as high penetration depth. This was done, for example, at the gravel pit in Reichenau on the Bonaduz gravels (Figure 39a). Mostly, errors in the ERT model result from very high resistivity values next to very low resistivity values, for example at the Eibsee rock avalanche, where large “splashed” boulders are interpreted to be contained in fine-grained paleolake sediments (Figure 22d). The significance of the ERT measurement is restricted due to the trapezium-shaped electric field, i.e. the maximum penetration can only be reached in the middle of the transect. Therefore, the electric cables need to be laid out on a much longer line before and after the spot of interest. For example, Tuma Padrusa was the only Toma hill in its close vicinity that we could assess with ERT measurements, given the possibility of a transect long enough to penetrate the Toma core in the middle of the transect (Figure 39d). Moreover, infrastructure sensitive to electric conductivity, such as power supply lines at the surface or gas pipelines in the underground (both present at the Flims rockslide), disturb the electric field, induced for ERT, significantly.

Age Dating

Radiocarbon dating of terrestrial organic matter found in event deposits in the lake sediments only yield relative ages. The ages demonstrate the maximum ages of the event, i.e. the plant or tree was alive before the event happened and was then entrained into the event deposits. If turbidites are present throughout the lake basin, their stratigraphic position can be used to decipher multistage rock-slope failures (Lake Oeschinen). However, if the lake system is wholly affected and thus too disturbed by a landslide event, as in the case of Lake Eibsee, this option is void. If a second catastrophic event subsequently enters the lake, deciphering of these two event deposits only based on dating techniques becomes unrealistic (e.g. Event 2 deposited on Event 1 in Lake Eibsee; here, sedimentology and reflection seismic data support the interpretation of two superimposed event deposits). Still, in combination with dating in the background sediments, which have been deposited before and after the event deposits, a suitable age model can be set up. Combined with varve chronology, which is regarded as a very accurate dating method, the age model can be additionally substantiated, for example in Lake Oeschinen (Figure 16b; Amann *et al.*, 2015). The relatively good fit shows that the age model obtained by radiocarbon dating is satisfying, although changes in sedimentation rates are possible due to the alteration of the lake system caused by the changing glacial environment and more incoming rock-slope failure deposits. At Lake Eibsee, however, varve chronology cannot be applied due to the lack of varves in the background sediment. In general, the dating approach in the lake described here can yield much smaller age ranges and refine recurrence rates of rock-slope failures compared with techniques often used on land for landslide dating, for example cosmogenic nuclide dating (e.g. Martin *et al.*, 2014; Ivy-Ochs *et al.*, 2017; Hilger *et al.*, 2018; Von Wartburg *et al.*, 2020). The power of radiocarbon dating of rock-slope failures revealed in lake sediment samples is demonstrated in the case of the Flims rockslide (Deplazes *et al.*, 2007; Ivy-Ochs *et al.*, 2009) and the Oeschinen rock avalanche (Knapp *et al.*, 2018; Köpfli *et al.*, 2018).

Limitations due to land use

Last but not least, fieldwork in densely populated Alpine regions is often confronted with restrictions due to land use. This fact is worth noting when evaluating results from fieldwork. Privately-owned land (e.g. Lake Eibsee, Toma hills on the golf course in Domat/Ems, or wildlife reserves at the Ils Aults and the Eibsee deposits etc.), large impassable infrastructure like railways or motorways, as well as natural obstacles like rivers (e.g. Hinterrhein River close to Bonaduz) can restrict access to points of interest.

6.3 Research Needs and Further Suitable Methods

Quantification

Volumes of the rock-slope failures and the resulting deposits need to be better quantified. The estimations often widely vary, for example at Lake Eibsee between 300-400 mio m³ based on the estimations of the deposit area (Jerz and Poschinger, 1995), and 165 mio m³ based on the modelled failed rock mass using a 2-D FEM model (Phase2 from Rocscience) (Leith *et al.*, 2016). Furthermore, postglacial valley infill is assumed to have been partially entrained. Further geophysical investigation, for example with ground-penetrating radar (GPR) or Seismic Refraction Tomography (SRT) would be necessary to distinguish between the event deposits and the underlying moraine material. By applying SRT, for example, the ERT model artefacts

caused by power supply lines or gas pipelines (like in Flims) could be avoided. In the lake, a detailed bathymetry would support subaqueous geomorphological mapping (e.g. Strupler *et al.*, 2019).

Simulation of runout
Based on improved volume estimations, the landslide runout can be modelled, for example with RAMMS (e.g. Preuth *et al.*, 2010; Schneider *et al.*, 2010), r.avaflow (Mergili *et al.*, 2020) or DAN3D (Sosio *et al.*, 2008). The field evidence gained by sedimentology and geophysics can further help to improve the parametrization of the runout models.

Simulation of impact wave
What is the significant factor that controls the interaction at the first impact of the landslide on the lake? What is more relevant for the height of the impact wave – the lake volume or the water depth? Further large-scale analogue models, such as the ones described by Miller *et al.* (2017), as well as studies collecting field evidence in order to verify the modelled wave height (Scholz *et al.*, 2019), are necessary.

Rock-avalanche entrainment
As outlined in chapter 3.1.5 (Knapp and Krautblatter, 2020), the role of entrainment needs to be assessed additionally in terms of energy budgets and the dependency of the entrained material (Iverson and Ouyang, 2015; Aaron and McDougall, 2019). To which degree is the mobility of a rock avalanche influenced by the lithology(-ies) of the entrained material?

Refine recurrence rates (age bracketing)
Radiocarbon dating can be supported by pollen analysis and Pb/Cs-dating in the lake, and further combined with cosmogenic nuclide dating (e.g. Ivy-Ochs *et al.*, 2017) or Th-dating on calcite cements (e.g. Ostermann *et al.*, 2017) in terrestrial deposits.

Knowledge transfer
Other lakes affected by (subaerial and subaqueous) landslides should be checked and dated in the close vicinity, for example a detailed comparison of Lake Eibsee and Lake Plansee (Oswald *et al.*, 2020). This way, regional triggers like earthquakes can be deciphered and hazard assessment can be improved for a whole region.

7 Outlook: Future Perspectives

7.1 Climate Change: Reaction to Atmospheric Warming

In alpine environments, climate change leads to enhanced deglaciation, which comes along with a sequence of geomorphological developments and landform-shaping processes such as the formation of new lakes (e.g. Ballantyne, 2002; Haeberli *et al.*, 2017). The transition from glacial conditions (Ice Age) to peri-/fluvioglacial and eventually fluvial processes is characterized by extreme denudation rates (Hinderer, 2001). The subglacial production of sediments decreases rapidly during the phase of glacier retreat, and with that the glacial transport of sediments. Erosional processes in steep bedrock terrain are especially influenced by weathering in response to climate and pre-deposition (Krautblatter and Moore, 2014), but also by rock-slope retreat due to an increasing number of slope failures, as outlined in this thesis. Thereby, destabilized slopes and resulting mass movements become the main “producers” of sediments, often transported in (glacio-) fluvial systems.

Climate scenarios, for instance for the Swiss Alps, show the most likely changes in temperature to be + 2-3 °C and in precipitation + 10% in winter and – 20% in summer for the time horizon 2050 (Haeberli and Hohmann, 2008). Already within the coming decades, a development in such a projected range would result in the vanishing of about 75% of the existing glacier surface and lead to a deep warming of permafrost in mountain peaks, as recent studies underline (e.g. Ravanel *et al.*, 2017; Scandroglio and Krautblatter, 2020; Schroeder *et al.*, 2020). There is a time delay between the relatively fast glacier meltdown and the disappearance of the stabilizing ice, both in the glaciers and in the permafrost, and the much slower redevelopment of a stabilizing vegetation cover (Haeberli and Hohmann, 2008). Whereas glacier forefields and moraine-covered slopes can essentially come to an end of modification after decades, slope deformation and the formation of alluvial fans may take centuries. Moreover, large rock-slope failures even occur after millennia have passed, initially caused, respectively prepared, by the paraglacial destabilization of the rock faces.

In conclusion, the probability of large rock/ice avalanches impacting lakes is likely to grow, resulting more often in impact waves and outburst floods. People and infrastructure may be endangered far beyond hazard zones existing before the new formation of the lakes. Therefore, the exposure to outburst floods in alpine environment will likely increase. The resulting socio-economical impact asks for risk-reduction strategies. As the basic knowledge and technologies necessary for anticipating future hazards are already available, much will depend upon an improved awareness of the challenges in science, policy and the public (Haeberli *et al.*, 2017).

7.2 Contribution to the Field of Research and Society

Site-specific knowledge on rock-slope stability is essential for risk analysis and hazard assessment. The monitoring of alpine permafrost degradation (e.g. Zugspitze or Steintälli; Krautblatter *et al.*, 2010; Scandroglio and Krautblatter, 2020; Schroeder *et al.*, 2020) or the monitoring of glacier retreat (e.g. at the Furggwanghorn glacier; Buchli *et al.*, 2018) often implies long-term observations at a specific site over a few years or decades. However, data often is not collected and/or analysed until an acute hazard potential leads to the study being

financed. Then, monitoring is carried out on short timescales, i.e. months or years (e.g. Höllentalklamm or Hochvogel; Jacobs *et al.*, 2020; Leinauer *et al.*, 2020). Instruments are installed on-site and record changes in order to improve the knowledge of active processes and enable an efficient risk analysis of the current hazard potential. Although huge amounts of data are collected in such studies, they often only go back in time to historical time scales at best. The site-specific knowledge gained is often not enough to assess the "failure character" of the specific site, which shows the long-term stability of the distinct rock slope and the rock-slope failure history over thousands of years. Ideally this would at least cover the Holocene, demonstrating immense changes after the last glacial period, which has been a key factor in destabilizing the rock slopes.

In my research, the complementary method approach, including the analysis of both lacustrine and terrestrial sediment archives makes it possible to get to know a specific site "as a whole system". This means that knowledge is gained on the site-specific event history, paleotopography, recurrence rates, magnitude and potential regional triggers of single catastrophic events reaching back in time up to thousands of years. This is especially important, because there are numerous "sleeping" rock walls, where locals and researchers assume that only one single large rock failure occurred thousands of years ago, i.e. before historic time, so it is considered to be stable now. This is the case not only at the Eibsee rock avalanche (~4000 years old), but also at the Oeschinen rock avalanche (thought to be ~9500 years old, now dated at ~2500 years), where the results of this thesis now show that there might be a much higher hazard potential from the rock walls of Mount Zugspitze and Mount Spitzstein, especially because we were able to decipher the multistage, progressive failure character, implying that more failures may happen in the future.

The present situation at Mount Spitzstein, also called "Spitze Stei" in Swiss German, impressively demonstrates how a community is asked for resolute action due to a rapidly increasing risk from a supposedly "stable" mountain flank. In fact, the youngest detected multistage event from Mount Spitzstein in our study occurred ~1000 years ago. Now, after this long time period, the summit of the "Spitze Stei" collapsed on 20 December, 2019. Monitoring of the movement started in summer 2018. In November 2019, about one month before the collapse, the summit moved 10 centimeters in 90 minutes. The results of our study now help to estimate possible failure volumes and model different scenarios based on the systematically gained knowledge of the site-specific failure history.

Finally, with my research I want to contribute not only to a better process understanding and systematic site-specific knowledge, but also to an improved communication within the scientific communities, which have long been separated along lines such as specialized research on rock-slope stability on the one hand, and lake studies on the other hand.

References

Aaron, J., and Hungr, O. (2016). Dynamic analysis of an extraordinarily mobile rock avalanche in the Northwest Territories, Canada. *Canadian Geotechnical Journal* 53(6)**,** 899-908.

Aaron, J., McDougall, S., Moore, J.R., Coe, J.A., and Hungr, O. (2017). The role of initial coherence and path materials in the dynamics of three rock avalanche case histories. *Geoenvironmental Disasters* 4(1)**,** 5.

Aaron, J., and McDougall, S. (2019). Rock avalanche mobility: The role of path material. *Engineering Geology* 257**,** 105126.

Abele, G. (1972). Kinematik und Morphologie spät- und postglazialer Bergstürze in den Alpen. *Z. Geomorph. N.F.* Suppl.-Bd. 14**,** 138-149.

Abele, G. (1974). Bergstürze in den Alpen – Ihre Verbreitung, Morphologie und Folgeerscheinungen. *Wiss. Alpenvereinshefte* 25**,** 1-230.

Abele, G. (1991). Durch Bergstürze mobilisierte Muren und durch Muren transportierte Bergsturzmassen. *Österr. Geogr. Ges., Jahresber. 1989/90***,** 33-39.

Abele, G. (1994). Large rockslides: their causes and movement on internal sliding planes. *Mountain Research and Development***,** 315-320.

Abele, G. (1997). Rockslide movement supported by the mobilization of groundwater-saturated valley floor sediments. *Zeitschrift fuer Geomorphologie* 41(1)**,** 1-20.

Aizebeokhai, A.P. (2010). 2D and 3D geoelectrical resistivity imaging: Theory and field design. *Scientific Research and Essays* 5(23)**,** 3592-3605.

Alexiades, C., and Jackson, M. (1967). Chlorite determination in clays of soils and mineral deposits. *American Mineralogist: Journal of Earth and Planetary Materials* 52(11-12)**,** 1855-1873.

Allen, S.K., Rastner, P., Arora, M., Huggel, C., and Stoffel, M. (2016). Lake outburst and debris flow disaster at Kedarnath, June 2013: hydrometeorological triggering and topographic predisposition. *Landslides* 13(6)**,** 1479-1491.

Alumbaugh, D.L., and Newman, G.A. (2000). Image appraisal for 2-D and 3-D electromagnetic inversion. *Geophysics* 65(5)**,** 1455-1467.

Amann, B., Mauchle, F., and Grosjean, M. (2014). Quantitative high-resolution warm season rainfall recorded in varved sediments of Lake Oeschinen, northern Swiss Alps: calibration and validation AD 1901–2008. *Journal of paleolimnology* 51(3)**,** 375-391.

Amann, B., Szidat, S., and Grosjean, M. (2015). A millennial-long record of warm season precipitation and flood frequency for the North-western Alps inferred from varved lake sediments: implications for the future. *Quaternary Science Reviews* 115**,** 89-100.

Anders, M.H., Fouke, B.W., Zerkle, A.L., Tavarnelli, E., Alvarez, W., and Harlow, G.E. (2010). The role of calcining and basal fluidization in the long runout of carbonate slides: an example from the Heart Mountain slide block, Wyoming and Montana, USA. *The Journal of Geology* 118(6)**,** 577-599.

Appleby, P. (2002). Chronostratigraphic techniques in recent sediments. In: *Tracking environmental change using lake sediments*. Springer, 171-203.

Archie, G.E. (1942). The electrical resistivity log as an aid in determining some reservoir characteristics. *Transactions of the AIME* 146(01)**,** 54-62.

Arias, A. (1970). Measure of earthquake intensity. *Massachusetts Inst. of Tech., Cambridge. Univ. of Chile, Santiago de Chile*.

Ariztegui, D., and Wildi, W. (2013). *Lake Systems from the Ice Age to Industrial Time.* Springer.

Arnaud, F., Revel, M., Chapron, E., Desmet, M., and Tribovillard, N. (2005). 7200 years of Rhone river flooding activity in Lake Le Bourget, France: a high-resolution sediment record of NW Alps hydrology. *The Holocene* 15(3)**,** 420-428.

Arnold, J.R., and Libby, W.F. (1949). Age determinations by radiocarbon content: checks with samples of known age. *Science* 110(2869)**,** 678-680.

Bach, F. (1935). *Naturkatastrophen im Frutigland: Quellenbändchen zur Heimatkunde von Frutigen. 1.* Heimatkunde-Vereinigung Frutigland: Buchdr. Geschäftsblatt A.G.

Bader, K. (1979). Exarationstiefen würmeiszeitlicher und älterer Gletscher in Südbayern (Trennung eisvorbelasteter und nicht eisvorbelasteter Sedimente aufgrund der seismischen Geschwindigkeiten). *E&G–Quaternary Science Journal* 29(1).

Bader, K. (1981). Die glazialen Übertiefungen im Saalachgletscher-Gebiet zwischen Inzell und Königssee. *E&G–Quaternary Science Journal* 31(1).

Ballantyne, C.K. (2002). Paraglacial geomorphology. *Quaternary Science Reviews* 21(18-19)**,** 1935-2017.

Bartelt, P., Buser, O., and Platzer, K. (2006). Fluctuation-dissipation relations for granular snow avalanches. *Journal of Glaciology* 52(179)**,** 631-643.

[Dataset] Bavarian Surveying and Mapping Authority (2006). *Airborne laser scan, Garmisch.*

Beigt, D., Villarosa, G., Gómez, E.A., and Manzoni, C. (2016). Subaqueous landslides at the distal basin of Lago Nahuel Huapi (Argentina): Towards a tsunami hazard evaluation in Northern Patagonian lakes. *Geomorphology* 268**,** 197-206.

Bennett, M.R., Huddart, D., and McCormick, T. (2000). The glaciolacustrine landform–sediment assemblage at Heinabergsjökull, Iceland. *Geografiska Annaler: Series A, Physical Geography* 82(1)**,** 1-16.

Bessette-Kirton, E.K., Coe, J.A., and Zhou, W. (2018). Using stereo satellite imagery to account for ablation, entrainment, and compaction in volume calculations for rock avalanches on glaciers: Application to the 2016 Lamplugh rock avalanche in Glacier Bay National Park, Alaska. *Journal of Geophysical Research: Earth Surface* 123(4)**,** 622-641.

Bieniawski, Z. (1967). Mechanism of brittle failure of rock Part I-Theory of fracture process. *Int J Rock Mech Min Sci Geomech Abstr* 4(4)**,** 395-406.

Bishop, M.P., and Houser, C. (2016). Geomorphological Mapping and Geospatial Technology. *International Encyclopedia of Geography: People, the Earth, Environment and Technology: People, the Earth, Environment and Technology***,** 1-13.

Blegen, N., Tryon, C.A., Faith, J.T., Peppe, D.J., Beverly, E.J., Li, B., et al. (2015). Distal tephras of the eastern Lake Victoria basin, equatorial East Africa: correlations, chronology and a context for early modern humans. *Quaternary Science Reviews* 122**,** 89-111.

Bøe, A.-G., Dahl, S.O., Lie, Ø., and Nesje, A. (2006). Holocene river floods in the upper Glomma catchment, southern Norway: a high-resolution multiproxy record from lacustrine sediments. *The Holocene* 16(3)**,** 445-455.

Boeckli, L., Brenning, A., Gruber, S., and Noetzli, J. (2012). Permafrost distribution in the European Alps: calculation and evaluation of an index map and summary statistics. *The Cryosphere* 6(4)**,** 807-820.

Boes, E., Van Daele, M., Moernaut, J., Schmidt, S., Jensen, B.J., Praet, N., et al. (2018). Varve formation during the past three centuries in three large proglacial lakes in south-central Alaska. *GSA Bulletin* 130(5-6)**,** 757-774.

Bowman, E.T., Take, W.A., Rait, K.L., and Hann, C. (2012). Physical models of rock avalanche spreading behaviour with dynamic fragmentation. *Canadian Geotechnical Journal* 49(4)**,** 460-476.

Bowman, S. (1990). *Radiocarbon dating.* Univ of California Press.

Brauer, A., Endres, C., Günter, C., Litt, T., Stebich, M., and Negendank, J.F. (1999). High resolution sediment and vegetation responses to Younger Dryas climate change in varved lake sediments from Meerfelder Maar, Germany. *Quaternary Science Reviews* 18(3)**,** 321-329.

Bronk Ramsey, C. (2013). OxCal version 4.2. 4. *University of Oxford Radiocarbon Accelerator Unit. Computer Program, Available at: c14. arch. ox. ac. uk/embed. php*.

Buchli, T., Kos, A., Limpach, P., Merz, K., Zhou, X., and Springman, S.M. (2018). Kinematic investigations on the Furggwanghorn rock glacier, Switzerland. *Permafrost and Periglacial Processes* 29(1)**,** 3-20.

Buser, O., and Bartelt, P. (2009). Production and decay of random kinetic energy in granular snow avalanches. *Journal of Glaciology* 55(189)**,** 3-12.

Bussmann, F., and Anselmetti, F.S. (2010). Rossberg landslide history and flood chronology as recorded in Lake Lauerz sediments (Central Switzerland). *Swiss Journal of Geosciences* 103(1)**,** 43-59.

Bütschi, D. (2008). *Gefürchtet, gebändigt und neu gedacht - die Kander. Die Geschichte eines Flusses und "seiner" Menschen (1800-1950).* Diploma, Historisches Institut der Universität Bern.

Calhoun, N.C., and Clague, J.J. (2018). Distinguishing between debris flows and hyperconcentrated flows: an example from the eastern Swiss Alps. *Earth Surface Processes and Landforms* 43(6)**,** 1280-1294.

Cardello, G.L., and Mancktelow, N.S. (2014). Cretaceous syn-sedimentary faulting in the Wildhorn Nappe (SW Switzerland). *Swiss Journal of Geosciences* 107(2-3)**,** 223-250.

Carling, P.A. (2013). Freshwater megaflood sedimentation: What can we learn about generic processes? *Earth-Science Reviews* 125**,** 87-113.

Carslaw, H.S., and Jaeger, J.C. (1959). *Conduction of Heat in Solids.* Oxford: Oxford University Press.

Chen, H., and Hawkins, A. (2009). Relationship between earthquake disturbance, tropical rainstorms and debris movement: an overview from Taiwan. *Bulletin of Engineering Geology and the Environment* 68(2)**,** 161-186.

Christen, M., Kowalski, J., and Bartelt, P. (2010). RAMMS: Numerical simulation of dense snow avalanches in three-dimensional terrain. *Cold Regions Science and Technology* 63(1-2)**,** 1-14.

Clague, J.J., and Evans, S.G. (2000). A review of catastrophic drainage of moraine-dammed lakes in British Columbia. *Quaternary Science Reviews* 19(17-18)**,** 1763-1783.

Clague, J.J., and O'Connor, J.E. (2015). Glacier-related outburst floods. In: *Snow and ice-related hazards, risks and disasters*. Elsevier, 487-519.

Coe, J.A., Baum, R.L., Allstadt, K.E., Kochevar Jr, B.F., Schmitt, R.G., Morgan, M.L., et al. (2016). Rock-avalanche dynamics revealed by large-scale field mapping and seismic signals at a highly mobile avalanche in the West Salt Creek valley, western Colorado. *Geosphere* 12(2)**,** 607-631.

Cohen, A.S. (2003). *Paleolimnology: the history and evolution of lake systems.* Oxford University Press.

Couston, L.-A., Mei, C.C., and Alam, M.-R. (2015). Landslide tsunamis in lakes. *Journal of Fluid Mechanics* 772**,** 784-804.

Crosta, G., Imposimato, S., and Roddeman, D. (2009). Numerical modelling of entrainment/deposition in rock and debris-avalanches. *Engineering Geology* 109(1-2)**,** 135-145.

Crosta, G.B., Frattini, P., and Fusi, N. (2007). Fragmentation in the Val Pola rock avalanche, Italian alps. *Journal of Geophysical Research: Earth Surface* 112(F1).

Crosta, G.B., Imposimato, S., and Roddeman, D. (2016). Landslide spreading, impulse water waves and modelling of the Vajont rockslide. *Rock Mechanics and Rock Engineering* 49(6)**,** 2413-2436.

Cruden, D., and Antoine, P. (1984). The slide from Mt. Granier, Isere and Savoie, France, on November 24, 1248. In: *Proceedings 4th International Symposium on Landslides*, 475-481.

Cruden, D., and Hungr, O. (1986). The debris of the Frank Slide and theories of rockslide–avalanche mobility. *Canadian Journal of Earth Sciences* 23(3)**,** 425-432.

Cruden, D.M., and Varnes, D.J. (1996). Landslides: investigation and mitigation. Chapter 3-Landslide types and processes. *Transportation research board special report* (247).

Dai, F., Lee, C.F., Deng, J., and Tham, L. (2005). The 1786 earthquake-triggered landslide dam and subsequent dam-break flood on the Dadu River, southwestern China. *Geomorphology* 65(3-4)**,** 205-221.

Davies, M.C., Hamza, O., and Harris, C. (2001). The effect of rise in mean annual temperature on the stability of rock slopes containing ice-filled discontinuities. *Permafrost and periglacial processes* 12(1)**,** 137-144.

Davies, T., and McSaveney, M. (2009a). The role of rock fragmentation in the motion of large landslides. *Engineering Geology* 109(1-2)**,** 67-79.

Davies, T., and McSaveney, M. (2012). Mobility of long-runout rock avalanches. *Landslides: Types, Mechanisms and Modeling***,** 50.

Davies, T.R., and McSaveney, M.J. (2009b). The role of rock fragmentation in the motion of large landslides. *Engineering Geology* 109(1-2)**,** 67-79.

De Blasio, F.V., and Medici, L. (2017). Microscopic model of rock melting beneath landslides calibrated on the mineralogical analysis of the Köfels frictionite. *Landslides* 14(1)**,** 337-350.

De Geer, G. (1912). A geochronology of the last 12000 years. In: *Proceedings 11th International Geological Congress (Stockholm 1912)*, 241-258.

Deevey, E.S., Gross, M.S., Hutchinson, G.E., and Kraybill, H.L. (1954). The natural C14 contents of materials from hard-water lakes. *Proceedings of the National Academy of Sciences of the United States of America* 40(5)**,** 285.

Delaney, K.B., and Evans, S.G. (2015). The 2000 Yigong landslide (Tibetan Plateau), rockslide-dammed lake and outburst flood: review, remote sensing analysis, and process modelling. *Geomorphology* 246**,** 377-393.

Deline, P., Hewitt, K., Reznichenko, N., and Shugar, D. (2015a). Rock avalanches onto glaciers. In: *Landslide hazards, risks and disasters*. Elsevier, Amsterdam, 263-319.

Deline, P., Gruber, S., Delaloye, R., Fischer, L., Geertsema, M., Giardino, M., et al. (2015b). Ice loss and slope stability in high-mountain regions. In: *Snow and Ice-Related Hazards, Risks, and Disasters.* Elsevier, Amsterdam**,** 521-561.

Deplazes, G., Anselmetti, F.S., and Hajdas, I. (2007). Lake sediments deposited on the Flims rockslide mass: the key to date the largest mass movement of the Alps. *Terra Nova* 19(4)**,** 252-258.

Dietrich, A., and Krautblatter, M. (2017). Evidence for enhanced debris-flow activity in the Northern Calcareous Alps since the 1980s (Plansee, Austria). *Geomorphology* 287**,** 144-158.

DIN EN ISO 17892-4 (2017-04). Geotechnical investigation and testing - Laboratory testing of soil - Part 4: Determination of particle size distribution (ISO 17892-4:2016); German version EN ISO 17892-4:2016.

Draebing, D., Haberkorn, A., Krautblatter, M., Kenner, R., and Phillips, M. (2017). Thermal and mechanical responses resulting from spatial and temporal snow cover variability in permafrost rock slopes, Steintaelli, Swiss Alps. *Permafrost and Periglacial Processes* 28(1)**,** 140-157.

Draebing, D., and Eichel, J. (2018). Divergence, convergence, and path dependency of paraglacial adjustment of alpine lateral moraine slopes. *Land Degradation & Development* 29(6)**,** 1979-1990.

Dramis, F., Guida, D., and Cestari, A. (2011). Nature and aims of geomorphological mapping. In: *Developments in earth surface processes*. Elsevier, Amsterdam, 39-73.

Dufresne, A., and Davies, T.R. (2009). Longitudinal ridges in mass movement deposits. *Geomorphology* 105(3-4)**,** 171-181.

Dufresne, A., Davies, T., and McSaveney, M. (2010). Influence of runout-path material on emplacement of the Round Top rock avalanche, New Zealand. *Earth Surface Processes and Landforms* 35(2)**,** 190-201.

Dufresne, A., Prager, C., and Clague, J.J. (2015). Complex interactions of rock avalanche emplacement with fluvial sediments: field structures at the Tschirgant deposit, Austria. In: *Engineering Geology for Society and Territory-Volume 2*. Springer, Dordrecht, 1707-1711.

Dufresne, A., Prager, C., and Bösmeier, A. (2016a). Insights into rock avalanche emplacement processes from detailed morpho-lithological studies of the Tschirgant deposit (Tyrol, Austria). *Earth Surface Processes and Landforms* 41(5)**,** 587-602.

Dufresne, A., Bösmeier, A., and Prager, C. (2016b). Sedimentology of rock avalanche deposits–case study and review. *Earth-Science Reviews* 163**,** 234-259.

Dufresne, A., and Dunning, S. (2017). Process dependence of grain size distributions in rock avalanche deposits. *Landslides* 14(5)**,** 1555-1563.

Dufresne, A., Geertsema, M., Shugar, D., Koppes, M., Higman, B., Haeussler, P., et al. (2018). Sedimentology and geomorphology of a large tsunamigenic landslide, Taan Fiord, Alaska. *Sedimentary Geology* 364**,** 302-318.

Dufresne, A., and Geertsema, M. (2020). Rock slide–debris avalanches: flow transformation and hummock formation, examples from British Columbia. *Landslides* 17(1)**,** 15-32.

Dykes, A.P. (2008). Geomorphological maps of Irish peat landslides created using hand-held GPS. *Journal of Maps* 4(1)**,** 258-276.

Eberhardt, E., Stead, D., Coggan, J., and Willenberg, H. (2002). An integrated numerical analysis approach applied to the Randa rockslide. In: *1st European Conference on Landslides*, 2002.

Eberhardt, E., Stead, D., and Coggan, J. (2004). Numerical analysis of initiation and progressive failure in natural rock slopes—the 1991 Randa rockslide. *International Journal of Rock Mechanics and Mining Sciences* 41(1)**,** 69-87.

Eden, D.N., and Page, M.J. (1998). Palaeoclimatic implications of a storm erosion record from late Holocene lake sediments, North Island, New Zealand. *Palaeogeography, Palaeoclimatology, Palaeoecology* 139(1-2)**,** 37-58.

Ekström, G., and Stark, C.P. (2013). Simple scaling of catastrophic landslide dynamics. *Science* 339(6126)**,** 1416-1419.

Erismann, T., Heuberger, H., and Preuss, E. (1977). Fused Rock of Kofels (Tyrol) - Frictionite Generated by a Landslide. *Tschermaks Mineralogische Und Petrographische Mitteilungen* 24(1-2)**,** 67-119.

Erismann, T.H., and Abele, G. (2001). *Dynamics of rockslides and rockfalls.* Springer Science & Business Media.

Evans, S., and Hungr, O. (1993). The assessment of rockfall hazard at the base of talus slopes. *Canadian Geotechnical Journal* 30(4)**,** 620-636.

Evans, S.G. (2006). Single-event landslides resulting from massive rock slope failure: characterising their frequency and impact on society. In: *Landslides from Massive Rock Slope Failure*. Springer, Dordrecht, 53-73.

Evans, S.G., Mugnozza, G.S., Strom, A.L., Hermanns, R.L., Ischuk, A., and Vinnichenko, S. (2006). Landslides from massive rock slope failure and associated phenomena. In: *Landslides from Massive Rock Slope Failure*. Springer, Dordrecht, 03-52.

Evans, S.G., Hermanns, R.L., Strom, A., and Scarascia-Mugnozza, G. (2011). *Natural and artificial rockslide dams.* Springer Science & Business Media.

Evers, F.M., and Hager, W.H. (2016). Spatial impulse waves: Wave height decay experiments at laboratory scale. *Landslides* 13(6)**,** 1395-1403.

Fäh, D., Giardini, D., Kästli, P., Deichmann, N., Gisler, M., Schwarz-Zanetti, G., et al. (2011). ECOS-09 earthquake catalogue of Switzerland release 2011 report and database. Public catalogue, 17. 4. 2011. Swiss Seismological Service ETH Zurich. *RISK*.

Fan, X., Zhan, W., Dong, X., van Westen, C., Xu, Q., Dai, L., et al. (2018). Analyzing successive landslide dam formation by different triggering mechanisms: The case of the Tangjiawan landslide, Sichuan, China. *Engineering geology* 243**,** 128-144.

Fan, X., Dufresne, A., Subramanian, S.S., Strom, A., Hermanns, R., Stefanelli, C.T., et al. (2020). The formation and impact of landslide dams–State of the art. *Earth-Science Reviews* 203**,** 103116.

Farinotti, D., Huss, M., Bauder, A., and Funk, M. (2009). An estimate of the glacier ice volume in the Swiss Alps. *Global and Planetary Change* 68(3)**,** 225-231.

Fine, I.V., Rabinovich, A.B., Thomson, R.E., and Kulikov, E.A. (2003). Numerical modeling of tsunami generation by submarine and subaerial landslides. In: *Submarine landslides and tsunamis*. Springer, Dordrecht, 69-88.

Fischer, K. (1999). *Massenbewegungen und Massentransporte in den Alpen als Gefahrenpotential: Symposion der Kommission für Geomorphologie der Bayerischen Akademie der Wissenschaften, München, am 24. und 25. November 1995.* Borntraeger.

Fischer, L., Kääb, A., Huggel, C., and Noetzli, J. (2006). Geology, glacier retreat and permafrost degradation as controlling factors of slope instabilities in a high-mountain rock wall: the Monte Rosa east face. *Natural Hazards and Earth System Sciences* 6(5)**,** 761-772.

Fischer, L., Purves, R.S., Huggel, C., Noetzli, J., and Haeberli, W. (2012). On the influence of topographic, geological and cryospheric factors on rock avalanches and rockfalls in high-mountain areas. *Natural Hazards and Earth System Science* 12(1)**,** 241-254.

Freundt, A., Strauch, W., Kutterolf, S., and Schmincke, H.-U. (2007). Volcanogenic tsunamis in lakes: examples from Nicaragua and general implications. *Pure and Applied Geophysics* 164(2-3)**,** 527-545.

Frey, H., Haeberli, W., Linsbauer, A., Huggel, C., and Paul, F. (2010). A multi-level strategy for anticipating future glacier lake formation and associated hazard potentials. *Natural Hazards and Earth System Sciences* 10(2)**,** 339-352.

Fritz, H.M., Mohammed, F., and Yoo, J. (2009). Lituya Bay landslide impact generated mega-tsunami 50 th Anniversary. In: *Tsunami Science Four Years after the 2004 Indian Ocean Tsunami*. Springer, Dordrecht, 153-175.

Gardner, A.S., Moholdt, G., Cogley, J.G., Wouters, B., Arendt, A.A., Wahr, J., et al. (2013). A reconciled estimate of glacier contributions to sea level rise: 2003 to 2009. *Science* 340(6134)**,** 852-857.

Geertsema, M. (2012). Initial observations of the 11 June 2012 rock/ice avalanche, Lituya mountain, Alaska. In: *The First Meeting of International Consortium of Landslides Cold Region Landslides Network, Harbin, China*, 49-54.

Genevois, R., and Tecca, P.R. (2013). The Vajont landslide: state-of-the-art. In: *Italian Journal of Engineering Geology and Environment-Book Series 6: International Conference on Vajont–1963–2013-Thoughts and Analyses After*.

Geotek, L. (2000). Multi-sensor Core Logger. *Daventry, United Kingdom*.

Ghaffari, H., Griffith, W., and Barber, T. (2019). Energy delocalization during dynamic rock fragmentation. *Geophysical Journal International* 217(2)**,** 1034-1046.

Gilli, A., Anselmetti, F.S., Glur, L., and Wirth, S.B. (2013). Lake sediments as archives of recurrence rates and intensities of past flood events. In: *Dating torrential processes on fans and cones*. Springer, Dordrecht, 225-242.

Girardclos, S., Schmidt, O.T., Sturm, M., Ariztegui, D., Pugin, A., and Anselmetti, F.S. (2007). The 1996 AD delta collapse and large turbidite in Lake Brienz. *Marine Geology* 241(1-4)**,** 137-154.

Glew, J.R., Smol, J.P., and Last, W.M. (2002). Sediment core collection and extrusion. In: *Tracking environmental change using lake sediments*. Springer, Dordrecht, 73-105.

Glew, J.R., and Smol, J.P. (2016). A push corer developed for retrieving high-resolution sediment cores from shallow waters. *Journal of Paleolimnology* 56(1)**,** 67-71.

Glur, L., Wirth, S.B., Büntgen, U., Gilli, A., Haug, G.H., Schär, C., et al. (2013). Frequent floods in the European Alps coincide with cooler periods of the past 2500 years. *Scientific reports* 3**,** 2770.

Goslar, T., van der Knaap, W.O., Hicks, S., Andrič, M., Czernik, J., Goslar, E., et al. (2005). Radiocarbon dating of modern peat profiles: pre-and post-bomb 14 C variations in the construction of age-depth models. *Radiocarbon* 47(1)**,** 115-134.

Grimstad, E., and Nesdal, S. (1990). The Loen rockslides - a historical review. In: *Rock Joints,* eds. M. Barton & W. Stephansson. Balkema, Rotterdam, 1-6.

Groll, M. (1903). Der Oeschinensee. *Jber. der Geogr. Ges. Bern* 19**,** 04.

Gruber, S., and Haeberli, W. (2007). Permafrost in steep bedrock slopes and its temperature-related destabilization following climate change. *Journal of Geophysical Research: Earth Surface* 112(F2).

Gruber, S. (2012a). Derivation and analysis of a high-resolution estimate of global permafrost zonation. *The Cryosphere* 6(1)**,** 221-233.

Gruber, S. (2012b). A Global view on permafrost in steep bedrock. In: *Proceedings of the 10th International Conference on Permafrost, June 2012, Salekhard, Russia*, 25-29.

Gylfadóttir, S.S., Kim, J., Helgason, J.K., Brynjólfsson, S., Höskuldsson, Á., Jóhannesson, T., et al. (2017). The 2014 L ake A skja rockslide-induced tsunami: Optimization of numerical tsunami model using observed data. *Journal of Geophysical Research: Oceans* 122(5)**,** 4110-4122.

Haas, U., Ostermann, M., Sanders, D., and Hornung, T. (2014). Quaternary sediments in the Werdenfels region (Bavaria, southern Germany). In: *From the foreland to the Central Alps - Excursion guide to the field trips of the DEUQUA Congress in Innsbruck, Austria, 24-29 September 2014,* eds. H. Kerschner, K. Krainer & C. Spötl. Geozon, Berlin, 18-30.

Haberkorn, A., Phillips, M., Kenner, R., Rhyner, H., Bavay, M., Galos, S.P., et al. (2015). Thermal regime of rock and its relation to snow cover in steep Alpine rock walls: Gemsstock, central Swiss Alps. *Geografiska Annaler: Series A, Physical Geography* 97(3)**,** 579-597.

Habib, P. (1975). Production of gaseous pore pressure during rock slides. *Rock Mechanics* 7(4)**,** 193-197.

Haeberli, W., Huggel, C., Kääb, A., Zgraggen-Oswald, S., Polkvoj, A., Galushkin, I., et al. (2004). The Kolka-Karmadon rock/ice slide of 20 September 2002: an extraordinary event of historical dimensions in North Ossetia, Russian Caucasus. *Journal of Glaciology* 50(171)**,** 533-546.

Haeberli, W., Hoelzle, M., Paul, F., and Zemp, M. (2007). Integrated monitoring of mountain glaciers as key indicators of global climate change: the European Alps. *Annals of glaciology* 46**,** 150-160.

Haeberli, W., and Hohmann, R. (2008). Climate, glaciers and permafrost in the Swiss Alps 2050: scenarios, consequences and recommendations. In: *9th International Conference on Permafrost, Fairbanks, Alaska, 29 Juni 2008 - 3 Juli 2008*, 607-612.

Haeberli, W., and Linsbauer, A. (2013). Global glacier volumes and sea level-small but systematic effects of ice below the surface of the ocean and of new local lakes on land. Brief communication. *The Cryosphere* 7(3)**,** 817-821.

Haeberli, W., Linsbauer, A., Cochachin, A., Salazar, C., and Fischer, U.H. (2016a). On the morphological characteristics of overdeepenings in high-mountain glacier beds. *Earth Surface Processes and Landforms* 41(13)**,** 1980-1990.

Haeberli, W., Buetler, M., Huggel, C., Friedli, T.L., Schaub, Y., and Schleiss, A.J. (2016b). New lakes in deglaciating high-mountain regions–opportunities and risks. *Climatic change* 139(2)**,** 201-214.

Haeberli, W., Schaub, Y., and Huggel, C. (2017). Increasing risks related to landslides from degrading permafrost into new lakes in de-glaciating mountain ranges. *Geomorphology* 293**,** 405-417.

Hajdas, I., Ivy, S.D., Beer, J., Bonani, G., Imboden, D., Lotted, A.F., et al. (1993). AMS radiocarbon dating and varve chronology of Lake Soppensee: 6000 to 12000 14 C years BP. *Climate dynamics* 9(3)**,** 107-116.

Hajdas, I., and Michczyński, A. (2010). Age-depth model of Lake Soppensee (Switzerland) based on the high-resolution 14 C chronology compared with varve chronology. *Radiocarbon* 52(3)**,** 1027-1040.

Hamdi, E., Romdhane, N.B., du Mouza, J., and Le Cleac'h, J.M. (2008). Fragmentation energy in rock blasting. *Geotechnical and Geological Engineering* 26(2)**,** 133-146.

Harris, C., Arenson, L.U., Christiansen, H.H., Etzelmüller, B., Frauenfelder, R., Gruber, S., et al. (2009). Permafrost and climate in Europe: Monitoring and modelling thermal, geomorphological and geotechnical responses. *Earth-Science Reviews* 92(3-4)**,** 117-171.

Hauck, C., and Mühll, D.V. (2003). Inversion and interpretation of two-dimensional geoelectrical measurements for detecting permafrost in mountainous regions. *Permafrost and Periglacial Processes* 14(4)**,** 305-318.

Hauck, C., and Kneisel, C. (2008). *Applied geophysics in periglacial environments.* Cambridge University Press.

Haug, Ø.T., Rosenau, M., Leever, K., and Oncken, O. (2016). On the energy budgets of fragmenting rockfalls and rockslides: Insights from experiments. *Journal of Geophysical Research: Earth Surface* 121(7)**,** 1310-1327.

Havenith, H.-B., and Bourdeau, C. (2010). Earthquake-induced landslide hazards in mountain regions: a review of case histories from Central Asia (An inaugural lecture to the society). *Geologica Belgica*.

Heckmann, T., Bimböse, M., Krautblatter, M., Haas, F., Becht, M., and Morche, D. (2012). From geotechnical analysis to quantification and modelling using LiDAR data: a study on rockfall in the Reintal catchment, Bavarian Alps, Germany. *Earth Surface Processes and Landforms* 37(1)**,** 119-133.

Heim, A. (1932). *Bergsturz und Menschenleben.* Fretz & Wasmuth, Zürich.

Heiri, O., Lotter, A.F., Hausmann, S., and Kienast, F. (2003). A chironomid-based Holocene summer air temperature reconstruction from the Swiss Alps. *The Holocene* 13(4)**,** 477-484.

Hengl, T., and Reuter, H.I. (2008). *Geomorphometry: concepts, software, applications.* Newnes.

Hermanns, R., Blikra, L., Naumann, M., Nilsen, B., Panthi, K., Stromeyer, D., et al. (2006). Examples of multiple rock-slope collapses from Köfels (Ötz valley, Austria) and western Norway. *Engineering Geology* 83(1-3)**,** 94-108.

Hermanns, R.L., Niedermann, S., Ivy-Ochs, S., and Kubik, P.W. (2004). Rock avalanching into a landslide-dammed lake causing multiple dam failure in Las Conchas valley (NW Argentina)—evidence from surface exposure dating and stratigraphic analyses. *Landslides* 1(2)**,** 113-122.

Hermanns, R.L., Hewitt, K., Strom, A., Evans, S.G., Dunning, S.A., and Scarascia-Mugnozza, G. (2011). The classification of rockslide dams. In: *Natural and artificial rockslide dams*. Springer, Dordrecht, 581-593.

Heuberger, H., Masch, L., Preuss, E., and Schröcker, A. (1984). Quaternary landslides and rock fusion in Central Nepal and in the Tyrolean Alps. *Mountain Research and Development***,** 345-362.

Hewitt, K. (2006). Rock avalanches with complex run out and emplacement, Karakoram Himalaya, Inner Asia. In: *Landslides from Massive Rock Slope Failure*. Springer, Dordrecht, 521-550.

Hewitt, K., Clague, J.J., and Orwin, J.F. (2008). Legacies of catastrophic rock slope failures in mountain landscapes. *Earth-Science Reviews* 87(1-2)**,** 1-38.

Hewitt, K., Clague, J.J., and Deline, P. (2011). Catastrophic rock slope failures and mountain glaciers. *Encyclopedia of Snow, Ice and Glaciers***,** 112-126.

Higman, B., Shugar, D.H., Stark, C.P., Ekström, G., Koppes, M.N., Lynett, P., et al. (2018). The 2015 landslide and tsunami in Taan Fiord, Alaska. *Scientific reports* 8(1)**,** 1-12.

Hilbe, M., and Anselmetti, F.S. (2015). Mass movement-induced tsunami hazard on perialpine Lake Lucerne (Switzerland): scenarios and numerical experiments. *Pure and Applied Geophysics* 172(2)**,** 545-568.

Hilbich, C., Hauck, C., Hoelzle, M., Scherler, M., Schudel, L., Völksch, I., et al. (2008). Monitoring mountain permafrost evolution using electrical resistivity tomography: A 7-year study of seasonal, annual, and long-term variations at Schilthorn, Swiss Alps. *Journal of Geophysical Research: Earth Surface* 113(F1).

Hilger, P., Hermanns, R.L., Gosse, J.C., Jacobs, B., Etzelmüller, B., and Krautblatter, M. (2018). Multiple rock-slope failures from Mannen in Romsdal Valley, western Norway, revealed from Quaternary geological mapping and 10Be exposure dating. *The Holocene* 28(12)**,** 1841-1854.

Hinderer, M. (2001). Late Quaternary denudation of the Alps, valley and lake fillings and modern river loads. *Geodinamica Acta* 14(4)**,** 231-263.

Hodell, D.A., Brenner, M., Kanfoush, S.L., Curtis, J.H., Stoner, J.S., Xueliang, S., et al. (1999). Paleoclimate of southwestern China for the past 50,000 yr inferred from lake sediment records. *Quaternary Research* 52(3)**,** 369-380.

Hornung, T., and Haas, U. (2017). Erläuterungen zur Geologischen Karte 1:25 000, 8531/8631 Zugspitze 8532/8632 Garmisch-Partenkirchen. *Bavarian Environmental Agency, Augsburg*.

Howarth, J.D., Fitzsimons, S.J., Norris, R.J., and Jacobsen, G.E. (2012). Lake sediments record cycles of sediment flux driven by large earthquakes on the Alpine fault, New Zealand. *Geology* 40(12)**,** 1091-1094.

Hsü, K.J. (1975). Catastrophic debris streams (sturzstroms) generated by rockfalls. *Geological Society of America Bulletin* 86(1)**,** 129-140.

Hsü, K.J., and Kelts, K. (1985). Swiss lakes as a geological laboratory. *Naturwissenschaften* 72(6)**,** 315-321.

Hu, W., and McSaveney, M. (2018). A polished and striated pavement formed by a rock avalanche in under 90 s mimics a glacially striated pavement. *Geomorphology* 320**,** 154-161.

Hu, W., Huang, R., McSaveney, M., Zhang, X.-h., Yao, L., and Shimamoto, T. (2018). Mineral changes quantify frictional heating during a large low-friction landslide. *Geology* 46(3)**,** 223-226.

Hu, W., Huang, R., McSaveney, M., Yao, L., Xu, Q., Feng, M., et al. (2019). Superheated steam, hot CO2 and dynamic recrystallization from frictional heat jointly lubricated a giant landslide: Field and experimental evidence. *Earth and Planetary Science Letters* 510**,** 85-93.

Hubbard, B., Heald, A., Reynolds, J.M., Quincey, D., Richardson, S.D., Luyo, M.Z., et al. (2005). Impact of a rock avalanche on a moraine-dammed proglacial lake: Laguna Safuna Alta, Cordillera Blanca, Peru. *Earth Surface Processes and Landforms* 30(10)**,** 1251-1264.

Huggel, C., Gruber, S., Caplan-Auerbach, S., Wessels, R.L., and Molnia, B.F. (2008). The 2005 Mt. Steller, Alaska, rock-ice avalanche: A large slope failure in cold permafrost. In: *9th International Conference on Permafrost, Fairbanks, Alaska,* 747-752.

Huggel, C. (2009). Recent extreme slope failures in glacial environments: effects of thermal perturbation. *Quaternary Science Reviews* 28(11-12)**,** 1119-1130.

Huggel, C., Salzmann, N., Allen, S., Caplan-Auerbach, J., Fischer, L., Haeberli, W., et al. (2010). Recent and future warm extreme events and high-mountain slope stability. *Philosophical Transactions of the Royal Society A: Mathematical, Physical and Engineering Sciences* 368(1919)**,** 2435-2459.

Huggel, C., Clague, J.J., and Korup, O. (2012). Is climate change responsible for changing landslide activity in high mountains? *Earth Surface Processes and Landforms* 37(1)**,** 77-91.

Huggel, C., Korup, O., and Gruber, S. (2013). Landslide hazards and climate change in high mountains. *Treatise on geomorphology: hazards, applied, anthropogenic and cultural geomorphology. Academic Press, San Diego*.

Huggel, C., Carey, M., Clague, J.J., and Kääb, A. (2015). *The High-Mountain Cryosphere.* Cambridge University Press.

Hung, J.-J., Lee, C.-T., and Lin, M.-L. (2002). Tsao-ling rockslides, Taiwan. In: *Catastrophic landslides, effects, occurrence, and mechanisms. Geological Society of America Reviews in Engineering Geology* 15**,** 91-115.

Hungr, O., and Evans, S. (2004). Entrainment of debris in rock avalanches: an analysis of a long run-out mechanism. *Geological Society of America Bulletin* 116(9-10)**,** 1240-1252.

Hungr, O. (2006). Rock avalanche occurrence, process and modelling. In: *Landslides from Massive Rock Slope Failure*. Springer, Dordrecht, 243-266.

Hungr, O., Leroueil, S., and Picarelli, L. (2014). The Varnes classification of landslide types, an update. *Landslides* 11(2)**,** 167-194.

Hunt, J.E., Wynn, R.B., Masson, D.G., Talling, P.J., and Teagle, D.A. (2011). Sedimentological and geochemical evidence for multistage failure of volcanic island landslides: A case study from Icod landslide on north Tenerife, Canary Islands. *Geochemistry, Geophysics, Geosystems* 12(12).

Hunt, J.E., Wynn, R., Talling, P., and Masson, D. (2013). Turbidite record of frequency and source of large volume (> 100 km3) Canary Island landslides in the last 1.5 Ma: Implications for landslide triggers and geohazards. *Geochemistry, Geophysics, Geosystems* 14(7)**,** 2100-2123.

Hunt, J.E., Wynn, R.B., and Croudace, I.W. (2015). "Identification, Correlation and Origin of Multistage Landslide Events in Volcaniclastic Turbidites in the Moroccan Turbidite System," in *Micro-XRF Studies of Sediment Cores*. Springer), 147-172.

Imre, B., Laue, J., and Springman, S.M. (2010). Fractal fragmentation of rocks within sturzstroms: insight derived from physical experiments within the ETH geotechnical drum centrifuge. *Granular matter* 12(3)**,** 267-285.

Iverson, R.M., Reid, M.E., and LaHusen, R.G. (1997). Debris-flow mobilization from landslides. *Annual Review of Earth and Planetary Sciences* 25(1)**,** 85-138.

Iverson, R.M. (2005). Regulation of landslide motion by dilatancy and pore pressure feedback. *Journal of Geophysical Research: Earth Surface* 110(F2).

Iverson, R.M., Reid, M.E., Logan, M., LaHusen, R.G., Godt, J.W., and Griswold, J.P. (2011). Positive feedback and momentum growth during debris-flow entrainment of wet bed sediment. *Nature Geoscience* 4(2)**,** 116-121.

Iverson, R.M., and Ouyang, C. (2015). Entrainment of bed material by Earth-surface mass flows: Review and reformulation of depth-integrated theory. *Reviews of Geophysics* 53(1)**,** 27-58.

Iverson, R.M. (2016). Comment on "The reduction of friction in long-runout landslides as an emergent phenomenon" by Brandon C. Johnson et al. *Journal of Geophysical Research: Earth Surface* 121(11)**,** 2238-2242.

Ivy-Ochs, S., Heuberger, H., Kubik, P., Kerschner, H., Bonani, G., Frank, M., et al. (1998). The age of the Köfels event-relative, 14C and cosmogenic isotope dating of an early Holocene landslide in the Central Alps (Tyrol, Austria). *Zeitschrift für Gletscherkunde und Glazialgeologie ZGG* 34**,** 57-68.

Ivy-Ochs, S., Poschinger, A., Synal, H.-A., and Maisch, M. (2009). Surface exposure dating of the Flims landslide, Graubünden, Switzerland. *Geomorphology* 103(1)**,** 104-112.

Ivy-Ochs, S., Martin, S., Campedel, P., Hippe, K., Alfimov, V., Vockenhuber, C., et al. (2017). Geomorphology and age of the Marocche di Dro rock avalanches (Trentino, Italy). *Quaternary Science Reviews* 169**,** 188-205.

Jacobs, B., Grabmaier, A., and Krautblatter, M. (2020). Benchmark rock fall hazard assessment and safety concept for touristically developed alpine gorges (Höllentalklamm, Bavarian Alps). In: *EGU General Assembly Conference Abstracts*, 18427.

Jerz, H., and Poschinger, A.v. (1995). Neuere Ergebnisse zum Bergsturz Eibsee-Grainau. *Geologica Bavarica* 99**,** 383-398.

Jibson, R.W. (1993). Predicting earthquake-induced landslide displacements using Newmark's sliding block analysis. *Transportation research record* (1411).

Jibson, R.W., Harp, E.L., and Michael, J.A. (2000). A method for producing digital probabilistic seismic landslide hazard maps. *Engineering Geology* 58(3)**,** 271-289.

Jibson, R.W. (2007). Regression models for estimating coseismic landslide displacement. *Engineering Geology* 91(2)**,** 209-218.

Joerin, U.E., Stocker, T.F., and Schlüchter, C. (2006). Multicentury glacier fluctuations in the Swiss Alps during the Holocene. *The Holocene* 16(5)**,** 697-704.

Johnson, B.C., Campbell, C.S., and Melosh, H.J. (2016). Reply to comment by Iverson on "The reduction of friction in long runout landslides as an emergent phenomenon". *Journal of Geophysical Research: Earth Surface* 121(11)**,** 2243-2246.

Kafle, J., Pokhrel, P.R., Khattri, K.B., Kattel, P., Tuladhar, B.M., and Pudasaini, S.P. (2016). Landslide-generated tsunami and particle transport in mountain lakes and reservoirs. *Annals of Glaciology* 57(71)**,** 232-244.

Kaser, G., Cogley, J., Dyurgerov, M., Meier, M., and Ohmura, A. (2006). Mass balance of glaciers and ice caps: consensus estimates for 1961–2004. *Geophysical Research Letters* 33(19).

Kastrup, U., Zoback, M.L., Deichmann, N., Evans, K.F., Giardini, D., and Michael, A.J. (2004). Stress field variations in the Swiss Alps and the northern Alpine foreland derived from inversion of fault plane solutions. *Journal of Geophysical Research: Solid Earth* 109(B1).

Keefer, D.K. (1984). Landslides caused by earthquakes. *Geological Society of America Bulletin* 95(4)**,** 406-421.

Keefer, D.K. (2000). Statistical analysis of an earthquake-induced landslide distribution—the 1989 Loma Prieta, California event. *Engineering geology* 58(3)**,** 231-249.

Keefer, D.K. (2002). Investigating landslides caused by earthquakes–a historical review. *Surveys in Geophysics* 23(6)**,** 473-510.

Kiefer, C., Krautblatter, M., Mayr, C., Oswald, P., and Strasser, M. (2020). The Influence of Debris Flow Activity on the Sediment of the Lake Plansee over 3.6 ka (Tyrol, Austria). In: *EGU General Assembly Conference Abstracts,* 21300.

Knapp, S. (2012). *The sedimentary archive of Lake Oeschinen (Bernese Alps, Switzerland): Reconstruction of the rockfall history.* ETH Zürich, Zürich. Unpublished master thesis, 73 p.

Knapp, S., Gilli, A., Anselmetti, F.S., Krautblatter, M., and Hajdas, I. (2018). Multistage Rock-Slope Failures Revealed in Lake Sediments in a Seismically Active Alpine Region (Lake Oeschinen, Switzerland). *Journal of Geophysical Research: Earth Surface* 123(4)**,** 658-677.

Knapp, S., and Krautblatter, M. (2020). Conceptual Framework of Energy Dissipation During Disintegration in Rock Avalanches. *Frontiers in Earth Science* 8(263).

Knapp, S., Mamot, P., Lempe, B., and Krautblatter, M. (2020a). Impact of an 0.2 km³ Rock Avalanche on Lake Eibsee (Bavarian Alps, Germany) – Part I: Reconstruction of the Paleolake and Effects of the Impact. *Earth Surface Processes and Landforms*.

Knapp, S., Anselmetti, F.S., Lempe, B., and Krautblatter, M. (2020b). Impact of an 0.2 km³ Rock Avalanche on Lake Eibsee (Bavarian Alps, Germany) – Part II: Catchment Response to Consecutive Debris Avalanche and Debris Flow. *Earth Surface Processes and Landforms*.

Kneisel, C. (2003). Electrical resistivity tomography as a tool for geomorphological investigations-some case studies (with 7 figures and 1 table). *Zeitschrift für Geomorphologie* Supplement**,** 37-49.

Kneisel, C., Emmert, A., and Kästl, J. (2014). Application of 3D electrical resistivity imaging for mapping frozen ground conditions exemplified by three case studies. *Geomorphology* 210**,** 71-82.

Knight, J., Mitchell, W.A., and Rose, J. (2011). Geomorphological field mapping. In: *Developments in earth surface processes*. Elsevier, Amsterdam, 151-187.

Köpfli, P., Grämiger, L.M., Moore, J.R., Vockenhuber, C., and Ivy-Ochs, S. (2018). The Oeschinensee rock avalanche, Bernese Alps, Switzerland: a co-seismic failure 2300 years ago? *Swiss Journal of Geosciences* 111(1-2)**,** 205-219.

Korup, O. (2005). Geomorphic hazard assessment of landslide dams in South Westland, New Zealand: Fundamental problems and approaches. *Geomorphology* 66(1-4)**,** 167-188.

Krautblatter, M., and Hauck, C. (2007). Electrical resistivity tomography monitoring of permafrost in solid rock walls. *Journal of Geophysical Research: Earth Surface* 112(F2).

Krautblatter, M., Verleysdonk, S., Flores-Orozco, A., and Kemna, A. (2010). Temperature-calibrated imaging of seasonal changes in permafrost rock walls by quantitative electrical resistivity tomography (Zugspitze, German/Austrian Alps). *Journal of Geophysical Research: Earth Surface* 115(F2).

Krautblatter, M., Huggel, C., Deline, P., and Hasler, A. (2012a). Research Perspectives on Unstable High-alpine Bedrock Permafrost: Measurement, Modelling and Process Understanding. *Permafrost and Periglacial Processes* 23(1)**,** 80-88.

Krautblatter, M., Moser, M., Schrott, L., Wolf, J., and Morche, D. (2012b). Significance of rockfall magnitude and carbonate dissolution for rock slope erosion and geomorphic work on Alpine limestone cliffs (Reintal, German Alps). *Geomorphology* 167**,** 21-34.

Krautblatter, M., Funk, D., and Guenzel, F. (2013). Why permafrost rocks become unstable: a rock–ice-mechanical model in time and space. *Earth Surf. Process. Landforms* 38(8)**,** 876-887.

Krautblatter, M., and Moore, J.R. (2014). Rock slope instability and erosion: toward improved process understanding. *Earth Surface Processes and Landforms* 39(9)**,** 1273-1278.

Krautblatter, M., and Leith, K. (2015). Glacier- and permafrost-related slope instabilities. In: *The High-Mountain Cryosphere: Environmental Changes and Human Risks,* eds. C. Huggel, M. Carey, J.J. Clague & A. Kääb. Cambridge University Press, Cambridge, 147-165.

Krautblatter, M., Kellerer-Pirklbauer, A., and Gärtner-Roer, I. (2018). Permafrost in den Alpen: Erscheinungsformen, Verbreitung und zukünftige Entwicklung. *Geographische Rundschau* (11)**,** 22-29.

Kremer, K., Simpson, G., and Girardclos, S. (2012). Giant Lake Geneva tsunami in ad 563. *Nature Geoscience* 5(11)**,** 756-757.

Kremer, K., Hilbe, M., Simpson, G., Decrouy, L., Wildi, W., and Girardclos, S. (2015). Reconstructing 4000 years of mass movement and tsunami history in a deep peri-Alpine lake (Lake Geneva, France-Switzerland). *Sedimentology* 62(5)**,** 1305-1327.

Kremer, K., Wirth, S.B., Reusch, A., Fäh, D., Bellwald, B., Anselmetti, F.S., et al. (2017). Lake-sediment based paleoseismology: Limitations and perspectives from the Swiss Alps. *Quaternary Science Reviews* 168**,** 1-18.

Krieger, M.L.H. (1977). *Large landslides, composed of megabreccia, interbedded in Miocene basin deposits, southeastern Arizona.* US Govt. Print. Off.

Lamoureux, S. (2002). Varve chronology techniques. In: *Tracking environmental change using lake sediments*. Springer, Dordrecht, 247-260.

Langlois, V.J., Quiquerez, A., and Allemand, P. (2015). Collapse of a two-dimensional brittle granular column: Implications for understanding dynamic rock fragmentation in a landslide. *Journal of Geophysical Research: Earth Surface* 120(9)**,** 1866-1880.

Larsen, M.C., Wieczorek, G.F., and Latrubesse, E. (2006). Geomorphic effects of large debris flows and flash floods, northern Venezuela, 1999. *Zeitschrift für Geomorphologie Neue Folge, Supplementband* 145**,** 147-175.

Lavé, J., Yule, D., Sapkota, S., Basant, K., Madden, C., Attal, M., et al. (2005). Evidence for a great Medieval earthquake (~ 1100 AD) in the central Himalayas, Nepal. *Science* 307(5713)**,** 1302-1305.

Leemann, A., and Niessen, F. (1994). Varve formation and the climatic record in an Alpine proglacial lake: calibrating annually-laminated sediments against hydrological and meteorological data. *The Holocene* 4(1)**,** 1-8.

Legros, F. (2006). Landslide mobility and the role of water. In: *Landslides from Massive Rock Slope Failure,* eds. S. G. Evans, G. Scarascia Mugnozza, A. Strom & R.L. Hermanns. Springer, Dordrecht, 233-242.

Leinauer, J., Jacobs, B., and Krautblatter, M. (2020). Process dynamics, real time monitoring and early warning at an imminent cliff fall (Hochvogel, Allgäu Alps). In: *EGU General Assembly Conference Abstracts*, 19073.

Leith, K., Moore, J.R., Amann, F., and Loew, S. (2014). In situ stress control on microcrack generation and macroscopic extensional fracture in exhuming bedrock. *Journal of Geophysical Research: Solid Earth* 119(1)**,** 594-615.

Leith, K., Hofmayer, F., Kessler, B., and Krautblatter, M. (2016). Preconditioning of the Eibsee rock avalanche by deglaciation and development of critical bedrock stresses. In: *EGU General Assembly Conference Abstracts*, 18256.

Lenhardt, W.A., Freudenthaler, C., Lippitsch, R., and Fiegweil, E. (2007). Focal-Depth Distributions in the Austrian Eastern Alps Based on Macroseismic Data. *Austrian Journal of Earth Sciences* 100.

Leonard, E.M. (1997). The relationship between glacial activity and sediment production: evidence from a 4450-year varve record of neoglacial sedimentation in Hector Lake, Alberta, Canada. *Journal of Paleolimnology* 17(3)**,** 319-330.

Linzer, H.-G., Decker, K., Peresson, H., Dell'Mour, R., and Frisch, W. (2002). Balancing lateral orogenic float of the Eastern Alps. *Tectonophysics* 354(3-4)**,** 211-237.

Locat, P., Couture, R., Leroueil, S., Locat, J., and Jaboyedoff, M. (2006). Fragmentation energy in rock avalanches. *Canadian Geotechnical Journal* 43(8)**,** 830-851.

Loke, M. (2006). RES2DINV ver. 3.55, Rapid 2-D resistivity & IP inversion using the least-squares method. *Software Manual* 139.

Lowe, D.R. (1975). Water escape structures in coarse-grained sediments. *Sedimentology* 22(2)**,** 157-204.

Maddock, R.H. (1986). Frictional melting in landslide-generated frictionites (hyalomylonit) and fault-generated pseudotachylites. *Tectonophysics* 128(1-2)**,** 151-153.

Magnin, F., Deline, P., Ravanel, L., Noetzli, J., and Pogliotti, P. (2015). Thermal characteristics of permafrost in the steep alpine rock walls of the Aiguille du Midi (Mont Blanc Massif, 3842 m asl). *The Cryosphere* 9(1)**,** 109-121.

Magnin, F., Westermann, S., Pogliotti, P., Ravanel, L., Deline, P., and Malet, E. (2017). Snow control on active layer thickness in steep alpine rock walls (Aiguille du Midi, 3842 m asl, Mont Blanc massif). *Catena* 149**,** 648-662.

Magnin, F., Etzelmüller, B., Westermann, S., Isaksen, K., Hilger, P., and Hermanns, R. (2019). Permafrost distribution in steep rock slopes in Norway: measurements, statistical modelling and implications for geomorphological processes. *Earth Surface Dynamics* 7, 1019-1040.

Mamot, P., Weber, S., Schröder, T., and Krautblatter, M. (2018). A temperature-and stress-controlled failure criterion for ice-filled permafrost rock joints. *The Cryosphere* 12(10)**,** 3333-3353.

Martin, S., Campedel, P., Ivy-Ochs, S., Vigano, A., Alfimov, V., Vockenhuber, C., et al. (2014). Lavini di Marco (Trentino, Italy): Cl-36 exposure dating of a polyphase rock avalanche. *Quaternary Geochronology* 19**,** 106-116.

Masson, D., Harbitz, C., Wynn, R., Pedersen, G., and Løvholt, F. (2006). Submarine landslides: processes, triggers and hazard prediction. *Philosophical Transactions of the Royal Society of London A: Mathematical, Physical and Engineering Sciences* 364(1845)**,** 2009-2039.

Mathews, W., and McTaggart, K. (1978). Hope rockslides, British Columbia, Canada. In: *Developments in Geotechnical Engineering*. Elsevier, Amsterdam, 259-275.

McArdell, B.W., Bartelt, P., and Kowalski, J. (2007). Field observations of basal forces and fluid pore pressure in a debris flow. *Geophysical Research Letters* 34(7).

McSaveney, M. (2002). Recent rockfalls and rock avalanches in Mount Cook national park, New Zealand. *Reviews in Engineering Geology* 15**,** 35-70.

McSaveney, M., and Davies, T. (2007). Rockslides and their motion. In: *Progress in Landslide Science*. Springer, Dordrecht, 113-133.

Mellor, M. (1973). Mechanical properties of rocks at low temperatures. In: *Permafrost: Second International Conference: Natl. Acad. of Sci. Washington, DC*, 334-344.

Mergili, M., Jaboyedoff, M., Pullarello, J., and Pudasaini, S.P. (2020). Back calculation of the 2017 Piz Cengalo–Bondo landslide cascade with r. avaflow: what we can do and what we can learn. *Natural Hazards & Earth System Sciences* 20(2).

Middleton, G.V. (1993). Sediment deposition from turbidity currents. *Annual review of earth and planetary sciences* 21(1)**,** 89-114.

Miles, S.B. (2001). *Seismic landslide hazard for the city of Berkeley, California*.

Miller, G.S., Andy Take, W., Mulligan, R.P., and McDougall, S. (2017). Tsunamis generated by long and thin granular landslides in a large flume. *Journal of Geophysical Research: Oceans* 122(1)**,** 653-668.

Milsom, J. (2003). *Field geophysics.* John Wiley & Sons.

Mitchell, T.M., Smith, S.A., Anders, M.H., Di Toro, G., Nielsen, S., Cavallo, A., et al. (2015). Catastrophic emplacement of giant landslides aided by thermal decomposition: Heart Mountain, Wyoming. *Earth and Planetary Science Letters* 411**,** 199-207.

Moernaut, J., Daele, M.V., Heirman, K., Fontijn, K., Strasser, M., Pino, M., et al. (2014). Lacustrine turbidites as a tool for quantitative earthquake reconstruction: New evidence for a variable rupture mode in south central Chile. *Journal of Geophysical Research: Solid Earth* 119(3)**,** 1607-1633.

Moernaut, J., Van Daele, M., Heirman, K., Wiemer, G., Molenaar, A., Vandorpe, T., et al. (2019). The subaqueous landslide cycle in south-central Chilean lakes: the role of tephra, slope gradient and repeated seismic shaking. *Sedimentary geology* 381**,** 84-105.

Monecke, K., Anselmetti, F.S., Becker, A., Schnellmann, M., Sturm, M., and Giardini, D. (2006). Earthquake-induced deformation structures in lake deposits: A Late Pleistocene to Holocene paleoseismic record for Central Switzerland. *Eclogae Geologicae Helvetiae* 99(3)**,** 343-362.

Moore, J.R., Sanders, J.W., Dietrich, W.E., and Glaser, S.D. (2009). Influence of rock mass strength on the erosion rate of alpine cliffs. *Earth Surface Processes and Landforms* 34(10)**,** 1339-1352.

Mörner, N.-A. (2014). Varve chronology. *Geochronology: Methods and Case Studies***,** 73-87.

Nasir, A., Lenhardt, W., Hintersberger, E., and Decker, K. (2013). Assessing the Completeness of Historical and Instrumental Earthquake Data in Austria and the Surrounding Areas. *Austrian Journal of Earth Sciences* 106(1).

Newmark, N.M. (1965). Effects of earthquakes on dams and embankments. *Geotechnique* 15 (2)**,** 139-160.

Nicoletti, P.G., and Sorriso-Valvo, M. (1991). Geomorphic controls of the shape and mobility of rock avalanches. *Geological Society of America Bulletin* 103(10)**,** 1365-1373.

Niklaus, M. (1967). *Geomorphologische und limnologische Untersuchungen am Oeschinensee.* Kommissionsverlag, Geographischer Verlag Kümmerly & Frey.

Noetzli, J., and Gruber, S. (2009). Transient thermal effects in Alpine permafrost. *The Cryosphere* 3(1)**,** 85-99.

Nowaczyk, N.R. (2002). Logging of magnetic susceptibility. In: *Tracking environmental change using lake sediments*. Springer, Dordrecht, 155-170.

O'Reilly, C.M., Alin, S.R., Plisnier, P.-D., Cohen, A.S., and McKee, B.A. (2003). Climate change decreases aquatic ecosystem productivity of Lake Tanganyika, Africa. *Nature* 424(6950)**,** 766-768.

Oohashi, K., Hirose, T., and Shimamoto, T. (2011). Shear-induced graphitization of carbonaceous materials during seismic fault motion: Experiments and possible implications for fault mechanics. *Journal of Structural Geology* 33(6)**,** 1122-1134.

Oohashi, K., Han, R., Hirose, T., Shimamoto, T., Omura, K., and Matsuda, T. (2014). Carbon-forming reactions under a reducing atmosphere during seismic fault slip. *Geology* 42(9)**,** 787-790.

Oppikofer, T., Jaboyedoff, M., and Keusen, H.-R. (2008). Collapse at the eastern Eiger flank in the Swiss Alps. *Nature Geoscience* 1(8)**,** 531-535.

Ostermann, M., Sanders, D., Prager, C., and Kramers, J. (2007). Aragonite and calcite cementation in "boulder-controlled" meteoric environments on the Fern Pass rockslide (Austria): implications for radiometric age dating of catastrophic mass movements. *Facies* 53(2)**,** 189-208.

Ostermann, M., Sanders, D., Ivy-Ochs, S., Alfimov, V., Rockenschaub, M., and Römer, A. (2012). Early Holocene (8.6 ka) rock avalanche deposits, Obernberg valley (Eastern Alps): Landform interpretation and kinematics of rapid mass movement. *Geomorphology* 171**,** 83-93.

Ostermann, M., and Prager, C. (2016). Field Trip 12: Rock slope failures shaping the landscape in the Loisach-, Inn-and Ötz Valley region (Tyrol, Austria). In: *Geo. Alp Conference Proceedings*.

Ostermann, M., Ivy-Ochs, S., Sanders, D., and Prager, C. (2017). Multi-method (14C, 36Cl, 234U/230Th) age bracketing of the Tschirgant rock avalanche (Eastern Alps): implications for absolute dating of catastrophic mass-wasting. *Earth Surface Processes and Landforms* 42(7)**,** 1110-1118.

Oswald, P., Huang, J.-J.S., Fabbri, S., Aufleger, M., Daxer, C., Strasser, M., et al. (2020). Strong earthquakes as main trigger mechanism for large pre-historic rock slope failures in Western Tyrol (Austria, Eastern Alps): constraints from lacustrine paleoseismology. In: *EGU General Assembly Conference Abstracts,* 14611.

Otto, J.-C., and Smith, M.J. (2013). Geomorphological mapping. *Geomorphological techniques* 2**,** 1-10.

Ouchterlony, F., Nyberg, U., Olsson, M., Bergqvist, I., Granlund, L., and Grind, H. (2004). Where does the explosive energy in rock blasting rounds go? *Science and technology of energetic materials* 65(2)**,** 54-63.

Owen, L.A., Kamp, U., Khattak, G.A., Harp, E.L., Keefer, D.K., and Bauer, M.A. (2008). Landslides triggered by the 8 October 2005 Kashmir earthquake. *Geomorphology* 94(1)**,** 1-9.

Paguican, E., de Vries, B.v.W., and Lagmay, A. (2014). Hummocks: how they form and how they evolve in rockslide-debris avalanches. *Landslides* 11(1)**,** 67-80.

Paris, R., Giachetti, T., Chevalier, J., Guillou, H., and Frank, N. (2011). Tsunami deposits in Santiago Island (Cape Verde archipelago) as possible evidence of a massive flank failure of Fogos volcano. *Sedimentary Geology* 239(3)**,** 129-145.

Patzelt, G. (2012a). Die Bergstürze von Tschirgant und von Haiming, Oberinntal, Tirol–Begleitworte zur Kartenbeilage. *Jahrbuch der Geologischen Bundesanstalt* 152(1-4)**,** 13-24.

Patzelt, G. (2012b). Die Bergstürze vom Pletzachkogel, Kramsach, Tirol. *Jahrbuch der Geologischen Bundesanstalt* 152(1-4)**,** 25-38.

Paul, F., Kääb, A., Maisch, M., Kellenberger, T., and Haeberli, W. (2004). Rapid disintegration of Alpine glaciers observed with satellite data. *Geophysical research letters* 31(21).

Paul, F., and Haeberli, W. (2008). Spatial variability of glacier elevation changes in the Swiss Alps obtained from two digital elevation models. *Geophysical Research Letters* 35(21).

Pavoni, N. (1968a). *Über die Entstehung der Kiesmassen im Bergsturzgebiet von Bonaduz-Reichenau (Graubünden).* Ecl. Geologic. Helvetica.

Pavoni, N. (1968b). Über die Entstehung der Kiesmassen im Bergsturzgebiet von Bonaduz-Reichenau (Graubünden). *Ecl. Geologic. Helvetica* 61/2**,** 494-500.

Penck, A., and Brückner, E. (1909). *Die Alpen im Eiszeitalter.* Tauchnitz, Leipzig.

Perret, S., Stoffel, M., and Kienholz, H. (2006). Spatial and temporal rockfall activity in a forest stand in the Swiss Prealps—a dendrogeomorphological case study. *Geomorphology* 74(1)**,** 219-231.

Peyron, O., Bégeot, C., Brewer, S., Heiri, O., Magny, M., Millet, L., et al. (2005). Late-Glacial climatic changes in Eastern France (Lake Lautrey) from pollen, lake-levels, and chironomids. *Quaternary Research* 64(2)**,** 197-211.

Pfiffner, O.-A., Schlunegger, F., and Buiter, S. (2002). The Swiss Alps and their peripheral foreland basin: Stratigraphic response to deep crustal processes. *Tectonics* 21(2)**,** 3-1-3-16.

Pfiffner, O.A., Ramsay, J., and Schmid, S. (2011). Structural map of the Helvetic Zone of the Swiss Alps. *Geological special map* 1(100,000).

Plafker, G., and Ericksen, G. (1978). Nevados Huascaran avalanches, Peru. In: *Developments in Geotechnical Engineering*. Elsevier, Amsterdam, 277-314.

Pollet, N., and Schneider, J.L.M. (2004). Dynamic disintegration processes accompanying transport of the Holocene Flims sturzstrom (Swiss Alps). *Earth and Planetary Science Letters* 221(1-4)**,** 433-448.

Pollet, N., Cojean, R., Couture, R., Schneider, J.-L., Strom, A.L., Voirin, C., et al. (2005). A slab-on-slab model for the Flims rockslide (Swiss Alps). *Canadian Geotechnical Journal* 42(2)**,** 587-600.

Poschinger, A., and Haas, U. (1997). Der Flimser Bergsturz, doch ein warmzeitliches Ereignis? *Bulletin für angewandte Geologie* 2(1)**,** 35-46.

Poschinger, A., and Kippel, T. (2009). Alluvial deposits liquefied by the Flims rock slide. *Geomorphology* 103(1)**,** 50-56.

Poschinger, A., and Ruegg, T. (2012). Die Churer Tomahügel, ein besonderes Zeugnis der Landschaftsgenese. *Jahresbericht der Naturforschenden Gesellschaft Graubünden* (117)**,** 93-100.

Poschinger, A.v., Wassmer, P., and Maisch, M. (2006). The Flims rockslide: history of interpretation and new insights. In: *Landslides from Massive Rock Slope Failure*. Springer, Dordrecht, 329-356.

Praet, N., Moernaut, J., Van Daele, M., Boes, E., Haeussler, P.J., Strupler, M., et al. (2017). Paleoseismic potential of sublacustrine landslide records in a high-seismicity setting (south-central Alaska). *Marine Geology* 384**,** 103-119.

Prager, C., Krainer, K., Seidl, V., and Chwatal, W. (2006). Spatial features of Holocene sturzstrom-deposits inferred from subsurface investigations (Fernpass rockslide, Tyrol, Austria). *Geo. Alp* 3**,** 147-166.

Prager, C., Zangerl, C., Patzelt, G., and Brandner, R. (2008). Age distribution of fossil landslides in the Tyrol (Austria) and its surrounding areas. *Natural Hazards and Earth System Sciences* 8**,** 377-407.

Prager, C., Ivy-Ochs, S., Ostermann, M., Synal, H.-A., and Patzelt, G. (2009). Geology and radiometric 14C-, 36Cl-and Th-/U-dating of the Fernpass rockslide (Tyrol, Austria). *Geomorphology* 103(1)**,** 93-103.

Preuth, T., Bartelt, P., Korup, O., and McArdell, B. (2010). A random kinetic energy model for rock avalanches: Eight case studies. *Journal of Geophysical Research: Earth Surface* 115(F3).

Pudasaini, S.P., and Krautblatter, M. (2014). A two-phase mechanical model for rock-ice avalanches. *Journal of Geophysical Research: Earth Surface* 119(10)**,** 2272-2290.

Pudasaini, S.P., and Mergili, M. (2019). A Multi-Phase Mass Flow Model. *Journal of Geophysical Research: Earth Surface* 124**,** 2920-2942.

Radić, V., Bliss, A., Beedlow, A.C., Hock, R., Miles, E., and Cogley, J.G. (2014). Regional and global projections of twenty-first century glacier mass changes in response to climate scenarios from global climate models. *Climate Dynamics* 42(1-2)**,** 37-58.

Rait, K.L., and Bowman, E.T. (2010). Dynamic fragmentation in rock avalanches: A numerical model of micromechanical behaviour. In: *Numerical Methods in Geotechnical Engineering,* eds. T. Benz & S. Nordal. Taylor & Francis Group, London, 435-440.

Ramsey, C.B. (1995). Radiocarbon calibration and analysis of stratigraphy; the OxCal program. *Radiocarbon* 37(2)**,** 425-430.

Ramsey, C.B. (2017). Methods for summarizing radiocarbon datasets. *Radiocarbon* 59(6)**,** 1809-1833.

Ravanel, L., Allignol, F., Deline, P., Gruber, S., and Ravello, M. (2010). Rock falls in the Mont Blanc Massif in 2007 and 2008. *Landslides* 7(4)**,** 493-501.

Ravanel, L., and Deline, P. (2011). Climate influence on rockfalls in high-Alpine steep rockwalls: The north side of the Aiguilles de Chamonix (Mont Blanc massif) since the end of the 'Little Ice Age'. *The Holocene* 21(2)**,** 357-365.

Ravanel, L., Magnin, F., and Deline, P. (2017). Impacts of the 2003 and 2015 summer heatwaves on permafrost-affected rock-walls in the Mont Blanc massif. *Science of the Total Environment* 609**,** 132-143.

Reimer, P.J., Baillie, M.G., Bard, E., Bayliss, A., Beck, J.W., Blackwell, P.G., et al. (2009). IntCal09 and Marine09 radiocarbon age calibration curves, 0–50,000 years cal BP. *Radiocarbon* 51(4)**,** 1111-1150.

Reimer, P.J., Bard, E., Bayliss, A., Beck, J.W., Blackwell, P.G., Ramsey, C.B., et al. (2013). IntCal13 and Marine13 radiocarbon age calibration curves 0–50,000 years cal BP. *Radiocarbon* 55(4)**,** 1869-1887.

Reusch, A., Moernaut, J., Anselmetti, F., and Strasser, M. (2016). Sediment mobilization deposits from episodic subsurface fluid flow—A new tool to reveal long-term earthquake records? *Geology* 44(4)**,** 243-246.

Reynolds, J.M. (2011). *An introduction to applied and environmental geophysics.* John Wiley & Sons.

Reznichenko, N.V., Davies, T.R.H., Shulmeister, J., and Larsen, S.H. (2012). A new technique for identifying rock avalanche-sourced sediment in moraines and some paleoclimatic implications. *Geology* 40(4)**,** 319-322.

Roberts, N.J., and Evans, S.G. (2013). The gigantic Seymareh (Saidmarreh) rock avalanche, Zagros Fold–Thrust Belt, Iran. *Journal of the Geological Society* 170(4)**,** 685-700.

Roberts, N.J., McKillop, R.J., Lawrence, M.S., Psutka, J.F., Clague, J.J., Brideau, M.-A., et al. (2013). Impacts of the 2007 landslide-generated tsunami in Chehalis Lake, Canada. In: *Landslide Science and Practice*. Springer, Dordrecht, 133-140.

Robinson, T.R., Davies, T.R., Reznichenko, N.V., and De Pascale, G.P. (2015). The extremely long-runout Komansu rock avalanche in the Trans Alai range, Pamir Mountains, southern Kyrgyzstan. *Landslides* 12(3)**,** 523-535.

Rödder, T., and Kneisel, C. (2012). Permafrost mapping using quasi-3D resistivity imaging, Murtèl, Swiss Alps. *Near Surface Geophysics* 10(2)**,** 117-127.

Rosendahl, B., Reynolds, D., Lorber, P., Burgess, C., McGill, J., Scott, D., et al. (1986). Structural expressions of rifting: lessons from Lake Tanganyika, Africa. *Geological Society, London, Special Publications* 25(1)**,** 29-43.

Rüffer, T. (1995). *Entwicklung einer Karbonat-Plattform: Fazies, Kontrollfaktoren und Sequenzstratigraphie in der Mitteltrias der westlichen Nördlichen Kalkalpen (Tirol, Bayern).* Geologisch-Paläontologisches Institut der Ruprecht-Karls-Universität, Heidelberg.

Samouëlian, A., Cousin, I., Tabbagh, A., Bruand, A., and Richard, G. (2005). Electrical resistivity survey in soil science: a review. *Soil and Tillage research* 83(2)**,** 173-193.

Sass, O. (2004). Rock moisture fluctuations during freeze-thaw cycles: Preliminary results from electrical resistivity measurements. *Polar Geography* 28(1)**,** 13-31.

Sass, O., and Krautblatter, M. (2007). Debris flow-dominated and rockfall-dominated talus slopes: Genetic models derived from GPR measurements. *Geomorphology* 86(1-2)**,** 176-192.

Sass, O., Krautblatter, M., and Morche, D. (2007). Rapid lake infill following major rockfall (bergsturz) events revealed by ground-penetrating radar (GPR) measurements, Reintal, German Alps. *The Holocene* 17(7)**,** 965-976.

Sassa, K., and Wang, G. (2005). Mechanism of landslide-triggered debris flows: Liquefaction phenomena due to the undrained loading of torrent deposits. In: *Debris-flow hazards and related phenomena*. Springer, Dordrecht, 81-104.

Scandroglio, R., and Krautblatter, M. (2020). Climate-change-induced changes in steep alpine permafrost bedrock. 13 years of 3D-ERT at the Steintälli ridge, Switzerland. In: *EGU General Assembly Conference Abstracts*, 18808.

Schäbitz, M., Janssen, C., Wirth, R., and Dresen, G. (2015). Microstructural and geochemical evolution of sliding surfaces in landslides and comparisons with crustal fault zones. In: *EGU General Assembly Conference Abstracts,* 5837.

Schaub, Y., Haeberli, W., Huggel, C., Künzler, M., and Bründl, M. (2013). Landslides and new lakes in deglaciating areas: a risk management framework. In: *Landslide Science and Practice*. Springer, Dordrecht, 31-38.

Scheidegger, A.E. (1973). On the prediction of the reach and velocity of catastrophic landslides. *Rock Mechanics and Rock Engineering* 5(4)**,** 231-236.

Scheller, E. (1970). *Geophysikalische Untersuchungen zum Problem des Taminser Bergsturzes.* Diss ETH Zürich, Zürich, Nr. 4560.

Schiefer, E., Menounos, B., and Wheate, R. (2007). Recent volume loss of British Columbian glaciers, Canada. *Geophysical Research Letters* 34(16).

Schmocker-Fackel, P., and Naef, F. (2010). More frequent flooding? Changes in flood frequency in Switzerland since 1850. *Journal of Hydrology* 381(1)**,** 1-8.

Schneider, D., Bartelt, P., Caplan-Auerbach, J., Christen, M., Huggel, C., and McArdell, B.W. (2010). Insights into rock-ice avalanche dynamics by combined analysis of seismic recordings and a numerical avalanche model. *Journal of Geophysical Research: Earth Surface* 115(F4).

Schneider, D., Huggel, C., Haeberli, W., and Kaitna, R. (2011). Unraveling driving factors for large rock–ice avalanche mobility. *Earth Surface Processes and Landforms* 36(14)**,** 1948-1966.

Schneider, J.-L., Pollet, N., Chapron, E., Wessels, M., and Wassmer, P. (2004). Signature of Rhine Valley sturzstrom dam failures in Holocene sediments of Lake Constance, Germany. *Sedimentary Geology* 169(1-2)**,** 75-91.

Schnellmann, M., Anselmetti, F.S., Giardini, D., and Mckenzie, J.A. (2006). 15,000 Years of mass-movement history in Lake Lucerne: Implications for seismic and tsunami hazards. *Eclogae Geologicae Helvetiae* 99(3)**,** 409-428.

Scholz, C.A. (2002). Applications of seismic sequence stratigraphy in lacustrine basins. In: *Tracking environmental change using lake sediments*. Springer, Dordrecht, 7-22.

Scholz, D., Krautblatter, M., Knapp, S., Poschinger, A., and Clague, J. (2019). Sedimentological reconstruction of an outburst flood in response to the Flims Rock Slide into the potential Lake Bonaduz. In: *EGU General Assembly Conference Abstracts*, 18773.

Schramm, J.M., Weidinger, J.T., and Ibetsberger, H.J. (1998). Petrologic and structural controls on geomorphology of prehistoric Tsergo Ri slope failure, Langtang Himal, Nepal. *Geomorphology* 26(1–3)**,** 107-121.

Schroeder, T., Scandroglio, R., Stammberger, V., Wittmann, M., and Krautblatter, M. (2020). New multi-phase thermo-geophysical model: Validate ERT-monitoring & assess permafrost evolution in alpine rock walls (Zugspitze, German/Austrian Alps). In: *EGU General Assembly Conference Abstracts*, 19984.

Schuster, R.L., and Alford, D. (2004). Usoi landslide dam and lake sarez, Pamir mountains, Tajikistan. *Environmental & Engineering Geoscience* 10(2)**,** 151-168.

Schwenk, M.A. (2017). *Sedimentological and geophysical analysis of rock-avalanche-related flooding deposits (Flims, CH).* LMU München, München. Unpublished master thesis, 98 p.

Shaller, P.J. (1991). Analysis of a large moist landslide, Lost River range, Idaho, USA. *Canadian Geotechnical Journal* 28(4)**,** 584-600.

Sheriff, R.E., and Geldart, L.P. (1995). *Exploration seismology.* Cambridge university press.

Siebert, L. (2002). Landslides resulting from structural failure of volcanoes. In: *Catastrophic landslides: effects, occurrence, and mechanisms*. Geological Society of America, 209-235.

Slingerland, R., and Voight, B. (1982). Evaluating hazard of landslide-induced water waves. *Journal of the Waterway Port Coastal and Ocean Division* 108(4)**,** 504-512.

Smith, M.J., and Wise, S.M. (2007). Problems of bias in mapping linear landforms from satellite imagery. *International Journal of Applied Earth Observation and Geoinformation* 9(1)**,** 65-78.

Smith, M.J. (2011). Digital Mapping: visualisation, interpretation and quantification of landforms. In: *Developments in Earth Surface Processes*. Elsevier, Amsterdam, 225-251.

Socco, L.V., Jongmans, D., Boiero, D., Stocco, S., Maraschini, M., Tokeshi, K., et al. (2010). Geophysical investigation of the Sandalp rock avalanche deposits. *Journal of Applied Geophysics* 70(4)**,** 277-291.

Sosio, R., Crosta, G.B., and Hungr, O. (2008). Complete dynamic modeling calibration for the Thurwieser rock avalanche (Italian Central Alps). *Engineering Geology* 100(1-2)**,** 11-26.

Sosio, R., Crosta, G.B., Chen, J.H., and Hungr, O. (2012). Modelling rock avalanche propagation onto glaciers. *Quaternary Science Reviews* 47**,** 23-40.

Spray, J.G. (1992). A physical basis for the frictional melting of some rock-forming minerals. *Tectonophysics* 204(3-4)**,** 205-221.

Spray, J.G. (2005). Evidence for melt lubrication during large earthquakes. *Geophysical Research Letters* 32(7).

Staub, R. (1910). Die Tomalandschaft im Rheintal von Reichenau bis Chur. *Jber. Geogr. Ges. Bern* (22)**,** 1-28.

Stewart, J.P., Chiou, S.-J., Bray, J.D., Graves, R.W., Somerville, P.G., and Abrahamson, N.A. (2002). Ground motion evaluation procedures for performance-based design. *Soil dynamics and earthquake engineering* 22(9)**,** 765-772.

Stockhecke, M., Timmermann, A., Kipfer, R., Haug, G.H., Kwiecien, O., Friedrich, T., et al. (2016). Millennial to orbital-scale variations of drought intensity in the Eastern Mediterranean. *Quaternary Science Reviews* 133**,** 77-95.

Stoffel, M. (2006). A review of studies dealing with tree rings and rockfall activity: The role of dendrogeomorphology in natural hazard research. *Natural Hazards* 39(1)**,** 51-70.

Stoll, V., Scandroglio, R., and Krautblatter, M. (2020). Modelling rock walls destabilization caused by hydrostatic pressure in frozen/unfrozen bedrock (Hochvogel & Zugspitze, Germany). In: *EGU General Assembly Conference Abstracts*, 14338.

Strasser, M., Anselmetti, F.S., Fäh, D., Giardini, D., and Schnellmann, M. (2006). Magnitudes and source areas of large prehistoric northern Alpine earthquakes revealed by slope failures in lakes. *Geology* 34(12)**,** 1005-1008.

Strasser, M., Monecke, K., Schnellmann, M., and Anselmetti, F.S. (2013). Lake sediments as natural seismographs: A compiled record of Late Quaternary earthquakes in Central Switzerland and its implication for Alpine deformation. *Sedimentology* 60(1)**,** 319-341.

Strupler, M., Anselmetti, F., Hilbe, M., and Strasser, M. (2019). Quantitative characterization of subaqueous landslides in Lake Zurich (Switzerland) based on a high-resolution bathymetric dataset. *Geological Society, London, Special Publications* 477(1)**,** 399-412.

Sturm, M., and Matter, A. (1978). Turbidites and varves in Lake Brienz (Switzerland): deposition of clastic detritus by density currents. *Modern and ancient lake sediments***,** 147-168.

Sturm, M. (1979). Origin and composition of clastic varves. In: *INQUA symposium on genesis and lithology of Quaternary deposits, Zurich, 1979*, 281-285.

Süfke, F., Gutjahr, M., Gilli, A., Anselmetti, F.S., Glur, L., and Eisenhauer, A. (2019). Early stage weathering systematics of Pb and Nd isotopes derived from a high-Alpine Holocene lake sediment record. *Chemical geology* 507**,** 42-53.

Supper, R., Ottowitz, D., Jochum, B., Römer, A., Pfeiler, S., Kauer, S., et al. (2014). Geoelectrical monitoring of frozen ground and permafrost in alpine areas: field studies and considerations towards an improved measuring technology. *Near Surface Geophysics* 12(1)**,** 93-115.

Tierney, J.E., Mayes, M.T., Meyer, N., Johnson, C., Swarzenski, P.W., Cohen, A.S., et al. (2010). Late-twentieth-century warming in Lake Tanganyika unprecedented since AD 500. *Nature Geoscience* 3(6)**,** 422-425.

Tinner, W., Kaltenrieder, P., Soom, M., Zwahlen, P., Schmidhalter, M., Boschetti, A., et al. (2005). Der nacheiszeitliche Bergsturz im Kandertal (Schweiz): Alter und Auswirkungen auf die damalige Umwelt. *Eclogae Geologicae Helvetiae* 98(1)**,** 83-95.

Tollmann, A. (1976). *Analyse des klassischen nordalpinen Mesozoikums; Stratigraphie, Fauna und Fazies der Nördlichen Kalkalpen.* Franz Deuticke Verlag, Wien.

Troesch, A. (1908). *Beiträge zur Geologie der westlichen Kientaleralpen (Blümlisalpgruppe).* Georges Bridel & Cie, Lausanne.

Turcotte, D.L. (1997). *Fractals and chaos in geology and geophysics.* Cambridge University Press.

Turnau, V. (1906). *Beiträge zur Geologie der Berner-Alpen, 1. Der prähistorische Bergsturz von Kandersteg, 2. Neue Beobachtungen am Gasteren-Lakkolith.* Buchdruckerei K.J. Wyss, Bern.

Ustaszewski, M., and Pfiffner, O.A. (2008). Neotectonic faulting, uplift and seismicity in the central and western Swiss Alps. *Geological Society, London, Special Publications* 298(1)**,** 231-249.

Van Daele, M., Van Welden, A., Moernaut, J., Beck, C., Audemard, F., Sanchez, J., et al. (2011). Reconstruction of Late-Quaternary sea-and lake-level changes in a tectonically active marginal basin using seismic stratigraphy: The Gulf of Cariaco, NE Venezuela. *Marine Geology* 279(1-4)**,** 37-51.

Van Daele, M., Moernaut, J., Doom, L., Boes, E., Fontijn, K., Heirman, K., et al. (2015). A comparison of the sedimentary records of the 1960 and 2010 great Chilean earthquakes in 17 lakes: Implications for quantitative lacustrine palaeoseismology. *Sedimentology* 62(5)**,** 1466-1496.

Van Daele, M., Haeussler, P.J., Witter, R.C., Praet, N., and De Batist, M. (2020). The sedimentary record of the 2018 Anchorage earthquake in Eklutna Lake, Alaska: Calibrating the lacustrine seismograph. *Seismological Research Letters* 91(1)**,** 126-141.

Vandekerkhove, E., Van Daele, M., Praet, N., Cnudde, V., Haeussler, P.J., and De Batist, M. (2020). Flood-triggered versus earthquake-triggered turbidites: A sedimentological study in clastic lake sediments (Eklutna Lake, Alaska). *Sedimentology* 67(1)**,** 364-389.

Vanneste, M., De Batist, M., Golmshtok, A., Kremlev, A., and Versteeg, W. (2001). Multi-frequency seismic study of gas hydrate-bearing sediments in Lake Baikal, Siberia. *Marine Geology* 172(1)**,** 1-21.

Varnes, D.J. (1978). Slope movement types and processes. *Special report* 176**,** 11-33.

Vidal, H. (1953). Neue Ergebnisse zur Stratigraphie und Tektonik des nordwestlichen Wettersteingebirges und seines nördlichen Vorlands. *Geologica Bavarica* 17**,** 56-88.

Vischer, D., Hager, W.H., and Cischer, D. (1998). *Dam hydraulics.* Wiley Chichester, UK.

Voight, B., and Faust, C. (1982). Frictional heat and strength loss in some rapid landslides. *Geotechnique* 32(1)**,** 43-54.

Voigtländer, A., Leith, K., and Krautblatter, M. (2018). Subcritical crack growth and progressive failure in Carrara marble under wet and dry conditions. *Journal of Geophysical Research: Solid Earth* 123(5)**,** 3780-3798.

Von Wartburg, J., Ivy-Ochs, S., Aaron, J.B., Martin, S., Leith, K., Rigo, M., et al. (2020). Constraining the age and source area of the Molveno landslide deposits in the Brenta Group, Trentino Dolomites (Italy). *Frontiers in Earth Science* 8**,** 164.

Walter, F., Amann, F., Kos, A., Kenner, R., Phillips, M., de Preux, A., et al. (2020). Direct observations of a three million cubic meter rock-slope collapse with almost immediate initiation of ensuing debris flows. *Geomorphology* 351**,** 106933.

Wang, G., Zhang, D., Furuya, G., and Yang, J. (2014). Pore-pressure generation and fluidization in a loess landslide triggered by the 1920 Haiyuan earthquake, China: a case study. *Engineering geology* 174**,** 36-45.

Wang, S., Sloan, S., Liu, H., and Tang, C. (2011). Numerical simulation of the rock fragmentation process induced by two drill bits subjected to static and dynamic (impact) loading. *Rock mechanics and rock engineering* 44(3)**,** 317-332.

Wanner, H., Beer, J., Bütikofer, J., Crowley, T.J., Cubasch, U., Flückiger, J., et al. (2008). Mid-to Late Holocene climate change: an overview. *Quaternary Science Reviews* 27(19-20)**,** 1791-1828.

Wanner, H., Solomina, O., Grosjean, M., Ritz, S.P., and Jetel, M. (2011). Structure and origin of Holocene cold events. *Quaternary Science Reviews* 30(21-22)**,** 3109-3123.

Weber, M. (1997). Quantitative Ableitung sedimentphysikalischer Parameter mit Hilfe eines Multi-Sensor Core Loggers neue Wege in der Analytik mariner Sedimente. *Zeitschrift angewandte Geologie* 43(3)**,** 144-153.

Weichert, D., Horner, R.B., and Evans, S.G. (1994). Seismic signatures of landslides: The 1990 Brenda Mine collapse and the 1965 Hope rockslides. *Bulletin of the Seismological Society of America* 84(5)**,** 1523-1532.

Weidinger, J.T., and Korup, O. (2009). Frictionite as evidence for a large Late Quaternary rockslide near Kanchenjunga, Sikkim Himalayas, India - Implications for extreme events in mountain relief destruction. *Geomorphology* 103(1)**,** 57-65.

Weidinger, J.T., Korup, O., Munack, H., Altenberger, U., Dunning, S.A., Tippelt, G., et al. (2014). Giant rockslides from the inside. *Earth and Planetary Science Letters* 389**,** 62-73.

Werder, M., Bauder, A., Funk, M., and Keusen, H.-R. (2010). Hazard assessment investigations in connection with the formation of a lake on the tongue of Unterer Grindelwaldgletscher, Bernese Alps, Switzerland. *Natural Hazards and Earth System Sciences* 10(2)**,** 227-237.

Wetzel, R.G. (2001). *Limnology: lake and river ecosystems.* gulf professional publishing.

Whalley, W. (1984). Rockfalls. In: *Slope Instability*. John Wiley and Sons, New York.

Whittall, J., Eberhardt, E., and McDougall, S. (2017). Runout analysis and mobility observations for large open pit slope failures. *Canadian Geotechnical Journal* 54(3)**,** 373-391.

Wick, L., Lemcke, G., and Sturm, M. (2003). Evidence of Lateglacial and Holocene climatic change and human impact in eastern Anatolia: high-resolution pollen, charcoal, isotopic and geochemical records from the laminated sediments of Lake Van, Turkey. *The Holocene* 13(5)**,** 665-675.

Wilhelm, B., Nomade, J., Crouzet, C., Litty, C., Sabatier, P., Belle, S., et al. (2016). Quantified sensitivity of small lake sediments to record historic earthquakes: Implications for paleoseismology. *Journal of Geophysical Research: Earth Surface* 121(1)**,** 2-16.

Wilson, B., Dewers, T., Reches, Z.e., and Brune, J. (2005). Particle size and energetics of gouge from earthquake rupture zones. *Nature* 434(7034)**,** 749-752.

Wilson, R.C. (1993). Relation of Arias intensity to magnitude and distance in California. US Geological Survey.

Wirth, S.B., Glur, L., Gilli, A., and Anselmetti, F.S. (2013). Holocene flood frequency across the Central Alps–solar forcing and evidence for variations in North Atlantic atmospheric circulation. *Quaternary Science Reviews* 80**,** 112-128.

Wolfe, B.B., Hall, R.I., Last, W.M., Edwards, T.W., English, M.C., Karst-Riddoch, T.L., et al. (2006). Reconstruction of multi-century flood histories from oxbow lake sediments, Peace-Athabasca Delta, Canada. *Hydrological Processes* 20(19)**,** 4131-4153.

Wolter, A., Stead, D., and Clague, J.J. (2014). A morphologic characterisation of the 1963 Vajont Slide, Italy, using long-range terrestrial photogrammetry. *Geomorphology* 206**,** 147-164.

Wynn, R., and Masson, D. (2003). Canary Islands landslides and tsunami generation: Can we use turbidite deposits to interpret landslide processes? In: *Submarine mass movements and their consequences*. Springer, Dordrecht, 325-332.

Xu, Q., Shang, Y., van Asch, T., Wang, S., Zhang, Z., and Dong, X. (2012). Observations from the large, rapid Yigong rock slide–debris avalanche, southeast Tibet. *Canadian Geotechnical Journal* 49(5)**,** 589-606.

Xu, Y., Matsuoka, H., and Sun, D. (2001). Fractal model for grain-size distribution of soils. *Powder and Grains 2001***,** 4.

Yarnold, J.C., and Lombard, J.P. (1989). A facies model for large rock-avalanche deposits formed in dry climates. In: Field trip guidebook—Pacific section. *Soc Econ Paleontol Mineral 62:9–31*

Yarnold, J.C. (1993). Rock-avalanche characteristics in dry climates and the effect of flow into lakes: insights from mid-Tertiary sedimentary breccias near Artillery Peak, Arizona. *Geological Society of America Bulletin* 105(3)**,** 345-360.

Zemp, M., Haeberli, W., Hoelzle, M., and Paul, F. (2006). Alpine glaciers to disappear within decades? *Geophysical Research Letters* 33(13).

Zemp, M. (2008). *Global glacier changes: facts and figures.* UNEP/Earthprint.

Zhang, M., Wu, L., Zhang, J., and Li, L. (2019). The 2009 Jiweishan rock avalanche, Wulong, China: deposit characteristics and implications for its fragmentation. *Landslides* 16(5)**,** 893-906.

Zhang, Z.-X. (2016). *Rock fracture and blasting: theory and applications.* Butterworth-Heinemann.

Zhang, Z., and Wang, L. (1995). Geological disasters in loess areas during the 1920 Haiyuan Earthquake, China. *GeoJournal* 36(2-3)**,** 269-274.

Zhao, T., Crosta, G.B., Utili, S., and De Blasio, F.V. (2017). Investigation of rock fragmentation during rockfalls and rock avalanches via 3-D discrete element analyses. *Journal of Geophysical Research: Earth Surface* 122(3)**,** 678-695.

Zolitschka, B., Francus, P., Ojala, A.E., and Schimmelmann, A. (2015). Varves in lake sediments–a review. *Quaternary Science Reviews* 117**,** 1-41.

Appendix

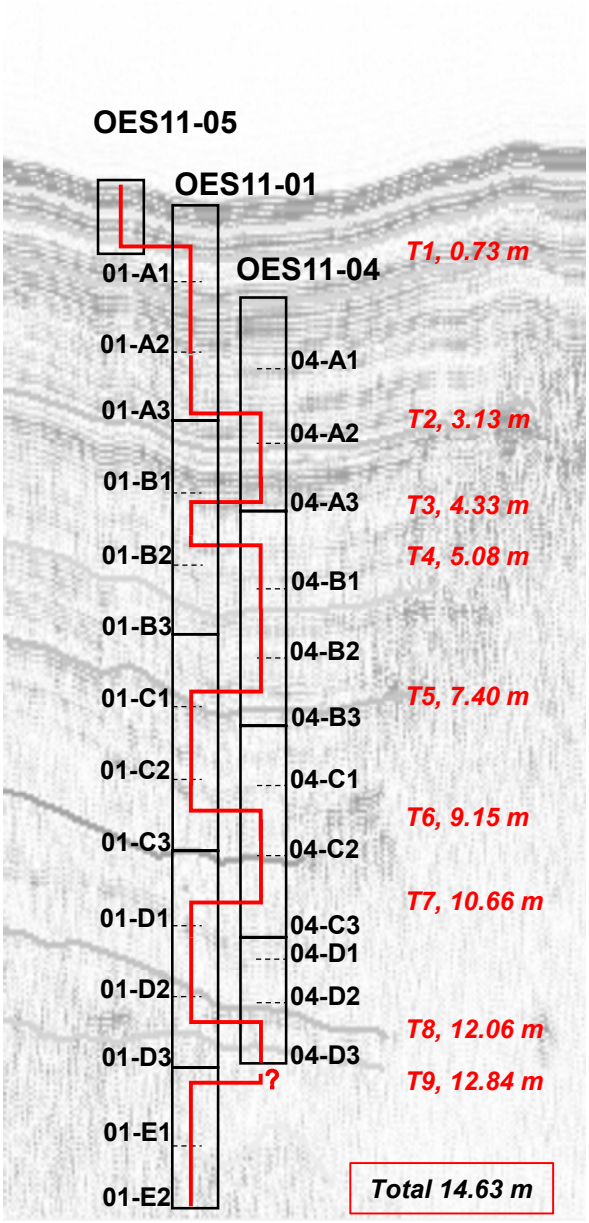

Figure S1. Scheme for assembling the composite core with nine tie points. Some core sections were shortened after settling out of the sediment in the lab (for instance, OES11-04-D1). Without scale.

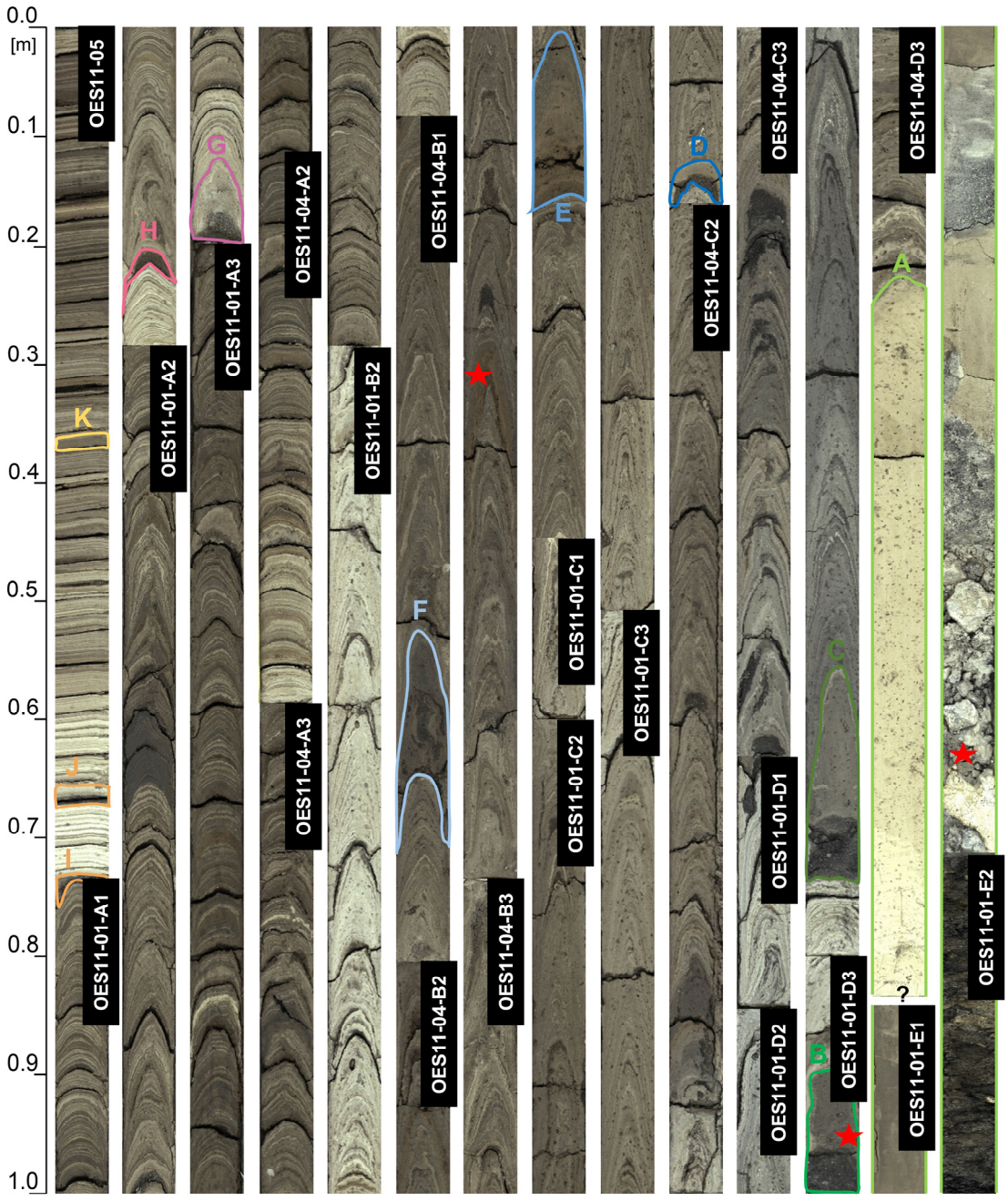

Figure S2. Composite-core sections (0-14 m) with marked turbidites related to the rock-slope failure events. Three wood samples were taken for radiocarbon dating (red stars). Sediment laminae are often deformed by piston coring due to high clay content. Color differences due to different stages of drying.

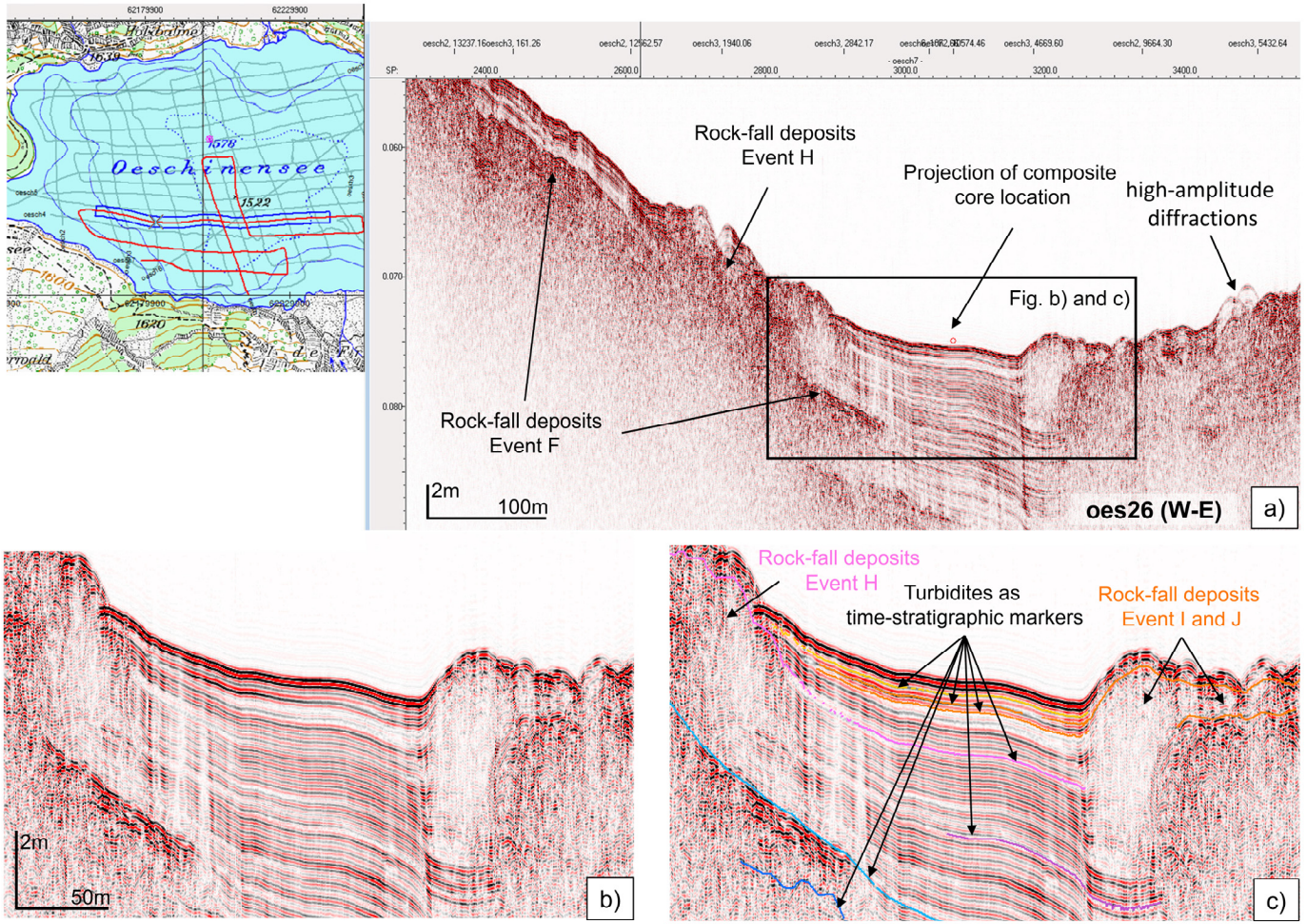

Figure S3. Detailed view of seismic stratigraphy in Lake Oeschinen on profile oes26 (see topo map in the upper left corner for location of profile). a) Event deposits F and H and event-related turbidite continuing towards the lake center and coring location; chaotic-to-transparent units and turbidites in the seismic data b) without interpretation and c) with arrows and colored horizons.

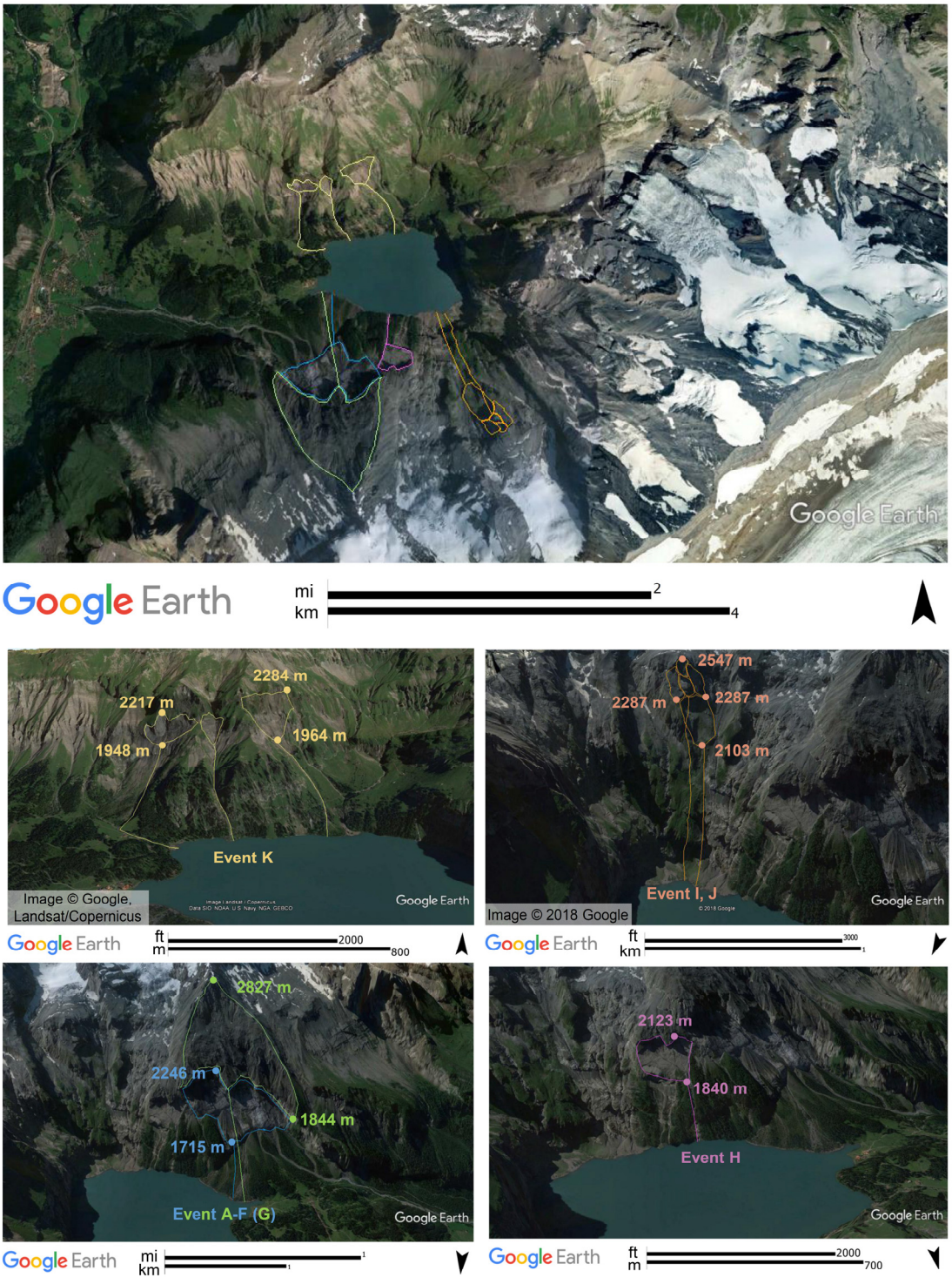

Figure S4. Detailed aerial images with scarp niches, elevations and assumed travel paths.

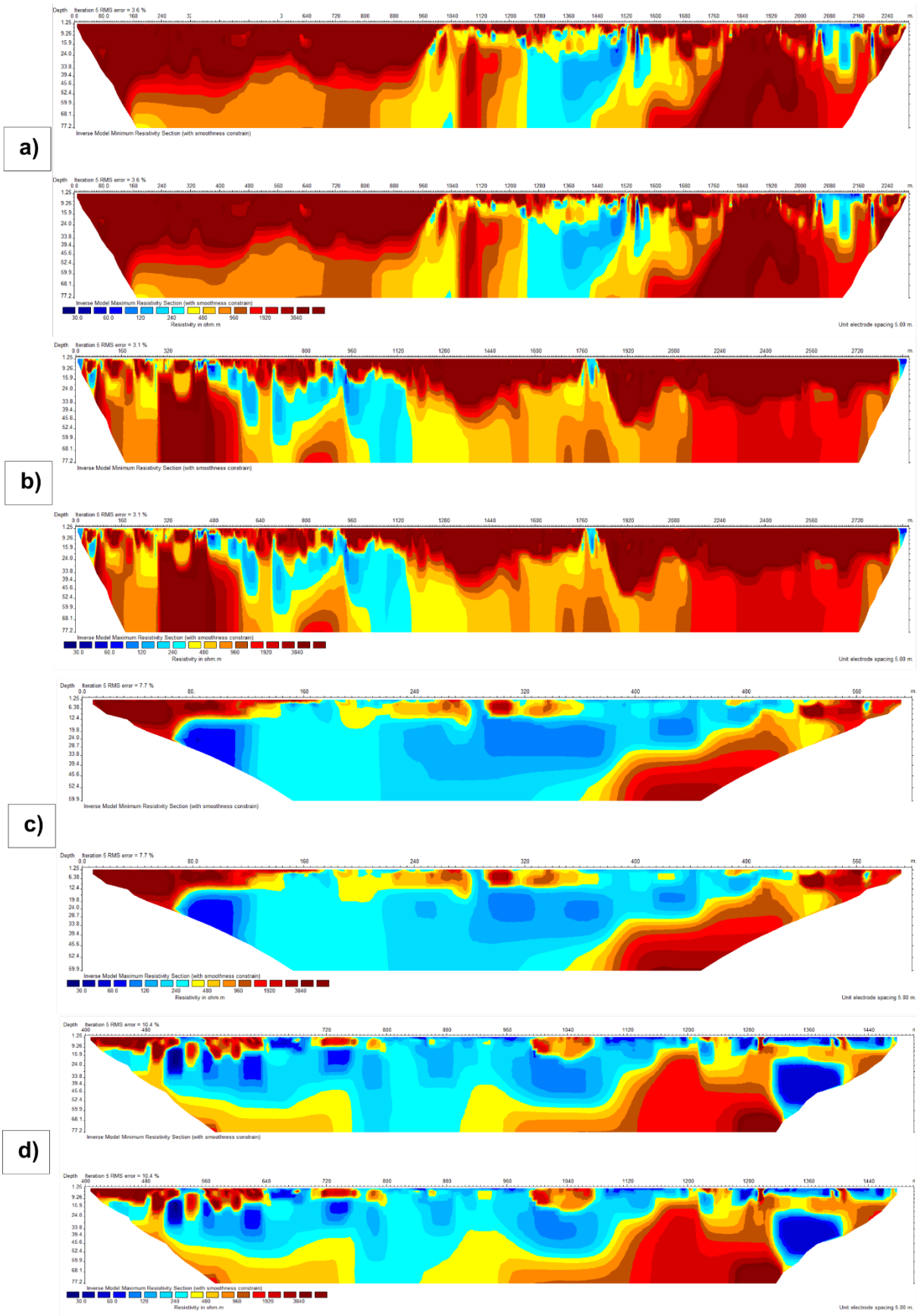

Figure S5: MinMax-Plots of ERT-profiles P1-P4 (a-d) depicting each the modelled inversion with the minimum values (top) and maximum values (bottom) within the error range. Colour differences occur only sparsely and according to the error range at the specific location.

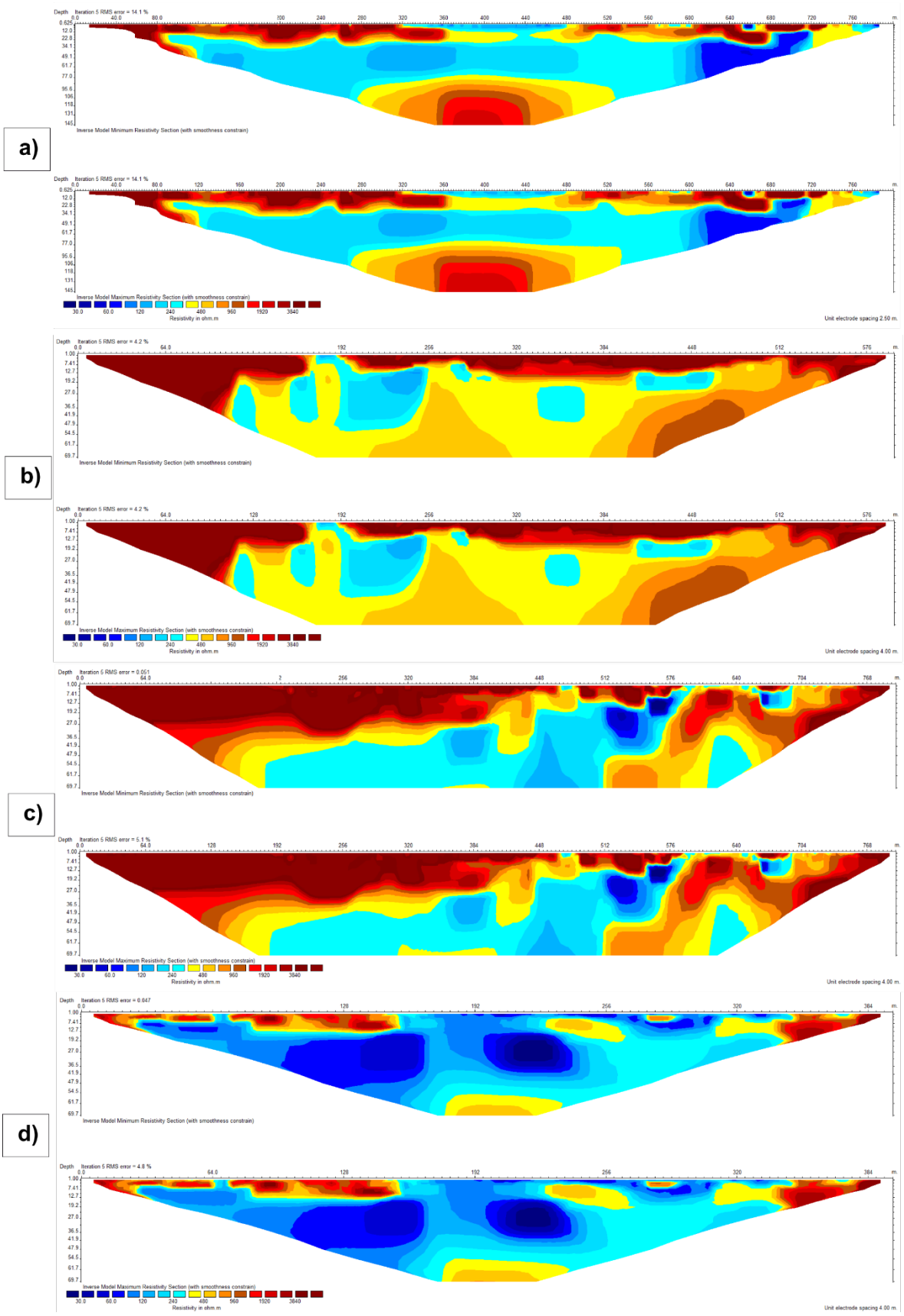

Figure S6: MinMax-Plots of ERT-profiles P5-P8 (a-d) depicting each the modelled inversion with the minimum values (top) and maximum values (bottom) within the error range. Colour differences occur only sparsely and according to the error range at the specific location.

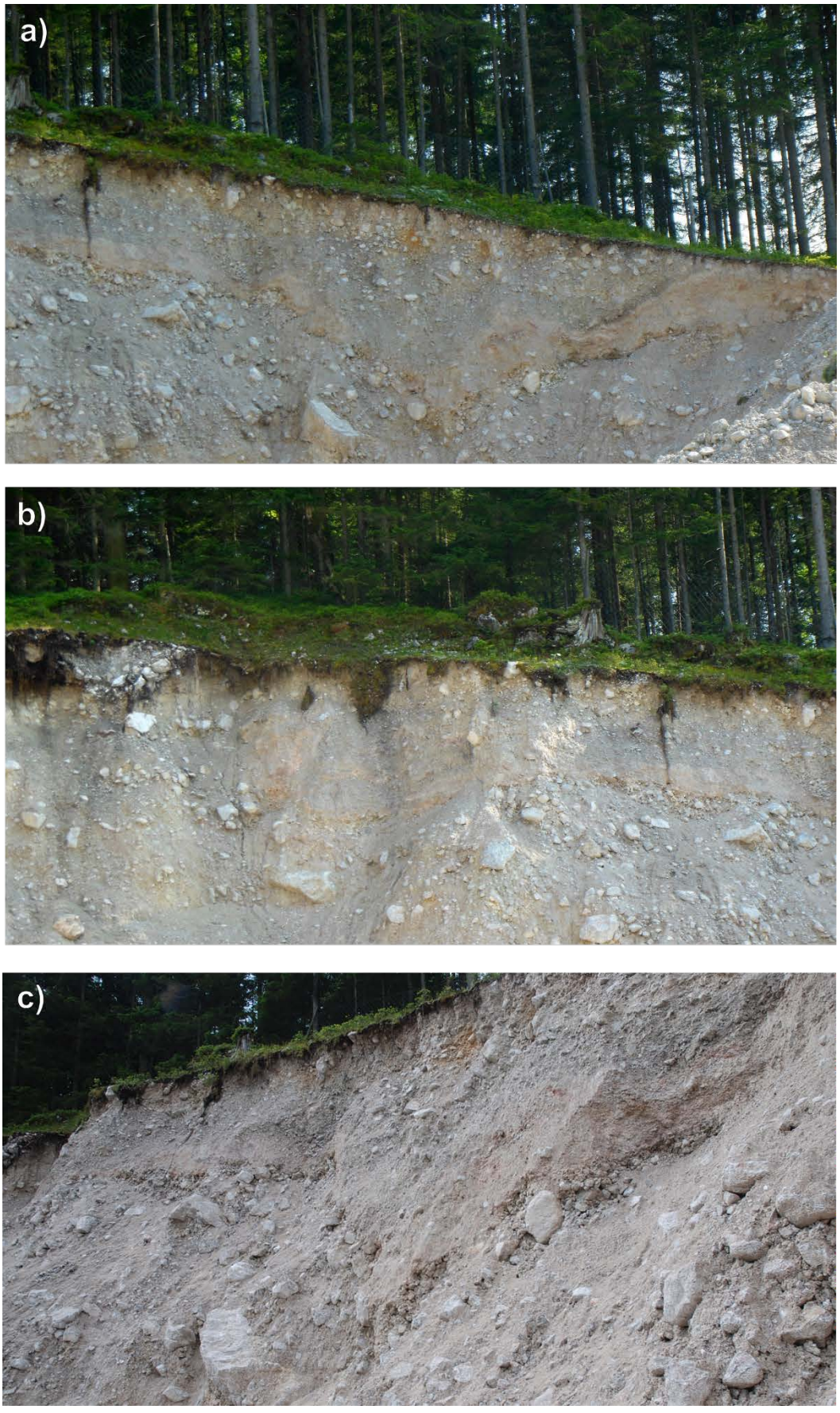

Figure S7: Raw pictures of the gravel pit at Zirmerskopf. a) and b) are E-W-oriented (rock avalanche flow towards the observer) and were taken on 06/07/2015, c) was taken on 18/06/2015 looking along the sediment surface to the East.

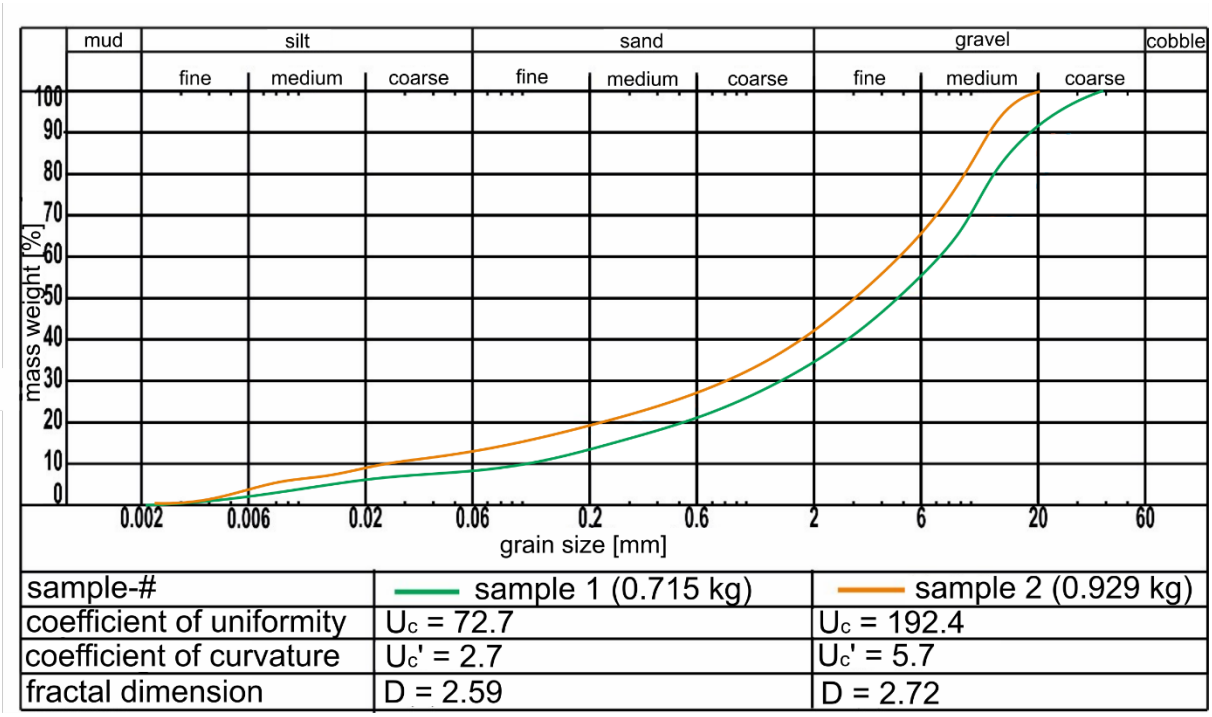

sample-#	sample 1 (0.715 kg)	sample 2 (0.929 kg)
coefficient of uniformity	U_c = 72.7	U_c = 192.4
coefficient of curvature	U_c' = 2.7	U_c' = 5.7
fractal dimension	D = 2.59	D = 2.72

Figure S8: Grain-size distributions of the two samples from the shear band between two rock-avalanche lobes with fractal dimensions.

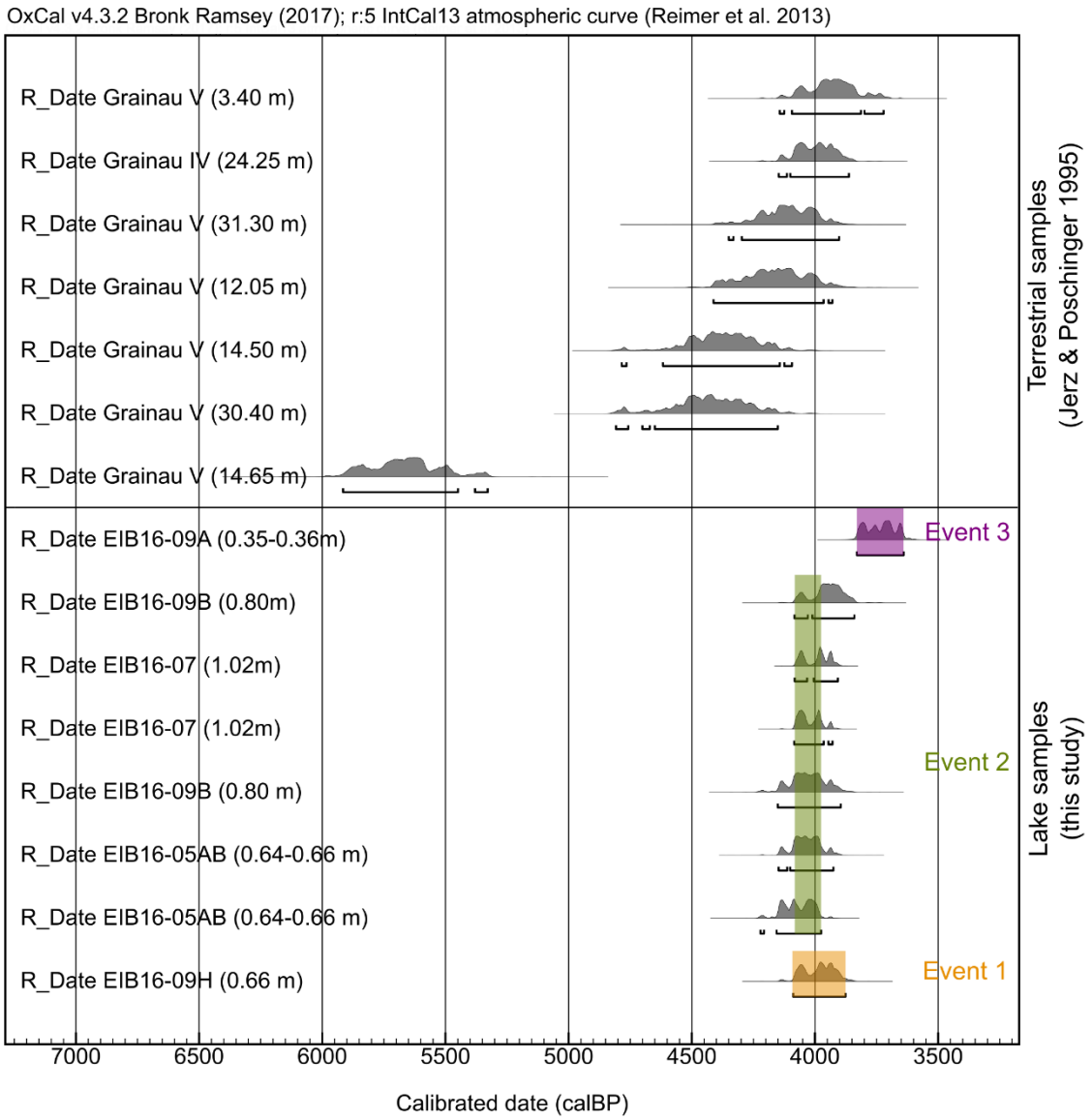

Figure S9: Comparison of calibrated, previously published radiocarbon ages on the Eibsee rock avalanche and our ages from Lake Eibsee. Our ages overlap at 4089-3976 cal yr BP.

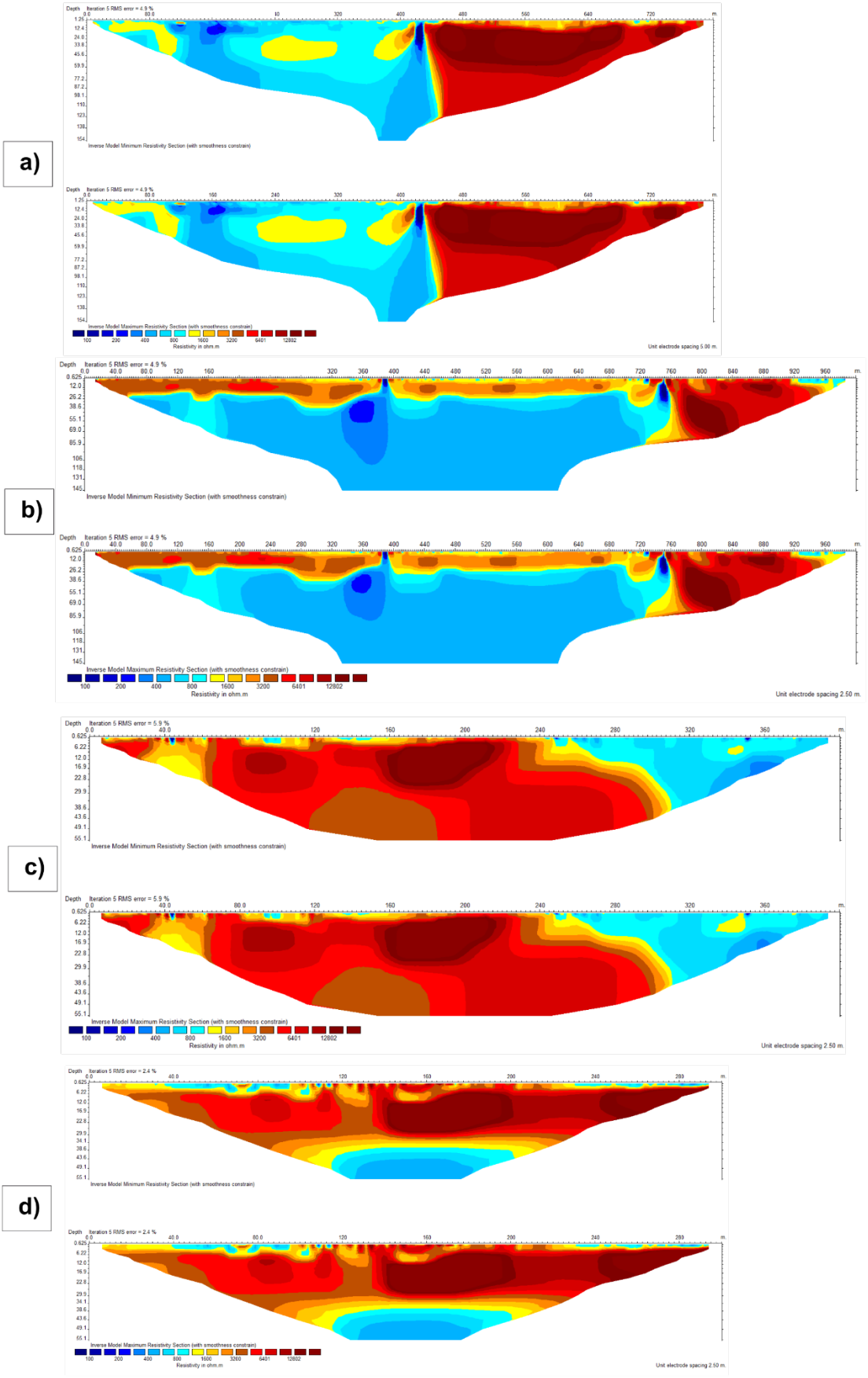

Figure S10: MinMax-Plots of ERT-profiles P1-P4 (a-d) depicting each the modelled inversion with the minimum values (top) and maximum values (bottom) within the error range. Colour differences occur only sparsely and according to the error range at the specific location.

Core number	Core section	Sediment depth [m]	Core type	Coordinates (CH1903/LV03)	Target
OES11-01	A1-A3 B1-B3 C1-C3 D1-D3 E1-E3	0.0-3.0 3.0-6.0 6.0-9.0 9.0-12.0 12.0-15.0	long	622024/149835 622024/149839	composite core (reaching top of rock avalanche forming initial lake basin)
OES11-02		-0.5-2.5	long	622034/149842	varve chronology (Amann et al., 2014; Amann et al., 2015)
OES11-03		2.0-5.0	long	622036/149844	
OES11-04	A1-A3 B1-B3 C1-C3 D1-D3	1.5-4.5 4.5-7.5 7.5-10.5 10.5-13.5	long	622030/149844 622034/149837	completion of composite core (combination of 11-01 and 11-04 overlapping)
OES11-05			short	622024/149838	top of composite core
OES11-06			short		varve chronology (Amann et al., 2014; Amann et al., 2015)
OES11-10		0.0-0.6	hammer	622219/149712	stratigraphy of uppermost deposits
OES11-11		0.0-1.2	hammer	622224/149709	
OES11-12		0.0-1.0	hammer	622134/149484	
OES11-13		0.0-0.7	hammer	622137/149490	
OES11-14		0.0-1.2	hammer	622144/149496	
OES11-15		0.0-0.9	short	622124/149581	
OES11-16		0.0-0.9	short	622046/149586	

Table S1. Overview of retrieved sediment cores and their location in the basin of Lake Oeschinen.

Core section	section depth [cm]		length [cm]	composite depth [cm]		tie points
	from	to		from	to	
OES 11-05 SC	3,5	76,4	72,9	0,0	72,9	T1
OES 11-01 A1	36,2	91,4	55,2	72,9	128,1	
OES 11-01 A2	6,5	99,0	92,5	128,1	220,6	
OES 11-01 A3	0,0	92,7	92,7	220,6	313,3	T2
OES 11-04 A2	53,5	98,0	44,5	313,3	357,8	
OES 11-04 A3	7,1	81,8	74,7	357,8	432,5	T3
OES 11-01 B2	10,4	86,2	75,8	432,5	508,3	T4
OES 11-04 B1	17,5	91,5	74,0	508,3	582,3	
OES 11-04 B2	7,4	99,7	92,3	582,3	674,6	
OES 11-04 B3	6,7	72,3	65,6	674,6	740,2	T5
OES 11-01 C1	75,8	95,5	19,7	740,2	759,9	
OES 11-01 C2	5,3	98,2	92,9	759,9	852,8	
OES 11-01 C3	3,0	65,0	62,0	852,8	914,8	T6
OES 11-04 C2	16,1	99,3	83,2	914,8	998,0	
OES 11-04 C3	9,5	77,0	67,5	998,0	1065,5	T7
OES 11-01 D1	76,0	95,4	19,4	1065,5	1084,9	
OES 11-01 D2	4,3	98,5	94,2	1084,9	1179,1	
OES 11-01 D3	3,0	30,1	27,1	1179,1	1206,2	T8
OES 11-04 D3	19,9	97,7	77,8	1206,2	1284,0	T9, gap
OES 11-01 E1	9,2	97,2	88,0	1284,0	1372,0	
OES 11-01 E2	2,9	94,2	91,3	1372,0	1463,3	

Table S2. Detailed information on the composite core using core sections of OES11-01, OES11-04 and OES11-05.

ERT profile	Orientation / related to flow direction	Length [m]	Penetration depth [m]	Lateral resolution (spacing) [m]	Target
P1	SE-NW / longitudinal, diagonal	2300	≤ 80	5	N-shoreline, dam, collision with bedrock, shearing / bulging, calibration site for rock-avalanche carapace (megaboulders)
P2	W-E / transversal	2900	≤ 80	5	W- and E-shoreline of paleolake, dam, thickness of rock-avalanche deposits
P3	SW-NE / longitudinal	600	≤ 60	5	N-paleolake dimension, calibration site for *Plattenkalk Limestone* and mixed sediments
P4	W-E / transversal	1100	≤ 60	5	N-paleolake dimension, paleotopography, “splash zone” of rock-avalanche deposits behind obstacle *(Zirmerskopf*)
P5	S-N / longitudinal	800	≤120	10	Paleotopography, bulldozing in distal facies, calibration site for mixed sediments
P6	SW-NE / transversal	600	≤ 60	4	Transitional shearing, dam characteristics
P7	SE-NW / diagonal	800	≤ 60	4	Paleotopography, thickness of rock-avalanche deposits
P8	N-S / transversal	400	≤ 60	4	Calibration lake sediments clay/silt

Table S3: Key parameters of ERT profiles P1-P8.

Material	Resistivity range [Ωm]	Source	Field-calibration site
Clay	5-100 < 100	Samouëlian et al. (2005) Kneisel (2003)	
Lake clay	< 100	Bader (1979, 1981)	Drilling V, Figure 23d
Moraine	90-2000	Samouëlian et al. (2005)	
Rock avalanche deposits (mixed)	< 3000	Socco et al. (2010)	Drilling IV, Figure 22c
Rock avalanche boulders (coarse)	> 10000	Socco et al. (2010)	Eibsee Hotel, Figure 22a
Rock avalanche debris (homogenous)	> 3000	Ostermann et al. (2012)	
Wetterstein Limestone	10000 (20°C) - 25000 (10°C)	Krautblatter et al. (2010)	Carapace boulders, Figure 22a
Hauptdolomite	> 3000 > 14900-16000 (10°C)	Laboratory test	Bedrock *Zirmerskopf*, Figure 22a
Plattenkalk Limestone	13100-17500	Laboratory test	Bedrock, Figure 22b; Drilling IV, Figure 22c
Eibsee rock avalanche body	3200-5000 (20°C)	Laboratory test	

Table S4: Calibration of ERT profiles with literature data, laboratory tests and field sites.

Coring location/ coordinates	Core number	Core section	Core type	Composition	Section depth in composite section [m]	Composite depth [m]
Location1: **4423170/ 5258127**	EIB16-01	EIB16-01	short	top	0.08-0.83	0.00-0.75
	EIB16-02	EIB16-02A	long	-	-	-
		EIB16-02B		-	-	-
		EIB16-02C		-	-	-
	EIB16-03	EIB16-03A	long	diffuse / gap?	0.08-0.72	0.75-1.39
		EIB16-03B		Consecutive	0.00-0.72	1.39-2.11
Location 2: **4422050/ 5258656**	EIB16-04	EIB16-04	short	top	0.06-0.64	0.00-0.58
	EIB16-05	EIB16-05AB	long	tie point	0.22-0.97	0.58-1.33
		EIB16-05C		consecutive	0.03-0.87	1.33-2.17
Location 3: **4421822/ 5258391**	EIB16-06	EIB16-06	short	top	0.05-0.54	0.00-0.49
	EIB16-07	EIB16-07	long	tie point	0.64-1.20	0.49-1.05
Location 4: **4423687/ 5258263**	EIB16-08	EIB16-08	short	top	0.05-0.67	0.00-0.62
	EIB16-09	EIB16-09A	long	tie point	0.26-1.01	0.62-1.37
		EIB16-09B		consecutive	0.04-0.99	1.37-2.32
		EIB16-09C		consecutive	0.00-0.40	2.32-2.72
		EIB16-09D	long	-	-	-
		EIB16-09E		diffuse/ gap?	0.28-1.01	2.72-3.45
		EIB16-09F		consecutive	0.00-0.55	3.45-4.00
		EIB16-09G	long	-	-	-
		EIB16-09H		tie point	0.17-0.88	4.00-4.71

Table S5: Key parameters of retrieved sediment cores with information on coring location and composition. Coordinates are given in Gauss-Krüger Zone 4.

Appendix A

Final published journal article:

Knapp, S., Gilli, A., Anselmetti, F.S., Krautblatter, M., Hajdas, I. (2018): Multistage Rock-Slope Failures Revealed in Lake Sediments in a Seismically Active Alpine Region (Lake Oeschinen, Switzerland). *Journal of Geophysical Research: Earth Surface 123(4): 658-677*.

https://doi.org/10.1029/2017JF004455

Appendix B

Final published journal article:

Knapp, S., and Krautblatter, M. (2020). Conceptual Framework of Energy Dissipation During Disintegration in Rock Avalanches. *Frontiers in Earth Science, 8*(263).

https://doi.org/10.3389/feart.2020.00263

Appendix C

Final published journal article:

Knapp, S., Mamot, P., Lempe, B., Krautblatter, M. (2021): Impact of an 0.2 km³ Rock Avalanche on Lake Eibsee (Bavarian Alps, Germany) – Part I: Reconstruction of the Paleolake and Effects of the Impact. *Earth Surface Processes and Landforms 46 (1), 296-306*.

https://doi.org/10.1002/esp.5024

Appendix D

Final published journal article:

Knapp, S., Anselmetti, F.S., Lempe, B., Krautblatter, M. (2021): Impact of an 0.2 km³ Rock Avalanche on Lake Eibsee (Bavarian Alps, Germany) – Part II: Catchment Response to Consecutive Debris Avalanche and Debris Flow. *Earth Surface Processes and Landforms 46 (1), 307-319.*

https://doi.org/10.1002/esp.5025